BULGARIAN CHEMICAL COMMUNICATIONS

2018 Volume 50 / Number 4

Journal of the Chemical Institutes
of the Bulgarian Academy of Sciences
and of the Union of Chemists in Bulgaria

Bulgarian Chemical Communications, Volume 50, Issue 4, (pp. 517 – 523) 2018

Improved synthesis of fluconazole by using nano-SSA as a green catalyst

L. Zamani[a], Z. Rezaei[a,b], S. Khabnadideh[a,b,*]

[a] Pharmaceutical Sciences Research Center, Shiraz University of Medical Sciences, Shiraz, Iran.
[b] Department of Medicinal Chemistry, Faculty of Pharmacy, Shiraz University of Medical Sciences, Shiraz, Iran

Received, September 19, 2016; Revised, January 29, 2018

In our on-going interest in the preparation of new antifungal agents, our attention was focused on fluconazole because of its broad antifungal spectrum, low toxicity and excellent pharmacokinetic properties. As a part of our program to develop a new method for synthesis of fluconazole, the conditions of some reactions, especially Grignard reactions, were screened and optimized. The best situation was achieved by using nano-silica sulfuric acid as a green and mild catalyst. The high yield and comfortable isolation in each step were the advantage points in this method.

Keywords: Fluconazole, Nano-SSA, Synthesis

INTRODUCTION

In recent years, life-threatening systemic fungal infections have become increasingly common, especially in immunocompromised hosts suffering from tuberculosis, cancer or AIDS and in organ transplant cases [1]. Though there are effective antifungal agents available in the market, they have shortcomings such as toxicity, limited range of activity for the fungal strains, high price and limited penetration through the central nervous system [1]. Several clinical drugs, including azoles, polyenes, echinocandins and allylamines have been developed to reduce the impact of fungal diseases. Among those, azole antifungal drugs, especially triazole agents such as fluconazole, voriconazole and itraconazole, posaconazole and ravuconazole [2] are marketed or in the late stages of clinical trials and proved to be more effective and thus are more widely used for the treatment of invasive fungal infections (Fig. 1). Fluconazole is an important antifungal agent used against various fungal strains which inhibits specific steps in fungal sterol biosynthesis [1, 3]. It is a 1,2,4-triazole based drug which has established an exceptional therapeutic record for *Candida* infections, including oropharyngeal and esophageal candidiasis, vulvovaginal candidiasis, candidemia, and disseminated candidiasis [4]. Usually azoles apply their antifungal activity through inhibition of CYP51 by a mechanism in which the heterocyclic nitrogen (N_3 of imidazole or N_4 of 1,2,4-tiazole) binds to the sixth coordination of heme iron atom of porphyrin in the substrate binding site of the enzyme [4a]. Based on the active site's structure of CYP51 and the extensive investigation of the structure- activity relationships of the azole antifungals, it was found that 1,2,4-triazole ring and 2,4-difluorophenyl group are essential for the high antifungal activity [4a]. Our investigation is based on the development of a new synthetic method for fluconazole by using a heterogeneous catalyst. We tried to set a new procedure in order to increase the rate and yield of the reaction and also reducing hazards to human and environment. Literature reports [5] didn't show any evidence concerning the use of heterogeneous catalysts for synthesis of fluconazole. Here we introduced nano-SSA as a green catalyst in some steps of fluconazole synthesis. In the presence of nano-SSA [6], the yield of the reaction increased and the reaction proceeded in a short time. We also inspected the Grignard reaction in three different states and compared their results with our method. For synthesis of fluconazole, we tried four different methods ***(a-d)***.

Method a: A Friedel-Crafts acylation was started from diflourobenzene ***(1)*** and chloroacetyl chloride ***(2)*** to get 2-chloro-1(2,4-difluorophenyl)1-ethanone ***(3)***. This step was applied under the same experimental conditions as in [5a]. Then in the second step for N_1-alkylation of 1*H*-1,2,4-triazole by ***(3)*** we first activated the carbonyl group of ***(3)*** by nano-SSA in toluene for 0.5 h and then 1,2,4-triazole was added.

* To whom all correspondence should be sent:
E-mail: : khabns@sums.ac.ir

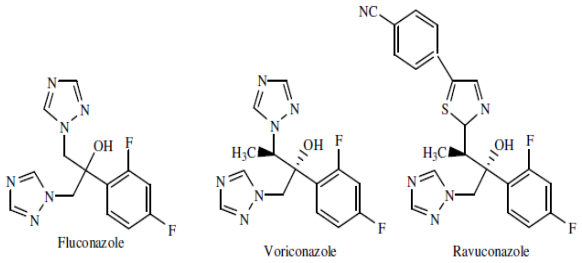

Fig. 1. Several clinical drugs including tri-azole rings

In the presence of nano-SSA, alkylation reaction was easily performed in high yield to get 1-(2,4-difluorophenyl)-2-(1*H*-1,2,4-triazole-1-yl)1-ethanone ***(5)***. In the third step the oxirane intermediate ***(6)*** was obtained by Corey–Chaykovsky epoxidation in the presence of trimethylsulfoxonium iodide and aqueous solution of NaOH. This step also was done according to the literature. Finally, in the last step again epoxide ring opening of **(*6*)** was achieved by activating oxirane with nano-SSA and then triazole was added to get fluconazole ***(7)*** (Scheme 1). In this method steps 2 and 4 were modified by nano-SSA catalyst. Our catalyst could increase dramatically the yield and the rate of reactions in these two steps. We suggested two intermediates (***3'*** and ***6'***) after using nano-SSA in the above steps.

This method has been used in the synthesis of fluconazole [7] but because it requires expensive material (for example, sulfoxide trimethyl iodide), and the formation yield of an epoxy compound is not very high, a direct result of the production cost of the final product fluconazole is difficult to reduce the impact of its promotion applications.

The present invention used the nano-SSA as a green catalyst; the reaction is easy to control, without complex special equipment. The original equipment can be put into use, each step takes place under mild reaction conditions, the simple and non-destructive environment is suitable for industrial promotion.

In our other approaches we tried to synthesize fluconazole by different methods of Grignard reactions and compared the results of each method in order to optimize the synthetic method for preparing of fluconazole.

Method b: In the second method (Grignard reaction 1) [1,2,4] triazol-1-yl-methanol ***(9)*** was synthesized by using 1,2,4-triazole ***(4)*** and 1,3,5-trioxan ***(8)***. Then ***(9)*** was chlorinated by thionyl chloride to achieve 1-chloromethyl-1*H*-[1,2,4] triazole ***(10)*** in high yield. Compound ***10*** then reacted with magnesium in dry ether under nitrogen gas to produce the Grignard intermediate ***(10')***. Finally, the reaction between ***(10')*** (eq. 2) and 2,4-difluoroethylbenzoate ***(11)*** (eq. 1) *via* Grignard reagent gave the product ***7*** (Scheme 2). In this procedure we used for the first time 1,3,5-trioxane for preparing fluconazole. This reagent easily substituted a hydroxymethyl group at position 1 of the triazole ring.

In method ***b*** we used trioxane for the first time as a hydroxymethylene group donor in the synthesis of fluconazole; in the previous work paraformaldehyde was used for the synthesis of hydroxymethyltriazole [7,8]. The present invention avoids the use of the expensive trimethyl iodide sulfoxide or trimethyl iodide sulfoxide, each step uses domestic raw material supply and low prices can effectively reduce production costs.

Method c: In the third procedure (Grignard reaction 2), we obtained 1-(2,4- difluorophenyl)-2-(1*H*-1,2,4-triazole-1-yl)1-ethanone***(5)*** by using nano-SSA catalyst, as mentioned in the first method. Then reaction between ***10'*** (eq. 1) and ***5*** (eq. 1) gave ***7*** (Scheme 3).

Method d: In the fourth procedure (Grignard reaction 3), as in the third one, we used both a Grignard reagent and our nano catalyst for synthesis of fluconazole. In this procedure we started from 1,3-dichloroacetone ***(12)*** and activated its carbonyl group by nano-SSA and then reacted it with triazole to get 1,3-bis-[1,2,4] triazol-1-yl-propan-2- one ***(13)***. In this method the Grignard reagent ***(15)*** was prepared from 2,4-difluorobromobenzene ***(14)*** with the same procedure as for compound ***10'***. This reagent was then reacted with ***(12)*** to get ***7*** (Scheme 4). Intermediate ***12'*** was our suggested structure in this way. However, each method has certain restrictions with regard to scope and reaction conditions; for example, each step of the method gives a low yield, the reaction with 1,3-dichloroacetone lacks selectivity, by-products are more difficult to separate, so there is no industrialization prospect [9]. To avoid these limitations, we investigated the use of nano-SSA for reacting 1,3-dichloro acetone and 1,2,4-1*H*- triazole. It is necessary to mention that using ionic liquids for this step, good results have been achieved [9].

We modified the processes used previously for synthesis of fluconazole by using nano-SSA as a green catalyst in some steps. Our results showed that this catalyst is more efficient as regards yield and time of the reactions (Method ***a***). We also used nano-SSA in the synthesis of one of the starting materials for Grignard reactions 3 (Method ***d***). The high yield and comfortable isolation in each step were the advantage points in this method.

This work was supported by Health Technology development Office, Deputy of Research and Technology, Ministry of Health and Medicinal Education, Ialamic Republic of Iran. The Grant number in Shiraz University of Medicinal Sciences is 6809.

EXPERIMENTAL

All chemicals were purchased from Merck and used without any additional purification. The products were characterized by FT-IR (ATR), ^{1}H-NMR, and a comparison of their physical properties with those reported in the literature. FT-IR (ATR) spectra were acquired on a Bruker, Eqinox 55 spectrometer.

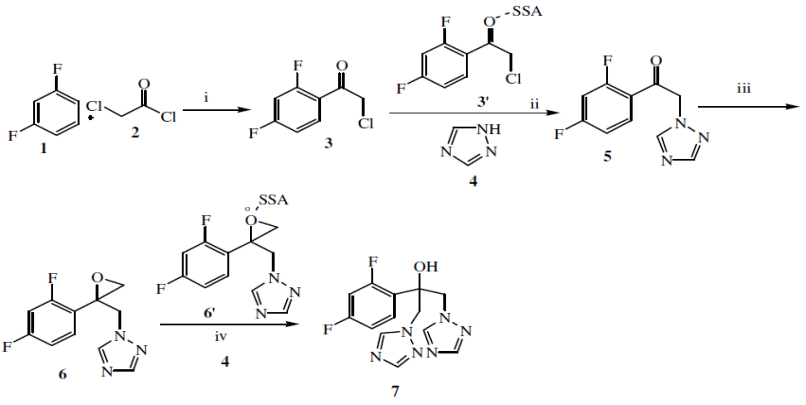

i)$AlCl_3$,R.T. ii) nano-SSA iii) Toluene, $NaHCO_3$, Reflux. iv) NaOH, TEAB, Trimethylsulfoxonium iodide, CH_2Cl_2. v)nano-SSA. vi) TEA, Ethanol, 80 C.

Scheme 1. Synthesis of fluconazole by nano-SSA (**method *a***).

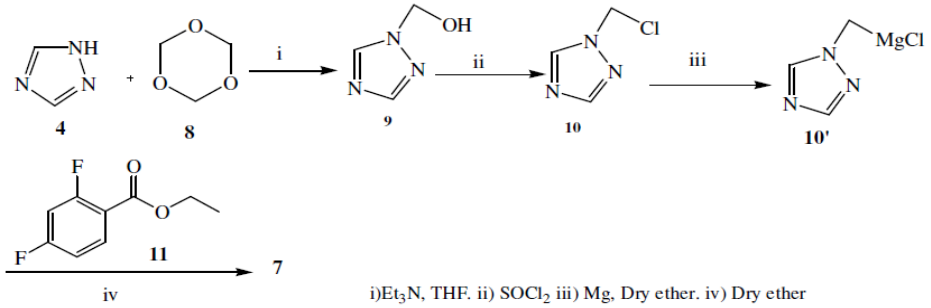

i)Et_3N, THF. ii) $SOCl_2$ iii) Mg, Dry ether. iv) Dry ether

Scheme 2. Synthesis of fluconazole by Grignard reaction 1 (**method *b***).

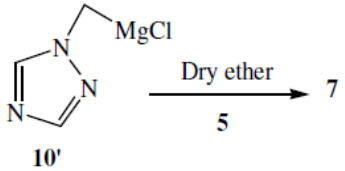

Scheme 3. Synthesis of fluconazole by Grignard reaction 2 (**method *c***).

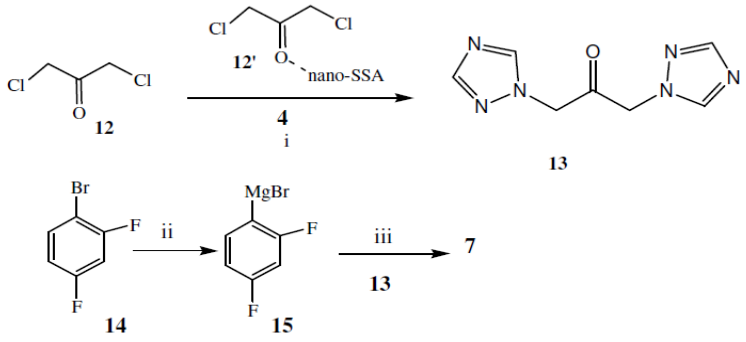

i) nano-SSA, Toluene. ii) Mg/Dry Ether. iii)Dry Ether

Scheme 4. Synthesis of fluconazole by Grignard reaction 3 (**method *d***).

A Bruker (NMR- 300MHz spectrometer) was used to record the ^{1}H NMR spectra. Spectrophotometer (UV/Vis biotek model UVIKONXL). Melting points were determined by using an Electrothermal 9100 digital melting point apparatus (Electrothermal, Essex, UK). The reaction progress and purity of the synthesized compounds were checked on Merck aluminium plates precoated with silica gel 60 F-254. UV radiation and/or iodine were used as the visualizing agents. Silica gel column chromatography was performed with silica gel 60G.

Preparation of nano-SSA

A 500 mL suction flask containing nano-silica gel (60.0 g) was equipped with a constant pressure dropping funnel containing chlorosulfonic acid (23.3 g, 0.2 mol) and gas inlet tube for conducting HCl gas over the adsorbing solution (water). Chlorosulfonic acid was added dropwise at room temperature over a period of 30 min. HCl gas was evolved from the reaction vessel immediately. After the addition was complete, the mixture was shaken for 30 min and a white solid of nano-SSA (76.0 g) was collected [6a].

2-Chloro-1-(2,4-difluoro-phenyl)-ethanone (3)

1,3-Difluorobenzene (5 mmol) and anhydrous aluminium chloride (6 mmol, 0.798 g) were stirred in 6 ml of dichloroethane at 30ºC for 30 min. The mixture was then cooled to 0ºC in ice bath and was charged dropwise with chloroacetyl chloride solution (5.1 mmol, 0.586 g) while stirring during 30 min. Stirring was continued for further 30 min keeping the reaction mixture at 0-10ºC. Then the mixture was warmed to room temperature and stirred for 24 h. After TLC showed complete conversion, the reaction was quenched by addition of hydrochloric acid (1M) and the mixture was extracted with dichloroethane at 0-5ºC. The combined organic layers were washed with 2×20 ml of saturated $NaHCO_3$ and then with cold water and brine, dried over anhydrous sodium sulfate (Na_2SO_4), and concentrated in vacuum. The white product was purified by recrystallization from *n*-hexane to get **3**, yield= 98%, mp= 44-48ºC.

1-(2,4-difluorophenyl)-2-(1H-1,2,4-triazole-1-yl)1-ethanone (5)

A flask equipped with a reflux condenser was charged with a mixture of 2-chloro-1-(2,4-difluoro-phenyl)-ethanone (4 mmol) and nano-SSA (0.1 g) in toluene solvent, the carbonyl group was activated after 0.5 h, then a mixture of 1,2,4 triazole (4 mmol, .0331g) and sodium bicarbonate (4.8 mmol, 0.404 g) in 4 ml of toluene was added to it and refluxed for 24 h. Then the reaction mixture was poured in crashed ice and extracted with ethyl acetate (2×5 ml). The combined organic layers were washed with water and brine, dried over anhydrous sodium sulfate and concentrated in vacuum. The yellow product ***5*** was obtained by recrystallization from diethyl ether; yield = 80%; mp=103-107˚C.

1-[2-(2,4-difluorophenyl)-2,3-epoxypropyl]-1H-1,2,4-triazole (6)

A mixture of 1-(2,4-difluorophenyl)-2-(1*H*-1,2,4-triazole-1-yl)1-ethanone in 15 ml of dichloromethane, trimethylsulfoxonium iodide (TMSI)**,** (1.8 mmol, 0.397 g) and 3 ml toluene was charged by sodium hydroxide solution (20%, 1.3 ml) and tetraethylammonium bromide (TEAB) (0.3 mmol, 0.063 g). The reaction mixture was heated at 60ºC for 7 h. Progress of the reaction was monitored by TLC. After completion of the reaction, the product was diluted with water and extracted with ethyl acetate (2×4 ml). The organic layer was washed and dried over anhydrous sodium sulfate and concentrated. White crystals were obtained by recrystallization from absolute ethanol; yield= 68%; mp=123-125˚C.

Fluconazole (7) via method a

A mixture of 1-[2-(2,4-difluorophenyl)-2,3-epoxypropyl]-1*H*-1,2,4-triazole (0.3 mmol) and nano-SSA (0.1 g) was stirred in 2 ml of absolute ethanol for 0.5 h. Then a mixture of triethylamine (0.18-0.29 ml) and 1,2,4 triazole (0.4 mmol, 0.0316 g) was added and refluxed in absolute ethanol for 15-24 h. TLC monitoring was used to control reaction progress. The mixture was filtered, concentrated and diluted with 3 ml of water. Then the filtrate was extracted with ethyl acetate (3×8 ml). The combined organic layers were washed with water and then with brine, dried over anhydrous sodium sulfate and concentrated in vacuum. The white product was purified by thin layer chromatography in a solvent system containing chloroform and methanol (88:12); yield = 55%; mp = 138-140˚C [7].

Hydroxymethyltriazole (9)

In a round-bottomed flask equipped with stirring system and cooler, dissolve triazole (1 mmol, 0.069 g), 1,3,5-trioxane (0.33 mmol, 0.03 g) and 0.5 mL of Et_3N in 5 mL of THF. Keep the reaction stirred under inert atmosphere and refluxing for 18 h. To purify the product, concentrate the solution in a rotavapor and wash the white solid formed with diethyl ether. The product was crystallized from hot acetone; yield = 88%; mp =70- 73˚C [7].

Chloromethyl-1H-[1,2,4]triazole (10)

Dissolve the product (**9**) (0.45 g) in 5 mL of THF and stir vigorously at 40°C for some time. Add slowly 0.6 mL of $SOCl_2$ using a dropping funnel and stir the reaction mixture, keeping the temperature at about 45°C. A white precipitate should form. Recover the precipitate by filtration and wash it with AcOEt; yield = 75%; mp =82-84˚ C [7].

Preparation of Grignard reagent from 1-chloromethyl-1H-[1,2,4]triazole (10')

0.05 g of Mg powder was placed in a dry reaction tube and 0.5 mL of anhydrous diethyl ether was added. In a separate dry vial, 0.117 g of 1-chloromethyl-1*H*-[1,2,4]triazole and 0.70 mL of anhydrous diethyl ether were mixed and immediately added to the reaction tube.

Fluconazole 7 via method b

2,4-difluoroethylbenzoate (1mmol, 0.186 g) was dissolved in 1 mL of anhydrous diethyl ether and added to the Grignard reagent (10′) under gentle reflux. After finishing the reaction, 0.5 mL of HCl (3 M) was added dropwise while stirring, forming a white precipitate. Ether was added to dissolve the precipitate, then the aqueous layer was removed and an equal volume of aqueous NaCl solution was added. The aqueous layer was again removed and the ether was evaporated. The final product was obtained; yield= 42%; mp = 138-141˚C [7].

Fluconazole 7 via method c

1-(2,4-difluorophenyl)-2-(1*H*-1,2,4-triazole-1-yl)1-ethanone (1 mmol, 0.22 g) was dissolved in 1 mL of anhydrous diethyl ether and added to the Grignard reagent (10′) under gentle reflux. After finishing the reaction, 2 mL of HCl (3 M) was added dropwise while stirring, forming a white precipitate. Ether was added to dissolve the precipitate, then the aqueous layer was removed and an equal volume of aqueous NaCl solution was added. The aqueous layer was again removed and the ether was evaporated. The final product was identified by TLC and spectroscopy data; yield = 38%; mp = 137-140˚C [7].

1,3-Bis-[1,2,4]triazol-1-yl-propan-2-one (13)

To 1,3-dichloroacetone (1 mmol, 0.127 g) in toluene, 0.1 g of nano-SSA was added, and stirred for 0.5 h. After activation of the carbonyl group, 1,2,4-triazole (2 mmol) was added and refluxed for 24 h. After completion the reaction, the mixture was cooled to room temperature and filtered. The catalyst was separated from the reaction mixture by boiling ethanol. The crude solid product was purified by recrystallization in ethanol: water, 80:20; yield = 80%; mp =136-138˚C [9].

Preparation of Grignard reagent from 1-bromo-2,4-difluoro-benzene (15)

0.07 g of Mg powder was placed in a dry reaction tube and 0.6 mL of anhydrous diethyl ether was added. In a separate dry vial, 0.19 g of 1-bromo-2,4-difluoro-benzene and 0.82 mL of anhydrous diethyl ether were mixed and immediately added to the reaction tube.

Fluconazole 7 via method d

0.36 g of 1,3-bis-[1,2,4]triazol-1-yl-propan-2-one was dissolved in 1 mL of anhydrous diethyl ether and added to the Grignard reagent (15) under gentle reflux. After finishing the reaction, 2 mL of HCl (3 M) was added dropwise while stirring, forming a white precipitate. Ether was added to dissolve the precipitate, then the aqueous layer was removed and an equal volume of aqueous NaCl solution was added. The aqueous layer was again removed and the ether was evaporated. The final product was identified by TLC and spectroscopy data; yield = 35%; mp = 139-140˚C [7].

Spectroscopy data

1-Chloro-1-(2,4-difluoro-phenyl)-ethanone (3): White solid; yield= 98%, mp= 44-48℃; FT-IR: ῡ (KBr) = 2900, 2800, 1703, 1614, 1486, 1433, 1392, 1316, 1269, 1193, 1142, 969, 822, 739, 606, 550 cm^{-1}.

1-(2,4-difluorophenyl)-2-(1H-1,2,4-triazole-1-yl)1-ethanone (5): Pale yellow solid; yield = 80%; mp =103-107 ˚ C; FT-IR: ῡ (KBr) = 3100, 2900, 2800, 1692, 1612, 1545, 1488, 1416, 1354, 1298, 1267, 1243, 1144, 1101, 994, 833, 608 cm^{-1}; ^{1}H NMR (300 MHz, DMSO-*d6*): 8.80 (s, 1H), 8.26 (s, 1H), 8.01-8.08 (m,1H), 7.50-7.58 (m, 1H), 7.28-7.35 (dt, *J*=11.6, *J*=2.4, 1H), 5.86 (d, *J*=3, 2H) ppm; ^{13}C- NMR (300 MHz, DMSO-*d6*) δ = 189, 167, 150, 145, 133, 113, 106, 105, 58 ppm, MS: (m/z, %), 141 (100), 70.1 (10).

1-[2-(2,4-difluorophenyl)-2,3-epoxypropyl]-1H-1,2,4-triazole (6): White solid; yield=55%; mp =123-125 ℃ FT-IR: ῡ (KBr)= 3139, 1621, 1558, 1508, 1458, 1424, 1383, 1242, 1160, 1033, 965, 882, 820, 797, 774, 654 cm^{-1}; ^{1}H NMR (300) MHz, DMSO): 8.70 (s, 1H), 8.16 (s, 1H), 7.19-7.31 (m, 2H), 6.98-7.05 (m, 1H), 4.83 (d, *J*= 20, 1H), 4.63 (d, *J*= 15, 1H), 3.12 (d, *J*= 4.8, 1H), 2.97 (d, *J*= 4.8, 1H) ppm; ^{13}C-NMR (300 MHz, DMSO) δ = 164, 162, 159, 150, 144, 130, 120, 112, 104, 56, 54, 52 ppm; MS: (m/z, %), 237 (4), 168 (60), 139 (100).

Fluconazole (7): White solid; isolated yield = 45%; mp = 138-140 ˚ C;FT-IR: ῡ (KBr) = 3119, 3012, 1773, 1620, 1504, 1451, 1414, 1272, 1210, 1137, 1075, 964, 910, 846, 767, 732, 710, 673, 613, 576 cm^{-1}; ^{1}H NMR (300 MHz, DMSO-*d6*): 8.32 (s, 2H), 7.80 (s, 2H), 7.11-7.25 (m, 2H), 6.84-6.91 (dt, *J*=18, *J*=2.4, 1H), 6.36 (s, 1H), 4.73 (d, *J*=14.2, 2H), 4.55 (d, *J*=14.2, 2H) ppm.

Hydroxymethyltriazole(9): White solid; yield = 88%; mp =70-73 ℃; FT-IR: ῡ (KBr) = 3104, 3038, 2957, 2738, 2637, 2544, 2402, 1555, 1419, 1360, 1104, 988, 856, 766, 654 cm^{-1}, ^{1}H NMR (300 MHz, DMSO): 6.45 (s, 2H), 8.30 (s, 1H), 9.17 (s, 1H) ppm.

1-Chloromethyl-1H-[1,2,4]triazole (10): White solid; isolated yield = 75%; mp = 82-84 C; ^{1}H NMR (300 MHz, DMSO): 6.27 (s, 2H), 8.30 (s, 1H), 9.17(s, 1H) ppm, ^{13}C-NMR (300 MHz, DMSO) δ = 55.4, 145.9, 151.7 ppm; MS: (m/z, %), 117 (35), 82 (100).

1,3-Bis-[1,2,4]triazol-1-yl-propan-2-one (13): White crystal; yield = 80%; mp =136-138 ˚ C; ^{1}H NMR (400 MHz, DMSO): 4.48 (s, 4H), 8.05 (s, 1H), 8.14 (s, 1H) ppm.

REFERENCES

1. H. B. Borate, S. R. Maujan, S. P. Sawargave, M. A. Chandavarkar, S. R. Vaiude, V. A. Joshi, R.D. Wakharkar, R. Iyer, R. G. Kelkar, S. P. Chavan, S. S. Kunte, *Bioorganic & Medicinal Chemistry Letters*, **20**, 722 (2010).
2. S. Yu, X. Chai, H. Hu, Y. Yan, Z. Guan, Y. Zou, Q. Sun, Q. Wu, *European Journal of Medicinal Chemistry*, **45**, 4435 (2010).
3. C. Biot, N. François, L. Maciejewski, J. Brocard, D. Poulain, *Bioorganic & Medicinal Chemistry Letters*, **10**, 839 (2000).
4. a) N. G. Aher, V. S. Pore, N. N. Mishra, A. Kumar, P. K. Shukla, A. Sharma, M. K. Bhat, *Bioorganic & Medicinal Chemistry Letters*, **19**, 759 (2009); b) S. C. X. Che, W. Wang, Y. Cao, Y. Xu, H. Ji, *European Journal of Medicinal Chemistry*, **44**, 4218 (2009).
5. a) Y. Xu, C. Sheng, W. Wang, X. Che, Y. Cao, G. Dong, S. Wang, H. Ji, Z. Miao, J. Yao, W. Zhang, *Bioorganic & Medicinal Chemistry Letters*, **20**, 2942 (2010); b) S. C. W. Wang, X. Che, H. Ji, Y. Cao, Z. Miao, *Bioorganic & Medicinal Chemistry Letters*, **19**, 5965 (2009).
6. a) M. A. A. H. Emtiazi, B. B. F. Mirjalili, *Arab. J. Chem.*, **8**, 793 (2015); b) A. B. B. B. F. Mirjalili, R. Vafazadeh, L. Zamani, *Bull. Korean Chem. Soc.*, **30**, 2440 (2009).
7. M. Song, Preparation method of broad-spectrum antifungal drug fluconazole, *Patents CN102344419 A*, (2012).
8. a) K. D. C. Steven, C. Zimmerman, Adam A. Galan, *J. Org. Chem.*, **54**, 1256 (1989); b) D. W. B. Wilhelm, Azolsubstituierte oximino-cyan-acetamid-derivate, *Patents, DE19823222961*, (1983).
9. M. W. J. Song, New method for preparing fluconazole, *Patents CN101891693 A*, (2010).

Подобрен синтез на флуконазол с използване на наносилика-сярна киселина като „зелен” катализатор

Л. Замани, З. Резаеи, С. Кабнадидех *

Факултет по фармация и фармацевтични науки, Изследователски център, Ширазки университет по мезицински науки, Шираз, Ислямска република Иран

Постъпила на 19 септември, 2016 г.;коригирана на 29 януари, 2018 г.

(Резюме)

В съответствие с нашия интерес към получаването на нови противогъбични агенти, насочихме вниманието си към флуконазола поради широкия му противогъбичен спектър, ниската токсичност и отличните фармакокинетични свойства. Като част от нашата програма за разработване на нов метод за синтез на флуконазол са изследвани и оптимизирани условията на някои реакции, включително Гринярдови реакции. Най-добри резултати са получени с използване на наносилика-сярна киселина като мек „зелен” катализатор. Предимства на метода са високият добив и лесната изолация на продуктите във всеки етап.

Bulgarian Chemical Communications, Volume 50, Issue 4 (pp. 524 – 529) 2018

Degradation of partially absorbable surgical mesh: a chemical and mechanical study

D. Pashkouleva[1*], M. Kirilova-Doneva[1,2], I. Borovanska[1], A. A. Apostolov[3]

[1]*Institute of Mechanics, Bulgarian Academy of Sciences, Bulgaria*
[2]*Faculty of Pharmacy, Medical University-Sofia, Bulgaria*
[3] *Faculty of Chemistry and Pharmacy, Sofia University St. Kliment Ohridski, Sofia, Bulgaria*

Received, January 17, 2017; Accepted, May 10, 2018

Chemical and mechanical testing of partially absorbable surgical mesh after being kept *in vitro* under physiological conditions for four months was performed. Differential scanning calorimetry and X-ray diffraction were used to investigate the degradation behavior and the changes in structure and crystallinity of this surgical mesh. The degradation of the copolymer poliglecaprone 25, which is a constituent of the mesh, was confirmed. The mechanical characteristics of the mesh were compared in two different directions by performing uniaxial tensile tests. A progressive loss of the tensile strength and elongation was established. Failure tests showed that the mechanical properties of the mesh are anisotropic. The lower tensile strength is in transversal direction.

Keywords: Polypropylene, Poliglecaprone, Structure, Mechanical properties, Surgical meshes.

INTRODUCTION

Mesh hernioplasty is a common surgical procedure – approximately 20 million hernia repairs occur each year worldwide [1]. Currently, hernia meshes are made of non-absorbable polymers: polypropylene (PP), polyethylene terephthalate (PET), polytetrafluorethylene (PTFE), as well as from absorbable polymers such as polyglactin (PGA) or poliglecaprone 25 (PGC) [2].

Non-absorbable hernia meshes keep their mechanical stability, but induce high inflammatory reactions. Absorbable and partially absorbable hernia meshes are used in the clinical practice in cases of large defects or damaged tissues. Absorbable meshes are completely replaced by connective tissue, but are only recommended for a temporary closure of the abdominal wall or an infected wound and not for implantation because of their rapid degradation [3]. When it became clear that the tensile strength required is much less than originally presumed the material of meshes was reduced by adding partially absorbable components or by primary reduction of the material used. Today light-weight and partially resorbable meshes are recommended as a golden standard in surgical practice because of their advantage for abdominal wall function.

Most light-weight hernia meshes (16-35 g/m^2) with large pores (diameter of >1 mm) are a combination of PP fibers and PGA or PGC fibers [4]. One of the most popular partially absorbable hernia meshes is ULTRAPRO, distributed by Johnson-Johnson Inc. (Neuss, Germany) and consisting of approximately equal parts of absorbable PGC-25 and non-absorbable PP monofilament fiber.

The mechanical properties and shrinkage of ULTRAPRO are investigated and compared with other meshes [5-7]. To present we could not find information about long-term changes of chemical composition of ULTRAPRO. Chemical degradation that leads to a reduction of the physical and mechanical properties is the primary obstacle to long-term mesh stability. One of the most popular polymers used for hernia meshes is polypropylene (PP). PP is a linear aliphatic hydrocarbon, which has methyl groups attached to chain backbone. It is nonpolar, highly hydrophobic and resistant to many chemical solvents, bases and acids [8]. Chain entanglement and intermolecular secondary bond forces (van der Waals-London forces) from induced dipole hydrogen bonds between chains define the mechanical properties of PP. This polymer is considered to be an inert material that provides stable service life *in vivo* as a mesh material [8]. Actually, the chronic inflammatory cells secrete highly reactive radicals as superoxide anions, as well as strongly oxidative chemicals, for example, hypochlorous acid and hydrogen peroxide, which are potentially detrimental to the PP mesh [9]. The created free radicals along the broken bonds are possible to bind to oxygen to form carbonyl groups [10]. Oxidization of polypropylene results in chain cracking, flaking, strands fissuring and surface crazing [9]. Surface oxidative degradation of PP gives as a result bulk property changes such as loss of mass, lowering the glass transition and melt temperatures and diminished molecular mobility

* To whom all correspondence should be sent:
E-mail: dessip@imbm.bas.bg

[11]. Both the polyester and ePTFE (i.e. expanded PTFE) have been shown to be much more inert to oxidation, which affects PP mesh at a greater severity [9].

In order to present all aspects of the degradation process of absorbable meshes we decided to characterize a pristine mesh ULTRAPRO before and after exposure to conditions similar to human physiology using Differential Scanning Calorimetry and X-ray Diffraction. The changes in the structure and crystallinity of this brand will be described. The information about long-term chemical, physical and mechanical changes of ULTRAPRO will be useful to determine the brand of explanted meshes.

MATERIALS AND METHODS

Materials

Partially absorbable light-weight mesh with brand name ULTRAPRO (Ethicon, a Johnson&Johnson Company, Germany) for surgical applications was used in this study. This monofilament mesh with large pores (3-4 mm) is made of two-component PROLENE™ (polypropylene – PP) and absorbable MONOCRYL™ (poliglecaprone 25 – PGC-25). PGC-25 is a copolymer of glycolide and ε-caprolactone [11], i.e., poly(glycolide-*co*-caprolatone). ULTRAPRO mesh has a different coloration (white and blue stripes) (Fig. 1). This design facilitates the orientation for positioning of the mesh. The pristine mesh was 150×150 mm^2, with thickness of 0.5 mm, fiber diameter of 90 μm and 55 g/m^2 average weight.

Fig. 1. Photo of ULTRAPRO mesh

Ageing of the mesh

In order to age the samples they were placed in the chamber of the digital thermostatic bath DIGIBATH-2 (Raypa, Spain) full of 0.9% saline solution. The chamber conditions were strictly controlled – 120 days at 37 ± 1°C temperature in saline solution exposure.

Various methods for chemical, physical and mechanical characterization of the mesh properties were used.

Differential scanning calorimetry (DSC)

Differential scanning calorimetry (DSC) was used as a test for identification of the changes in the structure of the surgical polymer mesh. DSC tests were performed on the Q200 DSC apparatus (TA, USA). The samples were investigated in a heating/cooling/second heating mode from -80 to 250ºC with a heating/cooling rate of 10ºC/min in nitrogen atmosphere. The crystallization (T_c) and melting temperature (T_m) were determined from the cooling and heating curves, respectively. In order to check if there is detectable glass transition in the two samples, separate experiments with a high heating rate of 50ºC/min from -80 to 250ºC were performed. In all cases the sample weight was between 1.5 and 3 mg.

X-ray diffraction (XRD)

This is another measurement tool, which assesses the physical structure of the materials. In our case the goal was to show which of the polymers present in the ULTARO mesh before and after the ageing was in crystalline form. A Siemens D500 diffractometer (Germany), with secondary monochromator and Cu-Kα radiation was used to obtain the diffractograms over the 2θ range of 10-40º with a step of 0.05º and count time of 5 s.

Mechanical characterization

In addition to the physical and chemical characterization, the mechanical properties of the mesh were determined. Uniaxial tensile test was conducted using a universal testing machine (Fu1000e, Germany) at room temperature and with the traverse velocity of 0.13 mm/s. All tests were performed in two perpendicular directions – longitudinal (along the loop columns) and transverse (across the loop columns) in order to determine the influence of anisotropy on the mechanical properties. Uniaxial testing in both directions may be not the perfect solution to describe the mechanical properties but is an established method. The orientation of ULTRAPRO mesh is easy to control, because the blue strips of the material are along the loop columns. For each direction, five specimens of 10 × 70 mm^2 were cut. The specimen's thickness was determined with a caliper. The force and the displacement were recorded. The relative breaking strain in % was computed as $\Delta L/L_o \times 100$, where L_o is the initial length before any load is applied and ΔL is the elongation of the sample. The tensile

strength was obtained using the expression *Force*/*Width*, where *Force* (N) is the load applied during the test and *Width* is the specimen width (mm). The stress cannot be computed, because the value of the thickness of the meshes is not measurable due to its discontinuous cross sectional area, where filaments and empty areas exist and are interspersed. The results are reported as mean ± standard error of the mean.

RESULTS AND DISCUSSION

Thermal characterization

The DSC curves of the pristine samples (white and blue stripes) and the sample soaked in solution are presented in Fig. 2 for the first heating (a), cooling (b) and second heating (c), respectively. The curves of the pristine white and blue samples are similar**.** Hence, these two parts of ULTRAPRO mesh are identical and the colouring does not influence its chemical characteristics. For this reason we will designate both as a pristine sample in contrary to the aged one.

There is a very weak low-temperature melting peak at ca. 55ºC, a very strong peak at ca. 169ºC of both pristine and aged sample in the thermograms of the first heating. An additional broad peak at around 183ºC is present in the thermogram of the first heating of the pristine sample (Fig. 2a).

The thermograms of cooling (Fig. 2b) are characterized by a single maximum at 114.3ºC for the pristine sample and a doublet at 114.3/129.0ºC after the stay in the physiologic solution. It is interesting to note the coincidence of the single peak at 129.0ºC for the aged sample with the high-temperature peak of the doublet for the aged one.

There is a peak of crystallization at 55.0ºC, a very strong peak of melting at 159.7ºC and a moderate peak of melting around 183ºC for the pristine sample in the thermogram of the second heating (Fig. 2c). A weak peak of melting at 55.0ºC and a strong one at 163.4ºC are also indicated in the thermogram of the aged sample (Fig. 2c).

A clear glass transition is indicated in the thermogram of fast heating of the pristine sample at 8.0ºC (Fig. 3). The registered melting T_m, glass transition T_g, and crystallization T_c temperatures together with the enthalpy of melting ΔH_m and DSC degree of crystallinity w_c are summarized in Table 1.

Generally, the changes in the shape of the first melting endotherms give some qualitative information about the content of different phases, as well as on the perfection of the crystal structure which depends on the prehistory of the material. The existence of multiple peaks in the DSC thermograms can appear in (a) a sample that consists of more than one plastic; (b) a sample that consists of only one plastic but with different molecular weights; (c) a sample that consists of crystals of different size and/or type; (d) a degraded sample [12].

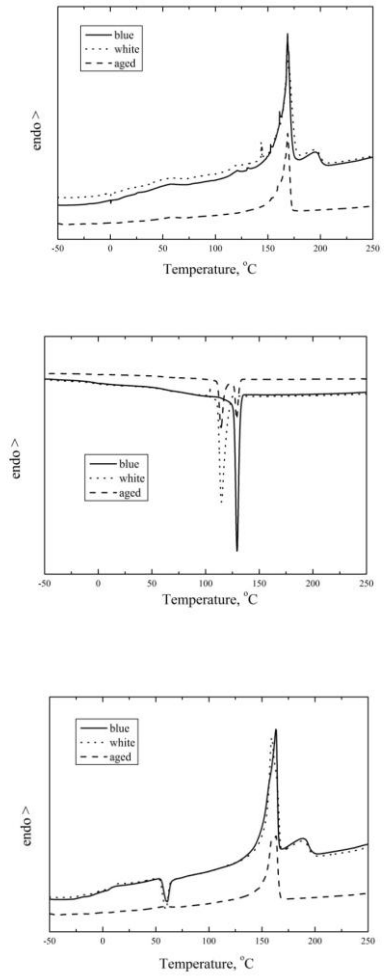

Fig. 2. DSC curves of pristine and aged samples of (a) first heating, (b) cooling and (c) second heating. (The curves are shifted vertically for the sake of clarity.)

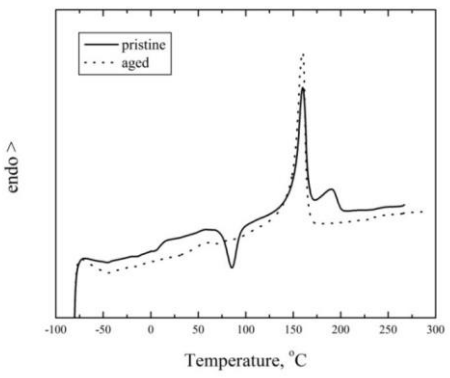

Fig. 3. DSC curves of heating of samples with a high heating rate of 50 ºC/min. (The curves are shifted vertically for the sake of clarity.)

Table 1. DSC characteristics of the pristine and aged sample.

Sample	First heating, 10°C/min			Cooling, 10°C/min	Second heating, 10°C/min			Heating, 50°C/min	
	T_m (°C)	ΔH_m (J/g)	w_c (%)	T_c (°C)	T_m, (°C)	ΔH_m (J/g)	w_c (%)	T_c (°C)	T_g (°C)
Pristine	55, 169.8 and 183	94.4	45.2	114.3	159.7, 183	82.5	41.2	55.0	8.0
Aged	168.8	89.5	42.8	114.3 /129.0	163.4	85.9	43.0	-	-

The melting at 169-170°C is obviously due to melting of PP crystals (Fig. 2). According to Wunderlicht [13] the melting temperature of 100% isotactic PP is 174 °C and that of 60% isotactic PP is 171-172°C. This is also supported by Keith and Padden [14] who state that 100% isotactic PP melts at 171°C, 60% at 165°C and 40% at 162°C. Other authors claim that perfectly isotactic PP has a melting point of 171°C, whereas commercial isotactic PP has a melting point that ranges from 160°C to 166°C, depending on atactic material and crystallinity. The observed melting temperature (Fig. 2a) of around 169-170°C in the first heating of both pristine and aged samples, respectively, matches that of homo-PP containing isotactic fraction of about 60-80%. The lower T_m of 163.4°C in the second heating may be attributed to worse crystallization conditions during the fast cooling, i.e., the created crystallites are imperfect and the crystallization has not taken fully place in both samples. This is indirectly proved by the additional crystallization at 55.0°C during the second heating of the pristine sample and also witnessed by the decrease in enthalpy of melting of the pristine sample from the first to the second heating by about 14 % (Table 1).

The observed peak at about 183°C for the pristine sample is probably due to melting of short polyglycolide blocks in the copolymer since polyglycolide melts at 225-230°C and the monomer glycolide melts at about 83°C [15], hence the glycolide oligomers melt in a very broad temperature interval depending on the length of the blocks. By the same token the observed melting peak at about 55°C is due to melting of short ε-caprolactone blocks in the copolymer since polycaprolactone melts at 60°C and caprolactone melts at -1,5°C. If we assume a mole ratio of the two components of poly(glycolide-*co*-caprolactone) of 1:1 (see e.g. [16]), then formation of both short glycolide and caprolactone blocks is possible. In fact we do not know the mole ratio of the PGC since it is a proprietary information and lacks in the producers‘s datasheets. Nary *et al*. [11] concluded that the best response from PGC 25, as well as its monofilament characteristic is related to its chemical composition, 25% ε-caprolactone and 75% glycolide. As can be easily calculated on the basis of the monomer molecular weights that this ratio corresponds to approximately 1:6 monomers capralactone: glycolide, i.e. oligoglycolide blocks will be formed thus explaining the melting around 183°C. Based on the above ratio, the caprolactone will form very short blocks, hence the corresponding very weak peak (Fig. 2a,c).

Both peaks around 55 and 190°C are not present in the thermograms of the aged sample (Fig. 2a,c) thus confirming the degradation of the copolymer during the ageing of the composite ULTRAPRO mesh.

The crystallization temperature of 129.0°C, registered at cooling (Fig. 2b) clearly indicates that the thermal history of the pristine sample has been cleared during the first heating. The presence of the low temperature crystallization peak at 114.3°C together with a peak at 129.0°C on the thermogram of the aged sample is probably due to inhomogeneous crystallization where the nuclei are the low molecular products formed after the degradation of the copolymer during the ageing.

The observed glass transition temperature of 8.0°C on the thermogram of the pristine sample (Fig. 3) may be attributed to the copolymer PGC since the glass transition temperature of its constituents is 35-40°C for polyglicolide and -60°C for the polycaprolactone. It is worth noticing that Lee *et al.* [16] reported T_g of PGC with glycolide/caprolactone feed ratio of 5.1/4.9 as -19.3°C, i.e. the slightly lower temperature may be explained by a slightly different feed ratio. The lack of T_g in the thermogram of the aged sample (Fig. 3) again indicates that degradation of the copolymer has taken place after the ageing. According to the literature [17], T_g of PP is -10°C. Nevertheless, it cannot be seen in the thermograms due to the relatively small quantity of amorphous PP; this is based on the fact that the composite ULTRAPRO mesh consists of equal parts of semicrystalline PP and PGC [15].

X-ray characterization

In Fig. 4 the normalized diffractograms of the two samples – the pristine and the aged one are shown. The two diffractograms match those of isotactic alpha-form of PP [18] and differ only slightly due to some change in the orientation in the aged sample, expressed by the decrease of the 111+131+041 complex maximum situated at 22.0 $^{o}2\theta$ as well as to the 200+220 complex maximum situated at 28.5 $^{o}2\theta$. An attempt to estimate the half-width of the three main maxima was made, but these half-widths of the corresponding maxima of the two samples turn out to be equal within the experimental error. Thus, no conclusions about an eventual process of worsening of the perfection of the PP crystallites due to the ageing can be made based on the diffraction line half-width. Since the well distinguished strong maximum of the β-phase at 21.31$^{o}2\theta$ is not seen, the latter is not present [18]. The presence of isotactic α-form of PP only is in agreement with the reported melting temperatures, see above. Since neither peaks of the copolymer PGC nor of its constituents (that are both crystalline as polymers) are seen, the copolymer PGC is random or blocky with short blocks. This is in agreement with the DSC data.

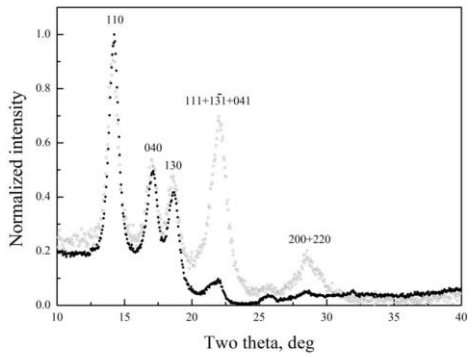

Fig 4. Normalized diffractograms of the two samples: ○-pristine sample and ●-aged sample. The Miller indices of the main maxima are shown.

Mechanical characterization

The characteristics of the mechanical properties are shown in Fig. 5. The results of the tensile test of the mesh are presented in a "longitudinal" (Fig. 5a) and a "transverse" (Fig. 5b) direction, as the anisotropic behavior was in agreement with the reported ones [6, 7].

The maximum equivalent stress for the pristine mesh in longitudinal and transverse direction is 37.7±0.9 N/cm and 5.5±0.7 N/cm, respectively. The equivalent stress is approximately 7 times higher in longitudinal than in transverse direction. The elongation at break is 151.8±2.5% in longitudinal and 191.2±23.8% in transverse direction. The obtained anisotropy of the ULTRAPRO mesh is also reported in [6, 7]. Unfortunately, the researchers use many different non-comparable settings for defining the mechanical characteristics of hernia meshes and the degree of anisotropy cannot be compared.

The degradation of PGC leads to a change in the mechanical properties of the mesh (see Fig. 5). The maximum equivalent stress in both directions slightly decreases (from 37.7±0.9 N/cm to 35.9±1.8 N/cm in longitudinal direction and from 5.5±0.7 N/cm to 2.0±0.3 N/cm transverse direction). The elongation at break also decreases (from 151.8±2.5% to 127.8±3.6% in longitudinal and from 191.2±23.8% to 131.5±17.5% in transverse direction).

CONCLUSIONS

It was shown that the poly(glycolide-lactone) copolymer in the ULTRAPRO mesh is a block copolymer, consisting of very short caprolactone blocks and much longer glycolide blocks. Degradation of the above copolymer during the ageing of the composite ULTRAPRO mesh was proven by DSC. Presence of only iso-PP in crystalline (α-) form in the mesh was proven by XRD both before and after the ageing. Degradation of PGC in the ULTRAPRO mesh was indicated by a change in the mechanical properties of the mesh after the ageing. Strong anisotropy of the mechanical properties in longitudinal and transverse direction was observed.

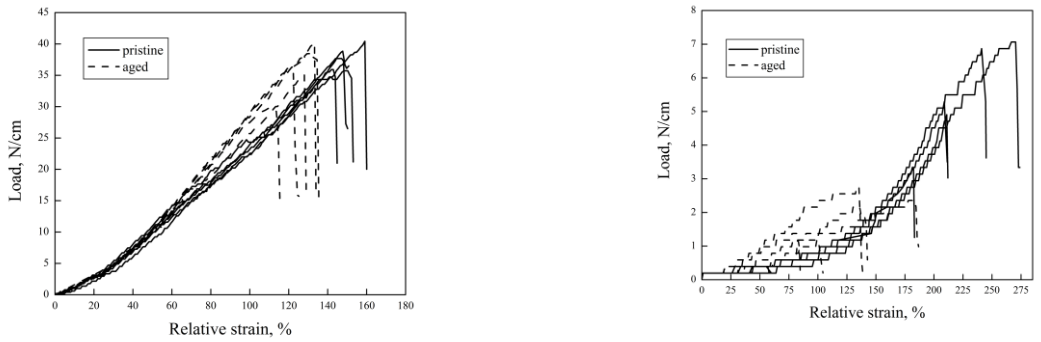

a) b)

Fig. 5. Strength-strain diagrams for ULTRAPRO mesh samples before and after saline solution exposure in (a) longitudinal and (b) transverse direction.

REFERENCES

1. A. Kingsnorth, *BMJ*, **328**, 59 (2004).
2. Y. Bilsel, I. Abci, *Intern. J. of Surgery*, **10**, 317 (2012).
3. B. Klosterhalfen, K. Junge, U. Klinge, *Exper. Rev. Med. Devices*, **2**, 103 (2005).
4. H. Kulacoglu, *Hippokratia*, **15**, 223 (2011).
5. A. Silvestre, G. Mathia, D. Fagundes, L. Medeiros, M. Rosa, *Hernia*, **15**, 629 (2011).
6. E. R. Saberski, S. B. Orenstein, Y. W. Novitsky, *Hernia*, **15**, 47 (2011).
7. P. Pott, M. Schwarz, R. Gundling, K. Nowak, P. Hohenberger, E. Roessner, *PLoS One*, **7**, e46978 (2012).
8. A. Wood, M. Cozad, D. Grant, A. Ostdiek, S. Bachman, S. Grant, *J. Mater. Sci.: Mater. Med.*, **24**, 1113 (2013).
9. C. Burns-Heffner, PhD Thesis, Clemson University, 2014.
10. F. Agresta, G. A. Baldazzi, L. F. Ciardo, G. Trentin, S. Giuseppe, F. Ferrante, N. Bedin, *Surg. Laparosc. Endosc. Percutan. Tech*., **17**, 91 (2007).
11. H. Nary Filho, L. E. M. Padovan, P. D. Ribeiro Júnior, T. Okamoto, *BCI*, **4**, 35 (1997).
12. I. Borovanska, T. Dobreva, R. Benavente, S. Djoumaliisky, G. Kotzev, *J. Elastom. Plast.*, **44**, 479 (2012).
13. B. Wunderlicht, Macromolecular Physics (vol. 3: Crystal Melting), Academic Press, New York, 1980.
14. H. Keith, F. Padden Jr., *J. Appl. Phys.*, **35**, 1286 (1964).
15. http://www.chemicalland21.com/specialtychem/nd/GLYCOLIDE.htm
16. S. H. Lee, B. S. Kim, S. H. Kim, S. W. Choi, S. I. Jeong, I. K. Kwon, S. W. Kang, J. Nikolovski, D. J. Mooney, Y. K. Han, Y. H. Kim, *J. Biomed. Mater. Res. A*, **66**, 29 (2003).
17. http://www.polymerprocessing.com/polymers/PP.html
18. S. C. Clark, Physical properties of Polymers Handbook, J. E. Mark (ed.), AIP Press, New York, 1996.

РАЗГРАЖДАНЕ НА ЧАСТИЧНО РЕЗОРБИРУЕМА ХИРУРГИЧНА МРЕЖА: ХИМИЧНО И МЕХАНИЧНО ИЗСЛЕДВАНЕ

Д. Пашкулева[1*], М. Кирилова-Донева[2], И. Борованска[1], А. А. Апостолов[3]

[1] Институт по механика, Българска академия на науките, София, България
[2] Факултет по фармация, Медицински университет-София, България
[3] Факултет по химия и фармация, Софийски университет „Св. Климент Охридски", София, България

Постъпила на 17 януари, 2017; приета на 10 май, 2018

(Резюме)

Химично и механично тестване на частично резорбируема хирургична мрежа е проведено след чегиримесечно престояване *in vitro* при физиологични условия. Диференциална сканираща калориметрия и рентгенова дифракция са използвани за изследване на разлагането и промените в структурата и кристалността на хирургичната мрежа. Потвърдено е разлагането на съполимера полиглекапрон 25, който е съставна част на мрежата. Механичните характеристики на мрежата са сравнени в две различни направления чрез провеждане на едноосови тестове на опън. Установена е прогресивна загуба на якост на опън и удължаване. Механичните изпитвания показват, че механичните свойства на мрежата са анизотропни. По-малка якост на опън е установена в напречно направление.

Bulgarian Chemical Communications, Volume 50, Issue 4 (pp. 530 – 537) 2018

Isolation and characterization of plant cell wall material from rose hip fruits

M. H. Ognyanov[1*], M. M. Hodzhova[1], N. T. Petkova[2], P. N. Denev[1], Y. N. Georgiev[1], M. G. Kratchanova[1]

[1]*Laboratory of Biologically Active Substances, Institute of Organic Chemistry with Centre of Phytochemistry, Bulgarian Academy of Sciences, 139, Ruski blvd., 4000 Plovdiv, Bulgaria*
[2]*Department of Organic Chemistry and Inorganic Chemistry, University of Food Technologies, 26, Maritza blvd., 4002 Plovdiv, Bulgaria*

Received, June 6, 2017; Revised, February 21, 2018

In the present study, plant cell wall material from rose hip fruits was isolated as alcohol-insoluble solids. Chemical composition of the cell wall material and initial fruits (edible part) was investigated and compared. The amounts of polyphenols (flavonoids), pigments, lipids, vitamin C were removed in a different extent during hot alcohol/acetone treatment. In contrary, proteins, polysaccharides and some polyphenols (condensed tannins) were co-precipitated due to the dehydration effect of alcohol, which was the main factor that restricted the extractability of 'contaminants'. In addition, carbohydrates (mainly pectins and cellulose) were found out to be the main constituents of the 'purified' rose hip cell wall preparation.

Keywords: Rose hip, Plant cell walls, Alcohol-insoluble solids, Characterization, Polysaccharides.

INTRODUCTION

Rose hip (RH) is widely distributed in particular regions of Europe (Balkan Peninsula), Asia (the Middle East), South and North America [1]. Fruits are mainly used for commercial production of jams, jellies, marmalades, tea, soups, food additives and functional ingredients. In traditional folk medicine RH is applied for curing infections, osteoarthritis and for the treatment of the common cold [2].

The RH fruits also attract attention as a rich source of low-molecular weight nutraceutical components, such as vitamins (C, B, E), carotenoids, phenols, essential oils, fatty acids and minerals, which have already been recognized as bioactive [3-8]. Although the impacts of low molecular weight biologically active substances are extensively studied, it seems that they are not responsible for all health beneficial effects.

Some of the studies dealing with RH fruits refer to the occurrence of polysaccharides [3, 5, 6]. However, the obtained polysaccharides were not fully characterized and therefore further investigation of the polymer composition and structure of the RH fruit cell walls is required. In addition, thorough knowledge of the composition of RH cell walls is crucial and essential for better understanding and assessing the quality of the fruits and their suitability for technological processing.

An extensive study of the RH polysaccharide fractions is related to the preparation of plant cell walls 'relatively' pure from intracellular components. It should be noted that the methods of cell wall preparation depend on the amounts of intracellular compounds in the initial plant material (starch, protein, polyphenols, etc.), the stages of ripeness, and used anatomical parts of the plant. Alcohol-insoluble solids (AIS) have usually been used as a source of cell wall material (CWM) by various researchers [9-12]. Generally, AIS are prepared by immersing the tissue in hot aqueous ethanol solution, followed by blending the mixture to disrupt the material and further solubilize low-molecular weight compounds. After filtration the residue is washed with absolute ethanol and acetone or petroleum ether. The advantage of this method for cell wall preparation is the fast inactivation of the most endogenous enzymes, which could alter polymers structure. However, dehydration with organic solvents is known to influence the solubility of the polysaccharides and additionally facilitate the formation of co-precipitate (artifacts) between cell wall components [9, 12].

In the current study a method for isolation of plant cell walls as AIS from RH fruits is described and the results of chemical composition analysis of the cell wall material and initial fruits are presented and compared.

EXPERIMENTAL

Plant material

The RH fruit material (with orange-red colour of the fruits) was obtained from a local producer (Smolyan, the Rhodope Mountains, Bulgaria). The material was enclosed in polyethylene bags and stored frozen (−18 ºC) before further treatment.

* To whom all correspondence should be sent:
E-mail: mogn@orgchm.bas.bg; mogn@abv.bg

Preparation of cell wall material

Cell wall material was obtained using the hot alcohol insoluble solids method. Extractions were carried out in a glass flask (4 L) placed in an incubator as follows: 200.0 g of chopped and freeze-dried rose hip fruits stripped of seeds was transferred into 2.0 L of ethanol/water 80:20 (v/v) solution (solid:liquid ratio = 1:10 w/v) pre-heated at 70 ºC. The obtained mixture was kept at 70ºC under vigorous shaking (every 10 min) for 1 h and then heating was discontinued. The resulting material was allowed to cool down and was left overnight at room temperature. Then the mixture was filtered through a nylon cloth to remove the solid particles. The same procedure was repeated as incubation was carried out for 1 h. After filtration, the insoluble residue was washed with ethanol/water 80:20 (v/v) (70ºC) solution (solid:liquid ratio = 1:5 w/v) for 1 h. Finally, the solid was washed with acetone (solid:liquid ratio = 1:4, w/v) at 30 ºC for 1 h. The solid material was vacuum-filtrated and additionally squeezed from excess of solvent through a cloth.

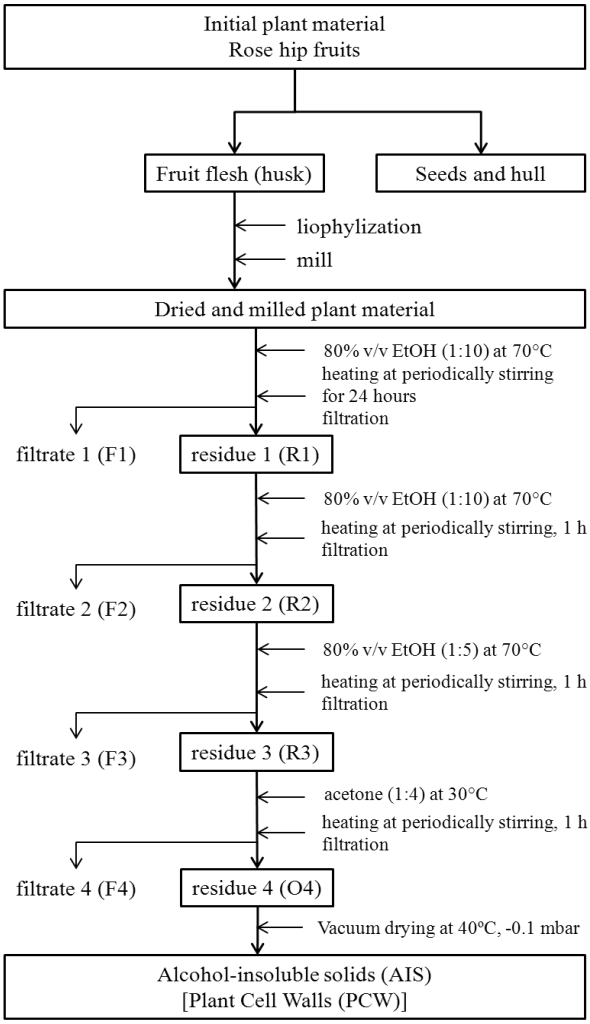

Fig. 1. Scheme of cell wall material preparation from rose hip fruits.

The obtained alcohol-insoluble residue was further vacuum-dried (40ºC, -0.1 mbar) to a constant weight. The general scheme of the cell wall material preparation from RH fruits followed in this investigation is presented in Fig. 1.

Moisture and ash content

For the moisture content, ground samples (~1.5 g) were dried in an automated moisture analyzer (KERN®DLB, Germany) at 105ºC until a constant weight. Results were used for dry solid calculation. Ash content was determined as the pulverized samples (0.5-2 g) were placed in a crucible, ignited in a muffle furnace at 550ºC to a constant weight.

Total carotenoids content

The total carotenoids were determined using acetone as a solvent according to Lichtenthaler and Wellburn [13]. For extraction of lycopene and *β*-carotene the method with acetone/petroleum ether solvents was used as previously described by Georgé *et al*. [14]. The concentrations of lycopene and *β*-carotene were calculated using the equations of Lime *et al*. [15].

Vitamin C content

The amount of ascorbic acid in the RH fruits was determined according to the 2,6-dichloroindophenol titrimetric method of AOAC [16].

Total carbohydrate content and monosaccharide composition analysis

Before analysis the samples were submitted to a prehydrolysis treatment with 72% (w/w) H_2SO_4 at 30 °C for 1 h, followed by a hydrolysis step with 1 M H_2SO_4 at 100 °C for 3 h. The total carbohydrates content in the hydrolyzates was assayed by the phenol-sulfuric acid method according to DuBois *et al*. [17] using glucose (10-80 μg/ml) as a reference. Absorbance was measured at 490 nm. The standard curve was constructed with glucose and galacturonic acid mixture (1.5:1.0) and was used for result calculation (AIS material). Individual neutral sugar composition of the obtained plant cell walls was determined [18] by gas chromatography using inositol as an internal standard. The constituent sugars released were analysed as their volatile alditol acetates [19]. The uronic acid content was determined by an automated colorimetric *m*-hydroxyl-diphenyl assay [20] using an auto-analyser Skalar San^{++} system (Skalar Analytical BV, Breda, The Netherlands). Galacturonic acid (12.5–100.0 μg/ml) was used for the calibration curve. The methylpentoses content was evaluated by the thioglycolic acid-sulfuric acid

method with L-Rha and L-Fuc (1:1) as standards [21].

Cellulose content

The cellulose determination was performed according to the Kürschner-Hoffer gravimetric method with modification [22]. Briefly, a sample (0.5 g) was boiled (30 min) with 25 ml of acetic-nitric reagent (acetic acid:H_2O:HNO_3 = 8:2:1 v/v) in a round-bottom flask. After cooling the insoluble residue was filtrated through a sintered glass filter (G3) under vacuum, washed successively with hot acetic-nitric reagent, then with deionized water to neutral pH, ethanol (96% v/v) and finally with an excess of petroleum ether. The obtained residue was dried in a laboratory ventilated oven at 50ºC to a constant weight.

Protein content

The crude protein content of the samples was estimated by the micro-Kjeldahl method [23]. The nitrogen as ammonia content in the digested samples was determined by the acetylacetone-formaldehyde colorimetric method using ammonium sulfate as a standard [24]. For calculation of crude protein, a value of the nitrogen-to-protein conversion factor of 6.25 was used.

Total lipids content

The powdered dried RH fruits (without seeds) (14.0-15.0 g) were packed in a cellulose thimble. An exhaustive extraction with petroleum ether (with boiling point: 40–60°C) (500 ml) was carried out for 8 h in a Soxhlet extractor. The obtained crude extract was dried under vacuum and its weight was used for calculation of the lipids content on the basis of dry weight of the samples.

Lignin determination

The lignin content of the prepared AIS was evaluated by two different analytical methods: the Klason lignin gravimetric method (KL) [25] and the spectroscopic acetyl bromide lignin (ABL) method [26].

Total phenols content

Freeze-dried fruits (edible part) or AIS (0.5 g) were mixed with 40 ml of 80% acetone in 0.2% formic acid and extracted on a magnetic stirrer at room temperature for 1 h. Then the samples were centrifuged (6000 g, 20 min) and supernatants were collected. Total phenolics were determined according to the method of Singleton and Rossi with Folin–Ciocalteu's reagent [27]. Gallic acid (10-200 μg/mL) was employed as a calibration standard and the results were expressed as mg gallic acid equivalents (GAE) per g dry weight.

Flavonoids and condensed tannins content

Freeze-dried fruits (edible part) or AIS (1.0 g powder) were mixed with 40 ml of 80% ethanol in 0.5% formic acid. Extraction was conducted on a magnetic stirrer at room temperature for 1 h. The samples were centrifuged (6000 g) for 20 min and clear supernatants were used for total flavonoids and tannins content analysis. The total flavonoid content was determined according to the method of Chang *et al*. [28] with $AlCl_3$ reagent. The results were presented as μg equivalents quercetin (QE) per g dry weight according to the calibration curve constructed with quercetin dihydrate (10-200 mg/L).

The methylcellulose precipitation assay was performed according to Sarneckis *et al*. [29] for determination of condensed tannin concentration. (-) epicatechin standard (≥ 90% HPLC, Fluka) aqueous solutions (10-200 mg/L) were used for calibration curve construction.

Antioxidant activity assays

Oxygen Radical Absorbance Capacity (ORAC) assay. ORAC was measured according to the method of Ou *et al*. [30] with some modifications described by Denev *et al*. [31]. ORAC analyses were carried out on a FLUOstar OPTIMA plate reader (BMG Labtech, Germany). A fluorescence filter with excitation wavelength of 485 nm and emission wavelength of 520 nm was used.

DPPH radical-scavenging ability. The extraction process was carried out with 100 % acetone in a ultrasonic bath [32]. DPPH assay was performed as described by Ivanov *et al*. [33]. The results were expressed as micromoles of Trolox equivalents (TE) per gram (μmol of TE/g) dry weight.

RESULTS AND DISCUSSION

Characterization of initial RH fruits

The current study started with removing of the edible part (fruit flesh) from seeds and hull. Mean fruit weight was 1.93 g that was based on randomly weighed 1 kg of fruits. The fruit flesh was the main usable part, as its proportion was 61.5%. The seeds and hull represented 38.5% of the fresh fruits weight. Average number of seeds in one fruit was 17 (from 100 fruits). Further, these parts were not subject of interest and analysis. The results for yields and chemical composition of initial RH fruits are summarized in Table 1. The dry matter content of the investigated fruit flesh was 47% which was

comparable with the previous study by Bonev *et al*. [34] who reported 43.4%. Rosu *et al*. [35] found that dry matter varied among rose species and they reported that *Rosa canina* L. Str. species had a slightly higher value (49.9%) than in our study.

Table 1. Yield, chemical composition and antioxidant capacities of initial RH fruits and isolated plant cell wall material (AIS)[a].

	Initial RH fruits	Plant cell wall material (AIS)
Yield (% w/w)	-	57
Dry matter (% w/w)	47	97
Ash (% w/w)	5.0	2.0
Crude protein (% w/w)	3.5	4.6
Total lipids (% w/w)	0.77	0.37
Total carbohydrates (% w/w)	34	52
Uronic acids (% w/w)	9.6	16.2
Cellulose (% w/w)	7.0	11.0
Methylpentoses (% w/w)	1.8	2.3
Lignin content (% w/w)		
Klason	-	8.0
ABSL	-	5.1
Vitamin C content (mg/100 g)	610	35
Total phenolics (mg GAE/g)	91	54
Total flavonoids (μg QE/g)	262	52
Total tannins (μg CE/g)	178	136
Total carotenoids (μg/g)	119.0	3.0
Lycopene	63.6	1.3
β-Carotene	54.0	1.5
ORAC (μmol TE/g)	2094.3	1372.9
DPPH (μmol TE/g)	2493.6	1870.8

[a] Values are the average of two replicates.

Initial RH fruit flesh was characterized with 5.0% ash content that was higher than the value previously found by Bonev *et al*. [34] (2.22%), but lower compared with the investigation of Demir and Özcan [5] for two RH samples from Turkey (7.35% and 6.48%).

The crude protein content of fruit flesh was evaluated to be 3.5% and it was in close agreement with the data of Michev *et al*. [36], but lower compared to these of Demir and Özcan [5] – 6.7 and 8.4%. According to the literature, the protein content of RH ranged between 2.3 and 4.58% dry matter [37] depending on maturity stage, agro-climate condition, and even correlated with altitude [35].

Our result for the lipid content (0.77%) was slightly lower than those reported by other authors who have shown for *R. canina* – 1.78% total fat content and 1.6 and 1.2% crude oil of two RH species [5]. In comparison with data in the literature, our result was in very good agreement with reports for fully ripened *R. canina* fruits (0.70-0.80%) [36].

It was shown that carbohydrates were the main constituents of the RH fruits based on dry matter (34%). Uronic acids and cellulose were accounted for nearly 10% and 7.0% of the dry matter, respectively. In addition, methylpentoses (Rha and Fuc) content was 1.8% and combined with those of uronic acid and cellulose occupied nearly 18.4%. Therefore, the soluble sugars should be accounted for the rest. The other authors who studied different RH species showed that cellulose content varied between 2.1% and 9.7% [34].

Vitamin C was recognized as one of the most important components of RH fruits based on our results. Its concentration was estimated to be 610 mg/100 g dry weight. This value was comparable with those found by Ercisli [6] who reported 727-943 mg/100 g ascorbic acid. Interestingly, higher levels of vitamin C content (1358 mg/100 g) were determined by Dimitrov and Bonev [4] for different RH species (31 sp.). In another study, Demir and Özcan [5] found considerably higher levels of vitamin C (2365 and 2712 mg/100 g).

It is well known that RH has been proposed as a source of health-promoting natural pigments, such as carotenoids [2, 3, 38]. In our study we found 119 μg/g total carotenoids content which value was comparable with the lower amounts of carotenoids (101.24 and 190.29 μg/g) detected in an earlier harvesting period [38]. Further, the concentrations of *β*-carotene (54.0 μg/g) and lycopene (63.6 μg/g) were found to constitute nearly 98% of the carotenoid content, which was similar to previous investigations [38]. With regard to previous studies [3], the total carotenoid content determined in *Rosa* species showed a wide range from 78 to 568 μg/g, which is in line with our results.

Initial RH had a high proportion of total phenolic content. The investigated species contained 91 mg GAE/g which was in close agreement with the reports for the same species [6] (96 mg GAE/g), but higher than reported by Denev

et al. [39] (56 mg/g). Our result was also higher than those determined by Demir *et al*. [40] who found variation in different *Rosa* species – between 31.08-52.94 mg/g. Among widely distributed polyphenols are the flavonoids, which consist of flavones, flavanols, anthocyanins and proanthocyanidins. Because of this it was of interest to evaluate total flavonoids and condensed tannins content. The investigated species contained 262 μg QE/g total flavonoids. This amount was lower than that obtained in recent studies [41], but it was of the same order (0.63 mg QE/g). The authors have also demonstrated a quantitative variation of phenolics between two RH species due to the different extraction solvent used. According to them, it seems that flavonoids of RH fruits can be totally extracted using water as an extraction solvent rather than a highly concentrated organic solvent (methanol, ethanol, acetone, etc.) as used in traditional extraction methods. Further, the measured concentration of total tannins in our *Rosa* species was 178 μg CE/g. Not enough studies discussed the quantitative amount of phenols and most of them have been focused on proanthocyanidin aglycones and glycosides characterization [42]. The tannins content was comparable to that in the report of Cunja *et al*. [43] who found values for proanthocyanidin trimer 1-3 ranging between 119.6-181.4 μg/g. In contrary, Taneva *et al*. [8] measured higher levels (3.86%, 3.76%, and 1.46%) for total tannin content in water, 50% (v/v) and 70% (v/v) ethanol extracts, respectively, suggesting that water was a better solvent for higher recovery of tannins. In addition, tannin content may vary widely during the growing season in particular anatomical plant parts, as Hashidoko [44] has noted that condensed tannins were more abundant in the underground parts of the plant and the polar phenol fraction contained higher amounts of catechin oligomers and polymers.

The antioxidant activity of *R. canina* hips was evaluated by ORAC and DPPH methods (Table 1). Initial RH sample showed high antioxidant activity (ORAC – 2094.3 μmol TE/g; DPPH – 2493.6 μmol TE/g). ORAC value was higher than earlier determined [7] – 1873.5 μmol TE/g.

Characterization of isolated plant cell wall material

The second main objective of our research was the isolation of plant CWM as AIS and its chemical characterization. We were particularly interested in how the chemical composition changed after plant material treatment with organic solvents. For easier comparison the results are presented in Table 1. During extraction of initial RH material with hot aqueous ethanol (70ºC) and acetone, 43% of the dry matter was solubilized. The AIS fraction represented 57% (w/w) of the lyophilized plant material. Although there were earlier studies concerning the carbohydrate constituents of the cell walls of suspension cultures from hip fruits [45, 46], yields of the AIS have not been reported before, and cannot be therefore compared. The result of the AIS content in the present study was lower comparing with data from our earlier experiments with RH fruits (76.1%) [47]. It should be pointed out that we followed a different procedure for AIS preparation and the starting RH material was differently prepared.

Ash content (2 %) was reduced to 60% due to aqueous organic solvent treatment.

Interestingly, the AIS had a high content of crude protein (4.6%) by reason of the co-precipitation of soluble protein with polysaccharides during alcohol treatment. In addition to the dehydration effects of aqueous alcohol and acetone, AIS was isolated from freeze-dried hips fruits material. Nevertheless, it is well-known, and also expected in our case, that AIS methods have advantage in cell wall enzymes inactivation. Also, initial RH fruit material seems not to be a rich source of protein such as in case of protein-rich soybean. Because of this we did not consider the necessity of additional extraction steps for removing co-precipitated proteins with chemical (detergents, PAW), enzyme (or both) treatment. This is consistent with the study of Renard [12] who found that the nitrogen content was significantly higher in the AIS procedures than in other methods and among these it was significantly higher in AIS prepared from freeze-dried material.

Total lipids content was reduced by nearly 52% compared to the initial content, logically due to organic solvent treatment.

Independently of the fact that lignin is typical for the second cell walls, hip fruits are composed of lignified elements. It was important to adapt an analytical method for lignin quantification in isolated plant cell walls. Reviews critically emphasized the relative advantages of the different methods published [25, 48, 49]. The most frequently used methods for lignin estimation are the classical gravimetric Klason and the spectroscopic ABL one. Klason lignin levels are determined as the amount of acid-insoluble material remaining after sulfuric acid (Seaman) hydrolysis. Despite the method simplicity, it should be noted that there are some weak points related to overestimation of lignin content due to protein and polysaccharide components, Maillard products, humin precipitates and lignin-like phenolic matter

formed during prolonged treatment with acid. Also, condensed tannins and tannin-protein complexes could affect the results [48].

ABL procedure requires isolation of plant cell wall with hot solvent, then its lignin constituent is solubilized into acetyl bromide/acetic acid solution followed by absorbance reading at 280 nm. This method seems to be a good alternative to the traditional gravimetric one, since it has been found that high protein content and carbohydrates did not interfere with lignin quantification [49]. However, higher amounts of non-lignin substances (precipitated and/or wall-bound) like phenolic compounds (tannins, acids, etc.) could have partial contribution to the total lignin content, since they have coincidental absorption spectra [48]. In this work, the lignin value using Klason method was higher (8.0%) than the ABL value (5.1%). The higher value could be attributed to the above mentioned plant 'contaminants'. In the literature, various data on the content of lignin in AIS of different fruits and vegetables can be found. Voragen *et al*. [50] reported that raspberry, pineapple, pear, carrot, cucumber, and especially cherry were rich in crude lignin (49-169 g/kg). They have also stated that the lignin content could be overrated by the method used. Another future research will be focused on the isolation of lignin with acidic 1,4-dioxane and determination of some basic chemical characteristics.

Vitamin C content was reduced by more than 94% in the AIS material and a value of 35 mg/100 g was measured. The result could find its explanation taking into account that various factors, including light, oxidation, metal ions, alkaline pH and high temperature, affected the stability and content of vitamin C [51]. During plant cell wall preparation, vitamin C was simultaneously extracted and degraded due to temperature, light and oxygen exposure. The similar tendency was observed with the total carotenoid pigments that seemed to be totally extracted. Their amount decreased by more than 97% compared to the initial plant material, probably due to better solubility in the organic solvent (acetone) used during cell wall isolation and instability in front of light, thermal treatment and oxygen. Lycopene and β-carotene contents were minimized (1.3 μg/g and 1.5 μg/g).

There was a tendency for reduction in the levels of polyphenol components in AIS as well. The total phenolic content was reduced by 41% or nearly 60% was recovered (54 mg GAE/g). Higher recovery could be due to the highly concentrated organic solvent (hot aqueous ethanol (70ºC, 80%) and acetone) used in plant cell wall isolation. Pure solvent led to co-precipitation of complex carbohydrate polymers in the cell walls that limited the polyphenol accessibility and efficiency of its extraction. Therefore, optimization of the extraction solvent is needed through reduction of ethanol concentrations (< 80%). This could alter the plant structure by swelling the matrix, enabling the solvent to more completely penetrate the plant material and solubilize extractable (non-wall-bound) phenolic compounds. On the other hand, the aqueous solvent would remove some additional water-soluble wall constituents (pectin). The possibility for interactions between intracellular polyphenols and plant cell walls components (protein, polysaccharides) should not be forgotten which could also affect extractability regardless of the extractants.

It was demonstrated that flavonoids were more fully removed from the initial RH material. Sequential treatment with different solvents was a good approach for removing low-molecular weight flavonoids from the wall, since the total content was reduced by 80% and the measured value was 52 μg QE/g. Also, there was a slight decrease (24%) in the level of condensed tannins in AIS (136 μg CE/g) suggesting that only a fraction of the tannins was extracted during AIS preparation. Probably, some of the non-extracted tannins were highly polymerized, wall-bound or co-precipitated in the highly concentrated organic solvents used. These findings were consistent with those of previous studies. For instance, Renard [12] noted that there was a clear trend for higher procyanidin content in the cell walls, when it was isolated as AIS. Earlier work [52] showed that 50% aqueous methanol is a poor solvent for proanthocyanidin polymers, whereas highly polymerized proanthocyanidin forms (DP > 10) dominated in the extracts of RH fruits. According to these authors unextractable proanthocyanidins were with an average DP higher than 14 [53]. The degree of polymerization may have a great influence on the extractability of condensed tannins. Regarding the antioxidant activity, there was a slight decrease in ORAC (34%) and DPPH (25%) activity, probably as a result of low-molecular weight components removal. Higher activities might be correlated with residual unextractable and co-precipitated phenolic compounds.

It was found that carbohydrates were the main constituents of the RH AIS (Table 1). The total carbohydrates represented nearly 52% of the AIS dry material. Further indication for cell wall polysaccharide types present in AIS could be obtained after neutral sugar composition analysis (Table 2). The major sugar moiety in RH AIS was glucose (19.1%) followed by galacturonic acid –

16.2% (Table 1). Cellulose was accounted for 11% of the dry matter (Table 1), suggesting that residual glucose (8.1%) constitutes the hemicellulose fraction (xyloglucan, etc.).

Table 2. Neutral sugar composition of RH cell wall material (% w/w)*.

Monosaccharides	Plant cell wall material (AIS)
Rha	0.4
Ara	4.1
Gal	4.0
Glc	19.1
Xyl	2.7
Fuc	0.8
Man	2.0
Total	33.1

*Values are the average of two replicates.

In addition, AIS was composed of generally recognized pectin monosaccharides. Amongst them, lower amounts of arabinose (4.1%), galactose (4.0%), mannose (2.0%) and xylose (2.7%) were found. Rhamnose content represented only 1.2% of the total neutral sugars, but it was indicative of pectin ramified region presence. In conclusion, the sugar composition of the AIS revealed the presence of different types of polysaccharides, such as pectin, cellulose and hemicelluloses. Due to the higher purity of the AIS used, the result of the neutral sugar composition content in the present study was higher compared with data from our earlier experiments with RH fruits [47]. It must be noted that we followed a different procedure for AIS preparation and the starting RH material was differently prepared. Additional comparison of our results with data in the literature cannot be done since the sugar composition of the RH AIS has not been previously reported. Such preparation 'virtually' free of contaminants could be effectively used to study major cell wall carbohydrate polymers in a further investigation.

CONCLUSIONS

Several conclusions may be drawn from the application of AIS as a method for plant cell wall preparation. The choice of the initial plant material treatment is strictly individual and it should depend on the major chemical constituents. Also, amounts of different chemical constituents are removed in different extents. There is no perfect method for the simultaneous and complete removal of all interfering substances without affecting the interaction between cell wall components. Therefore, we consider that the preparation of CWM is a matter of compromise with the aims of investigation. To the best of our knowledge, there are no published reports on the method for isolation of CWM from rose hip as AIS. Moreover, the current study is among the few ones presenting more detailed information about the chemical composition of fruit AIS.

Acknowledgements: *The first author acknowledges with gratitude the technical assistance of chemist I. Z. Yanakieva and Prof. Romualdo S. Fukushima, PhD from the Departamento de Nutrição e Produção Animal, Faculdade de Medicina Veterinária e Zootecnia da Universidade de São Paulo, Brazil for kindly provided reference and helpful comments. This work was funded by project № DFNP-214/16.05.2016 "Characterization and biological activity of pectic polysaccharide from the cell walls of rose hip fruits" of the Program for career development of young scientists, Bulgarian Academy of Sciences.*

REFERENCES

1. O. Nilsson, in: Flora of Turkey and the East Aegean Islands, P. H. Davis (ed.), Edinburgh University Press, Edinburgh, 1997, p. 106.
2. S. Patel, *Mediterr. J. Nutr. Metab.*, **6**, 89 (2013).
3. M. Bonev, S. Dimitrov, S. Yankov, G. Vladimirov, *Sci. Works Higher Institute Agric.-Plovdiv*, **16**, 175 (1967).
4. St. Dimitrov, M. Bonev, *Sci. Works Higher Institute Agric.-Plovdiv*, **16**, 183 (1967).
5. F. Demir, M. Özcan, *J. Food Eng.*, **47**, 333 (2001).
6. S. Ercisli, *Food Chem.*, **104**, 1379 (2007).
7. P. N. Denev, M. G. Kratchanova, M. Ciz, A. Lojek, O. Vasicek, P. Nedelcheva, D. Blazheva, R. Toshkova, E. Gardeva, L. Yossifova, P. Hyrsl, L. Vojtek, *Food Chem.*, **157**, 37 (2014).
8. I. Taneva, N. Tr. Petkova, I. Dimov, I. Ivanov, P. P. Denev, *J. Pharmacogn. Phytochem.*, **5**, 35 (2016).
9. R. R. Selvendran, *Phytochemistry*, **14**, 1011 (1975).
10. R. R. Selvendran, P. Ryden, in: Methods in Plant Biochemistry, P. M. Dey (ed.), vol. 2, Academic Press Limited, London, 1990, p. 549.
11. H. A. Schols, A. G. J. Voragen, in: Pectins and their manipulation, G. B. Seymour, J. P. Knox (eds.), Blackwell Publishing, CRC Press, Oxford, 2002, p. 1.
12. C. M. G. C. Renard, *Carbohydr. Polym.*, **60**, 515 (2005).
13. H. K. Lichtenthaler, A. R. Wellburn, *Biochem. Soc. Trans.*, **11**, 591 (1983).
14. S. Georgé, F. Tourniaire, H. Gautier, P. Goupy, E. Rock, C. Caris-Veyrat, *Food Chem.*, **124**, 1603 (2011).
15. B. J. Lime, F. P. Griffiths, R. T. O'Connor, D. C. Heinzelman, E. R. McCall, *J. Agric. Food Chem.*, **5**, 941 (1957).
16. AOAC Association of Official Analytical Chemists, Official methods of analysis, 18th edn. AOAC International, Gaithersburg, MD, 2000.
17. M. DuBois, K. A. Gilles, J. K. Hamilton, P. A. Rebers, F. Smith, *Anal. Chem.*, **28**, 350 (1956).

18. H. N. Englyst, J. H. Cummings, *Analyst*, **109**, 937 (1984).
19. A. B. Blakeney, P. J. Harris, R. J. Henry, B. A. Stone, *Carbohydr. Res.*, **113**, 291 (1983).
20. N. Blumenkrantz, G. Asboe-Hansen, *Anal. Biochem.*, **54**, 484 (1973).
21. M. N. Gibbons, *Analyst*, **80**, 268 (1955).
22. K. Kürschner, A. Hoffer, *Chem.-Ztg.*, **55**, 161 (1931).
23. R. B. Bradstreet, The Kjeldahl method for organic nitrogen, Academic Press, New York, 1965.
24. NFSS National Food Safety Standard of the People's Republic of China, GB 5009.5—2010 (2010).
25. C. W. Dence, in: Methods in Lignin Chemistry, S. Y. Lin, C. W. Dence (eds.), Springer-Verlag, Berlin, 1992, p. 33.
26. R. S. Fukushima, M. S. Kerley, *J. Agric. Food Chem.*, **59**, 3505 (2011).
27. V. Singleton, J. Rossi, *Am. J. Enol. Vitic.*, **16**, 144 (1965).
28. C.-C. Chang, M.-H. Yang, H.-M. Wen, J.-C. Chern, *J. Food Drug Anal.*, 10, 178 (2002).
29. C. J. Sarneckis, R. G. Dambergs, P. Jones, M. Mercurio, M. J. Herderich, P. A. Smith, *Aust. J. Grape Wine Res.*, **12**, 39 (2006).
30. B. Ou, M. Hampsch-Woodill, R. L. Prior, *J. Agric. Food Chem.*, **49**, 4619 (2001).
31. P. Denev, M. Ciz, G. Ambrozova, A. Lojek, I. Yanakieva, M. Kratchanova, *Food Chem.*, **123**, 1055 (2010).
32. N. Petkova, I. Ivanov, P. P. Denev, At. Pavlov, *Turk. J. Agric. Nat. Sci.*, **2**, 1773 (2014).
33. I. G. Ivanov, R. Z. Vrancheva, A. S. Marchev, N. T. Petkova, I. Y. Aneva, P. P. Denev, V. G. Georgiev, A. I. Pavlov, *Int. J. Curr. Microbiol. Appl. Sci.*, **3**, 296 (2014).
34. M. Bonev, S. Dimitrov, S. Yankov, G. Vladimirov, *Sci. Works Higher Institute Agric.-Plovdiv*, **15**, 243 (1966).
35. B. Michev, A. Naidenov, S. Chortanova, T. Malinov, Forest fruits – food and healing means, Zemizdat, Sofia, 1983.
36. I. Taneva, K. Dobreva, *Sci. Works University Food Technol.*, **60**, 468 (2013).
37. C. M. Rosu, C. Manzu, Z. Olteanu, L. Oprica, A. Oprea, E. Ciornea, M. M. Zamfirache, *Not. Bot. Horti Agrobot. Cluj-Napoca*, **39**, 203 (2011).
38. S. C. Andersson, K. Rumpunen, E. Johansson, M. E. Olsson, *Food Chem.*, **128**, 689 (2011).
39. P. Denev, A. Lojek, M. Ciz, M. Kratchanova, *Bulg. J. Agric. Sci*., **19**, 22 (2013).
40. N. Demir, O. Yildiz, M. Alpaslan, A. A. Hayaloglu, *LWT - Food Sci. Technol.*, **57**, 126 (2014).
41. J. D. Nađpal, M. M. Lesjak, F. S. Šibul, G. T. Anačkov, D. D. Četojević-Simin, N. M. Mimica-Dukić, I. N. Beara, *Food Chem.*, **192**, 907 (2016).
42. J.-P. Salminen, M. Karonen, K. Lempa, J. Liimatainen, J. Sinkkonen, M. Lukkarinen, K. Pihlaja, *J. Chromatogr. A*, **1077**, 170 (2005).
43. V. Cunja, M. Mikulic-Petkovsek, A. Zupan, F. Stampar, V. Schmitzer, *J. Plant Physiol.*, **178**, 55 (2015).
44. Y. Hashidoko, *Phytochemistry*, **43**, 535 (1996).
45. G. Chambat, J.-P. Joseleau, *Carbohydr. Res.*, 85, C10 (1980).
46. G. Chambat, J.-P. Joseleau, F. Barnoud, *Phytochemistry*, **20**, 241 (1981).
47. M. H. Ognyanov, PhD Thesis, IOCCP, Sofia, 2016.
48. P. J. Van Soest, in: Nutritional ecology of the ruminant, P. J. Van Soest (ed.), 2nd edn., Cornell University Press, Ithaca, New York, p. 177.
49. R. Hatfield, R. S. Fukushima, *Crop Sci.*, **45**, 832 (2005).
50. A. G. J. Voragen, J. P. J. Timmers, J. P. H. Linssen, H. A. Schols, W. Pilnik, *Z. Lebensm. Unters. Forsch.*, **177**, 251 (1983).
51. G. F. M. Ball, in: Water-soluble vitamin assays in human nutrition, G. F. M. Ball (ed.), Springer USA, 1994, p. 10.
52. L. Y. Foo, L. J. Porter, *Phytochemistry*, **19**, 1747 (1980).
53. J. K. Hellström, A. R. Törrönen, P. H. Mattila, *J. Agric. Food Chem.*, **57**, 7899 (2009).

ИЗОЛИРАНЕ И ХАРАКТЕРИСТИКА НА РАСТИТЕЛНИ КЛЕТЪЧНИ СТЕНИ ОТ ШИПКОВИ ПЛОДОВЕ

М. Хр. Огнянов[1*], М. М. Ходжова[1], Н. Тр. Петкова[2], П. Н. Денев[1], Й. Н. Георгиев[1], М. Г. Крачанова[1]

[1]*Лаборатория по биологично активни вещества, Институт по органична химия с Център по фитохимия, Българска академия на науките, бул. Руски 139, Пловдив 4000, България*
[2]*Катедра по органична и неорганична химия, Университет по хранителни технологии, бул. Марица 26, Пловдив 4002, България*

Постъпила на 6 юни, 2017; коригирана на 21 февруари, 2018

(Резюме)

В настоящото изследване бяха изолирани растителни клетъчни стени от шипкови плодове под формата на алкохолно-неразтворима част. Химичният състав на клетъчно-стенния материал и на изходните плодове (ядлива част) беше изследван и сравнен. Количеството на полифенолни вещества (флавоноиди), пигменти, липиди и витамин С беше отстранено в различна степен по време на обработката с горещ алкохол/ацетон. Противно на това, протеините, полизахаридите и някои полифеноли (кондензирани танини) бяха утаени поради дехидратиращия ефект на алкохола, който е и основният фактор, ограничаващ екстрахирането на „контаминантите“. В допълнение, въглехидратите (главно пектин и целулоза) бяха основните компоненти на „пречистения“ клетъчно-стенен материал от шипкови плодове.

Bulgarian Chemical Communications, Volume 50, Issue 4 (pp.538 – 544) 2018

Morchella esculenta (L.) growing in Bulgaria: chemical profile and hazard index

L. Dospatliev[1*], M. Ivanova[2], M. Lacheva[3], T. Radoukova[4]

[1]*Department of Pharmacology, Animal Physiology and Physiological Chemistry, Trakia University, 6000 Stara Zagora, Bulgaria*
[2]*Department of Informatics and Mathematics, Trakia University, 6000 Stara Zagora, Bulgaria*
[3]*Department of Botany, Agricultural University, 4000 Plovdiv, Bulgaria*
[4]*Department of Botany, Plovdiv University Paisii Hilendarski, 4000 Plovdiv, Bulgaria*

Received, July 21, 2017; Revised, July 31, 2018

Morchella esculenta (L.) Pers. (morel) is one of the most widely appreciated wild edible mushrooms. The mushroom *Morchella esculenta* has long been known for its medicinal properties, especially its health-promoting effects, including antioxidant activity, hepatoprotective activity, antimicrobial properties and antitumor effect. *Morchella esculenta* is rich in carbohydrates (79.06 g 100 g^{-1} dw), followed by proteins (11.19 g 100 g^{-1} dw), ash (7.32 g 100 g^{-1} dw) and fat (2.43 g 100 g^{-1} dw). Also moisture (89.41%), and total energy (1624.14 kJ 100 g^{-1} dw) were calculated. The concentrations of heavy metals: Pb (0.28 mg kg^{-1}), Cd (0.10 mg kg^{-1}), Cu (0.18 mg kg^{-1}), Co (0.28 mg kg^{-1}), Zn (0.82 mg kg^{-1}), Ni (0.46 mg kg^{-1}), Cr (0.28 mg kg^{-1}), Fe (17.01 mg kg^{-1}), and Mn (0.96 mg kg^{-1}), were assayed in *Morchella esculenta*. Hazard index values were calculated for children: 1-3 years old (0.665), 3-10 years old (0.347), 10-14 years old (0.186), 14-18 years old (0.131) and for adults > 18 years (0.230). According to this study, the edible wild mushroom *Morchella esculenta* could be used in human nutrition due to its good parameters. Heavy metal content of samples indicated that the Batak mountain is an ecologically pure region in Bulgaria, and therefore the mushrooms collected from this location could be consumed without any risk for human health.

Keywords: *Morchella esculenta*, Chemical profile, Hazard index

INTRODUCTION

Mushrooms have a long and strong relationship with human beings and can have vital economic impact. For a long time mushrooms have been consumed and used by men for their taste and pleasant aroma [1]. Mushrooms have a high nutritional value with high amount of vitamins, proteins, minerals, fibers, trace elements but have low calories and cholesterol [2-7]. Many of them are used in preparing medicines for many years and have potential in maintaining sound health and active immune system of the human body. Mushrooms are consumed as medicines in the form of capsules but not as food [8, 9]. Mushrooms are also rich sources of various bioactive substances like antibacterial, antifungal, antiviral, anti-parasitic, antioxidant, anti-inflammatory, antiproliferative, anticancer, antitumor, cytotoxic, anti-hiv, hypocholesterolemic, antidiabetic, anticoagulant, hepatoprotective compounds, etc. [10-14]. From 14 000 species which are known, 2 000 species are safe for human use and among them 650 possess medicinal properties [15, 16].

Morchella esculenta (L.) Pers. (morel) is a well known and extraordinary mushroom species. The head is distinctly conical in shape. The head surface comprises a honeycomb of sharp ridges and deep pits and is rich-brown in colour. The texture is sponge-like. The head and stem are generally hollow. It grows generally on chalky soil in grassy woodlands, field margins ad roadside verges. *Morchella esculenta* is picked up every year if the weather condition is suitable for growth in Bulgaria. It is collected especially in April and May, and marketed abroad either fresh or dried.

In the literature no data are available regarding *Morchella esculenta* in Bulgaria: Therefore, the aim of this study was to investigate the chemical profile and hazard index of *Morchella esculenta* from the Batak Mountain.

EXPERIMENTAL

Samples

Fifteen mushroom samples were collected in 2016 and 2017 from the Batak Mountain by the authors themselves.

The Batak Mountain is located in the western Rhodopes. Its western border is defined by the Chepinska river, the southern border – by Dospatska river and Dospat dam, the eastern border – by Vacha river and the northern border – by the Thracian Plane (GPS41°46'02.6"N 24°08'48.4"E). The region is industry-free and is characterised with forests, land and low buildings.

* To whom all correspondence should be sent:
E-mail: lkd@abv.bg

Reagents are qualified as "AR" (p.a. Merck & Fluka). The stock standard solutions for ICP determination of Fe, Ni, Cr, Cu, Co, Zn, Mn, Pb, and Cd at concentrations of 1000 mg L^{-1} were supplied by Merck, Darmstadt, Germany. Water was deionized in a Milli Q system (Millipore, Bedford, MA, USA) to a resistivity of 18.2 MΩ cm. All plastic and glassware was cleaned by soaking in dilute HNO_3 (1/9, v/v) and was rinsed with distilled water prior to use.

Sample preparation for nutritional analysis

The whole macrofungal samples were used in this study. Fresh samples, after the removal of extraneous material such as mud, bush, soil, plant, etc. by washing with demineralized water, were air-dried between Whatman filter papers. Approximately 5 g of each sample was taken immediately for the determination of moisture. Remaining samples were stored in a deep-freezer until use [17]. While examining the nutritional composition of mushroom samples, the maturation stage of them was not considered.

Proximate composition analysis

For determination of proximate value, the following parameters were studied by using the mushroom material.

Determination of crude protein: Protein content was determined using folin phenol reagent. 0.5 g of the powdered mushroom sample was extracted with 50 mL of 2% NaCl in a water bath at 60˚C for 1 h. The extract was filtered out and 50 mL of 3% copper acetate monohydrate was added to the filtrate to precipitate the protein. The precipitated protein was then centrifuged out and dissolves in 50 mL [18].

Determination of carbohydrates: Total carbohydrate was determined by adding 2 g of each sample in 50 mL distilled water, 0.2 mL of which was ten fold diluted. To 1 mL of the resulting solution and serial dilutions of glucose stock (10 mg 100 mL^{-1}) solution, 4 mL of anthrone reagent was added and the absorbance of the solutions was measured by a spectrophotometer at 620 nm against a reagent blank [19].

Determination of crude fat: Crude fat was determined by extracting 2 g moisture-free samples with petroleum ether in a soxhlet extractor, heating the flask on a sand bath for about 6 h till a drop taken from the drippings left no greasy stain on the filter paper. After boiling with petroleum ether, the residual petroleum ether was filtered using Whatman No 40 filter paper and the filtrate was evaporated in a preweighed beaker. Increase in weight of beaker gave the crude fat [20].

Determination of ash content: The powdered mushroom sample (3 g) was ashed in a previously ignited and cooled crucible of known weight in a Gallenkamp furnace at 55˚C for 6 h. The fairly cooled crucibles were put in desiccators and weighed [21].

Energy: Total energy was calculated according to the following equations: Total energy (kJ/100g) = 17 (g protein + g carbohydrate) + 37 (g lipid). The weight of individual nutrients is g/100 g dw sample [22].

Moisture content: The fresh weight of each mushroom sample was taken using a chemical balance. These samples were then oven-dried separately at 105˚C for 24 h. The loss in weight obtained after drying was regarded as the moisture content [23].

Digestion procedures

Multiwave 3000 closed vessel microwave system (maximum power was 1400 W, and maximum pressure in the Teflon vessels - 40 bar) was used in this study. The mushroom samples (0.25 g) were digested with 6 mL of HNO_3 (65%) and 1 mL of H_2O_2 (30%) in the microwave digestion system for 23 min and diluted to 25 mL with deionized water. A blank digest was carried out in the same way. All sample solutions were clear. Digestion conditions for the microwave system are given in Table 1.

Analytical procedure

Quantitative determination of the concentration of the studied trace elements (Fe, Ni, Cr, Cu, Co, Zn, Mn, Pb, Cd) was carried out in the mineralized samples by ICP Optima model 7000 DV spectrometer.

Accuracy and precision

In order to validate the method for accuracy and precision the certified reference material (CRM) - Virginia Tobacco Leaves (CTA-VTL-2) was analysed for the corresponding elements. The results are shown in Table 3. For evaluation of the correctness of the results, three generally accepted criteria were used as follows:

(1) $D = X - X_{CRM}$, where X is the measured value and X_{CRM} is the certified value. When D is within the limits of $\pm 2\sigma$, where σ is the standard deviation of the certified value, the result is considered to be good; when it is $-3\sigma \leq D \leq 3\sigma$ - satisfactory, and beyond these limits the result is unsatisfactory.

(2) $D\% = D / X_{CRM} \times 100$ - percentage difference. When the values of D% are in the limits $\pm 200\sigma / X_{CRM}$, the result is considered to be good;

when the value is in the limits ± 200σ / X_{CRM} and ± 300σ / X_{CRM} - satisfactory; and when it is out of the limits ± 300σ / X_{CRM}, the result is unsatisfactory.

(3) $Z = X - X_{CRM} / \sigma$. When $Z \leq 2$, the result is considered to be good; when $2 \leq Z \leq 3$ - satisfactory; when $Z > 3$ - unsatisfactory.

For evaluation of the accuracy of the digestion and measuring procedures, we have used the R criterion showing the extent of extraction of the element in percentage from the certified value. When the measured value X is within the limits of $X_{CRM} \pm U_{CRM}$, where U_{CRM} is the indefiniteness of the certified value, we accept the extent of extraction to be 100%. In all remaining cases, the extent of extraction is equal to $X / X_{CRM} \cdot 100$. As can be seen from the tables, the results obtained for all certified materials yield a recovery of 100% for all elements.

Method of risk assessment

The risk assessment of the heavy metals to human health due to the consumption of the mushrooms can be performed by calculating the hazard quotient (HQ) for each metal of interest and the hazard index (HI), which is the sum of the hazard quotients. The HQ is the ratio between the exposure and the reference dose (Eq. 1). One can assume the existence of a risk for mushroom consumption when the HQ > 1.

$$HQ_{metal} = \frac{DI.C_{metal}}{R_f D.BW} \quad (1)$$

where DI is the daily intake of mushrooms (kg day^{-1}), C_{metal} is the concentration of the metal in the mushroom given for dry weight (mg kg^{-1}), R_fD is the oral reference dose for the metal given for unit body weight (mg kg^{-1} day^{-1}), BW is the average human body weight (kg). The value of R_fD for Pb (0.004 mg kg^{-1} day^{-1}), for Cd (0.001 mg kg^{-1} day^{-1}), for Co (0.043 mg kg^{-1} day^{-1}), for Cu (0.04 mg kg^{-1} day^{-1}), for Mn (0.14 mg kg^{-1} day^{-1}), for Cr (0.003 mg kg^{-1} day^{-1}), for Ni (0.02 mg kg^{-1} day^{-1}) and for Zn (0.001 mg kg^{-1} day^{-1}), were taken from the Integrated Risk Information System. The average BW was taken as 70 kg for adults and 61, 43, 23, 12 kg for children: (14-18), (10-14), (3-10), (1-3) years old, respectively.

The HI provides information about the joint health risk caused by the heavy metals when a specific mushroom is consumed. We calculated the hazard index as given by Eq. 2:

$$HI = \Sigma HQ = HQ_{Cd} + HQ_{Pb} + HQ_{Ni} + HQ_{Cr} + HQ_{Cu} + HQ_{Co} + HQ_{Zn} + HQ_{Mn} \quad (2)$$

Statistical data processing

SPSS (Statistical Package for Social Science) program for Windows was used for statistical data processing.

RESULTS AND DISCUSSION

Chemical composition of Morchella esculenta

The main components of the chemical composition of *Morchella esculenta* are presented in Table 2. *Morchella esculenta* showed to be rich in carbohydrates (79.06 g 100 g^{-1} dw), which were the most abundant macronutrients. Proteins were present at 11.19 g 100 g^{-1} dw. Total energy value was established to be 1624.14 kJ 100 g^{-1} dw. A sample of *Morchella esculenta* growing in Portugal was also reported to have carbohydrates as the most abundant macronutrient [24]. The carbohydrates in mushrooms comprise various compounds: sugars (monosaccharides, their derivatives and oligosaccharides) and both reserve and structural polysaccharides [25].

Each value is expressed as mean ± SD (n = 15). Means with different letters within a row are significantly different ($p < 0.05$)

The results for the efficiency of microwave mineralization for Fe, Ni, Cr, Cu, Co, Zn, Mn, Pb and Cd determination in the certified reference material - Virginia tobacco CTA- VTA-2 are displayed in Table 3. The results from the descriptive analysis of the concentration of Fe, Ni, Cr, Cu, Co, Zn, Mn, Pb and Cd in *Morchella esculenta* samples are presented in Table 4.

Concentrations of nine metals (Fe, Ni, Cr, Cu, Co, Zn, Mn, Pb and Cd) were determined in this study. The trace element contents of the species depend on the ability of the species to extract elements from the substrate, and on the selective uptake and deposition of elements in tissues [26 - 32].

Table 1. Microwave acid digestion programme.

Step	Ramp time (min)	Hold time (min)	Cooling period (min)	Pressure (MPa)	Temperature (°C)
1	10	10	5	0.758	110
2	10	10	5	1.023	150
3	20	10	5	0.758	190

Table 2. Moisture (g 100 g^{-1} of fresh weight), macronutrients (g 100 g^{-1} of dry weight) and total energy (kJ 100 g^{-1} of dry weight) in the wild edible mushrooms.

Components	$\overline{X}$	SD	-95% Confid.	+95% Confid.
Moisture	89.41	± 1.73	88.45	90.37
Ash	7.32	± 0.76	6.90	7.74
Crude protein	11.19	± 0.76	10.77	11.61
Crude fat	2.43	± 0.29	2.27	2.59
Total carbohydrates	79.06	± 1.78	78.07	80.04
Total energy	1624.14	± 7.36	1620.07	1628.21

Table 3. Effectiveness of microwave mineralization in the determination of Fe, Ni, Cr, Cu, Co, Zn, Mn, Pb and Cd in Virginia Tobacco-CTA-VTA-2 certified reference material (n = 15).

Element	Certified value, mg kg^{-1}	Found value, mg kg^{-1} Microwave digestion	Recovery (%)
Fe	1083 ± 33	1160 ± 45	103
Ni	1.98 ± 0.21	1.92 ± 0.17	98.1
Cr	1.87 ± 0.16	1.83 ± 0.14	93.6
Cu	18.2 ± 0.8	18.1 ± 0.7	99.4
Co	0.429 ± 1.4	0.420 ± 0.02	98.0
Zn	43.3 ± 2.1	44.1 ± 1.6	101.8
Mn	79.7 ± 2.6	77.5 ± 2.1	97.2
Pb	22.1 ± 1.2	23.0 ± 0.8	104
Cd	1.52 ± 0.17	1.50 ± 0.05	98.7

Table 4. Concentration of heavy metals in mushroom samples (*Morchella esculenta*) collected from Batak Mountain, Bulgaria (n = 15)

Element	$\overline{X}$, mg kg^{-1}	SD, mg kg^{-1}	- 95% Confid.	+ 95% Confid.
Fe	17.01	± 3.65	14.99	19.03
Ni	0.46	± 0.11	0.40	0.52
Cr	0.28	± 0.18	0.18	0.38
Cu	0.18	± 0.02	0.17	0.19
Co	0.28	± 0.10	0.22	0.34
Zn	0.82	± 0.22	0.70	0.95
Mn	0.96	± 0.39	0.74	1.17
Pb	0.28	± 0.11	0.22	0.34
Cd	0.10	± 0.02	0.09	0.11

Fe was found to be the dominant ion as compared with other heavy metals in mushrooms, followed by manganese and zinc ions. Iron is vital for almost all living organisms, participating in a wide variety of metabolic processes, including oxygen transport, DNA synthesis, and electron transport. It is known that adequate iron in a diet is very important for decreasing the incidence of anemia. Iron deficiency occurs when the demand for iron is high, e.g., in growth, high menstrual loss, and pregnancy, and the intake is quantitatively inadequate or contains elements that render the iron unavailable for absorption. High concentrations of iron may lead to tissue damage, as a result of the formation of free radicals. The amount of Fe in the mushroom species varied from 14.99 to 19.03 mg kg^{-1}. Our data on the values of iron are lower than the values given in the cited reports. The reported iron values for mushroom samples were 1.190-628 mg kg^{-1} [7, 26–30].

Cr is a trace metal necessary for the normal metabolism of cholesterol, fat, and glucose. Chromium deficiencies in the diet produce elevated circulating insulin concentrations, hyperglycemia, elevated body fat, decreased sperm counts, reduced fertility, and shortened life span. The concentration of chromium in the mushroom species varied between 0.18 and 0.38 mg kg^{-1}. In other studies, chromium concentrations between 0.1 and 4 mg kg^{-1} were recorded [30, 33, 34].

Ni has no specific function in humans; however, it is a co-factor for some microbial intestine enzymes. Ni content in the adult human body should remain below 0.1 mg per day, and excess may cause damages to DNA and cell structures. The daily intake of Ni was estimated as 0.046 mg,

which represents approximately 3.3 % of R_fD established in 0.02 mg kg^{-1} per day, equivalent to 1.4 mg per day for a 70 kg adult [35]. Maximum and minimum values of Ni in the mushrooms were 0.40 and 0.52 mg kg^{-1}. Ni values found by the authors are in accordance with those of previous studies [30, 33, 34, 36].

Cu is an essential metal, which is a constituent of some metalloenzymes, and is required in hemoglobin synthesis and catalysis of metabolic growth. The average copper content of the analyzed mushroom samples was 0.18 mg kg^{-1}, which is below the safe limit of 40 mg kg^{-1} set by the WHO [35] in foods. According to the review reported by Kalac [36], copper concentrations accumulated in mushroom species usually varied from 20.0 to 100.0 mg kg^{-1}. Other workers have presented copper contents of mushroom samples to be in the ranges: 16.1-144.9 mg kg^{-1} [37], 2.6-72.4 mg kg^{-1} [5], 1.8-22.3 mg kg^{-1} [38], 5.0-83.0 mg kg^{-1} [30] and 13.7-182.4 mg kg^{-1} [39]. The results obtained in the current study indicated that copper content of the investigated mushroom samples was comparable to those reported in the literature.

The average concentration of Co in the analysed mushroom samples was 0.28 mg kg^{-1}, which is below the safe limit of 1 mg kg^{-1} set by the WHO [35] in foods. Based on the results from papers published until 2013, the reported Co content was found to vary between 0.1 and 7.0 mg kg^{-1} [36]. Cobalt is a constituent of vitamin B12.

Zn is one of the most important minerals needed by our body systems due to the fact that it is highly associated with protein- and carbohydrate-rich foods. Zinc is also used in medicines that treat rashes, acne, dandruff and athlete's foot [38]. It has biological significances for living organisms and mushrooms are known as good zinc accumulators. The average Zn content recorded in the studied samples was 0.82 mg kg^{-1}, respectively, which is below the safety limit of 60 mg kg^{-1}, determined by the WHO [35]. Zn levels reported in the literature were 29.3-158.0 mg kg^{-1} [7, 30, 34, 36, 38].

Mn is an essential metal needed for biological systems such as metalloproteins [34]. The average Mn content recorded in the studied samples was 0.96 mg kg^{-1}, which is below the toxicity limit of 400.0-1000.0 mg kg^{-1}. The reported levels of Mn in the literature are 12.9-93.3 mg kg^{-1} [7, 35-38].

Cd is accumulated mainly in kidneys, spleen and liver and its blood serum level increases considerably following mushroom consumption [25, 36-40]. Thus, cadmium seems to be the most deleterious among heavy metals in the mushrooms. It accumulates in bones and can take the role of calcium. The average concentration of Cd present in the studied wild mushrooms was 0.1 mg kg^{-1}, which is far below the 0.2 mg kg^{-1} limit set by the WHO [35].

The average concentration of Pb present in the studied wild mushrooms was 0.28 mg kg^{-1}, which is far below the 10.0 mg kg^{-1} limit set by the WHO [35]. Pb levels reported in the literature are 0.4-7.77 mg kg^{-1} [35-40]. Pb creates health disorders such as sleeplessness, tiredness, hearing and weight loss [26].

Hazard index

In order to assess the contribution of some heavy metals to the health risk of mushroom consumption, we calculated the hazard quotients. We evaluated the health risk of mushroom consumption concerning different age-groups relying on the hazard index (Table 5). Assuming that the mushroom season lasts 6 months (from May until October), in the calculus we reckoned with a weekly mushroom consumption of 1 kg (DI = 0.0143 kg day^{-1} fresh weight) for adults and adolescents beyond 14, and of 0.5 kg (DI = 0.0071 kg day^{-1} fresh weight) for children and teenagers.

CONCLUSIONS

Results of the studied area showed that the selected metals concentrations were below the safe limits of WHO/FAO set for edible mushrooms and for foodstuffs. The lower concentrations of essential and toxic metals in morels resulted in low HI values. This could be attributed to the lack of anthropogenic input like mining and industry and low-scale agricultural activities. From the obtained concentrations of heavy metals one can conclude that the locality Batak mountain is an ecologically clean area very suitable for collecting wild edible mushrooms that we can use in our daily menu.

Table 5. The hazard index values for mushrooms grown in the Batak mountain.

	Hazard index (HI)				
Age groups	1-3	3-10	10-14	14-18	adult
Average body weight (kg)#	12	23	43	61	70
Morchella esculenta	0.665	0.347	0.186	0.131	0.230

#Source: European Food Safety Authority Journal

REFERENCES

1. K. Das, *NeBIO*, **1**, 1 (2010).
2. S. Wasser, A. Weis, *Int. J. Med. Mushrooms*, **1**, 31 (1999).
3. D. Agrahar-Murugkar, G. Subbulakshmi, *Food Chem.*, **89**, 599 (2005).
4. A. Wani, H. Bodha, A. Wani, *J. Med. Plants Res.*, **4**, 2598 (2010).
5. A. Sen, K. Madhivanan, D. Mukherjee, R. Aguilar, *Biomol. Concepts*, **3**, 117 (2012).
6. L. Dospatliev, M. Ivanova, *CR Acad. Bulg. Sci.*, **70,** 795 (2017).
7. Q. Liu, H. Liu, C. Chen, J. Wang, Y. Han, Z. Long, *PLoS ONE*, 12(**3**), 1, (2017), https://doi.org/10.1371/journal.pone.0174618.
8. M. Elmastas, O. Isildak, I. Turkekul, N. Temur, *J. Food Comp. Anal.*, **20**, 337 (2007).
9. B. Ribeiro, P. Valentao, P. Baptista, R. Seabra, *Food Chem. Toxicol.*, **45**, 1805 (2007).
10. U. Lindequist, T. Niedermeyer, W. Julich, *Evid. Based. Complement. Alternat. Med.*, **2**, 285 (2005).
11. M. Rai, G. Tidke, *Nat. Prod. Rad.*, **4**, 246 (2005).
12. T. Ajith, K. Janardhanan, *J. Clin. Biochem. Nutr.*, **40**, 157 (2007).
13. L. Dospatliev, M. Ivanova, *Bulg. Chem. Commun.*, **49**, G, 5 (2017).
14. I. Türkekul, F. Çetin, M. Elmastaş, *J. Appl. Biol. Chem.*, **60**, 35 (2017).
15. N. Sheena, B. Lakshmi, K. Janardhanan, P. Karst, *Nat. Prod. Rad.*, **4**, 382 (2005).
16. A. Sharma, S. Sharma, S. Chandel, E. Vatsa, B. Parashar, *WJPPS*, **5**, 685 (2016).
17. A. Colak, E. Sahin, M. Yildirim, E. Sesli, *Food Chem.*, **103**, 1426 (2007).
18. M. Kadiri, I. O. Fasidi, *Nigerian J. Sci.*, **24**, 86 (1990).
19. D. Plummer, An Introduction to Practical Biochemistry, McGraw Hill, 1971, p. 112.
20. P. A. Sheikh, G. H. Dar, W. A. Dar, S. Shah, K. A. Bhat, S. Kousar, *Vegetos*, **28**(**2**), 124 (2015).
21. P. Manzi, A. Aguzzi, L. Pizzoferrato, *Food Chem.*, **73**, 321 (2001).
22. Dir. 90/496/CEE
23. AOAC, Association of Official Analytical Chemist. Official methods of analysis, 20th edn., Washington, DC, 2016.
24. A. Heleno, L. Barrosa, M. Sousa, A. Martins, C. Santos-Buelga, I. Ferreira, *LWT Food Sci. Technol.*, **44**, 1343 (2011).
25. D. Stojkovic, F. Reis, J. Glamoclija, A. Ćirić, L. Barros, L. Van Griensven, I. Ferreira, M. Soković, *Food Funct.*, **5**, 1602 (2014).
26. U. Udochukwu, B. Nekpen, O. Udinyiwe, F. Omeje, *Int. J. Curr. Microbiol. App. Sci.*, **3**, 52 (2014).
27. L. Dospatliev, P. Zaprjanova, K. Ivanov, V. Angelova, *Bulg. J. Agric. Sci.*, **20**, 1380 (2014).
28. J. Brzezicha-Cirocka, M. Mędyk, J. Falandysz, P. Szefer, *Environ Sci Pollut. Res.*, **23**, 21517 (2016).
29. M. Gebrelibanos, N. Megersa, A. Taddesse, *International Journal of Food Contamination*, **3**, 1 (2016).
30. M. Mleczek, P. Niedzielski, P. Kalač, A. Budka, M. Siwulski, M. Gąsecka, P. Rzymski, Z. Magdziak, K. Sobieralski, *Environ. Sci. Pollut. Res.*, **23**, 16280 (2016).
31. L. Dospatliev, M. Ivanova, *Chemistry*, **26,** 377 (2017).
32. J. Falandysz, A. Sapkota, A. Dryżałowska, M. Mędyk, X. Feng, *Environ. Sci. Pollut. Res.*, **24**, 15528 (2017).
33. R. Naresh, B. Udaya, R. Byragi, *Int. J. Env. Sci.*, **3**, 28 (2012).
34. A. Quarcoo, G. Adotey, *Mycosph.*, **4**, 960 (2013).
35. WHO, World Health Organization Evaluation of Certain Foods Additives and Contaminants (Twenty-Sixth Report of the Joint FAO/WHO Expert Committee on Food Additives); WHO Library Cataloguing-in-Publication Data; WHO: Geneva, Switzerland, 1982.
36. P. Kalač, *J. Sci. Food Agric.*, **93**, 209 (2013).
37. C. Elekes, G. Busuioc, G. Ionita, *Not. Bot. Hort. Agrobot. Cluj*, **38**, 147 (2010).
38. I. Okwulehie, J. Ogoke, *IJAMBR*, **1**, 7 (2013).
39. P. George, T. Ranatunga, S. Reddy, G. Sharma, *Am. J. Food Tech.*, **9**, 360 (2014).
40. L. Dospatliev, M. Ivanova, *Oxid. Commun.*, **40**, 993 (2017).

РАСТЕЖ НА ОБИКНОВЕНАТА СМРЪЧКУЛА В БЪЛГАРИЯ: ХИМИЧЕСКИ ПРОФИЛ И ЗДРАВЕН РИСК

Л. Доспатлиев[1*], М. Иванова[2], М. Лачева[3], Ц. Радукова[4]

[1]Катедра "Фармакология, физиология на животните и физиологична химия", Ветеринарно-медицински факултет, Тракийски университет, 6000 Стара Загора, България
[2]Катедра "Информатика и математика", Стопански факултет, Тракийски университет, 6000 Стара Загора, България
[3]Катедра "Ботаника", Агрономически факултет, Аграрен университет – Пловдив, 4000 Пловдив, България
[4]Катедра "Ботаника и методика на обучението по биология", Биологически факултет, Пловдивски университет „Паисий Хилендарски", 4000 Пловдив, България

Постъпила на 21 юли, 2017; коригирана на 31 юли, 2018

(Резюме)

Обикновената смръчкула е една от най-високо оценените диви ядливи гъби. Гъбата е известна със своите лечебни свойства, антиоксидантна активност, хепатопротективна активност, антимикробни свойства и антитуморен ефект. Обикновената смръчкула е богата на въглехидрати (79.06 g 100 g^{-1} сухо тегло), последвани от протеини (11.19 g 100 g^{-1} сухо тегло) и пепел (7.32 g 100 g^{-1} сухо тегло). Съдържанието на мазнини е 2.43 g 100 g^{-1} сухо тегло. Също така беше определена влагата (89.41%) и изчислена общата енергия (1624.14 kJ 100^{-1} g^{-1} сухо тегло). Беше определена концентрацията на тежките метали в обикновената смръчкула: Pb (0.28 mg kg^{-1}), Cd (0.10 mg kg^{-1}), Cu (0.18 mg kg^{-1}), Co (0.28 mg kg^{-1}) , Ni (0.46 mg kg^{-1}), Cr (0.28 mg kg^{-1}), Fe (17.01 mg kg^{-1}) и Mn (0.96 mg kg^{-1}). Стойностите на здравния риск са изчислени за деца на възраст от 1 до 3 години (0.665), 3-10 години (0.347), 10-14 години (0.186), 14-18 години (0.131) и възрастни над 18 години (0.230). Според това изследване, обикновената смръчкула е годна за консумация и може да се използва в храненето на хората поради добрите си параметри. Съдържанието на тежки метали в пробите показва, че Баташката планина е екологично чист район в България и поради това гъбите, събрани от това място, могат да се консумират без риск за човешкото здраве.

Bulgarian Chemical Communications, Volume 50, Issue 4 (pp. 545 – 552) 2018

Effect of polyphenol extract from *Polygonum multiflorum* Thunb. root on the storage of minced red tilapia (*Oreochromis* sp.)

P. T. Q. Le[1*], V. M. Nguyen[2]

[1] *Institute of Biotechnology and Food Technology, Industrial University of Ho Chi Minh City, Ho Chi Minh City, Vietnam*

[2] *Department of Food Technology, College of Agriculture and Applied Biology, Can Tho University, Can Tho City, Vietnam*

Received, August 12, 2017; Accepted, January 9, 2018

This study was carried out to evaluate the effects of the polyphenol extract from *Polygonum multiflorum* Thunb. root on lipid oxidation and sensory characteristics of minced red tilapia (*Oreochromis* sp.) during frozen storage. Fresh fillets were minced in aqueous solutions of the root extract with some polyphenol concentrations of 830, 415, 277 and 208 mg GAE/L, extract solution/sample ratio of 1/20 (v/w), then stored at -20±2ºC, for up to 100 days. The best oxidation inhibition results on minced fish were achieved at the highest polyphenol concentrations of 830 and 415 mg GAE/L. Significant differences ($p<0.05$) in all quality parameters (pH, PoV, MDA, color parameter and sensory evaluation) of treated and control samples (blank control and water-treated or water control) were registered during storage time. The advantages of polyphenol extract were discussed. It can extend the shelf-life of products during frozen storage and was more effective to improve qualities of minced fish, especially at a polyphenol concentration of 415 mg GAE/L. Therefore, it can be concluded that the polyphenol extract from *Polygonum multiflorum* Thunb. root can potentially be used as an alternative source of natural antioxidant.

Keywords: Antioxidant, Frozen storage, Lipid oxidation, Minced fish.

INTRODUCTION

Red tilapia (*Oreochromis* sp.) is widely cultured in South Vietnam, especially Tien Giang, Vinh Long, Dong Thap province and its production is expanding every year. Red tilapia flesh is tasty and can produce various products as frozen fillet, minced fish, salted fish, etc. [1]. The current demand for aquatic products, especially frozen fish products, has increased quite quickly worldwide. These products are a valuable natural resource with high protein content and are rich in polyunsaturated fatty acids [2]. Its qualities were studied in various fish species by many storage methods. There are two main problems associated with frozen storage of fish products: protein denaturation, hydrolysis and oxidation of lipids [3]. Among them, oxidation of lipids occurs in raw material during storage, processing, heat treatment, and in the final products during subsequent storage [4]. It causes degradation of the product qualities, leading to undesirable changes in flavor, color, texture and nutrition, especially in the organoleptic characteristics.

Using antioxidant compounds of synthetic or natural origin in the process or storage is one of the methods to reduce or retard oxidation and prevent the loss of quality and sensory attributes [5]. In recent years, consumers and food industry are concerned about food safety and health. Hence, the use of synthetic compounds in food industry was reduced, natural antioxidants as polyphenols substituting synthetics, especially polyphenols from plants, were requested. However, the activity of these compounds is quite difficult to predict, each polyphenol has different mechanisms involved in its antioxidant effect.

Polygonum multiflorum Thunb. is considered to be one of the most important natural antioxidant herbal extracts. It is valuable medicine plant and contains high levels of polyphenol compounds in its root such as tannins, anthraquinones, flavonoids, etc. In addition, these compounds were reported for hair-blacking, liver and kidney-tonifying, anti-aging effects and curing of other diseases [6]. The positive effects of polyphenols from various materials on fish products have been observed and prevented rancidity of many lipid systems, for instance, polyphenol in green tea and onion extract [7], date seed extract [8], red grape pomace (peels and seeds) [9], etc., but until now, no research has studies the combination between storage methods and polyphenols from *Polygonum multiflorum* Thunb. root to preserve minced fish.

The main objective of this study was to evaluate

* To whom all correspondence should be sent:
E-mail: lephamtanquoc@iuh.edu.vn

the effects of polyphenol extract from *Polygonum multiflorum* Thunb. root on the physicochemical and sensory parameters of minced red tilapia. A better understanding of the reactions that occur during the storage process enables better quality products to be obtained.

EXPERIMENTAL

Materials

Extract preparation: Polygonum multiflorum Thunb. roots were harvested from Cao Bang province (Vietnam). The roots were then cleaned by tap water, sliced and dried at 60°C until the moisture level was less than 12%. The slices were then ground into fine powder (diameter less than 0.5 mm) and vacuum-packed. Polyphenols from the dried powder of *Polygonum multiflorum* Thunb. roots were extracted in a microwave system with acetone concentration of 57.35%, solid/solvent ratio of 1/39.98 (w/v), extraction time of 289 sec and microwave power of 127 W. The crude extract was filtered through Whatman paper [10]. The filtered extract was evaporated at 45^{o}C until the solvent was completely removed and the extract was used for preparation of 830, 415, 277 and 208 mg GAE/L solution in distilled water.

Preparation of minced red tilapia: Red tilapia (*Oreochromis* sp.) fish samples (of average weight = 600-800 g) were purchased from Vinmart supermarket in Ho Chi Minh city (samples originated from Tien Giang province, Vietnam). Each sample was deheaded, cleaned, filleted and minced with various extract concentrations, using an extract solution/sample ratio of 1/20 (v/w). In addition, there were two control samples including untreated control (UC) and water control (the water/sample ratio of 1/20, v/w) (WC). Minced samples were placed in polyethylene bags and stored in the freezer at -50^{o}C and after that, all samples were moved to a -20^{o}C freezer and maintained at this temperature during the storage time. Samples were analyzed every 20 days until 100 days of storage at -20^{o}C.

Chemicals and reagents: Folin-Ciocalteu and DPPH (2,2-diphenyl-1-picrylhydrazyl) reagents were purchased from Merck (Germany). TBA (2-thiobarbituric acid) and TMP (tetramethoxy propane) were supplied by Sigma-Aldrich (USA). All other chemicals and organic solvents were of analytical reagent grade.

Determination of total phenolic content (TPC) and antioxidant capacity (AC) of extract

The TPC in the extract was determined by a slightly modified Folin-Ciocalteu colorimetric method [11]. The results were based on a standard curve obtained with gallic acid. TPC was expressed as mg of gallic acid equivalent per gram of dry weight (mg GAE/g DW).

The AC of the extract was determined by DPPH assay which was adapted and modified from studies of Soto *et al.* (2014) [12] and Chmelová *et al.* (2015) [13], with slight modification. Trolox was used as the standard. AC was expressed in TEAC (Trolox equivalent antioxidant capacity) determined as μmol of Trolox per gram of dry weight (μmol TE/g DW).

Chemical analysis

pH: According to Shim *et al.* (2012) [14], the pH value of 5 g samples blended with 20 mL distilled water for 60 s in a homogenizer (Panasonic 1L MX-AC400WRA, Japan) was determined with a pH meter (Trans Instruments BP3001, Singapore).

PoV: The PoV values were determined according to Seo *et al.* (2016) [15] with slight modifications. The lipids from the minced fish samples (5 g) were homogenized with 50 mL of acetic acid-isooctane for 5 min. Then, the samples were filtered through Whatman paper, 1 mL of saturated potassium iodide solution was added to the filtered extracts, shaken gently for 1 min and then 100 mL of distilled water and 0.5 mL of 0.1% starch solution were added. The obtained solution was titrated with 0.01 N sodium thiosulfate ($Na_2S_2O_3$) solution until the violet color disappeared. The results were expressed as meq oxygen/kg sample.

Thiobarbituric acid reactive substances (TBARS): TBARS values were determined by the method of Vyncke (1970) [16] with some slight modifications. Firstly, samples (5 g) were homogenized in 20 mL of 10% trichloroacetic acid (TCA) solution and 0.5 mL of BHT. Then, the samples were filtered through Whatman paper and made up to 100 mL with 10% TCA solution. The filtrate (5 mL) was mixed with 5 mL of 0.02 M 2-thiobarbituric acid (TBA) solution, heated in a boiling water bath at 100^{o}C for 35 min to develop the rose-pink color from the reaction between malondialdehyde and TBA; then cooled by tap water for 10 min. Absorbance was measured at 532 nm against a blank prepared with 5 mL of 0.02 M TBA solution and 5 mL of 10% TCA solution, using a spectrophotometer. TBARS values were μg of malondialdehyde (MDA)/kg of sample.

Color parameters: Color parameters consist of of L^* (lightness), a^* (from redness to greenness), b^* (from yellowness to blueness) values were recorded and determined on a Chroma Meter CR-400

(Minolta, Japan). The instrument was calibrated with a standard light plate and three different positions on the surface of each sample were measured for each storage time.

Sensory evaluations: Samples were prepared according to Masniyom *et al.* (2005) [17] with some slight modifications. The minced frozen samples were cut into 30×20×20 mm cubes, thawed, wrapped with aluminum foil and steamed for 15 min at 70°C. 60 non-trained panelists evaluated the steamed minced fish by color, odor, taste, texture and overall acceptability; using 9-point hedonic scales from 1 (dislike extremely) to 9 (like extremely) [18].

Data analysis

The experimental data were analyzed by the one-way analysis of variance (ANOVA) method and significant differences between the means from triplicate analyses at ($p<0.05$) were determined by Fisher's least significant difference (LSD) procedure using Statgraphics software (Centurion XV). The values obtained were expressed as mean±standard deviation (SD).

RESULTS AND DISCUSSION

Total polyphenol content and antioxidant capacity

The TPC and AC values of the extract were 47.53±0.79 mg GAE/g DW and 334.07±3.04 μmol TE/g DW, respectively. TPC and TEAC of samples from the MAE method were higher than those of samples from China which were extracted by the decoction method with deionized water as solvent (33.91±0.62 mg GAE/g DW; 257.9±3.7 μmol TE/g DW) and maceration methods with 50% ethanol as solvent (40.42±0.63 mg GAE/g DW; 256.7±0.7 μmol TE/g DW) [19].

The results showed that factors such as extraction methods, land, gender, etc., caused the differences in TPC and AC values. The crude extract was filtered and evaporated at 45°C until the solvent was completely removed. The extract was used for preparation of 830, 415, 277 and 208 mg GAE/L solution in distilled water to mince with fish fillet.

Changes in the pH value

Table 1 showed that the pH values were significantly different ($p<0.05$) from the storage time in the frozen storage. Indeed, they fluctuated and increased slightly after 100 days of frozen storage but all samples did not have any signs of damage such as rancid odor. However, the pH values of the initial samples were not affected by polyphenol in the extract.

The results showed that the shelf-life of the product would depend on the storage method and support of antioxidant as synthetic or natural additive, especially polyphenol from *Polygonum multiflorum* Thunb. roots. Phenolic compounds could affect the pH values and change some qualities of the product. Frozen storage can stabilize temperature of -20°C, inhibits micro-organisms, minimizes the biochemical processes of the product and extends the storage time with support of antioxidant.

In general, the change of pH value depends on many factors including material, diet, harvest season, stress levels, storage methods and support agents. The pH value of fish was approximately 7 initially, but then would decrease because glycogen would be hydrolyzed into lactic acid after death. The pH value would tend to increase again during storage.

Table 1. pH values of minced fish during the storage

Storage time (Days)	Polyphenol concentration of extract (mg GAE/L)					
	UC	WC	830	415	277	208
0	6.90 ± 0.09^{Aabc}	6.83 ± 0.07^{Aa}	6.85 ± 0.11^{Abc}	6.74 ± 0.10^{Aa}	6.79 ± 0.12^{Aab}	6.85 ± 0.14^{Aab}
20	6.84 ± 0.16^{Ca}	6.82 ± 0.01^{BCa}	6.61 ± 0.08^{Aa}	6.67 ± 0.04^{ABa}	6.70 ± 0.05^{ABCa}	6.78 ± 0.11^{BCa}
40	6.88 ± 0.03^{BCab}	6.90 ± 0.01^{Cab}	6.80 ± 0.05^{Ab}	6.83 ± 0.04^{ABb}	6.86 ± 0.06^{ABCbc}	6.90 ± 0.03^{Cabc}
60	7.03 ± 0.01^{Bc}	7.01 ± 0.10^{Bc}	6.90 ± 0.02^{Abc}	6.95 ± 0.02^{ABc}	6.98 ± 0.03^{ABd}	7.00 ± 0.01^{Bc}
80	6.99 ± 0.01^{BCbc}	7.01 ± 0.02^{Cc}	6.94 ± 0.02^{Ac}	6.94 ± 0.01^{Ac}	6.98 ± 0.02^{BCd}	6.96 ± 0.02^{ABbc}
100	6.85 ± 0.02^{Aa}	6.94 ± 0.01^{Cbc}	6.91 ± 0.02^{Bc}	6.92 ± 0.01^{BCc}	6.93 ± 0.01^{BCcd}	6.85 ± 0.01^{Aab}

Different superscript lower-case letters in the same column denote significant differences ($p<0.05$).
Different superscript capital letters in the same row denote significant differences ($p<0.05$).

These results are similar to those of Khalafalla *et al.* (2015) [20] who preserved Nile tilapia fillet (*Oreochromis niloticus*) using natural herbs such as thyme (*Thymus vulgaris*) extract and rosemary (*Rosmarinus officinalis*) extract, or Patagonian hake (*Merluccius hubbsi*) minces and fillets which were

preserved by the frozen method [21]. The increase of pH value might be due to endogenous enzymes in the material or microbial enzymes, which produced volatile bases such as ammonia or trimethylamine, which would increase the pH value [22]. Conversely, in some cases the pH did not change significantly, as shown in the study of Aubourg *et al.* (2004) [23] that preserved horse mackerel (*Trachurus trachurus*) by the freezing method with citric and ascorbic acid; or slightly decreased when Rostamzad *et al.* (2011) [24] preserved Persian sturgeon (*Acipenser persicus*) fillets by the freezing method with ascorbic acid. Although the change of pH values is negligible it is quite important in preservation, because it is related to structural changes and deterioration in the quality of materials during storage time.

Changes in the PoV value

The PoV values of all samples of this storage method was significantly different during storage time ($p<0.05$). The PoV values increased steadily after 100 days of storage, especially in control samples including UC and WC (6.53 and 6.84 meq/kg, respectively). The others kept a lower PoV value during storage time. The concentration of polyphenol extract increases with the decrease of PoV value (Table 2). Results show that polyphenol extract from *Polygonum multiflorum* Thunb. roots strongly affects the PoV value.

During storage time, the PoV value of the fish product steadily increases in spite of the storage methods used. The level of increase of PoV value could depend on many factors such as composition of raw material, storage method and antioxidants. There are some different mechanisms which affect lipid oxidation such as lipoxygenase enzyme, photo-oxidation, especially a free radical mechanism. Among them, autoxidation is a spontaneous reaction of molecular oxygen with lipids, leading to oxidative deterioration and proceeds by a free radical chain mechanism. The lipid oxidation is stopped by antioxidants that interrupt the free radical chain reaction. In addition, photo-oxidation also leads to the formation of hydroperoxides because of the presence of sensitizer and light which excite the reaction between oxygen and unsaturated fatty acids [25].

The presence of polyphenol extract may retard lipid oxidation by preventing the formation of free radicals or by interrupting the propagation of them through several mechanisms including scavenging species that initiate peroxidation, quenching $^{*}O_2$ - preventing formation of peroxides, breaking the autoxidative chain reaction, reducing localized O_2 concentrations and chelating metal ions so that they would be unable to generate reactive species or decompose lipid peroxides [26]. This result is in agreement with Ozen *et al.* (2011) [27] who stored minced chub mackerel (*Scomber japonicus*) muscle by the freezing method by adding red grape seed extracts and pomegranate seed extracts; or the study of Ozogul *et al.* (2010) [28] who refrigerated sardine (*Sardinella pilchardus*) fillets by immersing them in a solution of rosemary extract.

Changes in the TBARS value

Based on table 3, TBARS values of all samples are significantly different ($p<0.05$) and would tend to increase during storage time. Polyphenol concentrations increase with the decrease of the TBARS values. The combination of frozen storage and polyphenol extract produced positive effect on the inhibition of lipid oxidation. Extracts with concentrations of 830 and 415 mg GAE/L had the lowest TBARS values of 440.57 and 517.78 µg/kg while those of control samples were 781.35 and 1016.18 µg/kg after 100 days of storage. Those showed that TBARS values were dependent on storage method, raw material and antioxidant.

Table 2. PoV values (meq/kg) of minced fish during the storage

Storage time (Days)	Polyphenol concentration of extract (mg GAE/L)					
	UC	WC	830	415	277	208
0	1.12 ± 0.30^{Aa}	1.27 ± 0.11^{Aa}	1.27 ± 0.12^{Aa}	1.26 ± 0.21^{Aa}	1.06 ± 0.12^{Aa}	1.18 ± 0.21^{Aa}
20	1.85 ± 0.22^{ABb}	1.99 ± 0.35^{Bb}	1.53 ± 0.23^{Aa}	1.79 ± 0.21^{ABb}	1.86 ± 0.31^{ABb}	1.79 ± 0.19^{ABb}
40	3.05 ± 0.11^{Cc}	3.29 ± 0.28^{Cc}	2.20 ± 0.21^{Ab}	2.52 ± 0.12^{ABc}	2.58 ± 0.22^{Bc}	2.62 ± 0.17^{Bc}
60	4.31 ± 0.10^{CDd}	4.62 ± 0.27^{Dd}	2.66 ± 0.09^{Ac}	3.29 ± 0.29^{Bd}	3.62 ± 0.27^{Bd}	4.09 ± 0.15^{Cd}
80	5.12 ± 0.08^{De}	5.24 ± 0.13^{De}	3.38 ± 0.19^{Ad}	4.11 ± 0.15^{Be}	4.31 ± 0.29^{BCe}	4.50 ± 0.33^{Ce}
100	6.53 ± 0.13^{Df}	6.84 ± 0.33^{Df}	4.91 ± 0.23^{Ae}	5.45 ± 0.14^{Bf}	5.57 ± 0.20^{Bf}	6.09 ± 0.21^{Cf}

Different superscript lower-case letters in the same column denote significant differences ($p<0.05$).
Different superscript capital letters in the same row denote significant differences ($p<0.05$).

Table 3. TBARS values (μg MDA/kg) of minced fish during the storage

Storage time (Days)	Polyphenol concentration of extract (mg GAE/L)					
	UC	WC	830	415	277	208
0	238.39 ± 16.11^{Aa}	246.17 ± 9.19^{Aa}	243.27 ± 9.28^{Aa}	233.49 ± 24.65^{Aa}	233.02 ± 24.6^{Aa}	241.34 ± 9.21^{Aa}
20	355.09 ± 9.26^{Db}	388.65 ± 9.17^{Eb}	244.72 ± 9.14^{Aa}	272.16 ± 18.34^{Bbc}	277.64 ± 9.36^{Bb}	319.82 ± 24.26^{Cb}
40	408.57 ± 9.26^{Cc}	485.88 ± 9.21^{Dc}	276.37 ± 9.14^{ABb}	271.63 ± 18.31^{Ab}	276.53 ± 9.32^{ABb}	298.64 ± 18.67^{Bb}
60	480.56 ± 18.42^{Dd}	547.61 ± 9.26^{Ed}	330.99 ± 9.34^{Bc}	302.74 ± 9.14^{Ac}	361.88 ± 9.30^{Cc}	373.36 ± 9.32^{Cc}
80	786.69 ± 18.49^{De}	872.08 ± 18.49^{Ee}	544.36 ± 24.36^{Ae}	606.94 ± 18.38^{Be}	706.63 ± 24.46^{Ce}	780.67 ± 9.30^{De}
100	781.35 ± 16.01^{De}	1016.18 ± 9.24^{Ef}	440.57 ± 18.75^{Ad}	517.78 ± 9.21^{Bd}	653.26 ± 27.73^{Cd}	750.82 ± 16.04^{Dd}

Different superscript lower-case letters in the same column denote significant differences ($p<0.05$).
Different superscript capital letters in the same row denote significant differences ($p<0.05$).

TBARS value of the fish product always appears during storage time and was determined by the MDA content. During the secondary oxidation process, aldehydes, especially MDA, are formed [29], which are used to test for rancid food products. Changes of TBARS values also depend on lipoxygenase, peroxidase enzyme, autoxidation and photo-oxidation [25]. In addition, several proteins are bound to iron such as myoglobin, hemoglobin, ferritin and transferrin. During storage time, iron is released and then activates oxygen, which results in lipid oxidation [30]. The increase in TBARS value agreed with Maqsood *et al.* (2015) [8] who preserved minced mackerel (*Rastrelliger kanagurta*) by combination of iced storage date seed extract or with Aubourg *et al.* (2004) [23] who preserved horse mackerel (*Trachurus trachurus*) by the freezing method with citric and ascorbic acid.

Results proved that the presence of polyphenol extract from *Polygonum multiflorum* Thunb. roots inhibited the increase of TBARS value. The antioxidants had different abilities in preventing primary and secondary oxidation products formation [25]. However, the composition and content of fatty acid in the raw material also affected TBARS values during storage time; for instance, Tang *et al.* (2001) [31] refrigerated raw minced red meat, poultry and fish muscle during 10 days, and observed that the increase in TBARS values of all samples was completely different. Hence, to evaluate the quality of product, many quality factors are required to be assessed besides TBARS values.

Changes in the color parameters

The results of color analysis are presented in table 4. Color parameters (L^*, a^*, b^*) of the initial samples were slightly affected by the color of extract and they were significantly different ($p<0.05$) during storage time. The trend of color change was quite complex, L^*, a^* and b^* fluctuated slightly after 100 days of storage, but in general, they changed negligibly (except L^* values). The results obtained were similar with those of Paola and Isabel (2015) [32] with freezed mackerel fillet (*Scomber japonicus*); the L^* value slightly decreased, whereas a^* and b^* values changed insignificantly after 12 months.

Changes of fish product color were caused by the amount of soluble proteins which could strongly affect color parameters, especially L^* value. Protein structural changes resulted in the reflection of incident light and the light becomes scattered, causing interference, thus affecting the appearance of the flesh [33]. In addition, the color parameters were influenced by the retention of connective tissue and lipid content in the initial materials [34]. Besides, lipid oxidation could lead to an increase in the oxidation of oxymyoglobin to myoglobin, which would also causes color change [35]. Therefore, the color changes of the product could depend on several different factors including storage methods, antioxidants, raw material and process methods. Therefore, antioxidant usage would only restrict parts of the color changes in the products.

Changes in sensory attributes

Frozen storage proved most effective in extending shelf-life of products and in retaining quality index. In addition, the presence of polyphenol, especially in high polyphenol concentrations of 830 and 415 mg GAE/L, could inhibit the rise in PoV and TBARS values and would lessen the change of product color. However, the dark color of the botanical extracts could alter the visual perception of some food products. Sample of 415 mg GAE/L was chosen for sensory attributes evaluation and compared with control samples after 100 days of storage because this lower concentration did not affect natural odor and color of product.

Table 4. Color parameters of minced fish during the storage

Storage time (Days)	Polyphenol concentration of extract (mg GAE/L)					
	UC	WC	830	415	277	208
			L^*			
0	71.34 ± 0.05^{Ac}	70.78 ± 0.53^{Ac}	73.51 ± 1.43^{BCbc}	74.50 ± 0.63^{Ce}	74.07 ± 0.16^{BCf}	73.06 ± 0.53^{Bf}
20	71.37 ± 0.06^{Ec}	69.49 ± 0.09^{Ab}	69.92 ± 0.07^{Ba}	70.25 ± 0.04^{Cc}	73.08 ± 0.01^{Fe}	70.62 ± 0.04^{Dc}
40	74.55 ± 0.02^{Fd}	70.83 ± 0.07^{Cc}	72.66 ± 0.04^{Db}	73.42 ± 0.04^{Ed}	68.74 ± 0.06^{Bc}	68.18 ± 0.02^{Ab}
60	76.47 ± 0.04^{Fe}	75.48 ± 0.03^{Ed}	74.22 ± 0.06^{Cc}	74.68 ± 0.06^{De}	72.56 ± 0.03^{Bd}	72.25 ± 0.04^{Ae}
80	69.31 ± 0.03^{Db}	62.66 ± 0.03^{Aa}	73.38 ± 0.01^{Fbc}	67.11 ± 0.07^{Cb}	65.43 ± 0.06^{Bb}	71.14 ± 0.02^{Ed}
100	66.93 ± 0.01^{Da}	75.46 ± 0.06^{Fd}	70.41 ± 0.01^{Ea}	65.26 ± 0.03^{Ba}	64.69 ± 0.01^{Aa}	66.42 ± 0.04^{Ca}
			a^*			
0	2.23 ± 0.02^{Aa}	2.42 ± 0.04^{Bb}	4.79 ± 0.05^{Fd}	3.80 ± 0.07^{Df}	4.64 ± 0.03^{Ef}	3.60 ± 0.09^{Cd}
20	2.44 ± 0.02^{Bb}	1.02 ± 0.02^{Aa}	4.46 ± 0.07^{Ec}	3.62 ± 0.03^{De}	3.13 ± 0.02^{Cb}	4.51 ± 0.01^{Ef}
40	2.75 ± 0.01^{Ec}	5.83 ± 0.05^{Ff}	2.67 ± 0.02^{Da}	2.12 ± 0.01^{Ca}	1.39 ± 0.06^{Aa}	1.67 ± 0.02^{Bb}
60	2.47 ± 0.02^{Bb}	5.29 ± 0.07^{Ee}	3.76 ± 0.03^{Db}	3.53 ± 0.03^{Cd}	3.74 ± 0.03^{De}	1.29 ± 0.03^{Aa}
80	2.49 ± 0.05^{Ab}	3.04 ± 0.04^{Bc}	4.79 ± 0.07^{Dd}	3.36 ± 0.03^{Cc}	3.42 ± 0.08^{Cd}	2.45 ± 0.09^{Ac}
100	2.42 ± 0.07^{Ab}	3.25 ± 0.04^{Cd}	3.69 ± 0.06^{Db}	2.62 ± 0.06^{Bb}	3.26 ± 0.05^{Cc}	3.74 ± 0.06^{De}
			b^*			
0	9.79 ± 0.32^{Aa}	10.27 ± 0.02^{Bc}	12.3 ± 0.24^{Dd}	11.35 ± 0.30^{Cc}	11.73 ± 0.29^{Cd}	10.39 ± 0.06^{Cd}
20	10.32 ± 0.01^{Bb}	9.51 ± 0.07^{Aa}	12.00 ± 0.06^{Ec}	10.41 ± 0.05^{Bb}	10.61 ± 0.08^{Cb}	10.97 ± 0.04^{De}
40	10.52 ± 0.02^{Eb}	11.36 ± 0.05^{Fd}	9.44 ± 0.04^{Ca}	9.56 ± 0.02^{Da}	7.25 ± 0.03^{Aa}	7.84 ± 0.03^{Ba}
60	12.03 ± 0.06^{Bc}	12.42 ± 0.07^{Cf}	12.67 ± 0.01^{De}	12.9 ± 0.06^{Ee}	14.87 ± 0.06^{Fe}	9.09 ± 0.05^{Ab}
80	10.37 ± 0.08^{Bb}	9.83 ± 0.05^{Ab}	14.63 ± 0.06^{Ef}	11.87 ± 0.10^{Dd}	10.92 ± 0.04^{Cc}	9.73 ± 0.09^{Ac}
100	9.80 ± 0.08^{Aa}	11.54 ± 0.05^{Ee}	10.60 ± 0.08^{Bb}	11.18 ± 0.07^{Dc}	10.87 ± 0.06^{Cc}	11.61 ± 0.03^{Ef}

Different superscript lower-case letters in the same column denote significant differences ($p<0.05$).
Different superscript capital letters in the same row denote significant differences ($p<0.05$).

Table 5. Sensory evaluation of steamed minced fish

Samples	Texture	Color	Taste	Odor	Overall acceptability
UC	5.90 ± 0.99^{a}	6.22 ± 0.85^{b}	5.33 ± 1.11^{a}	5.03 ± 0.92^{a}	5.77 ± 0.85^{b}
WC	5.83 ± 0.69^{a}	5.87 ± 0.77^{a}	5.58 ± 0.72^{a}	5.18 ± 0.7^{a}	5.28 ± 0.74^{a}
415 mg GAE/L	6.27 ± 0.86^{b}	6.77 ± 0.93^{c}	6.75 ± 0.97^{b}	7.00 ± 0.76^{b}	7.03 ± 0.76^{c}

Different superscript lower-case letters in the same column denote significant differences ($p<0.05$).

The minced fish was evaluated in terms of consumer acceptability including odor, color, taste, texture and overall acceptability. Table 5 showed the results of the sensory evaluation of minced fish. There were no significant differences in texture, taste and odor ($p>0.05$) between control samples. However, all sensory scores of the sample of 415 mg GAE/L were higher than those of control samples and there were significant differences in all sensory attributes ($p<0.05$). Addition of polyphenol extract in minced fish did not adversely affect the odor, color, taste, texture and overall acceptability of steamed minced fish. It tended to increase the scores of sensory attributes. The overall acceptability scores of samples ranged from 5.28 to 7.03, with maximum acceptability obtained with polyphenol concentration of 415 mg GAE/L.

CONCLUSION

According to the present results, the use of polyphenol extract from *Polygonum multiflorum* Thunb. roots rendered minced fish less prone to oxidation than untreated samples. Polyphenol which acts as an antioxidant during minced fish storage offers many advantages such as extending the shelf-life of products and improving important qualities indexes. The antioxidant activities of polyphenol extract were recorded without any adverse effect on the sensory acceptability of the treated minced fish.

Acknowledgments: *The authors wish to thank Bui Long Bao, Tran Huu Dai, Chu Viet Ha, Dinh Thi Phuong Loan and Dr. Tran Thanh Truc for their supports.*

REFERENCES

1. N. T. N Ha, D. T. T. Huong, *J. Sci. Can Tho University*, **40**, 15 (2015).
2. K. Vareltzis, D. Koufidis, E. Gavriilidou, E. Papavergou, S. Vasiliadou, *Z. Lebensm. Unters. Forsch. A*, **205**, 93 (1997).
3. S. Simeonidou, A. Govaris, K. Vareltzis, *Z. Lebensm. Unters. Forsch. A*, **204**, 405 (1997).
4. S. Selmi, S. Sadok, *Pan-Am. J. Aquat. Sci*., **3**, 36 (2008).
5. M. Serdarglu, E. Felekoglu, *J. Food Qual*., **28**, 109 (2005).
6. L. Lin, B. Ni, H. Lin, M. Zhang, X. Li, X. Yin, C. Qu, J. Ni, *J. Ethnopharmacol*., **159**, 158 (2015).
7. S. Haghparast, H. Kashiri, G. Alipour, B. Shabanpour, *J. Agr. Sci. Tech*., **13**, 855 (2011).
8. S. Maqsood, P. Kittiphattanabawon, S. Benjakul, P. Sumpavapol, A. Abushelaibi, *Int. Food Res. J*., **22**, 1180 (2015).
9. I. Sanchez-Alonso, A. Jimenez-Escrig, F. Saura-Calixto, A. J. Borderıas, *Food Chem.*, **101**, 372 (2007).
10. L. P. T. Quoc, N.V. Muoi, *J. Sci. Technol*., **53**, 1 (2015).
11. A. Siddiqua, K. B. Premakumari, R. Sultana, S. Vithya, *Int. J. Chem. Tech. Res.*, **2**, 205 (2010).
12. C. Soto, E. Caballero, E. Pérez, M. E. Zúñiga, *Food Bioprod. Process*., **92**, 328 (2014).
13. D. Chmelová, M. Ondrejovič, M. Havrlentová, P. Hozlár, *J. Microbiol. Biotechnol. Food Sci*., **4**, 63 (2015).
14. S. Y. Shim, Y. S. Choi, H. Y. Kim, H. W. Kim, K. E. Hwang, D. H. Song, M. A. Lee, J. W. Lee, C. J. Kim, *Food Sci. Biotechnol*., **21**, 565 (2012).
15. H. W. Seo, J. K. Seo, H. S. Yang, *Korean J. Food Sci. Anim. Resour*., **36**, 198 (2016).
16. W. Vyncke, *Eur. J. Lipid Sci. Technol*., **72**, 1084 (1970).
17. P. Masniyom, S. Benjakul, W. Visessanguan, *LWT-Food Sci. Technol*., **38**, 745 (2005).
18. M. C. Meilgaard, G. V. Civille, B. T. Carr, Sensory evaluation techniques, CRC Press, New York, 2007.
19. H. B. Li, Y. Jiang, C. C. Wong, K. W. Cheng, F. Chen, *Anal. Bioanal. Chem*., **388**, 483 (2007).
20. F. A. Khalafalla, F. H. M. Ali, A. R. H. A. Hassan, *Beni-Suef University J. Basic Appl. Sci*., **4**, 33 (2015).
21. A. S. Ciarlo, R. L. Boeri, D. H. Giannini, *J. Food Sci*., **50**, 723 (1985).
22. M. Chaijan, S. Benjakul, W. Visessanguan, C. Faustman, *Food Chem*., **93**, 607 (2005).
23. S. Aubourg, F. Alenso, M. Gallardo, *Eur. J. Lipid Sci. Technol*., **106**, 232 (2004).
24. H. Rostamzad, B. Shabanpour, A. Shabani, *Int. Food Res. J*., **18**, 109 (2011).
25. E. Wsowicz, A. Gramza, M. Hes, H. H. Jelen, J. Korczak, M. Maecka, S. Mildner-Szkudlarz, M. Rudzinska, U. Samotyja, R. Zawirska-Wojtasiak, *Pol. J. Food Nutr. Sci*., **13**, 87 (2004).
26. W. F. Nawar, in: Food chemistry, O. R. Fennema (ed.), Marcel Dekker, New York, 1996, p. 225.
27. B. O. Ozen, M. Eren, A. Pala, I. Ozmen, A. Soyer, *Int. J. Food Sci. Technol*., **46**, 724 (2011).
28. Y. Ozogul, D. Ayas, H. Yazgan, F. Ozogul, E.K. Boga, G. Ozyurt, *Int. J. Food Sci. Technol*., **45**, 1717 (2010).
29. R. Guillén-Sans, M. Guzmán-Chozas, *Crit. Rev. Food Sci. Nutr*., **38**, 315 (1998).
30. A. J. Angelo, J. Vercellotti, T. Jacks, M. Legendre, *Crit. Rev. Food Sci. Nutr*., **36**, 175 (1996).
31. S. Tang, D. Sheehan, D. J. Buckley, P. A. Morrissey, J. P. Kerry, *Int. J. Food Sci. Technol*., **36**, 685 (2001).
32. A. S. Paola, Y. M. Isabel, *J. Food Res*., **4**, 135 (2015).
33. D. H. F. Robb, in: Farmed Fish Quality, S. C. Kestin, P. D. Warris (eds.), Blackwell Science, London, 2001, p. 220.
34. H. G. Kristinsson, A. E. Theodore, N. Demir, B. Ingadottir, *J. Food Sci*., **70**, 298 (2005).
35. W. K. M. Chan, C. Faustman, E. A. Decker, *J. Food Sci*., **62**, 709 (1997).

ВЛИЯНИЕ НА ПОЛИФЕНОЛОВ ЕКСТРАКТ ОТ КОРЕНИ НА *Polygonum multiflorum* THUNB. ВЪРХУ СЪХРАНЕНИЕТО НА НАРЯЗАНА ЧЕРВЕНА ТИЛАПИЯ (*Oreochromis* SP.)

П. Т. К. Ле[1*] , В. М. Нгуен[2]

[1] *Институт по биотехнология и технология на храните, Индустриален университет на град Хо Ши Мин, Хо Ши Мин, Виетнам*

[2]*Департамент по технология на храните, Колеж по селско стопанство и приложна биология, Университет на Кан То, Кан То, Виетнам*

Постъпила на 12 август, 2017; приета на 9 януари, 2018

(Резюме)

Целта на това изследване е да се оцени влиянието на полифенолов екстракт от корените на *Polygonum multiflorum* Thunb. върху окислението на липидите и сензорните характеристики на нарязана червена тилапия (*Oreochromis* sp.) по време на съхранението й в замразено състояние. Пресни рибни филета, потопени в 5% (v/w) водни разтвори на екстракта с концентрация на полифенола 830, 415, 277 и 208 mg GAE/L, са съхранявани при-20±2ºC за срок до 100 дни. Най-добри резултати за инхибицията на окислението на нарязаната риба са получени при най-високите концентрации на полифенол - 830 и 415 mg GAE/L. По време на съхранението са установени значителни разлики ($p<0.05$) при всички качествени параметри (pH, PoV, MDA, цвят и сензорна оценка) на обработените и контролните проби (празна проба и проба, обработена с вода). Обсъдени са предимствата на полифенолния екстракт – може да удължи търговския живот на продуктите при съхранението им в замразено състояние, като е най-ефективен при концентрация на полифенол 415 mg GAE/L. Следователно, може да се заключи, че полифенолният екстракт от корените на *Polygonum multiflorum* Thunb. би могъл да се използва като алтернативен източник на природни антиоксиданти.

Bulgarian Chemical Communications, Volume 50, Issue 4 (pp. 553 – 559) 2018

Polyphenol content and antioxidant activity of aqueous/methanol extracts from different tobacco species (*Nicotiana*)

M. H. Docheva[1*], V. T. Popova[2], T. A. Ivanova[2], V. V. Nikolova[1], T. H. Hristeva[1], N. N. Nikolov[1]

[1] *Tobacco and Tobacco Products Institute, 4108 Markovo, Bulgaria*
[2] *University of Food Technologies, 26, Maritsa Blvd., 4002 Plovdiv, Bulgaria*

Received, July 17, 2018; Revised, September 2, 2018

The aim of the study was to characterize the polyphenol content in the leaves of different tobacco species (*N. alata* Link & Otto, *N. rustica* L., *N. tabacum* L.), as well as to obtain extracts enriched in phenolic acids and flavonoids, and to evaluate their radical-scavenging activity. The content of chlorogenic acid in the leaves varied from 2.44 ± 0.21 mg/g (*N. rustica*) to 7.10 ± 0.50 mg/g (*N. alata*), and that of rutin – from 0.55 ± 0.05 mg/g (*N. alata*) to 10.85 ± 0.80 mg/g (*N. rustica*). The content of flavonoids was in the range from 0.66 ± 0.12 mg/g (*N. alata*) to 11.51 ± 0.8 mg/g (*N. rustica*). Two types of extracts were obtained using a macroporous resin – enriched in phenolic acids (PA) and enriched in flavonoids (F). The concentration of phenolic acids in Extracts PA was from 6.33 ± 0.50 mg/g (*N. tabacum*) to 3.88 ± 0.20 mg/g (*N. rustica*), and the recovery of phenolic acids – from 71 % to 86 %. Extracts F from *N. rustica* and *N. tabacum* were with flavonoid content of 9.7 ± 0.7 mg/g and 6.15 ± 0.4 mg/g, respectively, and those from the two genotypes of *N. alata* – with only 0.43 ± 0.09 mg/g. The recovery of flavonoids was 72 ± 9 %. Extracts PA were maximally purified from flavonoids, and Extracts F – from phenolic acids. All extracts revealed high antioxidant activity, having IC_{50} values from 5.82 ± 0.97 μg/ml (*N. rustica*) to 14.56 ± 2.61 μg/ml (*N. tabacum*). The results from the study give grounds for regarding the investigated *Nicotiana* species as a promising plant material for obtaining purified natural extracts with potential use in biopharmacy.

Keywords: Polyphenols, Tobacco, Aqueous/methanol extracts, Antioxidant activity

INTRODUCTION

The taxonomy of the genus *Nicotiana*, family *Solanaceae*, includes more than 70 species [1], of which only *Nicotiana tabacum* L. (common tobacco), and to a much lesser extent – *N. rustica* L. (also known as Aztec tobacco, or wild tobacco), are commercially cultivated and widely used for the manufacture of various tobacco products for smoking, snuffing, or oral use. Tobacco is an important cash crop in many countries throughout the world, and it is considered one of the most thoroughly investigated plant materials, along with tea and coffee. More than 4500 individual chemical constituents are identified in the different types, varieties, and selection lines of tobacco, or at different stages of its vegetation and processing. A significant part of these substances are biologically active, e.g., polyphenols, alkaloids, terpenes, saponins, carotenoids, *etc*. [2, 3]. Currently, more than 15 polyphenol metabolites have been identified in *N. tabacum* L., representing the groups of phenolic acids and flavonoids. The major polyphenols in tobacco are chlorogenic acid (3-*O*-caffeoylquinic acid) and its isomers neochlorogenic acid (5-*O*-caffeoylquinic acid) and 4-*O*-caffeoylquinic acid, and the flavonoids rutin (quercetin-3-rutinoside) and kaempferol-3-rutinoside [4–6]. Chlorogenic acid and rutin (vitamin P) possess a wide spectrum of biological activities, e.g., antioxidant, antibacterial, anti-inflammatory, anti-mutagenic and antitumor properties [7, 8].

The available information about the phytochemical characteristics of other *Nicotiana* species (e.g., *N. affinis, N. rustica, N. alata grandiflora, N. longiflora, N. sylvestris, N. wigandioides, etc*.) is relatively limited, and the research has been focused mainly on their alkaloid content [1, 9, 10].

Undoubtedly, over the last years, the interest in the obtaining and application of extracts from traditional or exotic medicinal plants has been constantly growing, and tobacco is a part of this tendency as well. It has been established that the extracts enriched in phenolic acids and flavonoids obtained from different types or varieties of cultivated tobacco have high radical-scavenging activity [5].

Due to the favorable impact of social, geographical and historical factors, Bulgaria has gained recognition over the centuries, as a producer and exporter of high-quality aromatic oriental tobacco. In the country there are traditions and

* To whom all correspondence should be sent:
E-mail: margarita_1980@abv.bg

distinctive achievements in the selection, development and improvement of oriental tobacco varieties. Parallel to this, consistent research aimed at the obtaining of diverse tobacco-derived bio-products has been carried out. As a part of its research program, the Tobacco and Tobacco Products Institute (Markovo, Bulgaria) started in 2015 the experimental growing of some *Nicotiana* species that had not been cultivated in the country, such as *N. alata* Link & Otto and *N. rustica* L.

The aim of this work was to determine the content of polyphenols in the leaves of different species of wild and cultivated tobacco (*N. alata* Link. & Otto, *N. rustica* L., and *N. tabacum* L.), as well as to obtain extracts enriched in phenolic acids and flavonoids and to evaluate their radical-scavenging activity.

MATERIALS AND METHODS

Plant material

The cured leaves of three tobacco species – *N. alata* Link & Otto, *N. rustica* var. *rustica* and *N. tabacum* L were used as the material in the study. One of them – *N. alata* Link & Otto, was represented by two genotypes (with white and pink petals, flowers at full blossom). Common tobacco – *N. tabacum* L., was represented by Plovdiv 7 (Pd7) variety, a Bulgarian variety of oriental tobacco, belonging to the Basma variety group, Ustina ecotype.

The plant material was provided by the Tobacco and Tobacco Products Institute, part of the Bulgarian Agricultural Academy. All plants were grown in 2016 on the experimental fields of the Institute, situated in the region of Plovdiv, South Bulgaria, under identical agro-ecological and meteorological conditions. The agrochemical characteristics of the soil were as follows: hummus-carbonate (rendzina) type; organic matter content (by Turin) – 2.31 %; total nitrogen content (by Kjeldahl) – 0.21 %; mobile forms of phosphorus P_2O_5 (by Egner-Reem) – 14.85 mg/100 g; available potassium K_2O (by Milcheva) – 67.5 mg/100 g; soil reaction (pH in H_2O) – 8.2 [11]. The vegetation period (June – September) was characterized by an average monthly temperature of 22 °C and an average amount of rainfall – 44.5 mm.

Tobacco leaves were hand-picked at maturity, stringed and sun-cured (48 h) following the traditional technology for oriental tobacco - oven-dried (40 °C; 6 h). Cured leaves were stored in cardboard boxes in an air-conditioned environment to avoid undesirable changes before processing and were finely milled at room temperature before analysis. The tobacco powder was stored in plastic bags in the dark.

Methods

Preparation of extracts enriched in phenolic acids and flavonoids: In order to obtain extracts enriched in phenolic acids or flavonoids we used the polymeric adsorbent (macroporous resin) Amberlite XAD 7, and adapted the method described by Docheva and Dagnon [12]. Samples of 0.5 g of dry tobacco powder were subjected to ultrasound-assisted extraction of polyphenols with 10 ml of 60% CH_3OH for 15 min. The extract was filtered and 3 g of the polymeric adsorbent Amberlite XAD 7 were added. The adsorption of polyphenols on the macroporous resin was carried out for 2 h under static conditions. The extracts enriched in phenolic acids (Extracts PA) and in flavonoids (Extracts F) were obtained by consecutive desorption of the absorbed polyphenols. First we desorbed the phenolic acids by using 70 ml of 30% CH_3OH (thus obtaining Extracts PA), and then – the flavonoids by using 65 ml of 100% CH_3OH (Extracts F). Both desorption steps were carried out under dynamic conditions on a mechanical shaker for 15 min. The content of polyphenols was determined in an aliquot of the obtained extracts by HPLC.

Determination of polyphenols in the plant material: A sample of 0.1 g of powdered tobacco was extracted with 5 ml of 60% CH_3OH for 15 min in an ultrasonic bath. The extract was filtered through a mechanical filter under vacuum. The polyphenols were purified by solid-phase extraction through a C-18 cartridge, and then the solution was filtered through a 0.45 μm membrane filter. The content of polyphenols was determined in an aliquot of the solution by HPLC according to the validated method by Dagnon and Edreva [13].

The separation of polyphenols was carried out on a chromatograph (Perkin Elmer Ltd., England) equipped with a UV/VIS detector at a single wavelength of 340 nm and an analytical column Kromasil C18, 150 mm, 5 μm, 4.6 mm i.d. (Supelco Park, PA, USA). The mobile phases were: phase A – CH_3OH:1% CH_3COOH = 5:95, and phase B – CH_3OH:1% CH_3COOH = 85:15. The gradient elution setup was: 100 % A 0 min; 15 min to 80% A; 35 min to 45 % A; 40 min to 45 % A. The flow rate of the eluent was 1.0 ml/min, and the volume of the injected sample – 10 μl.

Determination of polyphenols in the extracts: The content of polyphenols in an aliquot of the extracts was determined by Dagnon and Edreva [13]. The content of polyphenols was calculated from the peak area on a calibration curve in the

concentration range of 0.005 mg/ml to 0.1 mg/ml rutin and chlorogenic acid. The calculation took into account the sample quantity and the final volume of the sample.

Determination of the radical scavenging activity of extracts enriched in flavonoids (DPPH• method): In order to evaluate the free radical scavenging activity (RSA) by the DPPH• method, we evaporated the extracts enriched in flavonoids on a rotary vacuum evaporator, weighed the solid residue and dissolved it in CH_3OH.

A fresh solution of DPPH• with a concentration of 0.12 mM (0.0024 g of DPPH• dissolved in 50 ml of CH_3OH) was prepared. Then we mixed 2 ml of the DPPH• solution with 2 ml of the extract solutions in different concentrations (0.95 μg/ml; 1.9 μg/ml; 3.8 μg/ml; 7.6 μg/ml; 15 μg/ml; 30 μg/ml, and 60 μg/ml). The resultant solutions were incubated for 30 min in the dark at room temperature. The absorbance of the samples was read at 515 nm on a spectrophotometer. The radical scavenging activity of the samples was calculated by the equation:

$$RSA\ (\%) = [(A_0 - A_b)/A_0] \times 100,$$

where A_0 is the absorbance of the control blank (2 ml of DPPH• solution mixed with 2 ml of CH_3OH), and A_b is the absorbance of the respective sample.

For the interpretation of data the half-maximum inhibitory concentration IC_{50} (μg/ml) was used, defined as the concentration of the extract that achieves 50 % scavenging of DPPH•. The respective IC_{50} value was calculated by interpolation of a graph based on a linear regression model. The concentrations of the samples were plotted on the abscissa, and the mean values of RSA (%) calculated by the equation from three repetitions – on the ordinate.

RESULTS AND DISCUSSION

Polyphenols in the leaves of the studied tobacco species

The individual composition of the polyphenol complex of the two uncommon to the country and not cultivated *Nicotiana* species (*N. alata* and *N. rustica*) was similar to that of the commercial oriental tobacco (*N. tabacum*). The major components were represented by chlorogenic acid, neochlorogenic acid and 4-*O*-caffeoylquinic acid, and the flavonoids rutin (quercetin-3-rutinoside) and kaempferol-3-rutinoside. The observed differences between the samples were mainly quantitative.

The qualitative and quantitative composition of the studied tobacco species is presented in Table 1. Data revealed significant variations in the contents of all components of the polyphenol complex. The differences in the content of the two components having major contribution to the total polyphenol content – chlorogenic acid and rutin – were well defined. The content of chlorogenic acid varied from 2.44 ± 0.21 mg/g (*N. rustica*) to 7.10 ± 0.50 mg/g (*N. alata*), and that of rutin – from 0.55 ± 0.05 mg/g (*N. alata*) to 10.85 ± 0.80 mg/g (*N. rustica*). As data suggested, the *N. alata* species was characterized by a particularly low content of flavonoids (0.66 ± 0.12 mg/g, average for the two samples) in comparison with the other tobaccos studied, and a comparatively high amount of phenolic acids (7.2 ± 0.5 mg/g). The highest total content of polyphenols was found in the oriental tobacco (Pd7) – 16.8 mg/g, and the contents of phenolic acids (8.6 ± 0.6 mg/g) and flavonoids (8.2 ± 0.6 mg/g) were statistically identical.

The content of polyphenols in the sample was within the range characteristic for Bulgarian oriental tobacco [14].

Table 1. Polyphenols (mg/g) in the leaves of different tobacco species (n=3)

Tobacco	Components of the polyphenol complex (mg/g)					Ref.
	Phenolic acids			Flavonoids		
	Neochlorogenic acid	Chlorogenic acid	4-*O*-caffeoyl-quinic acid	Rutin	Kaempferol-3-rutinoside	
N. alata (1)[a]	0.04 ± 0.003	7.10 ± 0.50	0.47 ± 0.05	0.55 ± 0.05	0.20 ± 0.01	
N. alata (2)[b]	0.14 ± 0.01	6.10 ± 0.40	0.55 ± 0.06	0.48 ± 0.05	0.09 ± 0.01	
N. rustica	0.86 ± 0.07	2.44 ± 0.21	1.23 ± 0.14	10.85 ± 0.80	0.66 ± 0.07	
N. tabacum (Pd7)	1.46 ± 0.15	4.80 ± 0.30	2.32 ± 0.21	6.40 ± 0.50	1.80 ± 0.15	
Djebel Basma 1	1.44±0.11	8.03±0.6	3.18±0.2	8.52±0.60	1.39±0.11	[14]
Basma 79	1.28±0.10	5.10±0.4	3.12±0.2	6.71±0.50	1.47±0.11	[14]
Krumovgrad 90	1.41±0.09	4.80±0.3	2.53±0.17	6.80±0.50	1.92±0.13	[14]

[a] *N. alata* genotype with white flowers; [b] *N. alata* genotype with pink flowers

Polyphenols in the extracts

In compliance with the aim of the study, two types of extracts were obtained from the respective tobacco species – one enriched in phenolic acids (Extracts PA) and one enriched in flavonoids (Extracts F). The task was completed by carrying out a sequential separation of the polyphenol components, which was based on their different solubility in the eluent during desorption from the macroporous resin.This specific approach of two-stage desorption allows the targeted maximum amount of phenolic acids and minimum of flavonoids to be achieved in Extracts PA, and *vice versa* – in Extracts F. Therefore, the two types of extracts with different concentrations of the biologically active polyphenols could be regarded as individual products for targeted use in phytopharmaceutical formulations.

a) Extracts enriched in phenolic acids

Fig. 1 presents data about the total content of phenolic acids in the Extracts PA and in the leaves of the respective tobaccos. The analytical results reveal that the highest concentration of phenolic acids was achieved in the extract obtained from the Pd7 variety of oriental tobacco – 6.33 ± 0.50 mg/g, while the lowest – in the extract obtained from *N. rustica* – 3.88 ± 0.20 mg/g. There could be observed a proportionate correlation between the content of phenolic acids in the extracts and in the respective tobacco material. The recovery of phenolic acids was in the range from 71% to 86 %, for the different samples. These data were in compliance with previous research, which found that the average recovery of phenolic acids in extracts obtained by a similar extraction procedure from different Bulgarian cultivars of oriental tobacco was 76% [12]. Extracts PA were maximally purified from flavonoids. The extracts from *N. alata* (samples 1 and 2) were found to contain no flavonoids, while in those from *N. rustica* and *N. tabacum* only a minimal recovery of flavonoids was detected (8 %) despite the considerable flavonoid amount in the initial raw material – an average of 9.8 ± 2.3 mg/g (Table 1).

b) Extracts enriched in flavonoids

The content of flavonoids in the extracts obtained by the second stage of desorption varied considerably between the samples, being proportionate to their initial content in the respective tobacco material (Fig. 2). The highest content of flavonoids was found in the extract obtained from *N. rustica* tobacco – 9.7 ± 0.7 mg/g, followed by that in the extract from *N. tabacum* (Pd7) – 6.15 ± 0.4 mg/g. These are, respectively, the tobaccos characterized by the highest level of flavonoids (Table 1). The content of flavonoids in the extracts obtained from the two genotypes of *N. alata* (samples 1 and 2) was only 0.43 ± 0.09 mg/g on the average, which corresponds well to their lesser amount in the initial plant material (at an average of 0.66 ± 0.12 mg/g).

The recovery of flavonoids from tobacco was approximately equal for all samples – mean 72 ± 9 %, despite the distinctive differences in the content of flavonoids in the plant materials. In all extracts enriched in flavonoids, the detected content of phenolic acids was on the minimum – mean 0.33 ± 0.06 mg/g (e.g., recovery 5 %).

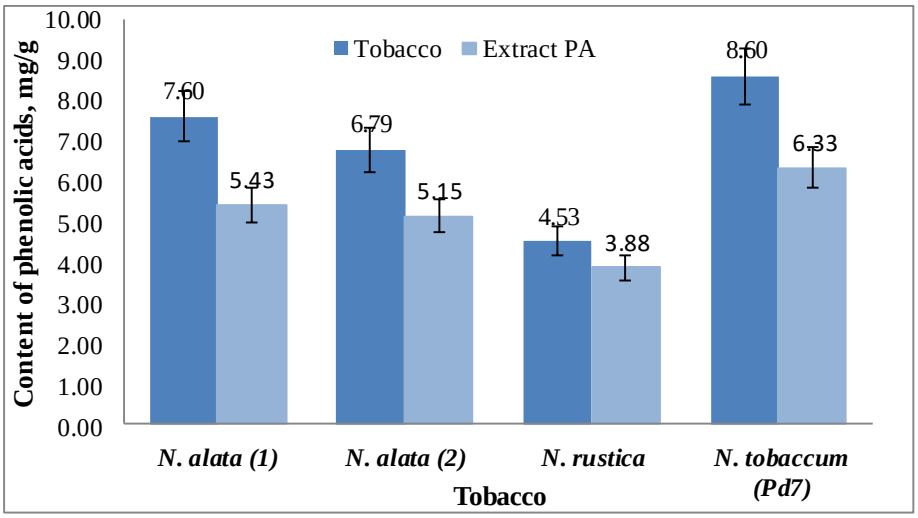

Fig. 1. Content of phenolic acids (mg/g) in the leaves of the studied tobaccos and in the obtained extracts enriched in phenolic acids

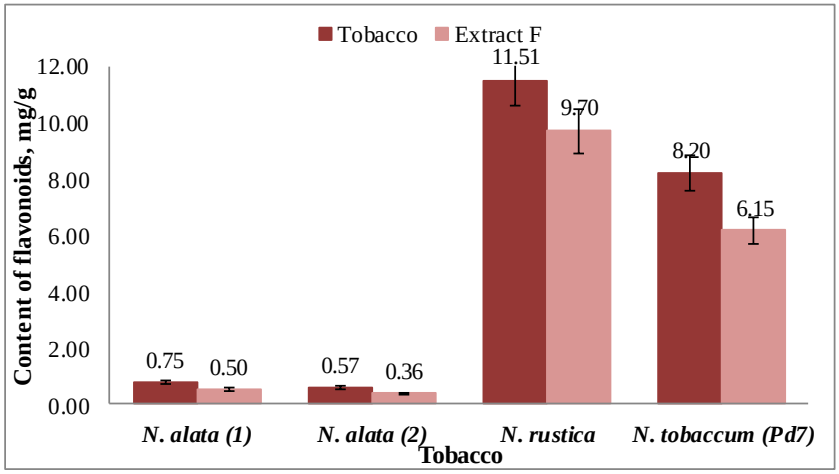

Fig. 2. Content of flavonoids (mg/g) in the leaves of the studied tobaccos and in the obtained extracts enriched in flavonoids

Those data were not significantly different from the findings by a previous research on Bulgarian oriental and Virginia tobacco (*N. tabacum*) cultivars, in which the mean recovery of phenolic acids was 92 %, and that of flavonoids – 6 % [12, 14].

Radical-scavenging activity of the extracts enriched in flavonoids (Extracts F)

Previous research [15] has found that the use of acetone and water as solvents, when applying the DPPH$^{\bullet}$ method, results in incorrect (lower) values of IC_{50}. Taking into consideration that finding, we investigated the radical-scavenging activity only of the extracts enriched in flavonoids, which were obtained by desorption with 100 % methanol.

Table 2 presents data about the content of flavonoids in the respective tobacco sample and the established radical-scavenging activity (IC_{50}) of the extracts. The high antioxidant activity of the extract obtained from *N. rustica* (IC_{50} = 5.82 ± 0.97 µg/ml) corresponds to the high content of flavonoids in the extract (9.7 ± 0.6 mg/g), and comes close to the radical-scavenging activity of the pure reference compound rutin (IC_{50} = 3.56 ± 0.5 µg/ml). Although the extract obtained from the Pd7 oriental tobacco was also characterized by a high content of flavonoids (6.15 ± 0.4 mg/g), it revealed the weakest radical-scavenging activity (IC_{50} = 14.56 ± 2.61 µg/ml). On the other hand, the extracts obtained from *N. alata* (samples 1 and 2) contained approximately equal amounts of flavonoids – mean 0.43 mg/g, but demonstrated significantly different radical-scavenging activities – IC_{50} = 6.71 ± 1.01 µg/ml and IC_{50} = 12.10 ± 2.07 µg/ml, respectively (Table 2). These findings about the radical-scavenging activity could be explained by the presence of biochemicals in the extracts other than flavonoids, which have hydroxyl groups and might be able to react with the free radical. The established radical-scavenging activity of the extracts obtained from *N. alata*, *N. rustica* and *N. tabacum* (variety Pd7) in our study was significantly higher than that of the extracts obtained by two different methods of purification – by adsorption resin and by column chromatography – from the Bulgarian oriental tobacco varieties Djebel Basma 1 and Krumovgrad 90, latter being respectively IC_{50} = 31 µg/ml, and IC_{50} = 40 µg/ml [12, 16].

The results from the study clearly reveal that the enriched-in-flavonoids extracts obtained from wild and cultivated tobacco species possess greater radical-scavenging activity compared to that of the five most active medicinal plants in Bulgaria – curly dock (*Rumex crispus* L.; IC_{50}=40.09 µg/ml), black raspberry (*Rubus occidentalis* L.; IC_{50}=45.23 µg/ml), monk's-rhubarb (*Rumex alpinus* L.; IC_{50}=46.69 µg/ml), sun spurge (*Euphorbia helioscopia* L.; IC_{50}=49.52 µg/ml), and red raspberry (*Rubus idaeus* L.; IC_{50}=50.52 µg/ml) [17].

CONCLUSIONS

A comparative study of the polyphenol content in three tobacco species (*N. alata* Link & Otto, *N. rustica* L. and *N. tabacum* L.) was completed. The results from the HPLC analysis of polyphenols revealed that the leaves of the wild tobacco species (*N. alata* and *N. rustica)* share similar qualitative composition with the cultivated tobacco (*N. tabacum)*, represented in the study by the Bulgarian oriental variety Plodviv 7. There are, however, substantial quantitative differences in the polyphenol profile between the tobacco species. The two types of extracts obtained after fractionation on the microporous resin Amberlite XAD7 showed high levels of phenolic acids and flavonoids, respectively.

Table 2. Content of flavonoids (mg/g) and radical-scavenging activity (μg/ml) of tobacco extracts, enriched in flavonoids (n=3)

Tobacco/plants	Flavonoids in the extract (mg/g)	IC_{50} (μg/ml)	Ref.
N. alata (1)[a]	0.50 ± 0.06	6.71 ± 1.01	
N. alata (2)[b]	0.36 ± 0.01	12.10 ± 2.07	
N. rustica	9.70 ± 0.60	5.82 ± 0.97	
N. tabacum (Pd7)	6.15 ± 0.40	14.56 ± 2.61	
-	Rutin	3.56 ± 0.50	
Djebel Basma 1	8.48±0.72	31.95±5.75	12, 16
Krumovgrad 90	6.12±0.53	39.05±7.03	12, 16
Rumex crispus L.	-	40.09	17
Rubus occidentalis L.	-	45.23	17
Rumex alpinus L.	-	46.69	17
Euphorbia helioscopia L.	-	49.52	17
Rubus idaeus L.	-	50.52	17

[a]*N. alata* genotype with white flowers; [b]*N. alata* genotype with pink flowers

The enriched-in-flavonoids extracts obtained from the untraditional tobacco species – *N. alata* and *N. rustica* – possessed radical-scavenging activity that was two to three times higher than that of the cultivated tobacco (*N. tabacum*). The observed differences in the IC_{50} values support the assumption that the radical-scavenging activity depends not only on the content of flavonoids in the extracts but also on the presence of the accompanying biochemicals with antioxidant properties.

The results from the study give grounds for regarding the investigated *Nicotiana* species as a promising plant material for obtaining purified natural extracts with potential use in biopharmacy.

REFERENCES

1. S. Knapp, M. Chase, J. Clarkson, *Taxon.*, **53**, 73 (2004).
2. J. Leffingwell, in: Tobacco: Production, Chemistry and Technology, D. Davis, M. Nielsen (eds.), Blackwell Science, London, 1999, p. 265.
3. A. Rodgman, T. Perfetti, The Chemical Components of Tobacco and Tobacco Smoke, CRC Press, Boca Raton, 2013.
4. L. Torras-Claveria, O. Jáuregui, C. Codina, A. Tiburcio, J. Bastida, F. Viladomat, *Plant Sci.*, **182,** 71 (2012).
5. X. Zhang, L. Zhon, H. Hunag, X. Ye, *Chem. Ind. Eng. Progress*, **31**, 2626 (2012).
6. G. Xiang, H. Yang, L. Yang, X. Zhang, Q. Cao, M. Miao, *Microchem. J.*, **95**, 198 (2010).
7. W. Ren, Z. Qiao, H. Wang, L. Zhu, L. Zhang, *Med. Res. Rev.*, **23**, 519 (2003).
8. S. Heleno, A. Martins, M. Queiroz, I. Ferreira, *Food Chemistry*, **173**, 501 (2015).
9. F. Saitoh, M. Noma, N. Kawashima, *Phytochemistry*, **24**, 477 (1985).
10. V. A. Sisson, R. F. Severson, *Beitr. Tabakforsch. Int.*, **14,** 327 (1990).
11. E. B. Arinushkina, Handbook for Chemical Analysis of Soil, Moscow University, 1970, p. 53.
12. M. Docheva, S. Dagnon, *C. R. Acad. Bulg. Sci.*, **68**, 183 (2015).
13. S. Dagnon, A. Edreva, *Beitr. Tabakforsch. Int*., **20,** 355 (2003).
14. M. Docheva, PhD thesis, PU, Plovdiv, 2016.
15. P. Molyneux, *Songklanakarin J. Sci. Technol*., **26**, 211 (2004).
16. M. Docheva, S. Dagnon, S. Statkova-Abeghe, *Nat. Prod. Res*., **28**, 1328 (2014).
17. M. Nikolova, L. Evstatieva, T. Nguyen, *Botanica Serbica*, **35**, 43 (2011).

ПОЛИФЕНОЛИ И АНТИОКСИДАНТНА АКТИВНОСТ НА ВОДНО-МЕТАНОЛНИ ЕКСТРАКТИ ОТ РАЗЛИЧНИ ВИДОВЕ ТЮТЮНИ

М. Х. Дочева [1*], В. Т. Попова[2], Т. А. Иванова[2], В. В. Николова[1], Ц. Х. Христева[1], Н. Н. Николов[1]

[1] *Институт по тютюна и тютюневите изделия, 4108 Марково, България*
[2] *Университет по хранителни технологии, бул. Марица 26, 4002 Пловдив, България*

Постъпила на 17 юли, 2018 г.; коригирана на 2 септември, 2018 г.

(Резюме)

Целта на изследването е да се характеризира съдържанието на полифеноли в листата на различни видове тютюн (*Nicotiana alata* Link & Otto, *N. rustica* L., *N. tabacum* L.), както и да се получат екстракти, обогатени на фенолни киселини и флавоноиди и да се определи тяхната радикал-улавяща активност. Съдържанието на хлорогенова киселина в листата варира от 2.44 ± 0.21 mg/g (*N. rustica*) до 7.10 ± 0.50 mg/g (*N. alata*), а това на рутина – от 0.55 ± 0.05 mg/g (*N. alata*) до 10.85 ± 0.80 mg/g (*N. rustica*). Съдържанието на флавоноиди е в границите от 0.66 ± 0.12 mg/g (*N. alata*) до 11.51 ± 0.8 mg/g (*N. rustica*). Два вида екстракти са получени с помощта на полимерен адсорбент (смола) – обогатени на фенолни киселини (PA) и на флавоноиди (F). Концентрацията на фенолните киселини в екстрактите PA е от 6.33 ± 0.50 mg/g (*N. tabacum*) до 3.88 ± 0.20 mg/g (*N. rustica*), а добивът на фенолни киселини – от 71 % до 86 %. Екстрактите F от *N. rustica* и *N. tabacum* са с флавоноидно съдържание съответно 9.7 ± 0.7 mg/g и 6.15 ± 0.4 mg/g, а тези от двата генотипа на *N. alata* – със само 0.43 ± 0.09 mg/g. Добивът на флавоноиди е 72 ± 9 %. Екстрактите PA са максимално пречистени от флавоноиди, а екстрактите F – от фенолни киселини. Всички екстракти показват висока антиоксидантна активност, със стойности на IC_{50} от 5.82 ± 0.97 μg/ml (*N. rustica*) до 14.56 ± 2.61 μg/ml (*N. tabacum*). Резултатите от проучването дават основание да се счита, че изследваните видове Nicotiana са обещаващ растителен материал за получаване на пречистени натурални екстракти с потенциално приложение в биофармацията.

Bulgarian Chemical Communications, Volume 50, Issue 4 (pp. 560 – 567) 2018

Instabilities during electrochemical deposition of Sn-Co alloys from gluconate/sulphate electrolyte

T. T. Valkova*, I. N. Krastev

Institute of Physical Chemistry, Bulgarian Academy of Sciences, 1113 Sofia, Bulgaria

Received, September 15, 2017; Accepted, July 30, 2018

Dull coatings with high cobalt content can be deposited from the investigated electrolyte. Depending on tin concentration, the deposition of coatings with cobalt content in the range from 0 up to 80 wt. % is possible. Electrochemical instabilities and spontaneous potential oscillations during galvanostatic deposition of Sn-Co alloys are observed and discussed.

Keywords: Electrodeposition, Tin-cobalt alloys, Oscillations

INTRODUCTION

Electrodeposited tin-cobalt alloy coatings are of commercial interest as a convenient and economic way to achieve an attractive finish [1, 2]. Bright tin-cobalt alloy coatings have mechanical and electrochemical properties similar to those of chromium coatings and can be considered as their effective substitution, especially where the high corrosion resistance of chromium is not needed [3]. Tin-cobalt alloys [4] and compositionally modulated Sn-Co multilayer alloy coatings [5] are alternative to lead-based alloys used as overlays for plain bearing.

Tin-based compounds have received particular attention in the field of lithium batteries for the synthesis of new negative electrode materials as alternatives to graphite materials. Tin-cobalt alloy found extensive application in this field [6-10], because it has been shown that the addition of Co gives the highest specific capacity [11], avoiding mechanical stress due to the Li-intercalation process [12].

According to the phase diagram Sn-Co alloy may be composed of various intermetallic compounds depending on its metal content [13]. The preparation of heterogeneous coatings offers possibilities for investigation of the self-organization phenomena as seen during the deposition of other cobalt alloys – i.e. those with indium and antimony [14].

The deposition of this alloy is performed from sulphate/gluconate [15-17], citrate [18] and pyrophosphate [19] electrolytes. All of them are environmentally friendly, non-toxic, and non-corrosive and electrodeposition process takes place at high energy efficiency.

Electrochemical oscillations observed during deposition of tin can be associated with both electro-oxidation and electro-reduction process. Cathodic potential oscillation of a Sn electrode immersed in alkaline (KOH) solution of SnO has been described by Piron *et al*. [20]. Oscillations took place only at current densities higher than the limiting current density and in a limited SnO concentration range. The potential increase is due to the depletion of tin ions near the electrode, and the potential decrease results from hydrogen evolution. Potential oscillations during deposition of tin from acidic stannous sulphate solution containing gelatine were investigated by cyclic voltammetry and chronopotentiometry. In the absence of gelatine damped potential oscillations are evident (dendritic growth). In its presence (gelatine acts as inhibitor and gives a smooth deposit) substantial potential oscillations occur [21].

Electrochemical oscillations during deposition of tin alloys were first reported by Survila *et al*. [22]. They found oscillations during the deposition of Cu-Sn alloy from an acidic solution containing Laprol 2402C. Later Nakanishi [23, 24] showed formation of layered nanostructures during electrodeposition of Cu and Sn in an acidic solution in the presence of cationic surfactant. The electrodeposition of the alloy is characterized by a negative differential resistance (NDR) and resulting current oscillations. Alloy films deposited during the oscillations have multi-layered structure composed of two alloy layers of different compositions. The multilayers have the period of thickness of 40-90 nm and were uniform over an area of *ca*. 1×1 mm. NDR arises from adsorption of a cationic surfactant on the alloy surface and the

* To whom all correspondence should be sent:
E-mail: krastev@ipc.bas.bg

oscillations occur from coupling of the NDR with the ohmic drop in the electrolyte [24].

In another work the same authors investigated the mechanism of oscillations and formation of nano-scale layered structures during induced co-deposition of some iron-group alloys (Ni-P, Ni-W and Co-W) by an *in situ* electrochemical quartz crystal microbalance technique [25]. They found that the electrodeposition of these alloys is connected with a negative differential resistance (NDR), from which the oscillations and the layer-structure formation arise.

Recently, Ihara *et al*. [26] showed that a large interfacial energy gradient is produced at the front of an electrochemical wave in Cu-Sn oscillatory electrodeposition. They observed the directional later motion of an oil droplet put on an electrode surface. During the deposition, when oscillations occur, surface composition changed periodically between Cu-rich and Sn-rich alloy layers.

Many other electrochemical systems are known to exhibit complex non-linear behaviour such as spontaneous oscillations of current or potential. Kaneko *et al.* [27] investigated potential oscillations during the deposition of cadmium and established that they result from the decrease in the surface concentration of cadmium ions (almost to zero) and as a result the potential shifts rapidly and reaches deposition of hydrogen. The evolved hydrogen improves the mass transport process by kind of agitating the electrolyte. As a result, the surface concentration of cadmium ions increases and the potential decreases again.

The oscillatory electrodeposition of Sn and some Sn containing alloys allows the assumption of the possible appearance of some oscillating electrochemical reactions also during deposition of tin-cobalt alloys.

The aim of the present work is to investigate the electrodeposition of a Sn–Co alloy from gluconate/sulphate electrolytes and to find out the conditions for the possible oscillating behaviour of the system.

EXPERIMENTAL

The composition of the electrolyte for deposition of Sn-Co alloy coatings is given in Table 1.

Table 1. Electrolyte composition

Composition	Concentration, g dm^{-3}
Sn as SnMS	0 - 15
Co as $CoSO_4.7H_2O$	0 - 15
Na_2SO_4.	0 - 50
$C_6H_{11}O_7Na$	0 - 150
NaOH	0 - 5

Distilled water and *pro analysi* grade reagents were used. The experiments were performed in a glass cell of 100 cm^{-3} at room temperature without stirring of the electrolyte. The working electrode (1 cm^2) and the two counter electrodes were made of platinum. A reference electrode Ag/AgCl with $E_{Ag/AgCl}$ = +0.197 V against the hydrogen electrode was used. All potentials in the present study are given against this reference electrode.

The cyclic voltammetric investigations were performed by means of a computerized potentiostat/galvanostat PAR 273A (Princeton Applied Research) using the PowerCorr software for electrochemical corrosion studies.

The sweep rate of the potential was 0.020 V s^{-1}. The alloy coatings, *ca*. 5 μm thick, were deposited on 0.3 mm thick copper substrates, 2×1 cm, in an electrolysis cell of 100 cm^3. The cobalt content in the coatings and their thickness was determined using a Fischerscope XDAL apparatus for X-ray fluorescence.

RESULTS AND DISCUSSION

Figure 1 shows the cyclic voltammetric curves in electrolytes containing ions of both metals separately and together. In this case, tin is the nobler component (the deposition peaks of tin are less cathodic (less negative) compared to the peak of pure cobalt). During the deposition of tin two cathodic reactions are observed again. The cobalt deposition from the same electrolyte in the absence of tin is characterized by one cathodic reaction. When cobalt is added to the solution of tin two cathodic maxima are observed again. The first one is in the form of a hump and the second one is well expressed. The first cathodic maximum corresponds to the deposition of pure tin and the second cathodic maximum to the co-deposition of cobalt.

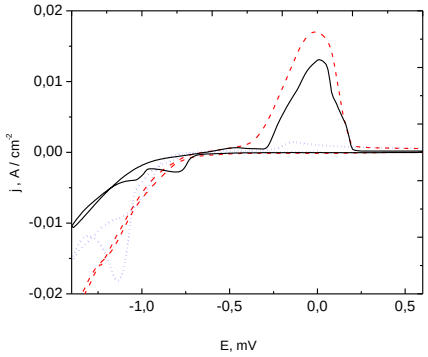

Fig. 1. CVA curves of tin, cobalt and SnCo alloy deposition from sulphate/gluconate electrolytes at pH=5. $C_{Na_2SO_4}$ = 40 g dm^{-3}; $C_{C_6H_{11}NaO_7}$ = 50 g dm^{-3}; v = 20 mV s^{-1}; —— C_{Sn} = 5 g dm^{-3};---- C_{Co} = 5 g dm^{-3} ; ···· C_{Sn} = 5 g dm^{-3}, C_{Co} =5 g dm^{-3}.

Two anodic reactions are detected in the case of dissolution of tin and one during dissolution of cobalt and the alloy. The main oxidation peak of the alloy is in the potential range where dissolution of tin and cobalt takes place.

Cobalt electrodeposition

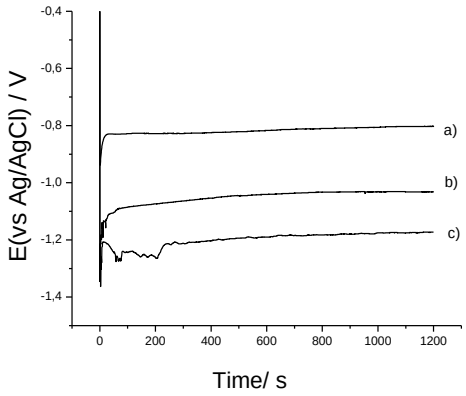

Fig. 2. Chronopotentiometric curves obtained at different current densities. C_{Co} = 5 g dm^{-3}; C_{Sn} = 0 g dm^{-3} (a) 0.2 A dm^{-2}, (b) 0.4 A dm^{-2}, (c) 1.4 A dm^{-2}

Figure 2 shows the chronopotentiometric curves obtained at different current densities at cobalt concentration of 5 g dm^{-3} and pH=4. The increase in the current densities leads to a small shift of the cathodic potential without appearance of any instabilities or oscillation reactions.

Tin electrodeposition

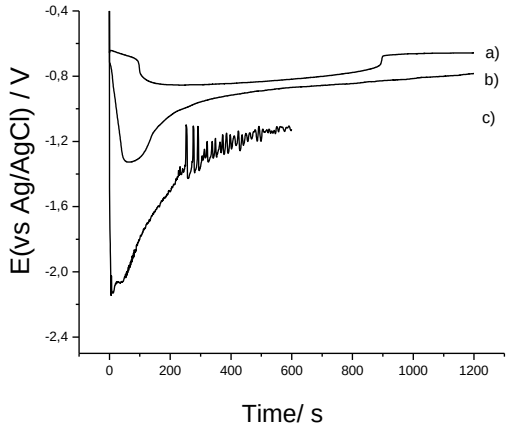

Fig. 3. Chronopotentiometric curves obtained at different current densities at pH=3.5. C_{Sn} = 10 g dm^{-3}; C_{Co} = 0 g dm^{-3}. (a) 0.4 A dm^{-2} (b) 0.6 A dm^{-2} (c) 1.6 A dm^{-2}

Figure 3 shows the chronopotentiometric curves obtained at different current densities at pH=3.5 and tin concentration of 10 g dm^{-3}. Up to the relatively high current density of 1.0 A dm^{-2} there are no instabilities appearing (curves a, b). The increase of the applied current density up to 1.6 A dm^{-2} leads to the appearance of irregular, not so well formed potential oscillations (curve c). They have maximal amplitude of about 300 mV and their period differs between 12 and 25 s. The oscillations appear at this pH value at the high current densities possibly due to the reduced passivation of the electrode in the acidic media.

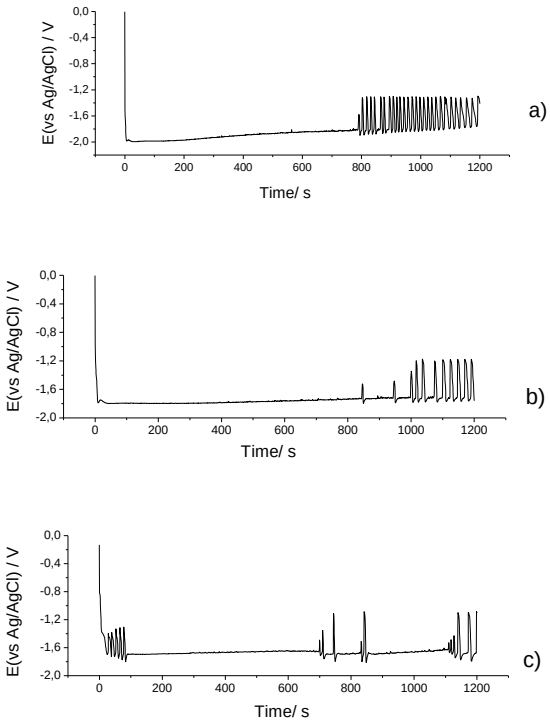

Fig. 4a. Chronopotentiometric curves obtained at different current densities at pH=5. C_{Sn} = 5 g dm^{-3}; C_{Co} = 0 g dm^{-3}. (a) 0.4 A dm^{-2} (b) 0.6 A dm^{-2} (c) 0.8 A dm^{-2}

Figure 4a shows the chronopotentiometric curves obtained at different current densities at increased pH value (pH=5) and a tin concentration of 5 g dm^{-3}. The increase of the pH of the electrolyte leads to appearance of potential oscillations at current densities between 0.4 A dm^{-2} and 1 A dm^{-2}. The oscillations have amplitude of about 600 mV. At current densities of 0.4 A dm^{-2} the period of the oscillations is about 15 s. At higher current densities the oscillations start at the beginning of the process with amplitude of about 500 mV, and after disappearing in a broad interval of about 700 s they appear again irregular with some higher amplitude of about 700 mV. At current densities 0.6 A dm^{-2} the period of the oscillations is about 25 s.

The influence of the concentration of tin in the electrolyte is shown in Fig 4b. This figure presents the chronopotentiometric curves obtained at a higher tin concentration of 10 g dm^{-3} at different current densities and pH=5. At current densities up to 0.2 A dm^{-2} no oscillations are registered.

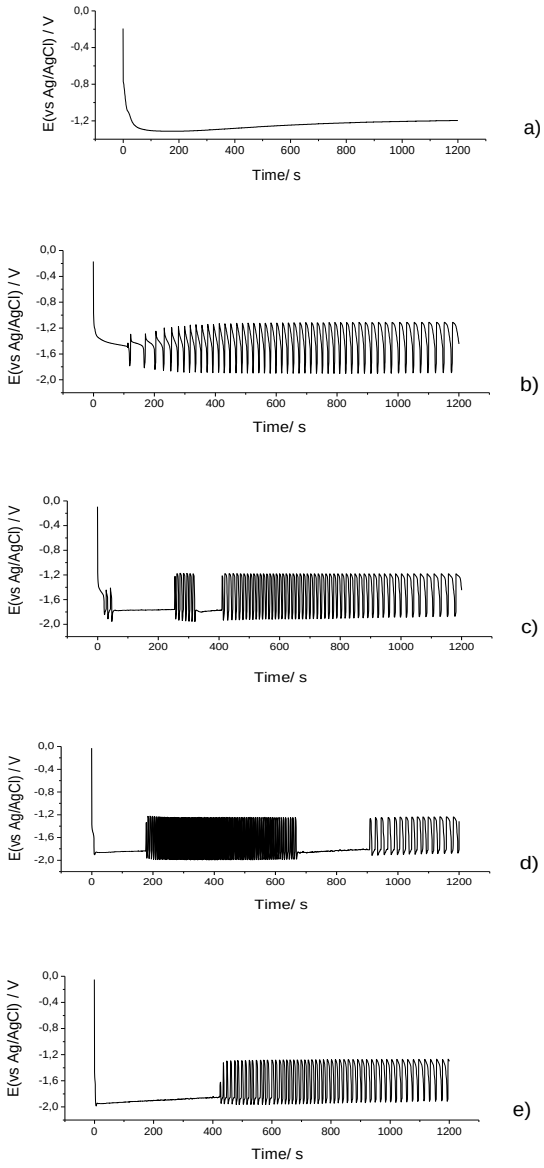

Fig. 4b. Chronopotentiometric curves obtained at different current densities at pH=5. C_{Sn} = 10 g dm^{-3}; C_{Co} = 0 g dm^{-3}. (a) 0.2 A dm^{-2}, (b) 0.4 A dm^{-2}, (c) 0.6 A dm^{-2}, (d) 1.0 A dm^{-2}, (e) 1.4 A dm^{-2}

The increase in the applied current density up to 0.4 A dm^{-2} leads to the appearance of regular potential oscillations with a high amplitude of about 700 mV, more regular than the oscillations obtained at 5 g dm^{-3} Sn (compare with Fig 4a). The period of the oscillations is about 12 s. At current densities of 1.0 A dm^{-2} the period of the oscillations differs between 5 s at the beginning and 20 s at the end of deposition. Similar results are observed at 15 g dm^{-3} Sn in the electrolyte. From the curves in Fig. 4b it is visible, that the period of oscillations increases with the time of deposition.

The effect of the concentration of the complex forming agent for tin ($C_6H_{11}O_7Na$ in this case) on the electrode processes is shown in Fig.5a.

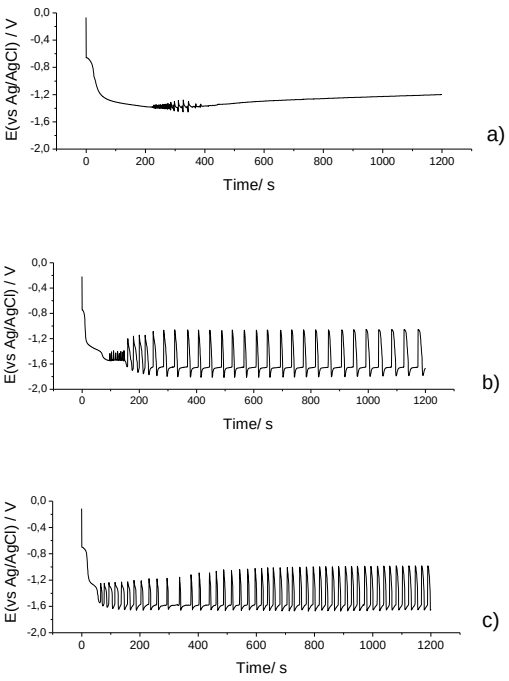

Fig. 5a. Chronopotentiometric curves obtained at current densities of 0.2 A dm^{-2} at pH=5. C_{Sn} = 5 g dm^{-3}; C_{Co} = 0 g dm^{-3}. (a) $C_{C_6H_{11}O_7Na}$ = 50 g dm^{-3}, (b) $C_{C_6H_{11}O_7Na}$ = 100 g dm^{-3}, (c) $C_{C_6H_{11}O_7Na}$ = 150 g dm^{-3}

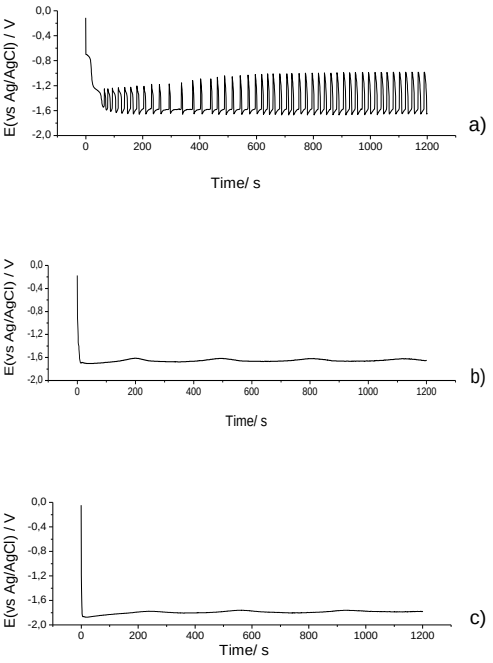

Fig. 5b. Chronopotentiometric curves obtained at different current densities at pH=5. C_{Sn} = 10 g dm^{-3}; C_{Co} = 0 g dm^{-3}; $C_{C_6H_{11}O_7Na}$ = 150 g dm^{-3}. (a) 0.2 A dm^{-2}, (b) 0.4 A dm^{-2}, (c) 0.6 A dm^{-2}

In a previous paper the function of the complex forming agent on the electrodeposition of Sn and SnCo alloy is described [28]. At low current densities of about 0.2 A dm^{-2} and 50 g dm^{-3} of

$C_6H_{11}O_7Na$ some small oscillations appear in a short period of the deposition (curve a). The increase of the concentration of gluconate up to 100 g dm^{-3} leads to the appearance of potential oscillations with a high amplitude of about 800 mV and a period of about 44 s (curve b). Similar results are obtained with 150 g dm^{-3} $C_6H_{11}O_7Na$ in the electrolyte, but with a smaller period of the oscillations about 28 s (curve c).

At a higher concentration of $C_6H_{11}O_7Na$ (100-150 g dm^{-3}) oscillations appear only at low current densities of about 0.2 A dm^{-2}. The increase of the current density results in the disappearing of the oscillations (Fig.5b).

Tin-cobalt electrodeposition

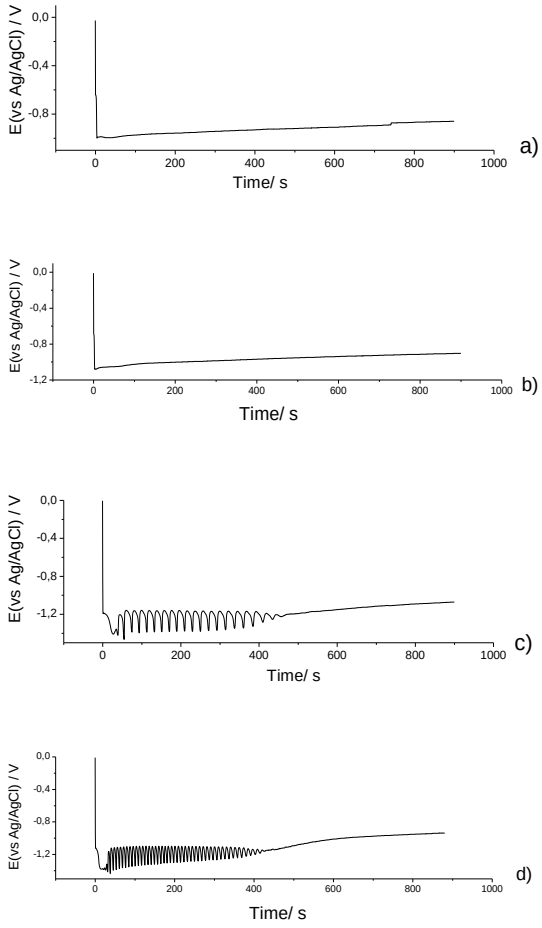

Fig. 6. Chronopotentiometric curves obtained at different current densities at pH=3.5. C_{Sn} = 5 g dm^{-3}; C_{Co} = 5g dm^{-3}. a) 0.8 A dm^{-2}, (b) 1.0 A dm^{-2}, (c) 1.6 A dm^{-2}, (d) 2.0 A dm^{-2}

Figure 6 shows chronopotentiometric curves obtained at different current densities at pH=3.5 and tin concentration of 5 g dm^{-3} and cobalt concentration of 5 g dm^{-3}. At low current densities up to 1.0 A dm^{-2} there are no oscillations registered (curves a, b). The increase of the applied current density up to 1.6 A dm^{-2} leads to the appearance of potential oscillations with an amplitude of about 200 mV. The period of the oscillations is about 20 s and they disappear after a deposition time of about 400 s. The further increase in the current density up to 2.0 A dm^{-2} leads to the appearance of potential oscillations with similar amplitude, but with a shorter period of about 9 s.

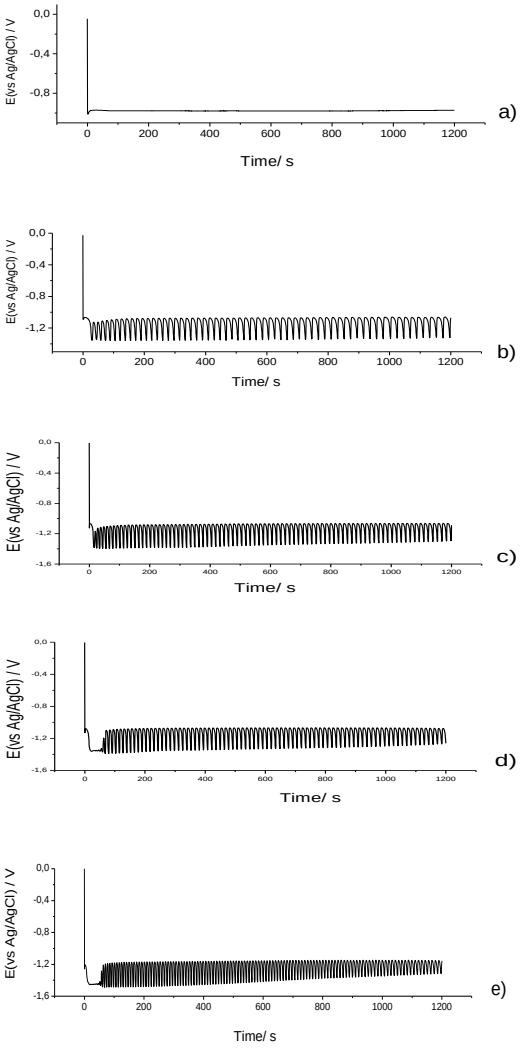

Fig. 7. Chronopotentiometric curves obtained at different current densities at pH=5. C_{Sn} = 5 g dm^{-3}; C_{Co} = 5g dm^{-3}. a) 0.6 A dm^{-2}, (b) 0.8 A dm^{-2}, (c) 1.0 A dm^{-2}, (d) 1.4 A dm^{-2}, (e) 2.0 A dm^{-2}

Figure 7 shows the chronopotentiometric curves obtained at different current densities at an increased pH value (pH=5), and the same concentrations of both metals in the electrolyte. In this case at current densities up to 0.6 A dm^{-2} no oscillations are observed (curve a). The appearance of potential oscillations starts at lower current densities compared to the more acidic electrolyte. At current densities 0.8 A dm^{-2} stable potential oscillations with amplitude of about 300 mV are registered. The period of the oscillations decreases

from about 26 s at 0.8 A dm^{-2} to about 10 s at 2.0 A dm^{-2}.

In order to find out the differences during deposition at a positive potential of the oscillations and at a negative one, two samples were deposited potentiostatically in the investigated alloy electrolyte at the potentials of -1.2 V and -1.5 V (the most positive and the most negative potentials in the oscillation curve (Fig.7 (curve b), current density 0.8 A dm^{-2}) for 300 s.

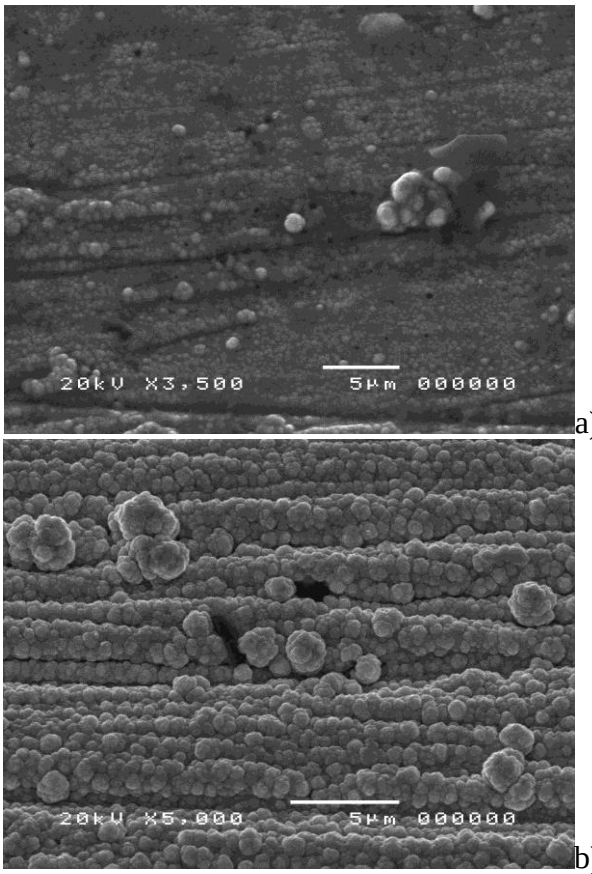

Fig. 8. Surface of tin-cobalt alloy coatings. C_{Sn} = 5 g dm^{-3}; C_{Co} = 5g dm^{-3}; pH=5. a) -1.2 V; 60 wt. % *Co*, b) -1.5 V; 50 wt. % *Co*

The appearance of the obtained coatings was different - the coating deposited at -1.2 V was silvery white while that, deposited at -1.5 V was dark-grey. The morphology of these coatings is shown in Fig. 8. The deposit obtained at -1.2 V contains about 60 wt. % of Co and the deposit obtained at -1.5 V about 50 wt. % of Co. The coatings obtained at the higher potentials are course-grained and rough and possibly that is the reason for the lower cobalt content.

Figure 9 shows the chronopotentiometric curves obtained at different current densities at pH=5 and higher tin concentration of 10 g dm^{-3} with a cobalt concentration of 5 g dm^{-3}. At current densities up to 0.8 A dm^{-2} no oscillations are registered (curve a) and the obtained coatings are bright. The increase in the applied current up to 1.0 A dm^{-2} leads to the appearance of potential oscillations with an amplitude of about 200 mV. The period of the oscillations is about 20 s. The increase in the current densities up to 1.4 A dm^{-2} leads to the formation of oscillations with a larger amplitude of about 300 mV and a shorter period of 12 s.

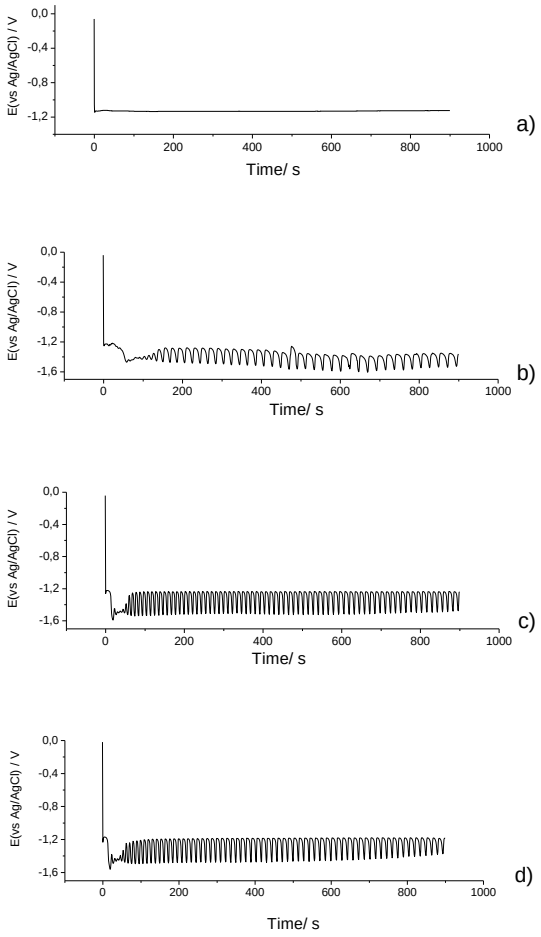

Fig. 9. Chronopotentiometric curves obtained at different current densities at pH=5. C_{Sn} = 10 g dm^{-3}; C_{Co} = 5g dm^{-3}. (a) 0.6 A dm^{-2}, (b) 1.0 A dm^{-2}, (c) 1.2 A dm^{-2}, (d) 1.4 A dm^{-2}

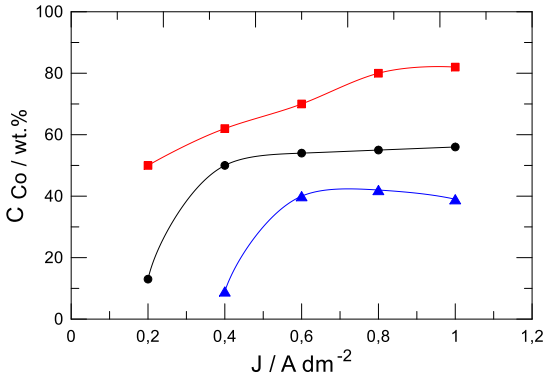

Fig. 10. Effect of the current density on the cobalt content in the alloy at different metal concentrations in the electrolyte. ● C_{Sn} = 5 g dm^{-3}; C_{Co} = 5 g dm^{-3}; ▲ C_{Sn} = 10 g dm^{-3}; C_{Co} = 5 g dm^{-3}; ■ C_{Sn} = 5 g dm^{-3}; C_{Co} = 10 g dm^{-3}

Figure 10 shows the effect of both tin concentration and cobalt concentration in an electrolyte at pH=5 on the composition of the alloy. At 5 g dm^{-3} of Sn and 5 g dm^{-3} of Co in the electrolyte the increase of the current density leads to an increase of the cobalt content in the coating up to 50 wt.%. At higher tin concentration of 10 g dm^{-3} in the electrolyte, pure tin coatings are deposited at low current densities and the cobalt content in the coatings increases up to about 40 wt.%. In both cases the deposition of coatings with almost constant composition is possible in a broad range of current densities. In this case oscillations of the cathodic potential are observed.

As expected, higher cobalt concentrations in the same electrolyte result in the rise of cobalt content in the alloy. At a cobalt concentration of 10 g dm^{-3} in the electrolyte, the cobalt content in the coatings is higher and reaches 80 wt.%.

CONCLUSIONS

1. Potential oscillations with different amplitude and period are registered during electrochemical deposition of Sn and Sn-Co alloys.

2. At lower pH values of the electrolyte the oscillations start at higher current densities during deposition of Sn and Sn-Co alloys due to the reduced passivation of the coatings in the more acidic electrolyte.

3. The period of the oscillations increases with the deposition time possibly due to the increase of the roughness of the coatings and decreases with the increase in the applied current densities.

4. The increase in Sn concentration in the electrolyte results in more regular potential oscillations.

5. The increase in the concentration of complexing agent (gluconate) leads to disappearing of the potential oscillations at high current densities.

6. The instabilities and the resulting potential oscillations during deposition of Sn-Co alloys are due to the Sn-component of the electrochemical system.

7. The observed potential oscillations during galvanostatic electrodeposition of Sn-Co alloys from gluconate/sulphate electrolytes are connected with some passivation phenomena of the cathode surface and the resulting hydrogen evolution.

Acknowledgements: *The authors express their gratitude to the National Science Foundation for the financial support of the project T 02/27- 2014.*

REFERENCES

1. J. D. C. Hemsley, M. E. Roper, *Trans. Inst. Met. Fin.*, **57,** 77 (1979).
2. P. K. Datta, Coatings and Surface Treatment for Corrosion and Wear Resistance, (K.N. Strafford, P.K. Datta, G.C. Gookan (eds.) Chichester: Ellis Horwood, 1984, p.74.
3. R. Sabitha, Malathy Pushpavanam, M. Mahesh Sugatha, T. Vasudevan, *Trans. Met. Fin. Assoc. of India*, **5,** 267 (1996).
4. I. Vitina, V. Belmane, A. Krumina, V. Rubene, *Surface and Coatings Tech*., **205,** 2893 (2011).
5. K. Chen, Dissertation, University of Loughborough, 2004.
6. F.-Sh. Ke, L. Huang, H.-B. Wei, J.-Sh. Cai, X.-Y. Fan, F.-Z. Yang, Sh.-G. Sun, *J. Power Sources*, **170**, 450 (2007).
7. K. Ui, S. Kikuchi, Y. Jimba, N. Kumagai, *J. Power Sources*, **196**, 3916 (2011).
8. G. Ferrara, R. Inguanta, S. Piazza, C. Sunseri, *J. Nanosci. Nanotechnol.*, **10** (12), 8328 (2010).
9. X.Y. Fan, F.S. Ke, G.Z. Wei, L. Huang, S.G. Sun, *J. Alloys Comp*., **476**, 70 (2009).
10. F. Zhan, H. Zhang, Y. Qi, J. Wang, N. Du, D. Yang, *J. Alloys Comp*., **570**, 119 (2013).
11. A. D. W. Todd, R. E. Mar, J.R. Dahn, *J. Electrochem. Soc*., **153**, A1998 (2006).
12. H. Guo, H. Zhao, X. Jia, X. Li, and W. Qiu, *Electrochim. Acta*, **52**, 4853 (2007).
13. T. Nishizawa, K. Ishida, *Bull. Alloy Phase Diagrams*, **4** (4), 387 (1983).
14. S. Nineva, Ts. Dobrovolska, I. Krastev, *Zastita Materiala*, **52 (**2) 80 (2011).
15. S. Rehim, S. Refaey, G. Schwitzgebel, F. Tara, M. Saleh, *J. Appl. Electrochem.*, **26**, 413 (1996).
16. E. Gómez, E. Guaus, J. Torrent, X. Alcobe, E. Vallés, *J. Appl. Electrochem.*, **31**, 349 (2001).
17. E. G. Vinokurov, *Russian J. Appl. Chem*., **83**, 258 (2010).
18. A. Survila, Z. Mockus, R. Juškėnas, *J. Appl. Electrochem*., **31**, 1109 (2001).
19. M. Damercheli, M. Aboutaebi, M. T. Salehi, *Galvanotechnik*, **104**, 1340 (2013).
20. D. L. Piron, I. Nagatsugawa, Ch. Fan, *J. Electrochem. Soc.* **138,** 3296 (1991).
21. S. Wen, J. A. Szpunar, *J. Electrochem. Soc.*, **153 (**3), E45-E51 (2006).
22. A. Survila, Z. Mockus, R. Juškenas, *Electrochim. Acta*, **43**, 909 (1998)
23. S. Nakanishi, S. Sakai, T. Nagai, Y. Nakato, *J. Phys. Chem. B*, **109** (5), 1750 (2005).
24. S. Sakai, S Nakanishi, K. Fukami, Y. Nakato, *Chemistry Letters*, **31**, 640 (2002).
25. S. Sakai, S. Nakanishi, Y. Nakato, *J. Phys. Chem. B*, **110** (24), 11944 (2006).
26. D. Ihara, T. Nagai, R. Yamada, S. Nakanishi, *Electrochim. Acta*, **55**, 358 (2009).
27. N. Kaneko, H. Nezu, N. Shinohara, *J. Electroanal. Chem. Interf. Electrochem*., **252**, 371 (1988).
28. T. Valkova, I. Krastev, *Bulg. Chem. Commun*., **48**, Special Issue B, 78 (2016).

НЕСТАБИЛНОСТИ ПРИ ЕЛЕКТРОХИМИЧНОТО ОТЛАГАНЕ НА Sn-Co СПЛАВИ ИЗ ГЛЮКОНАТНО-СУЛФАТЕН ЕЛЕКТРОЛИТ

Т. Т. Вълкова*, И. Н. Кръстев

Институт по физикохимия, Българска академия на науките, 1113 София, България

Постъпила на 15 септември, 2017, приета на 30 юли 2018

(Резюме)

Матови покрития с високо съдържание на кобалт могат да се отложат из изследвания електролит. В зависимост от концентрацията на калай е възможно отлагане на покрития със съдържание на кобалт от 0 до 80 wt. %. При галваностатичното отлагане на Sn-Co сплави са наблюдавани и дискутирани електрохимични нестабилности.

Bulgarian Chemical Communications, Volume 50, Issue 4 (pp. 568 – 574) 2018

One-pot synthesis of substituted imino- and imidazopyridines under catalyst-free conditions

F. N. Naghiyev, A. M. Maharramov, İ. M. Akhmedov, Kh. A. Asadov, A.N. Khalilov, A. V. Gurbanov, G. Z. Mammadova, A. R. Asgarova, E. Z. Guseynov, I. G. Mamedov*

Faculty of Chemistry, Baku State University, Baku AZ1148, Azerbaijan

Received, August 30, 2017; Revised, February 2, 2018

Substituted imino- and imidazopyridine derivatives were synthesized *via* a new one-pot, three-component reaction between benzylidenemalononitriles, malononitrile and amines under catalyst-free conditions at room temperature. When ethylenediamine was used as the amine component of the reaction, dihydro- and tetrahydroimidazopyridines were selectively obtained in good to high yields. On the other hand, the use of benzylamine led to the formation of 2-imino-1,2-dihydropyridine products. The reactions were found to tolerate the presence of electron-donating and withdrawing substituents on the benzylidenemalononitrile reactants. Products of these reactions are crystalline and can be isolated by a simple procedure at room temperature in good yields and with high purity.

Keywords: Benzylidenemalononitrile, Imidazopyridine, Iminodihydropyridine, X-ray analysis

GRAPHICAL ABSTRACT

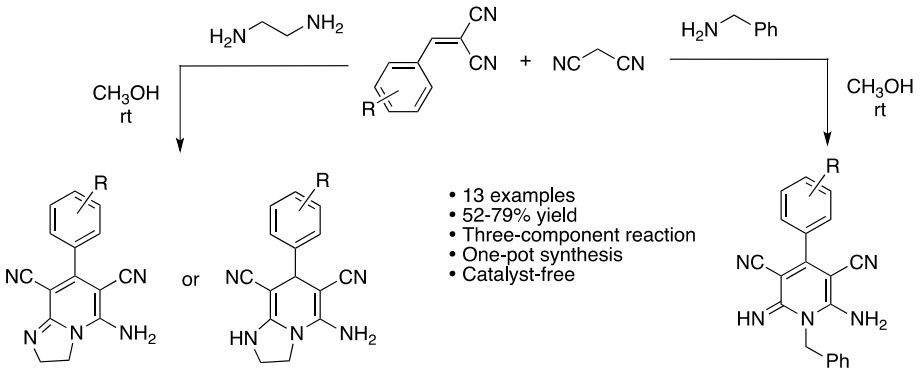

INTRODUCTION

Heterocyclic chemistry continues to be at the forefront of organic chemistry due to its importance across a variety of disciplines such as medicinal chemistry, agricultural chemistry and materials science [1,2]. Pyridine ring, a privileged structural core in heterocyclic chemistry, is present in many natural products such as nicotinic acid, nicotinamide and vitamin B_6 which play key roles in metabolism. In addition, functionalized pyridines have been shown to exhibit a broad range of biological activities including antimicrobial, antiulcer, anticancer, antipyretic and anti-inflammatory activities [3-7].

Due to all these attractive features of pyridine-containing compounds, numerous synthetic methods that enable the construction of substituted pyridines have been developed [8-10]. Recently, transition metal-catalyzed coupling reactions of enamides with alkynes, and TfOH-promoted reactions of enaminones with aldehydes were shown to be highly effective for the synthesis of substituted pyridines [11-13]. $Zn(NO_3)_2{\cdot}6H_2O$ was found to be a potent catalyst for the synthesis of unsymmetrical multisubstituted pyridines *via* the reaction of β-ketoesters with ketene *N,S*-acetals or ketene *N,N*-acetals [14]. Dong and co-workers reported in 2013 a copper-catalyzed, three-component reaction between sulfonyl azides, alkynes and 2-[(amino) methylene]malononitriles that gave rise to the formation of 4-amino- and 6-amino-2-iminopyridine derivatives [15]. An efficient one-pot methodology was reported by Ranu and co-workers in 2007 for the synthesis of substituted pyridines *via* the condensation of aldehydes, malononitrile and thiophenols promoted by the basic ionic liquid [bmIm]OH [16]. A multicomponent reaction of malononitrile and aldehydes with ammonium acetate catalyzed by Et_3N was developed for the synthesis of aminopyridine derivatives [17]. In

* To whom all correspondence should be sent:
E-mail: bsu.nmrlab@mail.ru

addition to these methods, efficient protocols for the synthesis of highly substituted pyridines and imidazopyridines starting from 2-aminopyridines, 2-bromopyridines, 2-(1*H*-benzo[*d*]imidazol-2-yl)acetonitrile [31], 2-amino-1-(2-propenyl)pyridinium bromide salt, α,β-unsaturated ketones, 1,3-dienes, and *O*-acetylketoximes have been successfully developed [18-32].

In this work, we report the development of a one-pot, three-component reaction between benzylidenemalononitriles, malononitrile and amines that lead to the synthesis of substituted imino- and imidazopyridines under catalyst-free conditions. Our interest in these compound classes stems from the attractive biological activity profiles observed for various pyridobenzimidazole derivatives (Figure 1) [33,34]. In a study reported by Denny and co-workers in 2011, 1-amino-2,4-dicyanopyrido[1,2-*a*] analogues (**1**) were found to effectively inhibit the cellular function of the pore-forming protein perforin [33]. More recently, Huttunen and co-workers reported in 2016 the reversible inhibition of the L-type amino acid transporter 1 (LAT1) by the pyridobenzimidazole analogue **2** (Fig. 1) [34]. Among the few synthetic methods available for the preparation of such pyridobenzimidazole derivatives [35-38], the reaction between 1H-benzimidazole-2-carbonitrile and arylidenemalononitriles reported by Bogdanowicz-Szwed and Czarny has been the most commonly utilized method [35]. The one-pot, three-component reactions that we have developed in this study operate under mild conditions, and result in rapid generation of complexity that leads to formation of multisubstituted imino- and imidazopyridines in an effective manner.

EXPERIMENTAL

All commercially available chemicals were obtained from Merck and Fluka companies and used without further purification. Melting points were measured on a Stuart SMP30 apparatus without correction. $^{1}H/^{13}C$ NMR spectra were recorded on a Bruker Avance 300-MHz spectrometer at 300 and 75 MHz, respectively (Figs. S1-13). X-Ray analyses were performed on a Bruker APEX equipment. Thin-layer chromatography (TLC) on commercial aluminum-backed plates of silica gel (60 F254) was used to monitor the purity of compounds and progress of reactions. Iodine vapor was used as a visualizing agent, eluent - 5:2 hexane/ethyl acetate.

*General procedure for the synthesis of compounds **6a–f**, **9g-i***

Mixture of benzylidenemalononitriles (**3a-f**, **3g-i**) (5.1 mmol) and malononitrile (5.2 mmol) was dissolved in 25 mL of methyl alcohol and stirred for 5-7 min. Ethylenediamine (5.2 mmol) was added to the mixture under vigorous stirring. The progress of the reaction was monitored by TLC (EtOAc/n-hexane, 2:1). The reaction mixture was stirred for 48-72 h. When the solvent was evaporated, crystals precipitated. Crystals were filtered through filter paper and recrystallized from a mixture of ethanol-water.

General procedure for the synthesis of compounds **13j-m**

Mixture of benzylidenemalononitriles (**10j-m**) (5.1 mmol) and malononitrile (5.2 mmol) was dissolved in 35 ml of methyl alcohol and stirred for 5-7 min. Benzylamine (5.2 mmol) was added to the mixture under vigorous stirring. The progress of the reaction was monitored by TLC (EtOAc/n-hexane, 2:1). The reaction mixture was stirred for 48-72 h. When the solvent was evaporated, crystals precipitated. Crystals were filtered through filter paper and recrystallized from a mixture of ethanol-water.

RESULTS AND DISCUSSION

We initiated our studies by the investigation of the three-component reaction between benzylidene-malononitrile (**3a-f**), malononitrile (**4**) and ethylene-diamine (**5**) (Table 1). Gratifyingly, the reaction was observed to proceed smoothly at room temperature in a methanol solution in the absence of a catalyst, and the dihydroimidazopyridine product **6a** was obtained in 52% isolated yield (Table 1, entry 1). Afterwards, the effect of the electronic properties of the substituents on the benzylidene-malononitrile component was investigated. When benzylidenemalononitrile reactants (**3b-d**) with -CH_3, -OCH_3 and -$N(CH_3)_2$ groups as electron-donating substituents were tested, the targeted dihydroimidazopyridine products **6b**, **6c** and **6d** were obtained in 66, 66 and 72% yields, respectively (entries 2-4). In addition, electron-withdrawing -F and -Br substituents were also found to be tolerated in this three-component reaction affording the dihydroimidazopyridine products **6e** and **6f** in good yields (entries 5 and 6). Finally, it is worth mentioning that, by the use of microwave (MW) irradiation, the reaction time could be decreased down to 175 min, compared to 48-72 h at room temperature (yields were similar at room temperature).

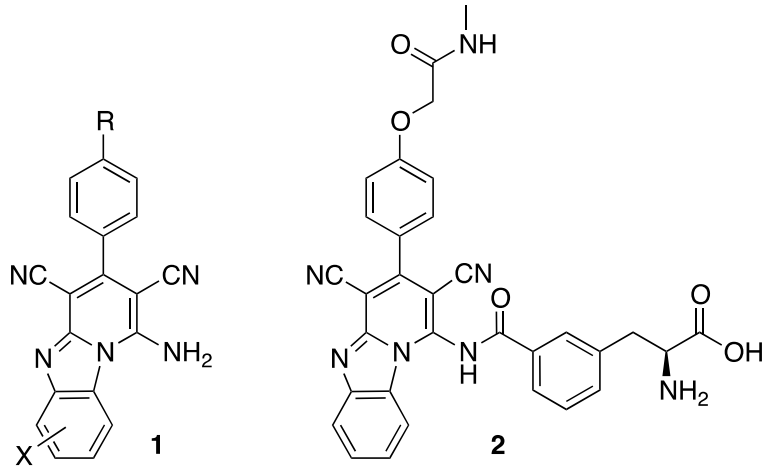

Fig. 1. Examples of biologically active pyridobenzimidazole analogues.

Table 1. Synthesis of dihydroimidazopyridine derivatives (**6a-f**) *via* three-component reaction between benzylidenemalononitriles, malononitrile and ethylenediamine.

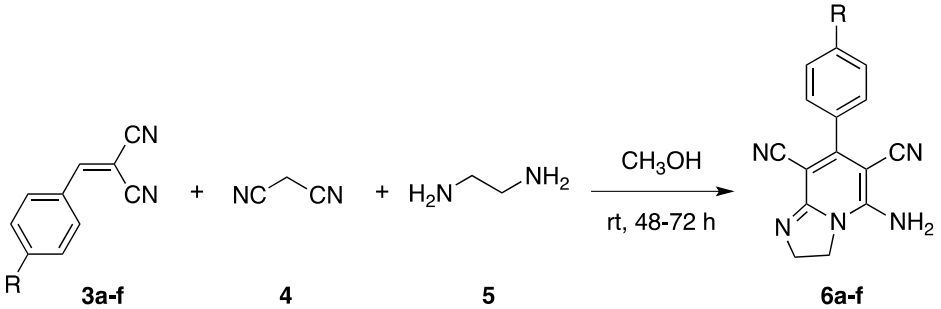

3a-f **4** **5** **6a-f**

Entry	R	Product	Yield (%)
1	H	6a	52
2	CH_3	6b	66
3	OCH_3	6c	66
4	$N(CH_3)_2$	6d	72
5	F	6e	68
6	Br	6f	62

The structures of the synthesized dihydroimdazopyridines were determined by NMR spectroscopy (Figs. S1-6). In addition, good quality crystals of three dihydroimidazopyridine products (**6b, 6c, 6e**) were obtained, and their structures were confirmed by single-crystal X-ray analysis (Fig. 2). Compound **6b** exhibits an intermolecular hydrogen bond in its crystal packing between one of the NH_2 hydrogens and the imine nitrogen of the dihydroimidazole moiety (Fig. 2a). On the other hand, compounds **6c** and **6e** were found to possess dimeric, hydrogen-bonded structures in which two intermolecular N-H···N≡C hydrogen bonds are present (Figs. 2b and 2c). This hydrogen bonding network is reminiscent of those previously observed for 2-cyanophenol derivatives [39,40]. Moreover, the crystal structure of **6e** revealed a F···F interaction with a distance of 2.77 Å between the two fluorine atoms [41]. The proposed reaction mechanism is shown in Scheme 1. Initially, ethylenediamine (**5**) is expected to act as a base and abstract one of the protons of malononitrile (**4**) to form the corresponding carbanion **7**. This carbanion could then undergo a Michael addition to benzylidenemalononitrile (**3a**) to give intermediate **8**. The incorporation of ethylenediamine (**5**) with separation of ammonia (NH_3) followed by a final oxidation would lead to the formation of the final dihydroimidazopyridine product **6a**. Surprisingly, when the three-component condensation of malononitrile and ethylenediamine with the dichloro-substituted benzylidenmalononitrile **3g** was tested, tetrahydroimidazopyridine product **9g** was obtained as the major product in 64% yield instead of the expected dihydroimidazopyridine compound (Table 2, entry 1). The generality of this outcome was examined with other dichloro-substituted benzylidenemalononitriles with –Cl substituents located at different positions (**3h** and **3i**). In accordance with our initial observation, these reactants afforded the tetrahydroimidazo-

pyridine products **9h** and **9i** in 73 and 79% yields, respectively (entries 2 and 3). In addition to the NMR spectroscopic analyses of the newly synthesized tetrahydroimidazopyridines (Figs. S7-9), the structure of product **9h** was further confirmed by single-crystal X-ray analysis (Fig. 3). In this crystal structure, molecules of **9h** form a hydrogen-bonded network by intermolecular hydrogen bonds with water molecules in addition to H···Cl interactions.

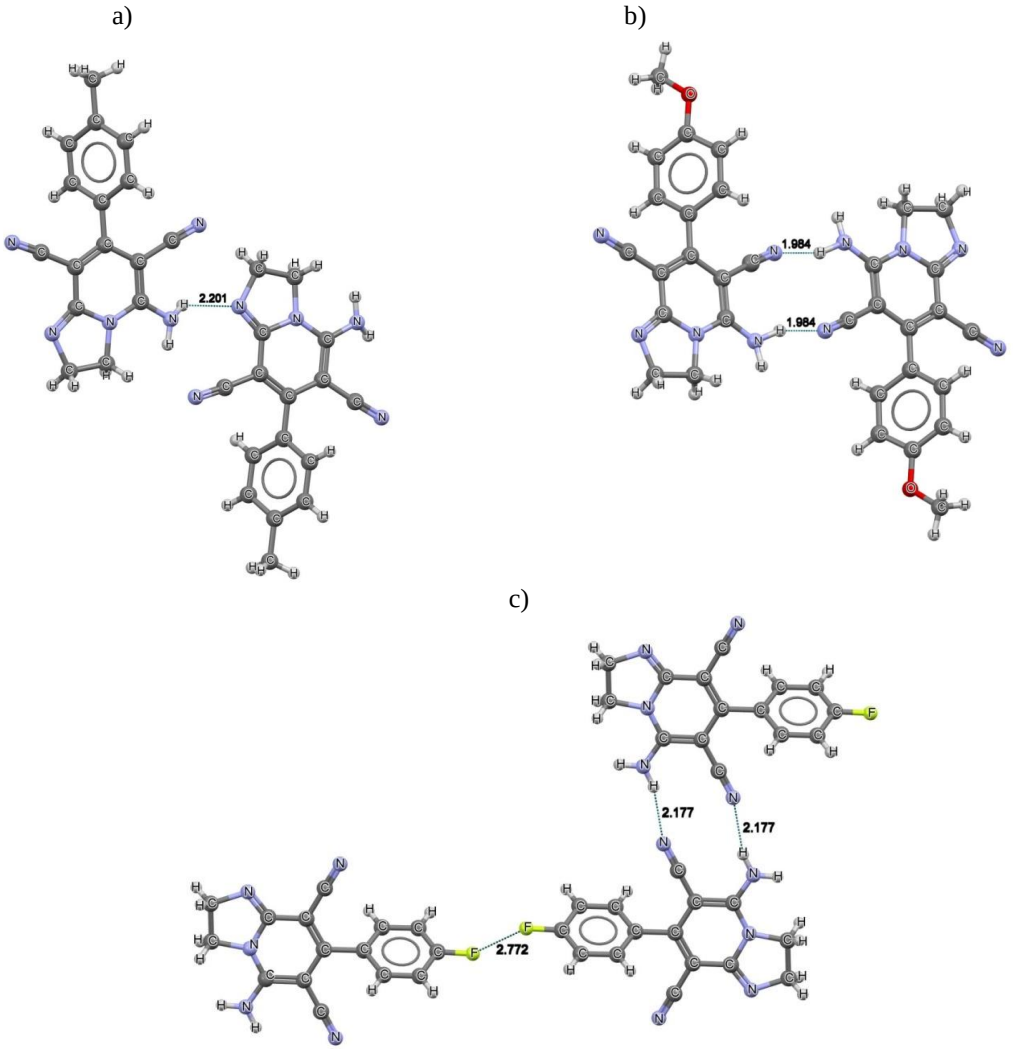

Fig. 2. X-ray structures of dihydroimidazopyridine products (a) **6b**; (b) **6c**; and (c) **6e**.

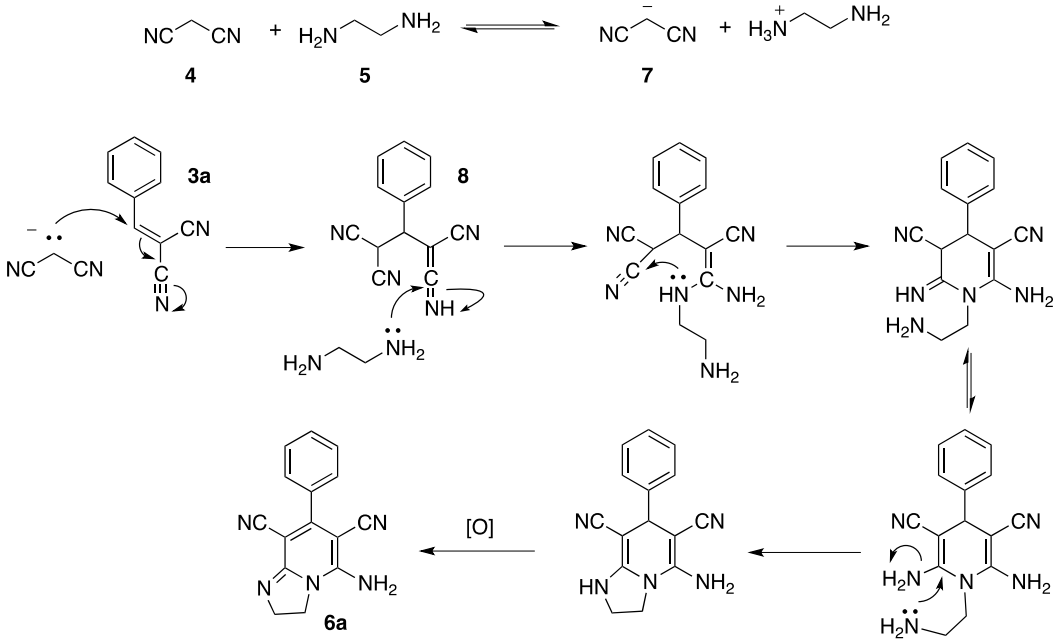

Scheme 1. Proposed reaction mechanism

Table 2. Synthesis of tetrahydroimidazopyridine derivatives (**9g-i**) *via* three-component reaction between dichloro-substituted benzylidenemalononitriles, malononitrile and ethylenediamine.

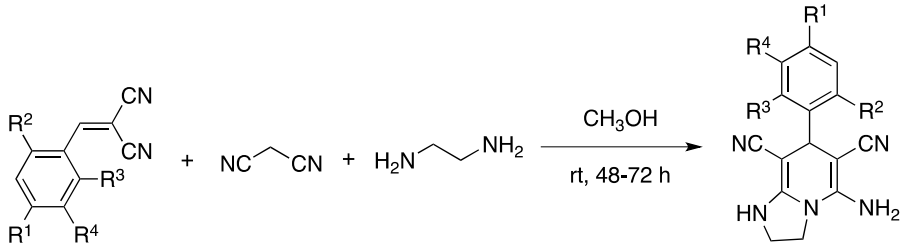

Entry	R_1	R_2	R_3	R_4	Product	Yield (%)
1	Cl	Cl	H	H	9g	64
2	H	Cl	Cl	H	9h	73
3	H	H	Cl	Cl	9i	79

Table 3. Synthesis of 2-imino-1,2-dihydropyridine derivatives (**13j-m**) *via* three-component reaction between para-substituted benzylidenemalononitriles, malononitrile and benzylamine

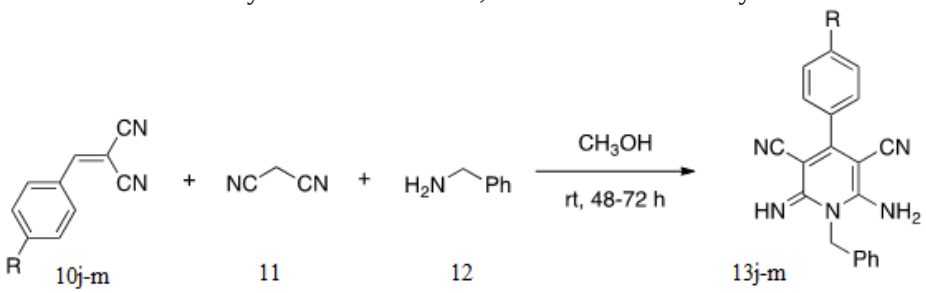

Entry	R	Product	Yield%
1	H	13j	63
2	OCH_3	13k	75
3	Br	13l	61
4	CF_3	13m	69

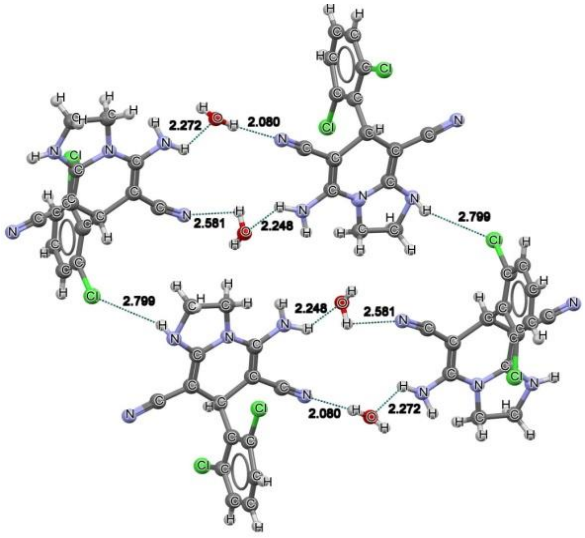

Fig. 3. X-ray structure of the tetrahydroimidazopyridine product **9h**.

Finally, the newly developed three-component reaction was tested using benzylamine (**12**) as the amine reactant in place of ethylenediamine (**5**). Fortunately, the reaction of benzylidenemalononitrile (**3a**) with malononitrile (**4**) and benzylamine (**12**) in methanol afforded the corresponding 2-imino-1,2-dihydropyridine product **13j** in 63% isolated yield (Table 3, entry 1, Figs. S10-13). The reaction was found to tolerate the presence of electron-donating (-OCH_3) and electron-withdrawing (-Br and -CF_3) groups on the phenyl ring, and the corresponding iminodihydropyridine products were obtained in good yields (75, 61 and 69% yields, respectively, entries 2-4).

CONCLUSION

We have developed an effective one-pot, three-component reaction for the synthesis of multisubstituted imino- and imidazopyridine starting from benzylidenemalononitriles, malononitrile and amines. The reactions are operationally simple, work at room temperature and under catalyst-free conditions. While dihydro- and tetrahydroimidazopyridines were obtained in a selective manner as the major products when ethylenediamine was used as the amine reactant, the use of benzylamine gave rise to the formation of 2-imino-1,2-dihydropyridine products. Investigation of the substrate scopes of the developed methodology indicated that the reactions tolerate a variety of benzylidene-malononitriles having electron-donating and withdrawing substituents, and the targeted products were obtained in good to high yields (52-79%).

REFERENCES

1. C. Cabrele, O. Reiser, *J. Org. Chem.*, **81**, 10109 (2016).
2. A. P. Taylor, R. P. Robinson, Y. M. Fobian, D. C. Blakemore, L. H. Jones, O. Fadeyi, *Org. Biomol. Chem.*, **14**, 6611 (2016).
3. F. E. Goda, A. A. Abdel-Aziz, O. A. Attef, *Bioorg. Med. Chem.*, **12**(8), 1845 (2004).
4. X. Haihua, L. Pingliang, G. Dongcai, H. Jinhui, C. Yuchao, H. Wei, *Med. Chem. Res*, **23**, 1941 (2014).
5. H. A. Ashraf, A. A. Dalal, L. Jochen, N. T. Heather, D. G. Bernard, A. P. Gary, A. O. A. Mohammed, *European Journal of Medicinal Chemistry*, **45**, 90 (2010).
6. A. M. E. Amal, A.H.F. Nahla, A. H. S. Gamal, *Bioorg. Med. Chem.*, **17**, 5059 (2009).
7. K. C. Rupert, J. R. Henry, J. H. Dodd, S. A. Wadsworth, D. E. Cavender, G. C. Olini, B. Fahmy, J. J. Siekierka, *Bioorg. Med. Chem. Lett.*, **13**(3), 347 (2003).
8. C. Allais, J.-M. Grassot, J. Rodriguez, T. Constantieux, *Chem. Rev.*, **114**, 10829 (2014).
9. J. A. Bull, J. J. Mousseau, G. Pelletier, A. B. Charette, *Chem. Rev.*, **112**, 2642 (2012).
10. J. A. Varela, C. Saá, *Chem. Rev.*, **103**, 3787 (2003).
11. Z. Mi-Na, R. Zhi-Hui, W. Yao-Yu, G. Zheng-Hui, *Chem. Commun.*, **48**, 8105 (2012).
12. W. Jicheng, X. Wenbo, Y. Zhi-Xiang, W. Jian, *J. Am. Chem. Soc.*, **137**, 9489 (2015).
13. W. Jie-Ping, J. Yanfeng, H. Changfeng, Sh. Shouri, *J. Org. Chem.*, **81**, 6826 (2016).
14. R. Qingyun, M. Wenyan, Y. Yongyan, H. Hongwu, G. Yucheng, *Synthetic Communications*, **40**, 303 (2010).
15. Z. Fenguo, L. Xu, Z. Ning, L. Yongjiu, Z. Rui, X. Xiaoqing, D. Dewen, *Organic Letters*, **15** (22), 5786 (2013).
16. C. R. Brindaban, J. Ranjan, S. Sowmiah, *J. Org. Chem.*, **72**, 3152 (2007).
17. M. Akbar, A. Sajad, A. B. Mohammad, *Synthetic Communications*, **46** (19), 1605 (2016).
18. M. Lijuan, W. Xianpei, Y. Wei, H. Bing, *Chem. Commun.*, **47**, 11333 (2011).
19. L. Zhi, C. Zhen-Chu, Z. Qin-Guo, *Synthetic Communications*, **34** (2), 361 (2004).
20. K. B. Avik, S. Sougata, M. Kamarul, H. Alakananda, *Chem. Commun.*, **51**, 1555 (2015).
21. A. H. Justin, S. H. Michael, D. R. Scott, *J. Org. Chem.*, **81**, 10376 (2016).
22. H. Huawen, C. Jinhui, T. Lichang, W. Zilong, L. Feifei, D. Guo-Jun, *J. Org. Chem.*, **81**, 1499 (2016).
23. R. R. Adam, L. D. Rick, *J. Org. Chem.*, **63**, 7840 (1998).
24. F. Yajie, W. Panpan, G. Xin, W. Ping, M. Xu, Ch. Baohua, *J. Org. Chem.*, **81**, 11671 (2016).
25. K. B. Chandan, D. U. Jayant, R. K. Pranab, *Synthetic Communications*, **43**, 2208 (2013).

26. B. Mohammad, K. Ali, H. Mahdieh, *Synthetic Communications*, **39**, 1002 (2009).
27. F. A. Abu-Shanab, Y. M. Elkholy, M. H. Elnagdi, *Synthetic Communications*, **32** (22), 3493 (2002).
28. G. Mehdi, M. Parham, A. Alireza, *Tetrahedron Letters*, **58**, 1887 (2017).
29. Z. Huiping, J. Linlin, *Tetrahedron Letters*, **56** (21), 2777 (2015).
30. K. Dilpreet, Kh. Rajni, K. K. Kamal, *Tetrahedron Letters*, **57**, 4464 (2016).
31. G. G. Fereshteh, O. Marzieh, S. Mina, S. Farhad, R. Ali, M. Mohammad, R. B. Ghasem, A. Tahmineh, F. Loghman, Sh. Abbas, F. Alireza, *Tetrahedron Letters*, **56** (5), 743 (2015).
32. A. Emad, E. Sina, S. Mehdi, Kh. Mehdi, M. Mohammad, *Tetrahedron Letters*, **58** (2), 121 (2017).
33. D. M. Lyons, K. M. Huttunen, K. A. Browne, A. Ciccone, J. A. Trapani, W. A. Denny, J. A. Spicer, *Bioorg. Med. Chem.*, **19**, 4091 (2011).
34. K. M. Huttunen, M. Gynther, J. Huttunen, E. Puris, J. A. Spicer, W. A. Denny, *J. Med. Chem.*, **59**, 5740 (2016).
35. K. Bogdanowicz-Szwed, A. Czarny, *J. Prakt. Chem.*, **335**, 279 (1993).
36. M. H. Elnagdi, K. U. Sadek, M. A. El-Maghraby, M. A. Selim, A. K. Khalafallah, M. A. E. M. Reaslan, *Phosphorus, Sulfur, and Silicon and the Related Elements*, **105**, 51 (1995).
37. N. M. Elwan, *J. Heterocyclic Chem.*, **41**, 281 (2004).
38. C. G. Yan, Q. F. Wang, X. K. Song, J. Sun, *J. Org. Chem.*, **74**, 710 (2009).
39. H. Bock, W. Seitz, Z. Havlas, J. W. Bats, *Angew. Chem. Int. Ed.*, **32**, 411 (1993).
40. H. Bock, W. Seitz, M. Sievert, M. Kleine, J. W. Bats, *Angew. Chem. Int. Ed.*, **35**, 2244 (1996).
41. R. J. Baker, P. E. Colavita, D. M. Murphy, J. A. Platts, J. D. Wallis, *J. Phys. Chem. A*, **116**, 1435 (2012).

ЕДНОСТАДИЕН СИНТЕЗ НА ЗАМЕСТЕНИ ИМИНО- И ИМИДАЗОПИРИДИНИ В ОТСЪСТВИЕ НА КАТАЛИЗАТОР

Ф. Н. Нагиев, А. М. Магеррамов, И. М. Ахмедов, Х. А. Асадов, А. Н. Халилов, А. В. Гурбанов, Г. З. Мамедова, А. Р. Асгарова, Е.З. Гусейнов, И. Г. Мамедов*

Факултет по химия, Държавен университет в Баку, Баку, AZ1148, Азербайджан

Постъпила на 30 август, 2017; коригирана на 2 февруари, 2018

(Резюме)

Заместени производни на имино- и имидазопиридини са синтезирани чрез нова едностадийна трикомпонентна реакция между бензилиденмалононитрили, малононитрил и амини в отсъствие на катализатор при стайна температура. При използване на етилендиамин като аминния компонент на реакцията се получават селективно дихидро- и тетрахидроимидазопиридини с добър до висок добив. Използването на бензиламин води до образуване на 2-имино-1,2-дихидропиридинови продукти. Установено е, че реакциите толерират присъствието на електрон-отдаващи и електрон-изтеглящи заместители върху бензилиденмалононитриловите реагенти. Продуктите на тези реакции са кристални и могат да се изолират с добър добив и висока чистота чрез лесна процедура при стайна температура.

Bulgarian Chemical Communications, Volume 50, Issue 4 (pp. 575 – 583) 2018

Synthesis and characterization of polymeric blend membranes enhanced by monoethanolamine for CO_2/CH_4 separation

A. Mushtaq*, H. Mukhtar, A. M. Shariff

Chemical Engineering Department, Universiti Teknologi PETRONAS, 32610 Seri Iskandar, Perak Darul Ridzuan, Malaysia

Received, December 8, 2017; Revised, August 1, 2018

Gas separation membranes for natural gas are widely used. For efficient separation of CO_2/CH_4, high-performance gas separating polymeric blend membranes are desired. The main objective of this study is to synthesize blend membranes for removal of CO_2 from CH_4 using glassy and rubbery polymers with the addition of amine. The methodology comprises various contents of polyvinyl acetate (PVAc) ranging from 5 to 20 wt% blended with polysulfone (PSU) and 10 wt% MEA in DMAc solvent used for the formation of flat sheet membranes *via* solution casting method. The synthesized blend membranes possessed homogenous surfaces and showed a uniform packed bed of spherical structure, as seen from FESEM images. The existence of a single glass transition temperature for different blend membranes indicated miscibility among the polymeric blends, shown by DSC analysis. Thermogravimetric analysis showed an improvement in the maximum degradation temperature with the increase in PVAc content in the membrane blends. FTIR analysis confirmed the polymer blend's miscibility with very few spectral peak shifts. The gas permeation results concerning MEA showed that CO_2 permeance increased, in PSU and PSU 80%/PVAc 20%, from 39.63% to 63.97% at 2 bar pressure. EPBM is an appropriate tool for the production of novel materials with joined characteristics that improved application properties with low-cost advantage.

Keywords: Polymeric blend membranes; Monoethanolamine; Morphology; Thermal degradation temperature; Spectral analysis.

INTRODUCTION

The performance of gas separating membranes is quite important for effective separation of CO_2 from natural gas. For membrane synthesis, permeance and selectivity are essential parameters that need to be addressed for efficient CO_2 separation [1, 2]. In gas separation, many glassy polymers have been used for membrane fabrication based upon industrial or scientific research work. Polysulfone was considered because of its good thermal, mechanical and chemical stability along with satisfactory gas performance [3, 4]. The same characteristics of polyvinyl acetate (PVAc) along with its comparatively low price, piezoelectric, pyroelectric and ferroelectric properties [5, 6] define its main advantages as flexibility, low density and formability [7]. Table 1 shows the different studies on polymer blended membranes [8-20] .

Different modifications were employed to improve membrane performance. Monoethanolamine (MEA), which belongs to primary amines, is widely used for removing CO_2 from natural gas; it is a relatively strong base having high reactivity with CO_2, low cost of solvent, thermal stability, but it was replaced by more efficient systems because of its corrosive properties, degradation of solvent issues, high heat of reaction with CO_2 and considerable energy requirements for regeneration of solvent used [21].

Numerous researchers have considered the chemistry of CO_2-amine solutions over many years due to its significant industrial application for CO_2 removal from gas streams. The Danckwerts' zwitterions mechanism has become the most frequently accepted mechanism for CO_2-amine reaction [22]. The reactions between CO_2 and primary amines are shown below, R representing the functional group for MEA:

R_1= -H, R_2= $-CH_2CH_2OH$

$$R_1R_2NH + CO_2 \leftrightarrow R_1R_2NH^+COO^-(\text{Zwitter ion}) \quad (1)$$

$$R_1R_2NH^+COO^- + R_1R_2NH \leftrightarrow R_1R_2NCOO^-(\text{Carbamate}) \quad (2)$$

Overall reaction is:

$$2R_1R_2NH + CO_2 \leftrightarrow R_1R_2NCOO^- + R_1R_2NH^+ \quad (3)$$

It is mean

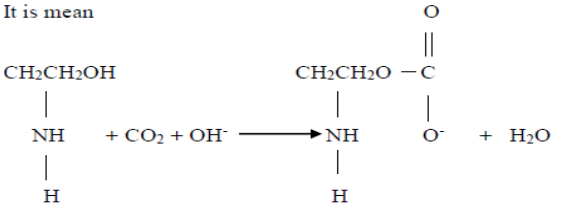

(4)

* To whom all correspondence should be sent:
E-mail: engrasimmushtaq@yahoo.com

The amine solution has shown efficient capability for natural gas purification in an absorption process [22]. Hence, it is expected that by blending with glassy polymer using different alkanolamine solutions, the separation ability of a blended polymeric membrane for the CO_2/CH_4 mixture will be enhanced. Different alkanolamines have different reaction rates with various acid gases. Furthermore, these alkanolamines differ in their equilibrium absorption characteristics for the many acid gases and have different sensitivities to corrosion factors and solvent stability. In MEA (primary amine), the CO_2 is captured by a chemical absorption process, in which the carbon dioxide reacts with the primary amine in the form of a carbamate. The main objective of this study is to synthesize an enhanced polymeric membrane with the addition of amine.

Table 1. Different studies on blend membranes

Year	Polymers	Gas type	Remarks	Permeance	Selectivity
2006	PU based PEI/PAI (Glassy/Glassy) blend	CO_2/N_2	CO_2/N_2 selectivity of PU-based blend membranes was increased	P_{CO2}=20.06 Barrer	$\alpha\frac{CO_2}{N_2}=22.56$
2006	PU/PDMS (Rubbery/Rubbery) cross-linked	CO_2/CH_4	Highest permeability, diffusivity, and solubility values are found for the PDMS membranes.	P_{CO2}=10 Barrer	$\alpha\frac{CO_2}{CH_4}=0.41$
2008	PES/PI (Glassy/Glassy) blend MMM	O_2/N_2	Ideal separation factors of O_2/N_2 is increased	P_{O2}=4.2 Barrer	$\alpha\frac{O_2}{N_2}=3.8$
2009	PVAm/PVA with porous PES support	CO_2/N_2	Ultra-thin membrane with good strength, stability and permeability/ selectivity	P_{CO2}=0.58 m^3(STP) /(m^2 h bar)	$\alpha\frac{CO_2}{N_2}=74$
2010	PEG/PDMS	CO_2/CH_4	Remarkably, the CO_2/H_2 selectivity is enhanced	P_{CO2}=530 Barrer	$\alpha\frac{CO_2}{CH_4}=10$
2010	PES/PI (Glassy/Glassy)	O_2/N_2	Gas permeance of N_2 increased with increase in feed pressure	P_{O2}=210.8 GPU	$\alpha\frac{O_2}{N_2}=5.4$
2011	SPEEK/ Matrimid	CO_2/CH_4	Cross-linked for anti-plasticization	P_{CO2}=9.43 Barrer	$\alpha\frac{CO_2}{CH_4}=27.98$
2011	PEI/PVP	CO_2/CH_4, CO_2/N_2	Significant improvement in selectivity	P_{CO2}=1.66 GPU	$\alpha\frac{CO_2}{CH_4}=55.33$
2012	PIM-1/ Matrimid	CO_2/CH_4, CO_2/N_2	Increased selectivity	P_{CO2}=50 Barrer	$\alpha\frac{CO_2}{CH_4}=31$
2013	PSF/PVP	CO_2/CH_4	Studied effect of solvents	P_{CO2}=275 GPU	$\alpha\frac{CO_2}{CH_4}=5.75$
2013	PU/PVA	CO_2/CH_4	Increased CO_2 permeability	P_{CO2}=49.5 Barrer	$\alpha\frac{CO_2}{CH_4}=10.1$
2013	PEG-PDMS	CO_2/N_2	Significant improvement in selectivity	P_{CO2}=20.0 GPU	$\alpha\frac{CO_2}{N_2}=18$
2014	CA/TiO_2 blend	CO_2/CH_4	Permeability of CO_2 was found to be increased for CA–TiO_2 blended	P_{CO2}=3.43x 10^3 Barrer	$\alpha\frac{CO_2}{CH_4}=23.3$
2015	PES/PVAc	CO_2/CH_4	CO_2 permeance increase due to the addition of PVAc in PES	P_{CO2}=4.15 GPU	$\alpha\frac{CO_2}{CH_4}=1.40$
2016	PSF/PI	CO_2/CH_4	Improved selectivity	P_{CO2}=3.3 Barrer	$\alpha(\frac{CO_2}{CH_4})=13.06$

Table 2. Blend composition of different polymer blend membranes

Membrane	Polymer		Amine, 10 wt.%
	PSU, wt. %	PVAc, wt. %	
M1	100%	0%	-
M2	0%	100%	
M3	95%	5%	MEA
M4	90%	10%	
M5	85%	15%	
M6	80%	20%	

METHODOLOGY

Materials

Polysulfone (PSU Udel® P-1800 powdered grade with a glass transition temperature (T_g) of 185°C) was purchased from Solvay Advanced Polymers, L.L.C, U.S.A. Polyvinyl acetate (PVAc beads, average Mw ~100,000 by GPC with a glass transition temperature (T_g) of 28°C) was supplied by Sigma-Aldrich, Germany. Dimethylacetamide (DMAc 99.99% pure) was acquired from Merck, Germany. MEA amine 99.99% pure was purchased from Merck, Germany. Amines were used for the fabrication of polymeric amine blend membranes.

Method

Two different types of membranes were prepared in this work: polymeric blend membranes and polymeric amine blend membranes. To prepare the membranes, the following procedure is given:

i. PSU was heated at 110°C to remove moisture content. Then, the PSU and PVAc were allowed to dissolve completely in DMAc solvent.

ii. Then the amine was added in the blend with continuous stirring for 24 h to obtain a homogeneous dope solution.

iii. To remove air bubbles, the solution was ultrasonicated in Transonic Digital S, Elma® for 3 h at a frequency of 100 Hz.

iv. This blend was poured and cast on a glass plate using a casting knife with an opening of 200 µm. After 1 h of evaporation, the casted film was dried in an oven at 70°C for 2 h. These membranes were also dried at ambient temperature for five days to allow the evaporation of the solvent.

The synthesized membranes were then peeled off for further characterization. The different compositions of polymers and amines of blend membranes are shown in Table 2.

The enhanced polymeric blend membrane was developed by blending polysulfone glassy polymer and rubbery polymer polyvinyl acetate with mono ethanol amine was carried out in the solvent dimethylacetamide. Figure 1 represents the flow diagram of a methodology for fabrication of amine polymer blend membrane. These synthesized membranes were characterized by the following methods:

The thermal degradation temperature of the synthesized polymeric blended membranes was determined by TGA (thermal gravimetric analysis). Approximately 10 mg of the sample was heated at a rate of 2°C/min with the Perkin Elmer TGA. The CO2SMU apparatus was used for the gas permeation experiment, where CO_2/CH_4 flow rate (0.1 m^3/sec) was controlled by a flow meter/controller. These trials were accomplished at room temperature (302±2K) under ambient pressure (101±2 kPa).

The FTIR spectrum was taken on a Perkin Elmer Spectrum One FTIR spectrometer, to investigate the interaction between both polymers and amine. The scans were 20 in the wavelength range of 4000 cm^{-1} – 450 cm^{-1} and the spectra were obtained from a 200-µm diameter sampling area. Membrane samples were cut from casted membrane films at random positions dried for more than 48 h at room temperature and then fixed to the plate. All spectra were corrected for the FTIR characteristic progressive increase in the absorbance at lower wave numbers, using the equipment software.

RESULTS AND DISCUSSION

Morphology of enhanced polymeric blend membranes (EPBM)

MEA amine was blended with different compositions of PVAc in a PSU matrix, the morphology of blended membranes is shown in Figures 2 to 5. It is evident from the top surfaces of Figures 2 (a) to 5 (a) that their surfaces were likewise uniform without any pin holes and no indications of phase separation. Respectively, on distinct cross-sections of Figures 2 (b) to 5 (b) the enhanced polymeric blend membranes ьre highly packed with uniform microspheres known as a packed bed of spheres. Nevertheless, the measure of the structure is

somewhat dissimilar because of 5-20 wt. % compositions of PVAc in PSU with 10 wt. % of MEA.

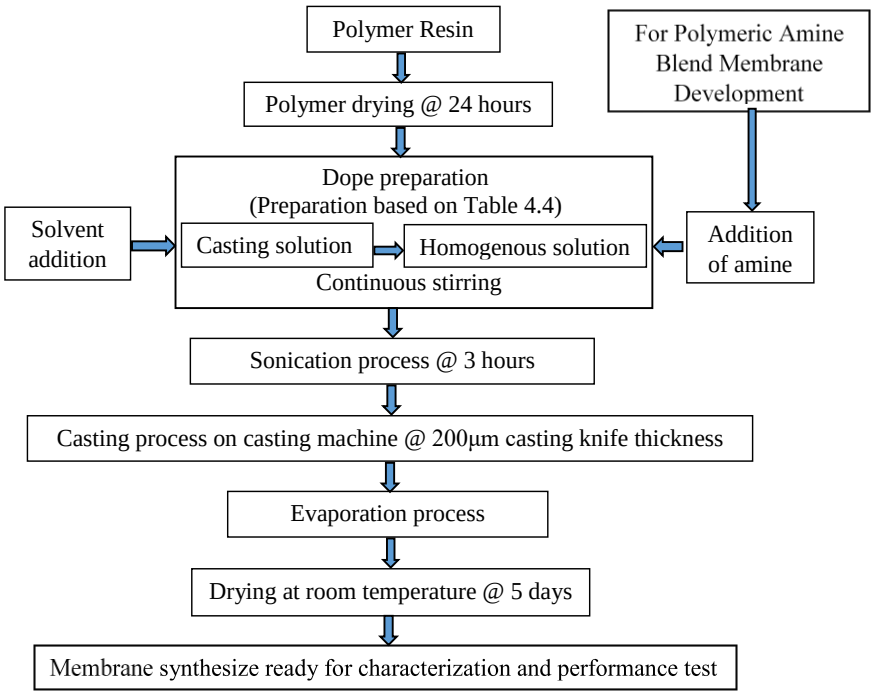

Fig. 1. Methodology for fabrication of amine polymer blend membrane

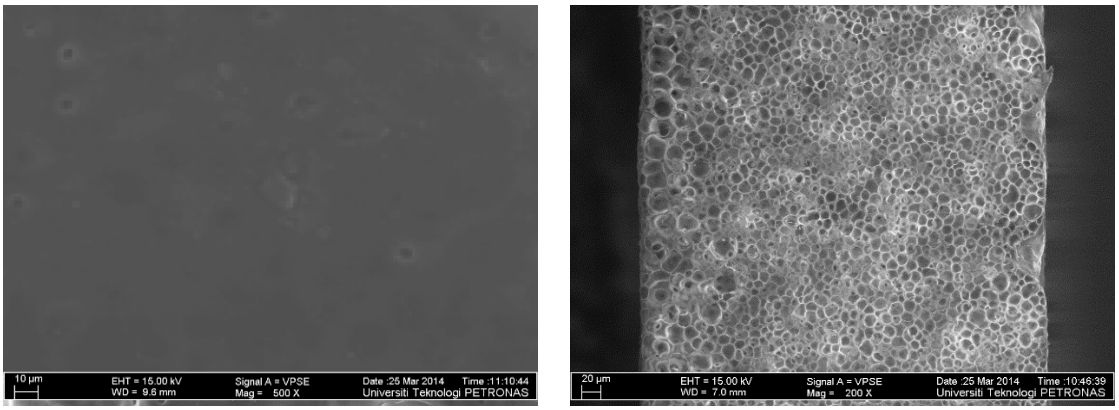

(a) (b)

Fig. 2. Blend membrane of PSU/PVAc (95/5) wt. % / MEA (a) Top view (500 ×) (b) Cross section view (200 ×)

For EPBM with MEA these figures show that membranes top surfaces were uniform and without any phase separation which suggests that miscibility exists between PSU/PVAc and MEA. Similarly, on comparing the cross-sections in Figures 2 (b) to 5 (b), the EPBM contained a uniform packed bed of spheres. The sizes of the packed bed of spheres structure increase the percentage of PVAc from 5-20 wt. % with MEA, the sphere size was found from 22.40-9.73µm and extent toward 41.06-10.64µm.

To decrease the interfacial area with dispersed morphology in blends, shape relaxation of the deformed particles may occur latter, tending to acquire a spherical shape [23]. When the different compositions of PVAc are blended in PSU with different amines the wall area decreases because PVAc and amines are incorporated into the spheres. From the microporous structures of the blended membranes it is apparent that the surfaces are reasonably homogeneous indicating miscibility between the PSU/PVAc polymers and amines [24]. In addition, the number of spheres differs depending on PVAc composition and addition of MEA amine. This is probably because thermodynamic instability overcomes the kinetic process [24].

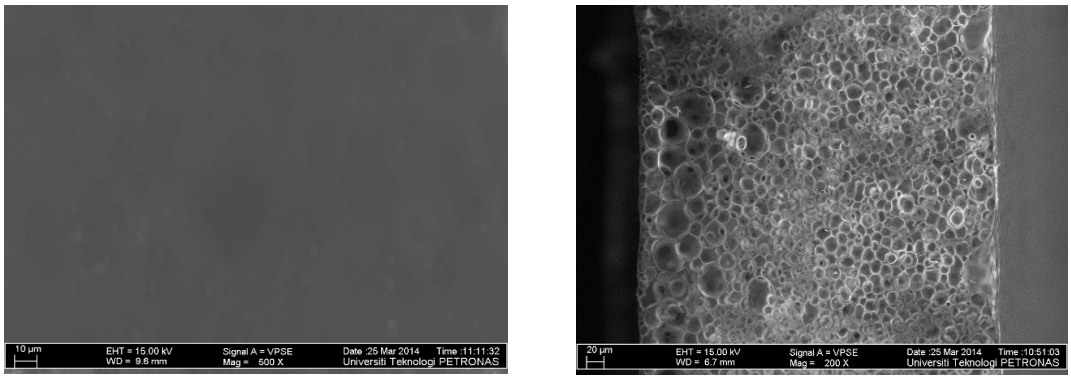

(a) (b)

Fig. 3. Blend membrane of PSU/PVAc (90/10) wt. % / MEA (a) Top view (500 ×) (b) Cross section view (200 ×)

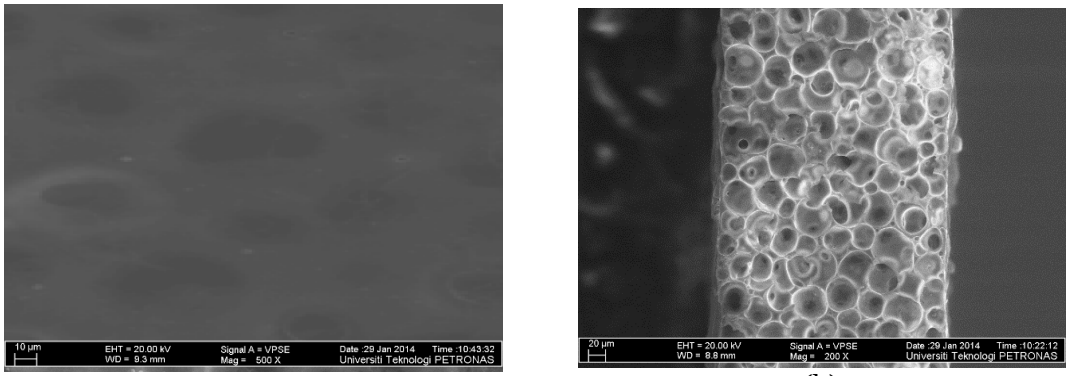

(a) (b)

Fig. 4. Blend membrane of PSU/PVAc (85/15) wt. % / MEA (a) Top view (500 ×) (b) Cross section view (200 ×)

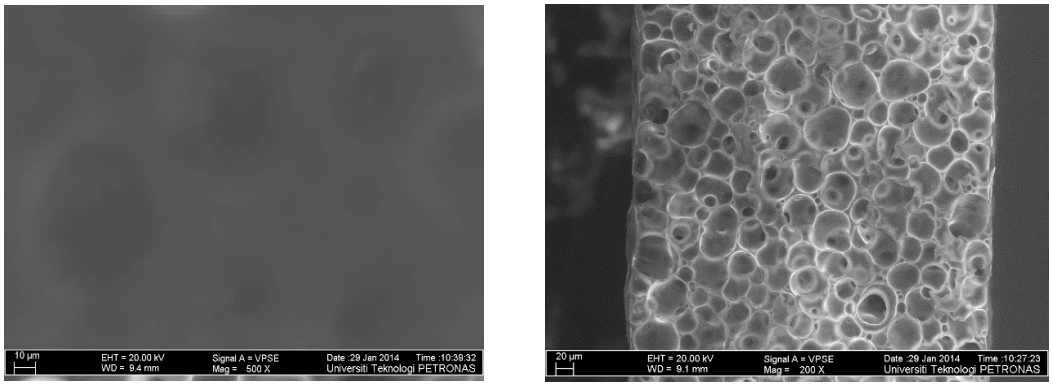

(a) (b)

Fig. 5. Blend membrane of PSU/PVAc (80/20) wt. % / MEA (a) Top view (500 ×) (b) Cross section view (200 ×)

Increasing number of mobile linkages in the polymer backbone increasing the free volume of the polymer when PVAc (rubbery) polymer was used. For PSU (glassy) polymer, to increase polymer free volume through chain backbone packing, the efficiency and cohesive energy density decreased [3, 25]. Morphology of homogenous polymer blend relies upon the composition blend, consistency of the individual segments and the preparation history [23, 26]. The two-stage morphology can altogether impact the pervasion properties of the films. Structures of the developed membranes revealed a packed bed of spheres rather than finger-like microvoids in the sub-porous layer; this indicates the absence of defects and pinholes at the membrane surfaces [3, 27]. Due to the well-known interaction between CO_2 and $–NH_2$ groups, the amine molecules that occupy the micropores will increase the CO_2 adsorption of these materials [23, 24]. In addition, as MEA amine was added, a significant improvement in the membrane's perm-selectivity was also observed. As a consequence of the solubility of CO_2 in MEA amine, the presence of amine enhanced the CO_2 solubility across the membrane. This research into the morphology of different polymer blends with amines was not found in the literature.

Thermal gravimetric analysis of enhanced polymeric blend membranes

Figure 6 shows the degradation behavior when MEA amine was added in different compositions of PSU/PVAc. The stability of synthesized blend membrane was changed. From this figure for M3 to M6, the primary bend demonstrates the weight reduction of 10 wt. % for MEA at 166.42°C (M3). The second bend shows a mass loss of 5-20 wt. % of PVAc at 326.62°C and the third bend of PSU at 528.32°C demonstrates the 50-60 wt. % mass loss in the blend membranes.

On the contrary, this trend is also shown with M6, degradation onsets at 523.57°C, and maximum degradation temperature is 559.74°C. It is also observed that the amount of residue for all membranes at 800°C has decreased by the addition of MEA and PVAc in PSU. At the end of the degradation, almost 20-25 wt. % of residue remained. For an effective separation, the polymer should have good interaction with one of the components of the mixture. Molecular structure, arrangement and specific nature of chemical groups attached to the main chain are some factors that affect the properties of the membrane and their performance. In comparison, alkanol amines decompose at a lower temperature than PSU/PVAc because of the substitution of NH group [28, 29]. Table 3 summarized the thermal degradation results.

The degradation products of MEA are mainly formate, hydroxyethyl formamide, hydroxyethyl imidazole and oxalate. Glycolate and acetate are also present, however, in low concentrations. Adding MEA to the blend changed the thermal stability of PSU/PVAc blend. This is probably due to the properties of the amine, specifically its basicity and the number of –OH groups present. These results are in good agreement with previous studies [28-30].

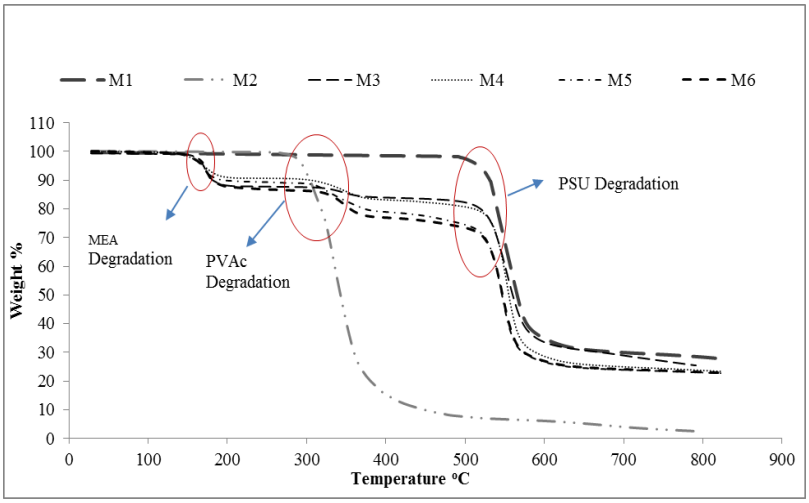

Fig. 6. Effect of TGA on enhanced polymeric blend membranes with various composition of PVAc in PSU with MEA amine

Table 3. Thermal degradation temperature of polymeric MEA amine blend membranes

Membrane Sample	Polymer Blend			Degradation MEA amine onset temperature (°C)	Maximum MEA amine degradation temperature (°C)	Degradation onset PVAc temperature (°C)	Maximum degradation PVAc temperature (°C)	Degradation onset PSU temperature (°C)	Maximum degradation PSU temperature (°C)
	PSU wt. %	PVAc. wt. %	Amine 10wt.%						
M1	100	-	-	-	-	-	-	535.13	570.48
M2	-	100	-	-	-	318.54	355.38	-	-
M9	100	-	MEA	165.65	200.88	-	-	522.12	543.04
M18	95	5		166.42	178.90	326.62	356.64	528.32	569.44
M19	90	10		164.11	177.56	323.37	355.57	527.76	566.26
M20	85	15		163.94	174.06	322.78	352.24	525.50	561.16
M21	80	20		159.74	173.51	320.80	350.63	523.57	559.74

Spectral analysis of enhanced polymeric blend membrane

FTIR spectral analysis of enhanced polymeric blend membranes is shown in Figure 7. A broad frequency of FTIR spectra for PVAc, PSU, and MEA was examined. A complete spectral analysis was also done to confirm the hydrogen-bonding behavior of the amine blended membranes [38].

Figure 7 shows the FTIR spectra of the synthesized PSU/PVAc/MEA polymeric blend membranes at 10 wt. % MEA with various composition of PVAc in the PSU matrix. The functional groups (S=O, CSO_2C, C-O, C_6H_6, C=O and C-H) of PSU/PVAc blend slightly change their positions, but remain stable in the range. Spectral shifts are observed for the benzene ring by the addition of MEA. The amine group (C-N) appears at 1058.23-1094.71 cm^{-1} for PSU/PVAc/MEA (M3-M6) blend membranes. The N-H group's peaks for M3 to M6 are observed at 3442.77 cm^{-1} - 3494.04 cm^{-1}. The hydrogen bonding is a strong intermolecular interface that affects miscibility.

Similarly, by the addition of MEA in the PSU/PVAc blend, the O-H peak appears at 3219.45-3307.86 cm^{-1} for M3 to M6. Hydrogen bonding is important for hydroxy compounds, but the effect tends to be weaker than for the hydroxy group, and the overall effect on the spectrum is slightly less pronounced. This condition changes the amino salts and related ammonium, where strong hydrogen bonding is experienced, and a consistent broadening of the NH^+ absorption is observed [31]. This figure shows the incorporation of MEA into PSU/PVAc matrix by confirming the presence of the particular frequency bands of the characteristic peaks which is evidence that the amine had an interaction with the polymer.

The structural differences between different alkanolamine are important, and they strongly influence the chemistry and reactivity of nitrogen and the N-H group. Hydrogen bonding disturbs NH^+ and OH^- groups by altering the electronic field, which then provides the enthalpy that favours mixing [32]. These results indicated that hydrogen-bonding interactions existed between the ester carbonyl and carboxyl end groups of PSU and the OH groups of PVAc/amine [23]. Hence, these results of the structural analysis support the compatible nature of PSU/PVAc/amines blend membranes indicated by the microscopic and macroscopic observations.

Polymer blends compatibility, the peak shifts of certain significant bands to other frequencies point to the existence of particular interactions taking place amongst the characteristic groups of the pure PSU/PVAc polymers and amines. The summarized form of different shifts in the FTIR spectra is presented in Table 4 and supports the development of the interactions among the polymers which indicates their miscibility in the form of blended membranes [6, 32-34]. The limited degree of peak shifting revealed by FTIR studies confirmed the miscibility of the tested polymer blends.

Moreover, there was no cross-linking and formation of intermediates, and the frequency shifts observed were peaks that characterized diaryl sulfone, C=O, C-O and N-H groups of PSU/PVAc/amine. These spectral changes point to molecular interactions between the polymer components in the blends, highlighting their compatibility [26]. These observations are in good agreement with previous studies [16, 34, 35].

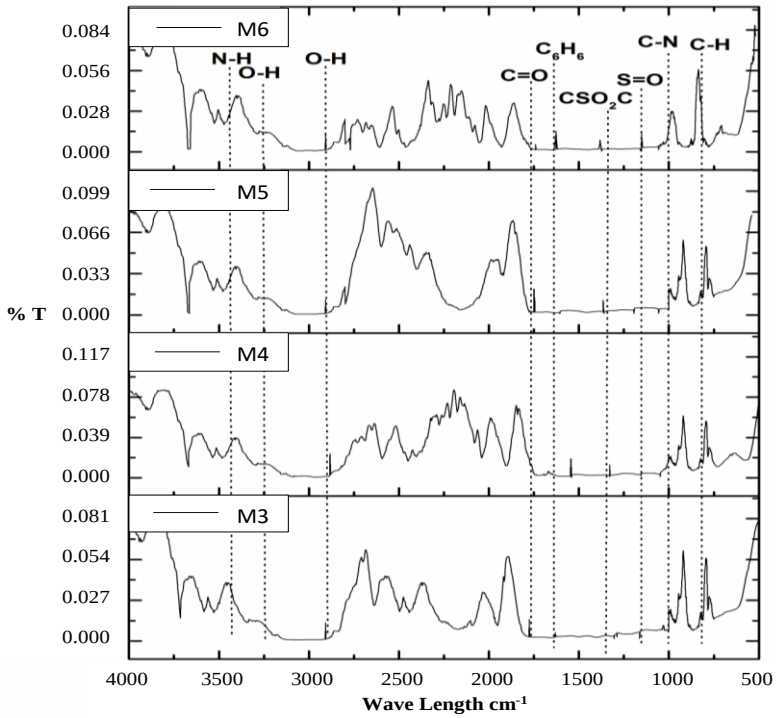

Fig. 7. Comparative FTIR spectra of the polymeric blend membranes with MEA amine.

Table 4. Summary of the FTIR spectral data of enhanced polymeric blend membranes

Spectral assignment	Wave number, cm^{-1}	PSU/PVAc/DEA blend membranes Observed wave number, cm^{-1}	PSU/PVAc/MDEA blend membranes Observed wave number, cm^{-1}	PSU/PVAc/MEA blend membranes Observed wave number, cm^{-1}
S=O symmetric stretch	1150-1100	1087.73-1123.15	1105.35-1130.74	1118.13-1140.28
CSO_2C asymmetric stretch	1322, 1370-1250	1305.39-1320.16	1307.28-1324.63	1310.93-1334.52
C-O asymmetric stretch	1244, 1260-1000	1057.78-1068.83	1039.92-1052.54	1034.41-1049.26
C_6H_6 ring stretch	1587-1489	1566.80-1585.27	1542.67-1569.39	1570.43-1581.62
OH aliphatic and aromatic stretch	2886, 2938 and 2971	2806.42-2819.88	2871.72-2889.44	2847.29-2867.08
C=O stretch	1736, 1760-1600	1715.21-1722.56	1734.66-1744.27	1730.57-1755.36
C-H phenyl ring substitution band	850, 870-675	802.73-844.06	819.83-867.81	821.52-835.18
C-N stretch	1340-1020	1181.29-1203.19	1207.21-1241.65	1058.23-1094.71
N-H stretch	3500-3300	3488.67-3499.93	3374.21-3378.29	3442.77-3494.04
O-H stretch	3640-3160	3608.18-3625.08	3240.93-3270.11	3219.45-3307.86

CONCLUSION

An enhanced polymeric blend membrane was successfully developed. The morphology of the enhanced polymeric blend membrane showed uniform microspherical structure known as a packed bed of spheres. After addition of amine in the PSU/PVAc polymer blend, the thermal behaviour showed a deviation from the expected trend and the degradation temperature decreased. Furthermore, as MEA amine was added, a remarkable improvement in the membrane's properties was observed. These enhanced polymeric amine blend membranes have a high capability of capturing carbon dioxide from natural gas. In conclusion, the synthesis of EPBM was found to have a promising application for natural gas purification.

Acknowledgement: *The authors would like to acknowledge the Universiti Teknologi PETRONAS for supporting this research work and the NED University of Engineering & Technology, Karachi, Pakistan for financial support to Asim Mushtaq, studying at this University.*

REFERENCES

1. H. Yang, Z. Xu, M. Fan, R. Gupta, R.B. Slimane, Bland, *J. Environ. Sci.*, **20**, 14 (2008).
2. P. Šimon, M. Rybár, *Polymer Degradation and Stability*, **38**, 255 (1992).
3. M. A. Aroon, A. F. Ismail, M. M. Montazer-Rahmati, T. Matsuura, *Sep. Purif. Technol.*, **72**, 194 (2010).
4. A. F. Ismail, L. I. B. David, *J. Membr. Sci.*, **193**, 1 (2001).
5. A. F. Ismail, W. Lorna, *Sep. Purif. Technol.*, **30**, 37 (2003).
6. K. R. Devi, R. Madivanane, *IRACST-Eng. Sci. Tech. (ESTIJ)*, **2**, 795 (2012).
7. R. W. Baker, in: Membrane Technology and Applications 3rd Edn, R. W. Baker (eds), Wiley, California, 2012.
8. G. C. Kapantaidakis, G. H. Koops, M. Wessling, *Desalination*, **145** (1**)**, 353 (2002).
9. M.-J. Kim, B. Sea, K.-H. Youm, K.-H. Lee, *Desalination*, **193**, 43 (2006).
10. P. Tremblay, M. Savard, J. Vermette, R. Paquin, *J. Membr. Sci.*, **282**, 245 (2006).
11. A. F. Ismail, R. A. Rahim, W. A. W. A. Rahman, *Sep. Purif. Technol.*, **63**, 200 (2008).
12. L. Deng, T.-J. Kim, M.-B. Hägg, *J. Membr. Sci.*, **340**, 154 (2009).
13. M.A. Semsarzadeh, B. Ghalei, *J. Membr. Sci.*, **401-402**, 97 (2012).
14. S. R. Reijerkerk, M. H. Knoef, K. Nijmeijer, M. Wessling, *J. Membr. Sci.*, **352**, 126 (2010).
15. A. L. Khan, X. Li, I. F. J. Vankelecom, *J. Membr. Sci.*, **380**, 55 (2011).
16. S. Rafiq, Z. Man, S. Maitra, A. Maulud, F. Ahmad, N. Muhammad, *Korean J. Chem. Eng.*, **28**, 2050 (2011).
17. T. Hu, G. Dong, H. Li, V. Chen, *J. Membr. Sci.*, **432**, 13 (2013).
18. S. Farrukh, S. Javed, A. Hussain, M. Mujahid, *Asia-Pacific J. Chem. Eng.*, 543 (2014).

19. S.H.A. Abdul Hadi, H. Mukhtar, H. Abdul Mannan, T. Murugesan, *Appl. Mech. Mater.*, **754**, 44 (2015).
20. H. Mukhtar, H.A. Mannan, D. Minh, R. Nasir, D.F. Moshshim, T. Murugesan, *IOP Conference Series: Earth and Environmental Science*, **36**, 1 (2016).
21. R.W. Baker, *Ind. Eng. Chem. Res.*, **41**, 1393 (2002).
22. P.V. Danckwerts, *Chem. Eng. Sci.*, **34**, 443 (1979).
23. S. Thomas, Y. Grohens, P. Jyotishkumar (eds.), John Wiley & Sons, 2014, p. 18.
24. Y. Mansourpanah, A. Gheshlaghi, *J. Polym. Res.*, **19**, (2012).
25. B.D. Freeman, *Macromolecules*, **32**, 375 (1999).
26. A. Linares, J. L. Acosta, *J. Appl. Polym. Sci.*, **92**, 3030 (2004).
27. T. O. Leiknes, King Abdullah University of Science and Technology, 2008, p. 3.
28. S. Zhou, S. Wang, C. Chen, *Ind. Eng. Chem. Res.*, **51**, 2539 (2012).
29. J. G. Thompson, *Aerosol Air Qual. Res.*, **14**, 550 (2014).
30. Y.-L. Zhao, W. H. Jones, F. Monnat, F. Wudl, K. N. Houk, *Macromolecules*, **38**, 10279 (2005).
31. D. Shillady, *CRC Press*, 2011, p. 291.
32. H. W. Siesler, Springer, Berlin-Heidelberg, 1984, p. 1.
33. S. Rafiq, Z. Man, A. Maulud, N. Muhammad, S. Maitra, *J. Membr. Sci.*, **378**, 444 (2011).
34. R. Raslan, A. W. Mohammad, *J. Appl. Sci.*, **10**, 2628 (2010).
35. I. Ahmed, A. Idris, M. Y. Noordin, R. Rajput, *Ind. Eng. Chem. Res.*, **50**, 2272 (2011).

СИНТЕЗ И ОХАРАКТЕРИЗИРАНЕ НА ПОДСИЛЕНИ С МОНОЕТАНОЛАМИН СМЕСЕНИ ПОЛИМЕРНИ МЕМБРАНИ ЗА РАЗДЕЛЯНЕ НА CO_2/CH_4

А. Муштак*, Х. Мухтар, А. М. Шариф

Департамент по инженерна химия, Технологичен университет PETRONAS, 32610 Сери Искандар, Перак Дарул Риджуан, Малайзия

Постъпила на 8 декември 2017; коригирана на 1 август, 2018

(Резюме)

Мембрани за разделяне на газове се използват широко. За ефективно разделяне на CO_2/CH_4, са необходими високоефективни смесени полимерни мембрани. Основната задача на това изследване е да се синтезират смесени мембрани за отстраняване на CO_2 от CH_4 с помощта на стъкловидни и каучуковидни полимери с добавка на амин. Методологията използва различни съдържания на поливинилацетат (PVAc) от 5 до 20 wt% смесен с полисулфон (PSU) и 10 wt% MEA в разтворител DMA за получаване на плоски филмови мебрани по метода на леене от разтвор. Получените смесени мембрани имат хомогенна повърхност и еднороден слой със сферична структура, както се вижда от FESEM снимките. DSC анализът показва съществуването на еднаква температура на стъкловиден преход за всички полимерни смеси. Термогравиметричният анализ сочи, че максималната температура на деградация се повишава с увеличаване на съдържанието на PVAc в полимерните смеси. Чрез много малкия брой изместени пикове при FTIR анализа е потвърдена смесваемостта на полимерните компоненти. Резултатите за газовата проницаемост в присъствие на MEA показват, че проницаемостта към CO_2 нараства в PSU и PSU 80%/PVAc 20%, съответно от 39.63% на 63.97% при налягане 2 bar. Смесената полимерна мембрана е подходяща за получаване на нови материали с подобрени свойства, които съчетават широки възможности за приложение с ниска себестойност.

Bulgarian Chemical Communications, Volume 50, Issue 4 (pp. 584 – 591) 2018

Effect of MEA on the performance of polysulfone/polyvinyl acetate blend membranes

A. Mushtaq*, H. Mukhtar, A. M. Shariff

Chemical Engineering Department, Universiti Teknologi PETRONAS, 32610 Seri Iskandar, Perak Darul Ridzuan, Malaysia

Received, January 9, 2018; Revised, August 2, 2018

Separation of CO_2 from natural gas within the field of membrane technology has been carried out for a long time. For efficient separation of CO_2/CH_4, high-performance gas separating membranes are desired. The blending technique enhances the chemical and thermal stability, also taking heed in the improvement of separation properties with the economic sustainability. This research studies the perm-selective performance of polymeric blend membranes, glassy polymer (polysulfone) and rubbery polymer (polyvinyl acetate) with monoethanolamine (MEA). The polymeric amine blend membranes with enhanced properties were synthesized with different blending ratios in dimethylacetamide (DMAc) solvent. In this study, various compositions of polyvinyl acetate (PVAc) ranging from 5 to 20 wt. % were blended with polysulfone (PSU) and MEA, and were used for the formation of flat sheet membranes *via* evaporation method. The gas permeation results showed that the CO_2 permeance increased with increasing feed pressure.

Keywords: Methane, Carbon dioxide separation, Polymeric blend, Enhanced polymeric blend membrane, Permeance, Selectivity.

INTRODUCTION

The separation of carbon dioxide from natural gas in the area of membrane technology has been a much-known practice. It provides multitudes of benefits in comparison with other techniques, which points to its feasibility for gas separation. The performance of gas separating membranes is quite important for effective separation of CO_2 from natural gas. Thus, in the development of the membrane, permeance and selectivity factors are essential that need to be addressed for efficient CO_2 separation [1, 2].

Numerous glassy polymeric materials were utilized for membrane fabrication in gas separation established over scientific or industrial research practices. Polysulfone (PSU) was selected due to its good mechanical, thermal and chemical stability with adequate gas performance [3, 4]. Combining these features with low price, polyvinyl acetate (PVAc) is a useful polymer displaying piezoelectric, ferroelectric and pyroelectric properties [5]. The typical benefits of polyvinyl acetate are formability, flexibility, and low density [6].

Monoethanolamine (MEA), which belongs to primary amines, is widely used for removing CO_2 from natural gas. It is a relatively strong base having high reactivity with CO_2, low cost of solvent and thermal stability. However, it was replaced by more efficient systems because of its corrosive properties, degradation of solvent issues, high heat of reaction with CO_2 and substantial energy consumption for regeneration of the used solvent. The carbon dioxide loading capacity for primary and secondary amines is in the range from 0.5–1 mole of CO_2 per mole of amine, such as a fraction of the carbamate species is hydrolyzed to form hydrogen carbonates [7].

Numerous researchers have examined the behavior of CO_2-amine solutions because of their significant industrial application for removal of CO_2 from gas streams. The Dankwerts' zwitterions mechanism is widely accepted for amine reaction with CO_2 [8]. The reactions between CO_2 and primary amines, where R represents the functional group, for MEA are:

R_1= -H, R_2= -CH_2CH_2OH

$$R_1R_2NH + CO_2 \leftrightarrow R_1R_2NH^+COO^-(\text{Zwitter ion}) \quad (1)$$

$$R_1R_2NH^+COO^- + R_1R_2NH \leftrightarrow R_1R_2NCOO^-(\text{Carbamate}) \quad (2)$$

Overall reaction is:

$$2R_1R_2NH + CO_2 \leftrightarrow R_1R_2NCOO^- + R_1R_2NH^+ \quad (3)$$

It is mean

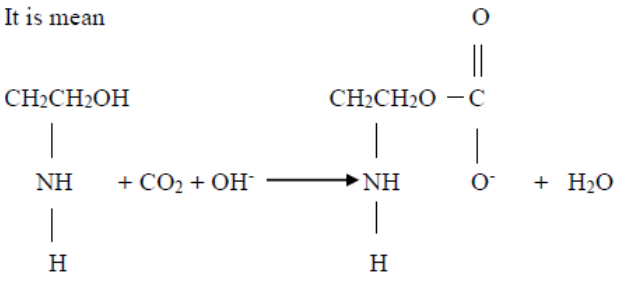

(4)

Monoethanolamine has the tendency to sanitize the acid gas from natural gas [9]. Hence, by blending

* To whom all correspondence should be sent:
E-mail: engrasimmushtaq@yahoo.com

a PSU/PVAc with monoethanolamine solutions, the separation capability is enhanced for the CO_2/CH_4 mixture. Diverse amines have unlike reaction rates with respect to various acid gases. Accumulatively, the separate amines differ in their equilibrium absorption characteristics for the various acid gases and hence display various sensitivities regarding solvent stability and corrosion factors.

On account of essential amines like MEA, the CO_2 is caught by a chemical absorption process in which the CO_2 reacts with the amine as a carbamate. The main objective of this study is to develop an enhanced polymeric membrane with the addition of the amine. The different studies regarding blend membrane are summarized in Table 1 [5, 10-23].

METHODOLOGY

Materials and Membrane Synthesis

Polysulfone (PSU) Udel® P-1800, with a glass transition temperature (T_g) of 185°C, was attained from Solvay Advanced Polymers; L.L.C, U.S. in powdered form. Polyvinyl acetate (PVAc) was purchased from Sigma-Aldrich in the form of beads having a glass transition temperature (T_g) 30°C and average M_w ~100,000 by GPC.

Table 1. Different studies on polymeric blend membranes

Year	Polymers	Gas type	Remarks	Permeance	Selectivity
2006	PU based PAI-PEI (glassy-glassy) blend	CO_2/N_2	CO_2/N_2 selectivity of PU-based blend membranes is increased	P_{CO2}=20.06 Barrer	$\alpha\frac{CO_2}{N_2}=22.56$
2006	PU-PDMS (rubbery-rubbery) cross-linked	CO_2/CH_4	Highest permeability, diffusivity, and solubility values are found for the PDMS membranes	P_{CO2}=10 Barrer	$\alpha\frac{CO_2}{CH_4}=0.41$
2008	PI-PES (glassy-glassy) blend MMM	O_2/N_2	Ideal separation factors of O_2/N_2 is increased	P_{O2}=4.2 Barrer	$\alpha\frac{O_2}{N_2}=3.8$
2009	PVAm-PVA with porous PES support	CO_2/N_2	Ultra-thin membrane with good permeability and selectivity	P_{CO2}=0.58 m^3(STP) /(m^2 h bar)	$\alpha\frac{CO_2}{N_2}=74$
2010	PEG-PDMS	CO_2/CH_4	Remarkably, the CO_2/H_2 selectivity is enhanced	P_{CO2}=530 Barrer	$\alpha\frac{CO_2}{CH_4}=10$
2010	PES-PI (glassy-glassy)	O_2/N_2	Gas permeance of N_2 increased with increase in feed pressure	P_{O2}=210.8 GPU	$\alpha\frac{O_2}{N_2}=5.4$
2011	SPEEK-Matrimid	CO_2/CH_4	Cross-linked for anti-plasticization	P_{CO2}=9.43 Barrer	$\alpha\frac{CO_2}{CH_4}=27.98$
2011	PEI-PVP	CO_2/CH_4, CO_2/N_2	Significant improvement in selectivity	P_{CO2}=1.66 GPU	$\alpha\frac{CO_2}{CH_4}=55.33$
2012	PIM-1/Matrimid	CO_2/CH_4, CO_2/N_2	Increased selectivity	P_{CO2}=50 Barrer	$\alpha\frac{CO_2}{CH_4}=31$
2013	PSF-PVP	CO_2/CH_4	Studied effect of solvents	P_{CO2}=275 GPU	$\alpha\frac{CO_2}{CH_4}=5.75$
2013	PU-PVA	CO_2/CH_4	Increased CO_2 permeability	P_{CO2}=49.5 Barrer	$\alpha\frac{CO_2}{CH_4}=10.1$
2013	PEG-PDMS	CO_2/N_2	Significant improvement in selectivity	P_{CO2}=20.0 GPU	$\alpha\frac{CO_2}{N_2}=18$
2014	CA-TiO_2 blend	CO_2/CH_4	Permeability of CO_2 was found to be increased for CA–TiO_2 blended	P_{CO2}=3.43× 10^3 Barrer	$\alpha\frac{CO_2}{CH_4}=23.3$
2015	PES-PVAc	CO_2/CH_4	CO_2 permeance increase due to the addition of PVAc in PES	P_{CO2}=4.15 GPU	$\alpha\frac{CO_2}{CH_4}=1.40$
2016	PSF/PI	CO_2/CH_4	Improved selectivity	P_{CO2}=3.3 Barrer	$\alpha(\frac{CO_2}{CH_4})=13.06$

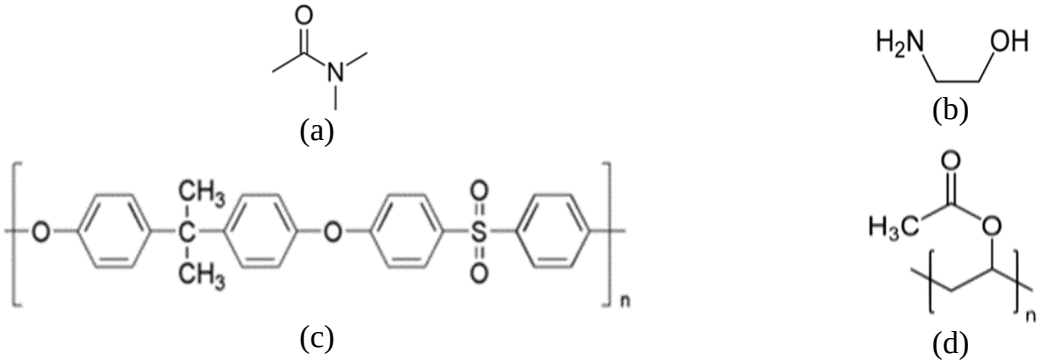

Fig. 1. Chemical structure of solvent, amine and polymers (a) DMAc (b) MEA (c) PSU (d) PVAc

Table 2. Composition of enhanced polymeric blend membranes

Membrane	Polymer, wt. %		Amine 10 wt. %
	PSU	PVAc	
1	100%	0%	-
2	0%	100%	
3	95%	5%	MEA
4	90%	10%	
5	85%	15%	
6	80%	20%	

Monoethanolamine (MEA) (boiling point 170.0ºC) and dimethyl acetamide solvent (boiling point 160ºC) with 99.99% purity were purchased from Merck. The chemical structures of the solvent, amine and polymers are shown in Figure 1. This study includes the blending of glassy (PSU) and rubbery (PVAc) polymers, and methyl diethanolamine was taken in DMAc solvent. Blending of 20% wt/wt was performed. The different compositions of enhanced polymeric blend membranes are presented in Table 2. Polysulfone was preheated for one night to eliminate moisture. Firstly, the polyvinyl acetate was allowed to dissolve completely in dimethylacetamide. Then PSU and MEA were added under continuous stirring for 24 h at room temperature to attain a homogeneous blend. To clear the solution from air bubbles, bath sonication in a Transonic Digital S, Elma® for one hour was performed. Polysulfone and amine were completely dissolved without any evidence of deposition, which qualified it as a miscible polymer blend. The blend was then cast on a glass plate *via* casting knife with an opening of 200 μm. These casted membranes were sited in a drying room at ambient temperature for five days to allow for the evaporation of the solvent. The membranes were then peeled from the glass plate to check the performance of CO_2 and CH_4 separation. Table 2 shows the composition of the polymer blended membranes. The equipment used for the gas permeation performance was a CO2SMU unit, where CO_2/CH_4 flow rate (0.1cm^3/sec) was measured by a flow controller meter. These trials were performed under ambient pressure (101 ± 2kPa) at room temperature (302 ± 2K). Figure 2 shows the methodology for fabrication of polymeric amine blend membrane.

The permeance of the CO_2 and CH_4 gases was calculated by the following equations [24]:

$$\frac{P_{CO_2}}{l} = \frac{J_{CO_2}}{\Delta P_{CO_2}} \quad (5)$$

$$\frac{P_{CH_4}}{l} = \frac{J_{CH_4}}{\Delta P_{CH_4}} \quad (6)$$

where J is the flux of CH_4 and CO_2 gases, ΔP is the differential partial pressure across the membrane for the gases and l denotes the thickness of the membrane. Thus, the gas selectivity (α_{CO_2/CH_4}) was calculated by taking the ratios of the CO_2 and CH_4 permeance [24]:

$$\alpha_{CO_2/CH_4} = \frac{P_{CO_2}/l}{P_{CH_4}/l} \quad (7)$$

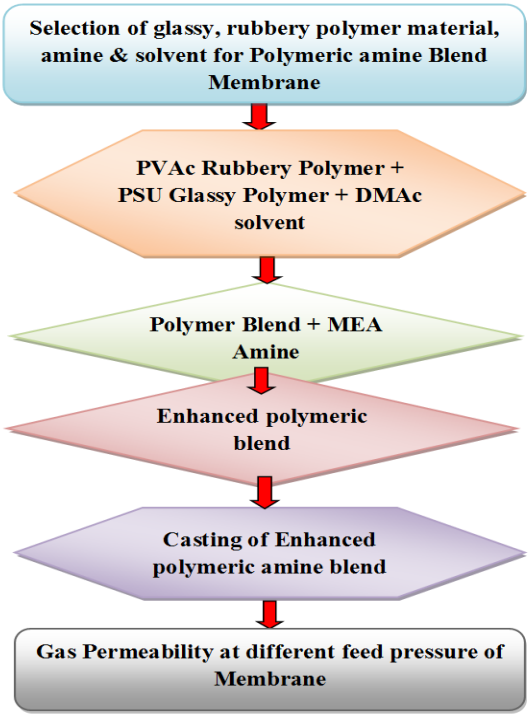

Fig. 2. Methodology for fabrication of polymeric amine blend membranes

RESULTS & DISCUSSION

Gas Permeance Evaluation

In this study, when the gases CO_2 and CH_4 will pass through the EPBM, the amine absorbs the maximum CO_2. The CO_2 permeation rate will be higher as compared to CH_4; the membrane will not absorb the maximum amount of CH_4 so its permeation rate in the membrane will be less.

Figure 3 shows that base polysulfone membrane's permeance of CO_2 was reduced with increasing pressure due to the fact that the glassy polymer is a mixture of crystalline and amorphous phases. The crystallites act as effectual cross-links to decrease the area accessible for permeation, thus permeance of PSU decreases [25]. On the other hand, for the base PVAc membrane, the permeance of CO_2 (14.48±0.01 to 40.24±0.08 GPU) and CH_4 (3.34±0.1 to 15.09±0.08 GPU) increases with the increase of pressure (2-10 bar) as shown in Figures 3 and 4. Due to PVAc membrane that exists above T_g there is a large intersegmental polymer chain motion [26, 27]. Figure 3 represents the increasing trend of CO_2 permeance when MEA amine is blended in PSU and PVAc. The CO_2 permeance increased in various compositions of PSU/PVAc with MEA amine membranes. The maximum CO_2 permeance for PSU80%/PVAc20%/MEA was 12.14±0.02 GPU to 53.20±0.29 GPU with an increase in the pressure from 2 to 10 bar as shown in Figure 3. The PVAc percentage increased in PSU with MEA 10 wt. %, the permeance of CO_2 also rose with pressure increase due to the fact that MEA amine has captured the CO_2. The high CO_2 permeance of membranes with increased PVAc content in PSU was likely due to the blended membrane's rising affinity for CO_2, especially since CO_2 has a non-polar linear structure and smaller kinetic diameter (3.3Å) [28-33]. In Figure 4 the CH_4 permeance slightly increased in various compositions of PSU/PVAc with MEA amine membranes, for PSU80%/PVAc20%/MEA from 1.33±0.01 GPU to 1.78±0.02 GPU with an increase in the pressure from 2 to 10 bar. As compared to CO_2, the slow moving CH_4 molecule has a kinetic diameter of 3.8Å and a tetrahedral structure [28]. By addition of MEA amine in the PSU/PVAc blend membranes, the CO_2 permeance increased. Figure 5 shows that pure PSU selectivity CO_2/CH_4 is rising with pressure from 2 to 10 bar whereas selectivity (CO_2/CH_4) of pure PVAc membrane decreased with pressure increase. The enhanced polymeric membrane's selectivity also rose with increased feed pressure as shown in Figure 5. In the blend MEA amine molecules conjoint into the pores of the microporous materials. So for the blended membranes, the maximum selectivity of the PSU95%/PVAc5%/MEA is 9.43±0.1–30.17±0.7 from 2 to 10 bar. The membrane microporous structure incorporates MEA molecules. These amine molecules increase CO_2 adsorption due to interactions between CO_2 and $-NH_2$ groups [34, 35].

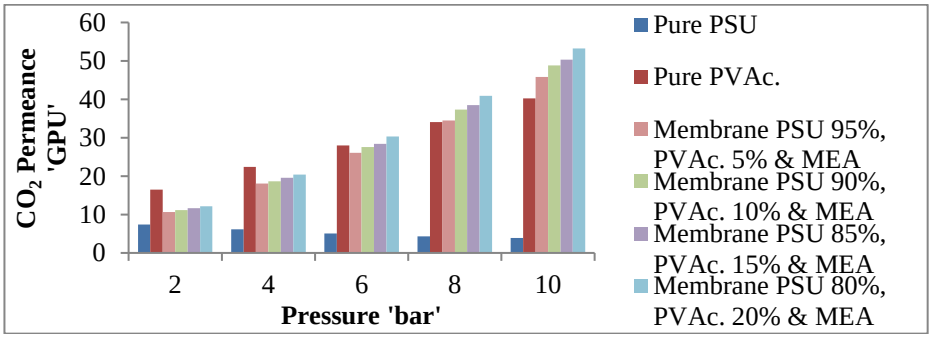

Fig. 3. Comparison of CO_2 permeance at various feed pressures for MEA amine polymeric blend membrane.

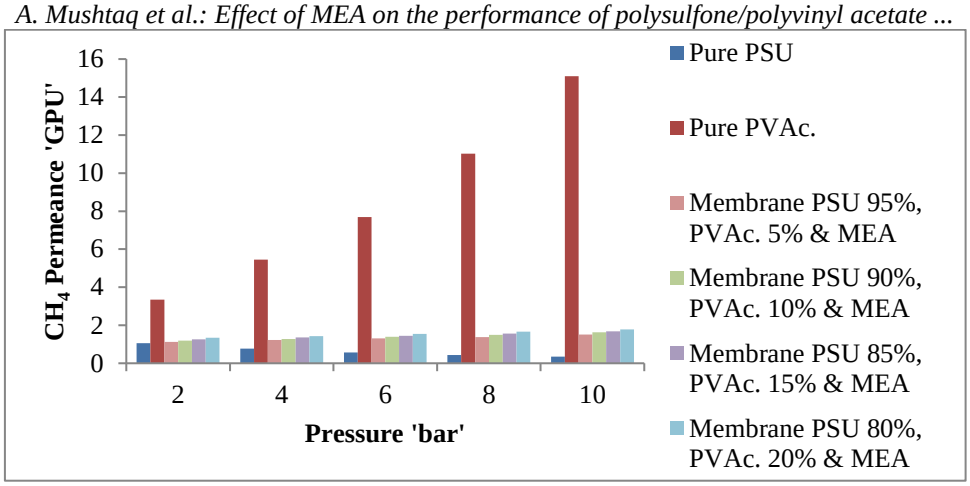

Fig. 4. Comparison of CH_4 permeance at various feed pressures for MEA amine polymeric blend membrane

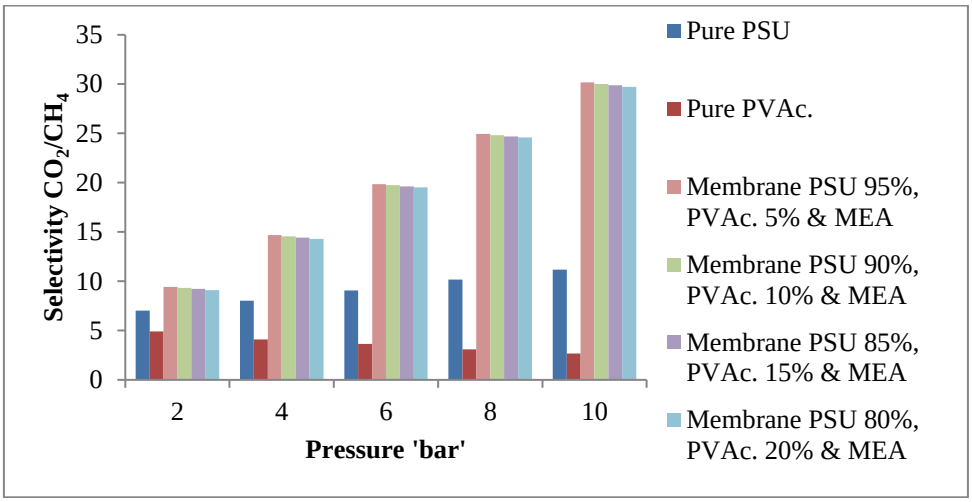

Fig. 5. Comparison of selectivity (CO_2/CH_4) at various feed pressures for MEA amine polymeric blend membrane

Hence, it was concluded that base polysulfone and polyvinyl acetate membrane and enhanced polymeric blend membranes were completely miscible and also characteristically increased CO_2 permeance and selectivity with rising feed pressure. The pressure difference across the membrane increased the volume of CO_2 gas across the membrane surface, increasing the formation rate of CO_2–amine complexes. Therefore, most amine molecules became involved in CO_2–amine interactions as the amine carrier concentration gently reached a state of saturation. Transporter saturation with a gradual reduction in gas flux under increased pressure describes the behavior of facilitated transport membranes. The observed results are in good agreement with former ones [29-33, 36].

Regression Graph between Pressure & Experimental Data for CO_2 Permeance, CH_4 Permeance & Selectivity CO_2/CH_4 of Different Polymeric Blend Membranes

Figures 6 and 7 show the correlation coefficients between the pressure and experimental values as given by a polynomial quadratic fit obtained with an R^2 value of 0.999. Hence, a proof is provided of the accuracy of the values obtained through the experimental setup based on the permeance performance of the different blend membranes.

Correlationship Graph between Polynomial Predicted & Experimental Data for CO_2 and CH_4 Permeance & Selectivity CO_2/CH_4 of Polymeric Blend Membrane

Data analysis aims at understanding information gathered in an experiment and assessing the expected extent of one variable to rely on another which is autonomously known.

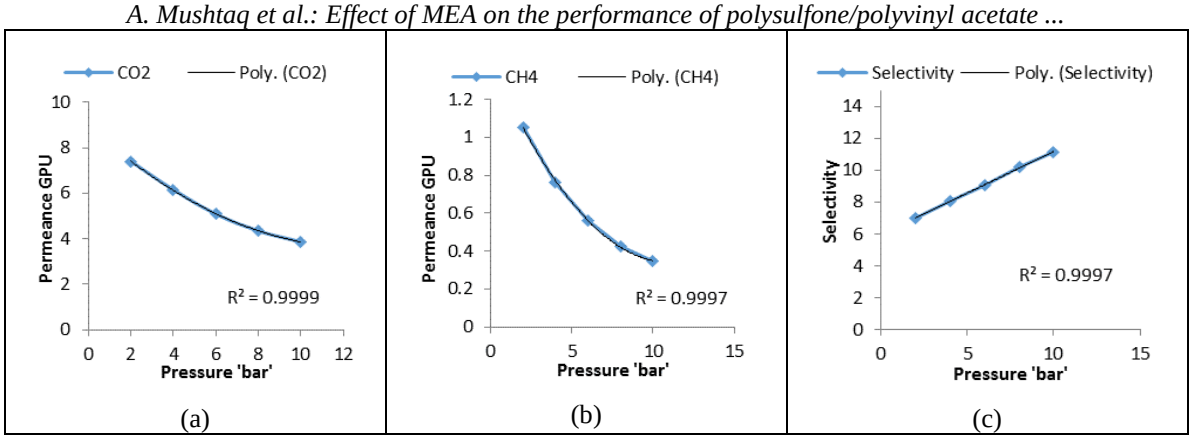

Fig. 6. Permeance (a) CO_2 (b) CH_4 in 'GPU' and (c) Selectivity CO_2/CH_4 against pressure 'bar' along with the correlation coefficient for base polysulfone membrane

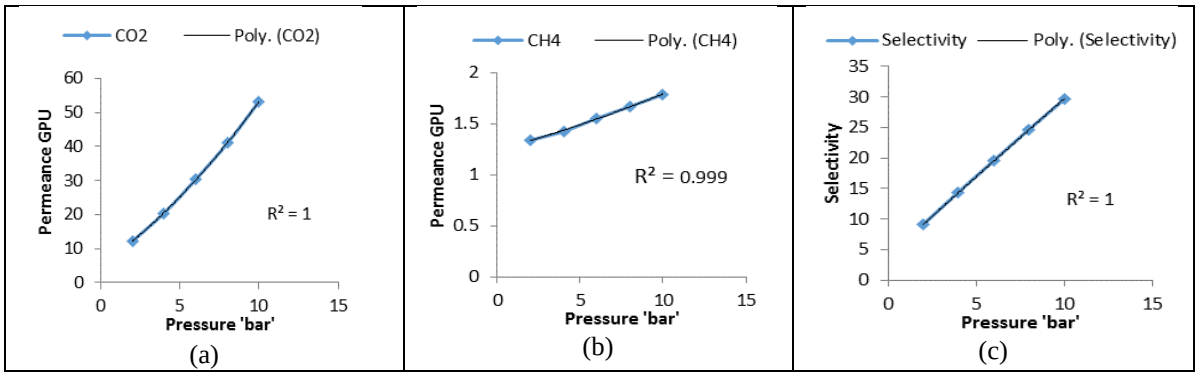

Fig. 7. Permeance (a) CO_2 (b) CH_4 in 'GPU' and (c) Selectivity CO_2/CH_4 against pressure 'bar' along with the correlation coefficient for PSU 80%/PVAc20%/MEA membrane.

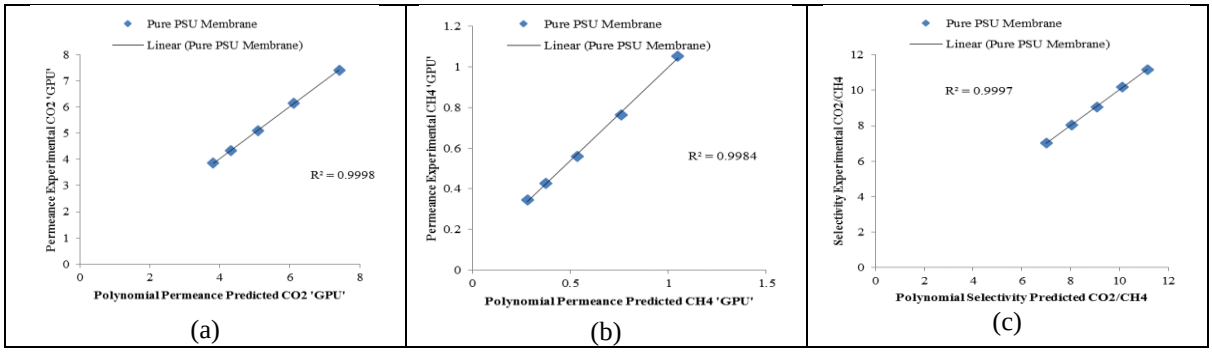

Fig. 8. Experimental permeance against polynomial predicted permeance and their selectivity along with the correlation coefficient for base polysulfone membrane

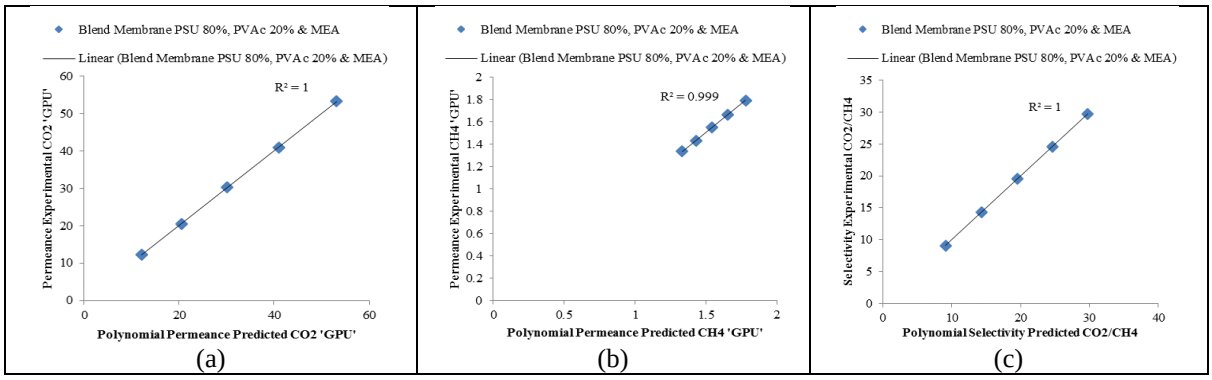

Fig. 9. Experimental permeance against polynomial predicted permeance and their selectivity along with the correlation coefficient for PSU 80%/PVAc20%/MEA membrane.

It will just manage the (regular) one-dimensional case in which the indigent variable is an element of one autonomous variable. The objective is to identify and evaluate the relationship between the two variables. The relationship between the polynomial-predicted, and experimental permeance values given in Figures 8 and 9 are in accordance with the linear fit obtained with an R^2 value of 0.999. Hence, a proof is provided of the accuracy of the values obtained through the experimental setup based on the permeance performance of the different blend membranes comprising pure PSU membrane and PSU 80%/PVAc 20%/MEA membrane. On the whole, a model fits the data if the difference between the experimental and the predicted values is small and unbiased.

CONCLUSION

An enhanced polymeric blend membrane was successfully developed. Moreover, the addition of MEA made an incredible improvement in the membrane's perm-selectivity. The soluble nature of CO_2 in MEA enhanced CO_2 solubility across the membrane. The enhanced polymeric amine blend membranes have a high proficiency of capturing CO_2 from natural gas. The relationship between the polynomial-predicted and experimental permeance values by a linear fit was obtained with an R^2 value of 0.999. For future work, propensity to add inorganic fillers such as zeolites or carbon molecular sieves in the blend would promote the enhanced polymeric blend membrane.

Acknowledgement: *The authors would like to acknowledge the Universiti Teknologi PETRONAS for supporting this research work and the NED University of Engineering & Technology, Karachi, Pakistan for financial support to Asim Mushtaq studying at this University.*

NOMENCLATURE

DMAc	Dimethyl acetamide
GPU	Gas Permeation Unit
MEA	Monoethanolamine
PSU	Polysulfone
PAI	Polyamide-imide
PDMS	Polydimethylsiloxane
PEA	Aromatic polyether amide
PEG	Polyethylene glycol
PEI	Polyether imide
PEO	Polyethylene oxide
PES	Polyethersulfone
PI	Polyimide
PIM-1	Polymer of intrinsic microporosity
PPO	Polypropylene oxide
PU	Polyurethane
PVA	Polyvinyl alcohol
PVAc	Polyvinyl acetate
PVAm	Polyvinyl amine
PVDF	Polyvinylidene fluoride
PVP	Polyvinyl propylene
SPEEK	Sulfonated aromatic poly(ether-ether-ketone)

REFERENCES

1. H. Yang, Z. Xu, M. Fan, R. Gupta, R.B. Slimane, Bland, *J. Environ. Sci.*, **20**, 14 (2008).
2. R. Abedini, A. Nezhadmoghadam, *Pet. Coal*, **52**, 69 (2010).
3. J. Ahn, W.-J. Chung, I. Pinnau, M.D. Guiver, *J. Membr. Sci.*, **314**, 123 (2008).
4. M. A. Aroon, A. F. Ismail, M. M. Montazer-Rahmati, T. Matsuura, *Sep. Purif. Technol.*, **72**, 194 (2010).
5. S. H. A. Abdul Hadi, H. Mukhtar, H. Abdul Mannan, T. Murugesan, *Appl. Mech. Mater.*, **754**, 44 (2015).
6. R. W. Baker, in: Membrane Technology and Applications 3rd Edn, R. W. Baker (eds), Wiley, California, 2012.
7. P. M. M. Blauwhoff, G. F. Versteeg, W. P. M. van Swaaij, *Chem. Eng. Sci.*, **39**, 207 (1984).
8. P. V. Danckwerts, *Chem. Eng. Sci.*, **34**, 443 (1979).
9. C.-H. Yu, *Aerosol and Air Quality Research*, 745 (2012).
10. G. C. Kapantaidakis, G. H. Koops, M. Wessling, *Desalination*, **145** (1), 353 (2002).
11. M.-J. Kim, B. Sea, K.-H. Youm, K.-H. Lee, *Desalination*, **193**, 43 (2006).
12. P. Tremblay, M. Savard, J. Vermette, R. Paquin, *J. Membr. Sci.*, **282**, 245 (2006).
13. A. F. Ismail, R.A. Rahim, W.A.W.A. Rahman, *Sep. Purif. Technol.*, **63**, 200 (2008).
14. L. Deng, T.-J. Kim, M.-B. Hägg, *J. Membr. Sci.*, **340**, 154 (2009).
15. S. R. Reijerkerk, M. H. Knoef, K. Nijmeijer, M. Wessling, *J. Membr. Sci.*, **352**, 126 (2010).
16. J. Han, W. Lee, J.M. Choi, R. Patel, B.-R. Min, *J. Membr. Sci.*, **351**, 141 (2010).
17. A. L. Khan, X. Li, I.F.J. Vankelecom, *J. Membr. Sci.*, **380**, 55 (2011).
18. W. N. W. Salleh, A. F. Ismail, *AlChE J.*, **58**, 3167 (2012).
19. W. F. Yong, F. Y. Li, Y. C. Xiao, P. Li, K. P. Pramoda, Y. W. Tong, *J. Membr. Sci.*, **407-408**, 47 (2012).
20. P. Moradihamedani, N. A. Ibrahim, W. M. Z. W. Yunus, N. A. Yusof, *J. Appl. Polym. Sci.*, **130**, 1139 (2013).
21. M.A. Semsarzadeh, B. Ghalei, *J. Membr. Sci.*, **432**, 115 (2013).
22. T. Hu, G. Dong, H. Li, V. Chen. *J. Membr. Sci.*, **432**, 13 (2013).
23. S. Farrukh, S. Javed, A. Hussain, M. Mujahid, *Asia-Pacific J. Chem. Eng.*, 543 (2014).
24. A. Javaid, *Chem. Eng. J.*, **112**, 219 (2005).
25. A. Y. Houde, S. S. Kulkarni, M. G. Kulkarni, *J. Membr. Sci.*, **71**, 117 (1992).
26. C. J. Orme, M. K. Harrup, Th. A. Luther, R.t P. Lash, K. S. Houston, D. H. Weinkauf, F. F. Stewart, *J. Membr. Sci.*, **186**, 249 (2001).

27. T. C. Merkel, R. P. Gupta, B. S. Turk, B. D. Freeman, *J. Membr. Sci.*, **191**, 85 (2001).
28. R. W. Baker, K. Lokhandwala, *Ind. Eng. Chem. Res.*, **47**, 2109 (2008).
29. R. Raslan, A. W. Mohammad, *J. Appl. Sci.*, **10**, 2628 (2010).
30. A. Torres-Trueba, F.A. Ruiz-Treviño, G. Luna-Bárcenas, C.H. Ortiz-Estrada, *J. Membr. Sci.*, **320**, 431 (2008).
31. F.G. Kerry, in: Industrial gas handbook: gas separation and purification 1st Edn, F.G. Kerry (eds), CRC Press, New York, 2007.
32. L. Wang, Y. Cao, M. Zhou, S.J. Zhou, Q. Yuan, *J. Membr. Sci.*, **305**, 338 (2007).
33. M. Ulbricht, *Polymer*, **47**, 2217 (2006).
34. J. Franco, D. de Montigny, S. Kentish, J. Perera, G. Stevens, *Sep. Sci. Tecnol.*, **43**, 225 (2008).
35. P.D. Vaidya, E.Y. Kenig, *Chem. Eng. Sci.*, **62**, 7344 (2007).
36. Y. Tanabe, in: Macromolecular Science and Engineering, R. Hull . R. M. Osgood, Jr. H. Sakaki . A. Zunger (eds), Springer, Berlin Heidelberg, 2013.

ВЛИЯНИЕ НА МОНОЕТАНОЛАМИН ВЪРХУ ЕФЕКТИВНОСТТА НА СМЕСЕНИ ПОЛИСУЛФОН/ПОЛИВИНИЛОВИ МЕМБРАНИ

А. Муштак*, Х. Мухтар, А. М. Шариф

Департамент по инженерна химия, Технологичен университет PETRONAS, 32610 Сери Искандар, Перак Дарул Риджуан, Малайзия

Постъпила на 9 януари, 2018; коригирана на 2 август, 2018

(Резюме)

Разделянето на CO_2 от природния газ с мембранна технология е използвано отдавна. За успешно разделяне на CO_2/CH_4 са необходими ефективни мембрани. Техниката на смесване повишава химичната и термичната стабилност, подобрява разделителната способност и икономическата устойчивост. В настоящата работа е изследвана ефективността на селективната проницаемост на смесените полимерни мембрани, стъкловидния полимер (полисулфон) и каучуковидния полимер (поливинилацетат) при добавяне на моноетаноламин (MEA). Амин-съдържащи смесени полимерни мембрани с подобрени свойства са синтезирани при различни съотношения в разтворител диметилацетамид. Поливинилацетат с различна концентрация в интервала от 5 до 20 wt.% е смесен с полисулфон и MEA и е използван за получаване на плоски мембранни филми по метода на изпаряване. Резултатите показват, че проницаемостта по отношение CO_2 нараства с увеличаване на захранващото налягане.

Bulgarian Chemical Communications, Volume 50, Issue 4 (pp. 592 – 601) 2018

Comparative study of sunset yellow dye adsorption onto cornelian cherry stones-based activated carbon and carbon nanotubes

F. O. Erdogan*

Department of Chemistry and Chemical Processing Technologies, Kocaeli Vocational School, Kocaeli University, 41140, Kocaeli, Turkey

Received, December 13, 2017; Accepted, July 20, 2018

The objective of the study was to prepare low-cost activated carbon from cornelian cherry stones (*Cornus mas* L.) and compare its adsorption behavior for a food dye with that of commercial multiwalled carbon nanotubes. The cornelian cherry stones activated carbon (AC) and commercial multi-walled carbon nanotubes (MWCNT) were characterized by N_2 adsorption isotherms and SEM (scanning electron microscopy). Adsorption of a food dye, sunset yellow FCF, by AC and MWCNT was examined in detail. Batch adsorption test showed that the extent of sunset yellow adsorption was dependent on dye concentration, contact time, solution temperature and adsorbent dosage. The experimental adsorption equilibrium data were compared to the Langmuir, Freundlich, Temkin and DR isotherm models and the isotherm model parameters were determined. The maximum adsorption capacity was found to be 125.3 and 43.8 mg/g for AC and MWCNT, respectively. Pseudo-first-order, pseudo-second-order and Elovich equations were fitted to the kinetic data, and the rate constants were evaluated. Thermodynamic parameters enthalpy, entropy and Gibbs free energy changes were established. Results showed that activated carbon produced from cornelian cherry stones is suitable for the adsorption of sunset yellow food dye and could be used as a low-cost effective adsorbent in the treatment of industrial wastewater.

Keywords: Cornelian cherry stones, Adsorption isotherms, LiOH activations, Sunset yellow, Multiwalled carbon nanotubes.

INTRODUCTION

Activated carbon is one of the widely used adsorbents in removal of dyes because of its large surface area, favorable pore size distribution and high adsorption capacities. Activated carbon is produced from a variety of carbonaceous raw materials such as cherry stones, apricot seed kernels, almond shells, peach stones, orange peels, pistachio shells, coal, petroleum coke, lignite, wood, resin, coconut husks, tomato stems, olive stones, waste tires, waste paper, fish waste [1-16]. The surface properties and adsorption characteristics of activated carbons depend on the physical and chemical properties of the raw materials and the activation methods. Activated carbons can be produced by physical or chemical activation. Chemical activation, is a single-step method of preparation of the raw material in the presence of chemical agents such as $ZnCl_2$, $AlCl_3$, LiOH, KOH, NaOH, K_2CO_3, Na_2CO_3, H_3PO_4 and H_2SO_4 [17-22]. Many studies have been reported for activated carbon production using various raw materials and activation agents. Philip [16] produced activated carbon from apricot stones by activation with H_3PO_4. The highest specific surface area, micropore volume and mean pore radius were found as 1603 m^2 g^{-1}, 0.752 cm^3 g^{-1} and 9.4 Å, respectively. Fu *et al*. [9] produced activated carbon from tomato stems at different carbonization temperatures (500, 600, 650, 700, 750 and 800 °C) and impregnation ratios (1, 1.5, 2, 2.5 and 3). In this study, BET surface area, micropore area, total volume, and micropore volume of activated carbon obtained at 700 °C with impregnation ratio of 2.5 were 971 m^2 g^{-1}, 838 m^2 g^{-1}, 0.576 cm^3 g^{-1} and 0.425 cm^3 g^{-1}, respectively. Tian *et al*. [23] produced activated carbon from cotton stalk with KOH and investigated the effects of micropore development on the physicochemical properties of the activated carbons. Al-Rahbi and Williams [24] produced activated carbon from waste tyres with alkali chemical reagents (KOH, K_2CO_3, NaOH, and Na_2CO_3). The maximum surface areas obtained by chemical activation with KOH, K_2CO_3, NaOH, and Na_2CO_3 were 621, 133, 128 and 92 m^2 g^{-1}, respectively. To the best of our knowledge, no study has been reported on the preparation of activated carbon from cornelian cherry stones by chemical activation with LiOH.

Carbon nanotubes are newly emerged carbonaceous materials, their characteristic structures and electronic properties make them interact strongly with dyes, *via* non-covalent forces such as hydrogen bonding, van der Waals forces and hydrophobic interactions [25]. Carbon

* To whom all correspondence should be sent:
E-mail: foerdogan@gmail.com

nanotubes with different diameters would have different surface area, which would affect their adsorptive properties [26].

Dyes (synthetic organic substances) are widely used in food, textile, leather, paper, cosmetic, pharmaceutic and automotive industries. Sunset yellow (SY) is a pyrazolone dye used in food products such as beverages, candies, dairy, pharmaceuticals and bakery products [27, 28]. Many methods have been employed to remove dyes from aqueous solution, and adsorption is considered superior to the other techniques.

The main objects of this study are: (i) to study the feasibility of using the activated carbon produced from cornelian cherry stones as a low-cost adsorbent for the removal of sunset yellow (SY) dye; (ii) to compare its adsorption behavior for the food dye to that of commercial multiwalled carbon nanotubes (MWCNT); (iii) to determine the various parameters affecting sorption, such as contact time, amount of adsorbents and temperature of the solution; (iv) to determine the applicability of various isotherm models ((i.e., Langmuir, Freundlich, Temkin and DR) to find out the best-fit isotherm equation; and (v) to determine thermodynamic and kinetic parameters and explain the nature of the adsorption.

MATERIALS AND METHODS

Materials

In this study, cornelian cherry stones were obtained from Havza in Samsun province in Turkey. The precursor, cornelian cherry stones were first air dried, then crushed and sieved in order to get standardized particle dimensions Then, cornelian cherry stones were contacted with a dilute 10 vol.% sulfuric acid solution for 8 h (sulfuric acid contributes to the removal of inorganic components from lignocellulosic materials) and washed with hot distilled water. Multiwalled carbon nanotubes were provided by CNT CO., LTD (Korea) [44].

Preparation of the activated carbons

10 g of dried cornelian cherry stones (<2 mm) were mixed in a beaker with 200 mL of LiOH solution which corresponded to an impregnation ratio of 4:1 (weight of impregnation reagent/weight of cornelian cherry stones) for 8 h at 65 °C. The impregnated sample was then dried overnight in a moisture oven at 120 ˚C. Then, the impregnated sample was carbonized in a tube furnace (Protherm STF) under N_2 flow at a heating rate of 10 °C/min up to 700 ˚C for 1 h. After the activation the sample was allowed to cool down to room temperature under N_2 flow before its removal from the furnace. The activated sample was washed several times with HCl and hot distilled water to remove residual chemicals until gave no chloride reaction with $AgNO_3$. The activated sample was dried for about 6 h at a temperature of 120 ºC. Activated sample was stored in a sealed flask and labelled. The pores of activated carbon were characterized by analysis of N_2 adsorption–desorption isotherms at 77 K using Micromeritics TriStar II 3020.

Adsorbate

The commercial food dye sunset yellow FCF ($C_{16}H_{10}N_2Na_2O_7S_2$, molecular weight 452.37 g/mol, C.I. 15985, λmax=482 nm, chemical structure shown in Figure 1) was supplied by Sigma-Aldrich. Distilled water was used to prepare all solutions.

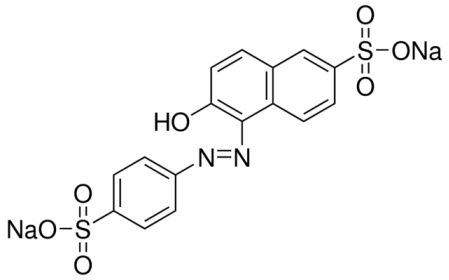

Figure 1. Chemical structure of sunset yellow FCF.

Adsorption equilibrium studies

Adsorption of SY on cornelian cherry stones-based activated carbon (AC) and MWCNT was studied by batch experiments. Equilibrium adsorption studies were conducted in a set of 60 mL capped volumetric flasks containing different amounts of adsorbent in the range of 0.05-0.09 g/L for AC and 0.01-0.03 g/L for MWCNT, 50 mL initial concentrations of SY solutions (10-50 mg/L for AC, 10-100 mg/L for MWCNT). Flasks were shaken in a mechanical shaker (GFL 1086) at 100 rpm and different temperatures (30, 40 and 50°C). After adsorption, samples were filtered and then the concentrations of SY in the supernatant solution were analyzed. All concentrations were measured on a UV spectrophotometer (LaboMed Inc.) at 482 nm. The adsorption efficiency (E) was calculated using equation (1):

$$E = \frac{(C_0 - C_e)}{C_0} 100 \qquad (1)$$

where C_0 and C_e (mg/L) are the initial and equilibrium liquid-phase concentrations of dye, respectively. The SY uptake at equilibrium (q_e (mg/g)), was calculated using equation (2):

$$q_e = \frac{(C_0 - C_e)V}{W} \qquad (2)$$

where V (L) is the volume of the solution, and W

(g) is the mass of the adsorbent used in the experiments. The equilibrium data were simulated using the Freundlich, Langmuir, Temkin and DR isotherm models [27].

Adsorption kinetics

Kinetic adsorption experiments were carried out by adding 0.05 g/L of AC or 0.01 g/L of MWCNT to 50 mL of 10 mg/L SY dye aqueous solutions at temperatures of 30, 40 and 50°C. The uptake of SY at time t, q_t (mg/g) was calculated by the following equation:

$$q_t = \frac{(C_0 - C_t)V}{W} \quad (3)$$

where C_t (mg/L) is the liquid-phase concentration of dye at time t, (min).

In order to predict the adsorption behavior of sunset yellow FCF on the adsorbents, pseudo-first-order and pseudo-second-order kinetic equations, which are described with equations (4) and (5), respectively, were applied for modeling experimental data:

$$log\left(q_e - q_t\right) = log\, q_e - \frac{k_1 t}{2.303} \quad (4)$$

$$\frac{t}{q_t} = \frac{1}{k_2 q_e^2} + \frac{t}{q_e} \quad (5)$$

where k_1 (1/min) and k_2 (g/mg min) are the adsorption rate constants of the pseudo-first-order and pseudo-second-order, respectively [27, 29]. Elovich equation has been generalized and frequently used in the adsorption studies of many pollutants in aqueous solution:

$$q_t = \left(\frac{1}{\beta}\right) ln(\alpha\beta) + \left(\frac{1}{\beta}\right) ln\, t \quad (6)$$

where α is the chemisorption rate (mg/g min) and β is a coefficient related with the extension of covered surface and activation energy of chemisorption (g/mg). The equation constants can be determined by plotting the straight line of q_t *versus lnt* [30].

Adsorption thermodynamics

The rate constant (pseudo-first or pseudo-second order) of dye adsorption is expressed as a function of the temperature by the Arrhenius relationship [31,32]:

$$ln\, k = lnA - \left(\frac{E_a}{R}\right)\frac{1}{T} \quad (7)$$

where E_a is the Arrhenius activation energy (kJ/mol), A is the Arrhenius factor, R is the molar gas constant (8.314 J/mol K) and T is the absolute temperature (K).

To describe the thermodynamic behavior of the adsorption of SY dye onto AC or MWCNT, the thermodynamic parameters including the changes in free energy (ΔG°), enthalpy (ΔH°) and entropy (ΔS°) were calculated by the following equations:

$$\Delta G^0 = -RT\, ln\, K_c \quad (8)$$

$$ln\, K_c = -\frac{\Delta H^0}{RT} + \frac{\Delta S^0}{R} \quad (9)$$

where R is the universal gas constant (8.314 J/mol K), T is the temperature (K) and $K_C = C_{ads}/C_e$ is the equilibrium constant of the SY adsorption equilibrium (which is a ratio of C_{ads}, the SY concentration in the adsorbent, and C_e, the SY concentration in the adsorbate [29].

RESULTS AND DISCUSSION

Characterization of the carbonaceous materials

The surface physical properties of the adsorbents were characterized with an automated gas sorption apparatus using N_2 as adsorbate at 77.4 K. Nitrogen adsorption is a standard technique widely used for the determination of porosity of adsorbents. Figures 2 and 3 show the isotherms of the LiOH treated sample (AC) and MWCNT, respectively. Appearance of hysteresis loop indicates the presence of mesopores. The pore structure of the adsorbents was calculated by using the t-method analysis from the adsorption branch of the nitrogen isotherms [9, 27].

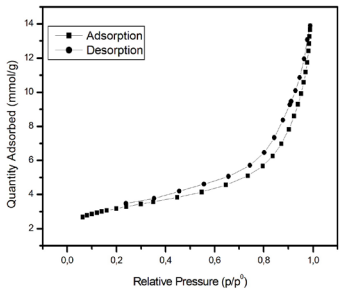

Figure 2. Adsorption-desorption isotherms of AC.

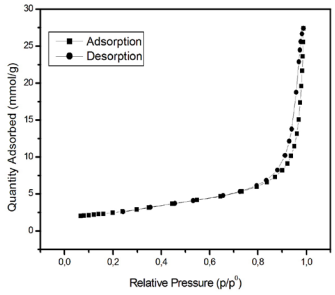

Figure 3. Adsorption-desorption isotherms of MWCNT.

Table 1. Textural parameters of the adsorbents.

Properties	AC	MWCNT
BET surface area (m^2/g)	249.5	193.7
Langmuir surface area (m^2/g)	337.3	265.2
Total pore volume (mL/g)	0.445	0.250
Micropore volume (mL/g)	0.039	0.062
Average pore width (nm)	7.14	15.51

Table 1 shows the BET and Langmuir surface areas, total pore volume and avarage pore size for the adsorbents. N_2 adsorption-desorption experiments showed that AC has high surface area of 249.5 m^2/g. The average pore width (L=7.14 nm) suggests that AC is a mesoporous adsorbent. MWCNT has lower surface area (193.7 m^2/g) and pore volume (0.250 mL/g) [44] than AC, which is similar to the values reported by Li *et al*. [25]. The value of the average pore width (15.51 nm) shows that multiwalled carbon nanotubes have a mesoporous structure which may have come from the inner cavities and the agglomerations of MWCNTs. A similar phenomenon was reported by Li *et al*. [25]. Carbon nanotubes form aggregated pores due to the entanglement of tens and hundreds of individual tubes that have adhered to each other as a result of van der Waals forces of attraction. The aggregated pores have the dimensions of a mesopore or higher [25].

SEM was used to observe the surface physical morphology of the adsorbents. SEM micrographs of AC and MWCNT are shown in Figures 4 and 5.

Figure 4 shows that surface of AC containing cavities and pores of various sizes and shapes. These cavities were caused by the evaporation of the impregnated LiOH derived compound, leaving the space previously occupied by the reagent.

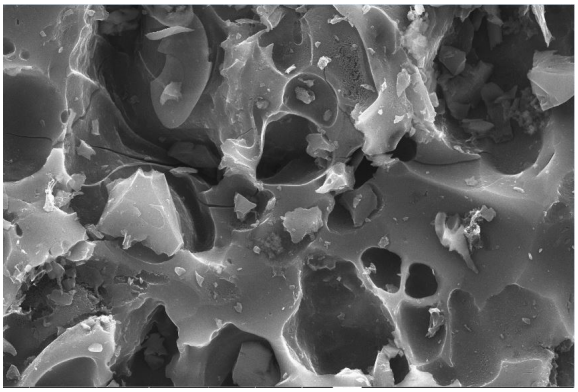

Figure 4. Scanning electron micrograph of activated carbon produced from cornelian cherry stones.

Effects of adsorbent dosage and contact time

Figure 6 presents the adsorption isotherms of the SY dye as the relationship between the amount of dye adsorbed per unit mass of a given carbonaceous adsorbent and time.

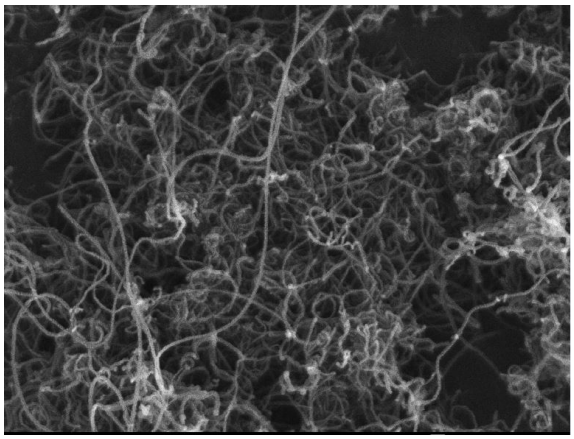

Figure 5. Scanning electron micrograph of MWCNT.

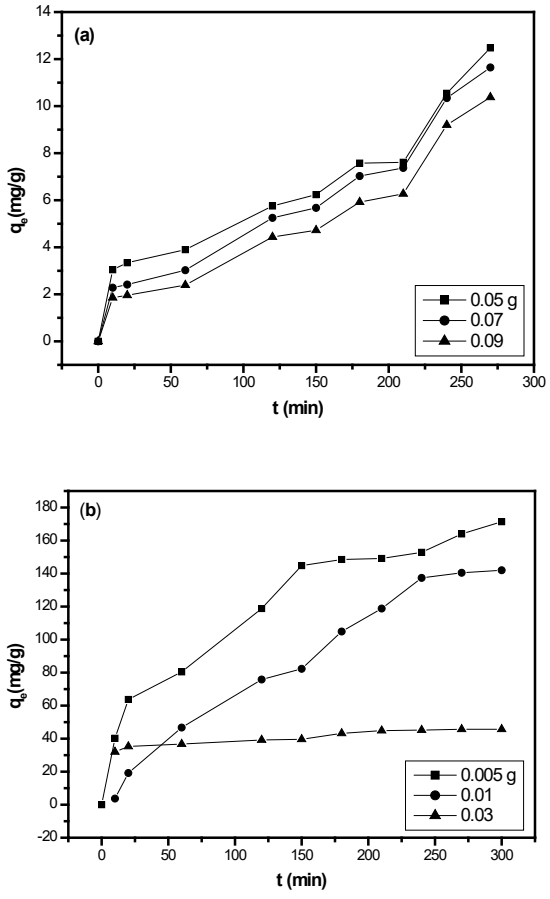

Figure 6. Effects of adsorbent dosage and contact time on the adsorptive uptake of food dye onto AC (a) and MWCNT (b) (conditions: C_0=10 mg/L; temperature=40 °C).

Fig. 6 (a) shows that the adsorption capacities at equilibrium (q_e) decreased with an increase in adsorbent dose from 0.05 to 0.09 g/L. Similar result have been observed for the adsorption of phenol onto activated carbon and fungal biomass [42]. In a batch of adsorption studies, the adsorption

efficiency (E) increased from 60.43% to 90.47% when the adsorption dosage of AC increased from 0.05 to 0.09 g/L at 40 °C. This corroborates the reports of our previous study [29]. Similar behavior was reported in the literature [35, 43]. Figure 6 (b) showed that the adsorption capacities at equilibrium (q_e) decreased with an increase in adsorbent dose from 0.005 to 0.03 g/L. The adsorption capacity of MWCNT at equilibrium decreased from 171.41 to 45.02 mg/g with an increase in adsorbent dosage from 0.005 to 0.03 g/L. This is explained as a consequence of partial aggregation, which occurs at high adsorbent amount resulting in decreased active sites. Similar results have been reported for the sorption of various adsorbate onto various adsorbents in the literature [29, 34-36].

Effect of the solution temperature

The temperature dependence of sunset yellow sorption onto AC was studied at optimum adsorbent dosage of 0.05 g/L. Figure 7 shows that the food dye adsorption increased with the temperature, which may be attributed to the enhanced reaction rate at a higher temperature. The possible explanation is that a high temperature expands the pore volume and the surface area and thus provides more chances for sunset yellow dye to pass the external boundary layer and penetrate more easily. This corroborates the reports of our previous studies [27, 29]. Similar behavior has been reported in the literature [37]. The temperature dependence of SY sorption onto MWCNT was studied at optimum adsorbent dosage of 0.005 g/L. Figure 8 presents the adsorption capacity of SY dye onto MWCNT at temperatures from 30 to 50 °C. The result shows that the equilibrium adsorption capacity of SY dye decreased while increasing the solution temperature from 30 to 50 °C. The adsorption capacity of MWCNT at equilibrium decreased from 171.41 to 141.09 mg/g with an increase in the temperature from 30 to 50 °C. This decrease may be due to weakening of the bonds between the dye molecules and the active sites of MWCNT. Similar phenomena have been observed in the adsorption of remazol brilliant blue [38] and methylene blue [39] dyes onto orange peel adsorbent.

Adsorption isotherms

The equilibrium adsorption isotherms are essential to the practical design and optimization of the adsorption process. The adsorption isotherm describes how adsorbates interact with adsorbents 29]. The equilibrium data of food dye adsorption onto adsorbents was explored using the isotherm models of Langmuir, Freundlich, Temkin and DR. The calculated parameters of the four isotherm models are and presented in Table 2.

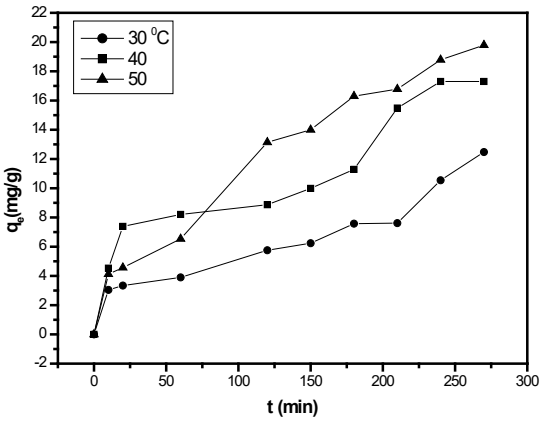

Figure 7. Effect of solution temperature on the adsorption of the food dye onto AC (conditions: W=0.05 g/L; C_0=10 mg/L).

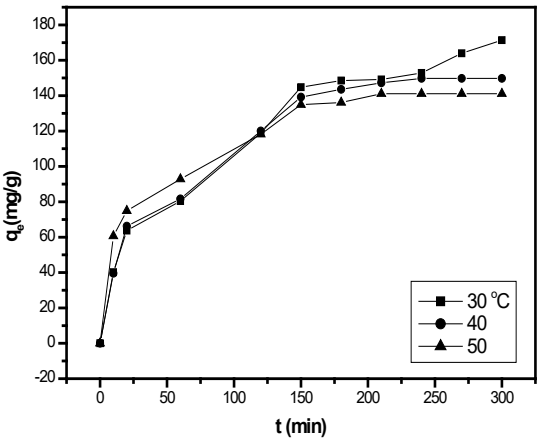

Figure 8. Effect of solution temperature on the adsorption of the food dye onto MWCNT (conditions: W=0.005 g/L; C_0=10 mg/L).

The correlation coefficients decreased in the order: DR> Langmuir> Temkin> Freundlich for AC. Langmuir adsorption isotherms constants related to adsorption capacity, Q_0, were found as 125.31 and 43.78 mg/g for AC and MWCNT, respectively. The relatively large adsorption capacity of AC could be attributed to its relatively large surface area (249.5 m^2/g) and total pore volume (0.445 mL/g). The results revealed that the adsorption of food dye on AC was best described by the Langmuir isotherm, indicating the adsorption was homogeneous and a monolayer was present.

Table 2. Freundlich, Langmuir, Temkin and DR isotherm constants for the adsorption of SY dye onto AC and MWCNT at 40 °C

Isotherms	Parameters		
Freundlich	K_F (mg/g)(L/mg)$^{1/n}$	n	R^2
AC	0.4312	1.6397	0.523
MWCNT	460.29	2.291	0.453
Langmuir	Q_0 (mg/g)	K_L (L/mg)	R^2
AC	125.31	0.0087	0.905
MWCNT	43.78	0.206	0.198
Temkin	A (L/g)	b (J/mol)	R^2
AC	0.228	176.79	0.642
MWCNT	7.63E-4	-75.64	0.454
DR	q_m (mg/g)	E (J/mol)	R^2
AC	40.55	119.56	0.911
MWCNT	2199.51	325.44	0.920

Table 3. Kinetic models parameters for the adsorption of SY onto AC at different dye concentrations and temperatures.

AC		Pseudo-first order			Pseudo-second order			Elovich		
m_{ads} (g/L)	q_e (mg/g) exp	k_1 $(min)^{-1}$	q_e (mg/g)	R^2	k_2 (g/mg min)	q_e (mg/g)	R^2	β	α	R^2
10	12.475	0.0055	11.649	0.824	1.34-3	11.541	0.765	0.435	11.534	0.696
20	25.693	0.0051	27.265	0.714	2.57E-4	26.144	0.439	0.190	57.993	0.614
30	31.374	0.0061	35.238	0.753	1.01E-4	42.265	0.331	0.136	0.5435	0.699
40	46.337	0.0062	54.141	0.720	2.05E-5	96.246	0.104	0.089	176.40	0.687
50	36.052	0.0046	39.771	0.740	3.59E-5	60.827	0.104	0.127	0.4979	0.611
T (°C)										
30	12.475	0.0055	11.649	0.824	1.34E-3	11.541	0.765	0.435	11.534	0.696
40	17.302	0.0070	15.052	0.741	1.16E-3	17.559	0.820	0.435	0.459	0.696
50	19.790	0.0104	20.944	0.932	6.33E-4	22.769	0.864	0.203	0.6895	0.901

Langmuir adsorption isotherm constant related to adsorption capacity, Q_0 was found as 125. 31 mg/g. To confirm the favorability of the adsorption, the separation factor R_L was calculated by the following equation:

$$R_L = \frac{1}{1 + K_L C_0} \qquad (10)$$

where the adsorption process is either unfavorable ($R_L > 1$), linear ($R_L = 1$), favorable ($0 < R_L < 1$) or irreversible ($R_L = 0$). Here, the value of R_L was found to be 0.696 and 0.327 for AC and MWCNT, respectively, which further confirmed that the Langmuir isotherm was favorable for the adsorption of the food dye on the two adsorbents. Similar observation was reported for the adsorption of remazol brilliant blue dye on an orange peel adsorbent [38]. The value of n (from the Freundlich equation) was found to be 1.64 and 2.29 for AC and MWCNT, respectively, which is an evidence of the good adsorption of SY dye on the two adsorbents [38].

Adsorption kinetics

Adsorption kinetics provides an understanding of the mechanism of adsorption, which in turn governs the mass transfer and the equilibrium time. Sunset yellow was adsorbed on adsorbents as a function of time. Pseudo-first order and pseudo-second order and also Elovich models were obtained at temperatures of 30, 40 and 50 °C for various dye concentrations (10-50 mg/L for AC and 10-80 mg/L for MWCNT). The regression coefficients (R^2) were evaluated for all models. The results are shown in Table 3. As shown in Table 3, the highest R^2 values were obtained for the pseudo-first order kinetic model and the experimental q_e values matched well with the calculated data. It can be seen that k_1 values are increasing as the temperature increases. The higher regression coefficients indicated that the pseudo-first order model was a better fit than the pseudo-second order model.

Table 4. Kinetic models parameters for the adsorption of SY onto MWCNT at different dye concentrations and temperatures.

MWCNT		Pseudo-first order			Pseudo-second order			Elovich		
m_{ads} (g/L)	q_e (mg/g) exp	k_1 (min^{-1})	q_e (mg/g)	R^2	k_2 (g/mg min)	q_e (mg/g)	R^2	β	α	R^2
10	171.41	0.0101	153.50	0.963	1.37E-4	182.82	0.966	0.026	9.034	0.959
20	238.24	0.0142	79.590	0.803	9.93E-4	239.23	0.999	0.075	2254.2	0.977
50	406.56	0.0147	444.15	0.912	4.44E-5	460.83	0.902	0.039	22.436	0.855
80	130.88	0.0067	126.51	0.696	9.15E-5	136.24	0.647	0.011	5.434	0.626
T (°C)										
30	171.41	0.0101	153.50	0.963	1.37E-4	182.82	0.966	0.026	9.034	0.959
40	149.75	0.0180	154.31	0.965	2.01E-4	165.02	0.982	0.029	10.169	0.966
50	141.09	0.0174	116.95	0.953	3.69E-4	149.70	0.992	0.038	23.234	0.969

Table 5. Thermodynamic parameters for the adsorption of SY onto adsorbents.

Adsorbent	Ea (kJ/mol)	ΔH° (kJ/mol)	ΔS° (J/mol)	ΔG° (kJ/mol)		
				30 °C	40 °C	50 °C
AC	25.84	110.7	368.3	-1.07	-4.28	-8.44
MWCNT	40.20	-14.58	-48.37	0.018	0.678	0.977

Therefore, it can be said that the pseudo-second order model is not suitable to explain the adsorption process accurately. Similar results have been found in our previous study [29]. Table 3 presents the results deduced from linear plots of q_t *versus lnt*, where β is a constant related to the extension of covered surface, and α is in relationship with chemisorption rates [30]. The Elovich constants were determined from the intercepts and slope of plots. It was noted that all β values of AC were similar. The chemisorption rates, indicated by the coefficient α, vary with dye concentration; the best value was obtained in the case of 40 mg/L dye concentration.

Kinetic parameters for the removal of sunset yellow by MWCNT are represented in Table 4. The results for the MWCNT showed good agreement with the three kinetic models, especially with the pseudo-second order kinetic model, suggesting the presence of chemisorption for MWCNT.The values for k_2 are 0.000137, 0.000201 and 0.000369 g/mg min at 30, 40 and 50 C, respectively. Similar results have been reported for the sorption kinetics of various adsorbate onto various adsorbents in literature [27, 30, 31, 40, 41]. The Elovich model was applied to the adsorption of sunset yellow on MWCNT. It was noted that all β values of MWCNT were similar, and increased with increasing temperature. Conversely, they decreased with increasing concentration. Similar results have been reported for the sorption kinetics of basic and reactive dyes onto granular activated carbon [30]. The chemisorption rates (α), vary with dye concentration, the best value was obtained in case of 10 mg/L dye concentration. The correlation coefficients of the Elovich model for MWCNT were also high, which indicates good linearity. From the R^2 values it may be deduced that the Elovich model can be accepted as one of the characteristics of the adsorption reaction onto MWCNT. Elovich model, initially used to express the beginning of the sorption process, long before equilibrium, can be correctly used in case of chemisorption with highly heterogeneous adsorbents [30].

Adsorption thermodynamics

The activation energy (E_a) of adsorption can be evaluated using the pseudo-first order rate and pseudo-second order constants for AC and MWCNT, respectively. The linear plot between ln k_1 or ln k_2 versus 1/T was used to calculate E_a using equation 7 and the results are given in Table 5. The E_a gives an idea about the type of adsorption process (physical or chemical). Low energies (E_a: 5-40 kJ/mol) are characteristic for physical adsorption, while higher activation energies (E_a: 40-800 kJ/mol) suggest chemical adsorption [31]. The value of E_a given in Table 5 confirms the nature of the physisorption process of SY onto AC. The E_a value was thus determined to be 40.2 kJ/mol for the second adsorption process, which indicates the chemisorption nature of SY adsorption onto the MWCNT.

The values of ΔH° and ΔS°, determined from the slope and intercept or the plot of $\ln K_C$ *vs* 1/T are reported in Table 5. The negative values of ΔG° obtained at different temperatures as seen in Table 5, show that the SY adsorption on AC was spontaneous and physical in nature, but SY adsorption on MWCNT was non-spontaneous which was revealed by the positive values of ΔG° at all temperatures under study. The increase in the

magnitude of ΔG° with increase in temperature showed an increase in the feasibility of adsorption at higher temperatures [9, 23,24]. The positive value of both ΔH° and entropy ΔS° obtained for SY adsorption on AC showed that the adsorption process was endothermic and had random characteristics. This further confirmed the results of the studies on the effect of solution temperature on the adsorption for AC. Similar results were reported for the adsorption of disperse yellow 211 dye using low-cost adsorbents [29]. ΔH° was determined to be -14.58 kJ/mol, indicating the exothermic nature of the adsorption process for SY on MWCNT. This result is in aggrement with the decrease in the equilibrium adsorption capacity with increasing temperature. The negative values of ΔS° suggest decreased randomness at the solid/solution interface and no significant changes occurring in the internal structure of the adsorbent through the adsorption of SY onto MWCNT. Similar results were reported for adsorption of basic violet 10 using MCM-41 [33].

CONCLUSIONS

The present investigation showed that biowaste cornelian cherry stones can be effectively used as a raw material for the preparation of activated carbon *via* chemical activation using LiOH. The BET surface area and total pore volume of the produced activated carbon were 249.5 m^2/g and 0.445 mL/g, respectively. This activated carbon (AC) and commercial multiwalled carbon nanotubes (MWCNT) were used to remove sunset yellow FCF food dye (SY) from aqueous solutions at various temperatures. In batch adsorption studies, the efficiency of SY adsorption by AC or MWCNT increased with adsorbent dosage, but the equilibrium adsorption capacity decreased significantly. Adsorption capacities of SY onto AC and MWCNT were 125.3 and 43.8 mg/g, respectively. The results showed that the adsorption capacity of AC is about 2.8 times higher than that of MWCNT. The Freundlich, Langmuir, Temkin and DR isotherm models were used for the mathematical description of the adsorption of SY dye onto AC or MWCNT at various temperatures and the results suggested that the adsorption equilibrium data fitted well to the Langmuir and DR models for AC and DR model for MWCNT. The pseudo-first order, pseudo-second order and Elovich kinetic models were used to analyze the data obtained for SY adsorption onto the prepared activated carbon and MWCNT. The kinetic calculations showed that the adsorption followed the pseudo-first order model with a multi-step diffusion process for AC. These results finally confirmed that the adsorption of SY onto AC is controlled by both physisorption and chemisorption processes. The pseudo-second order kinetic model agrees very well with the dynamic behavior for the adsorption of SY onto MWCNT at different temperatures.

Thermodynamic constants were also evaluated using equilibrium constants changing with temperature. The negative value of ΔG° indicated the spontaneity and confirmed the favorable adsorption of SY onto AC. As the temperature increased from 30 to 50 °C, the positive values of ΔH° confirmed that the process was endothermic. The positive value of ΔS° suggested the increased randomness of SY adsorption onto AC. The enthalpy change (ΔH°) for the SY adsorption onto MWCNT was -14.58 kJ/mol, which was also found to be exothermic and the adsorption capacity decreased with the increase in temperature. The ΔG° values were positive, therefore the SY adsorption onto MWCNT was non-spontaneous and the negative value of ΔS° showed the stability of the sorption process. The activation energy of the adsorption process was calculated by performing kinetic analysis at different temperatures (30-50 °C). Activation energies were 25.84 and 40.2 kJ/mol for AC and MWCNT, respectively. This study revealed that cornelian cherry stones-based activated carbon can be used as a highly efficient and economically viable adsorbent for SY dye removal from aqueous solutions.

Acknowledgements: *The author acknowledges the financial support provided by Kocaeli University Scientific Research Projects Unit. (Project No: 2014/113, 2016/019 HD and 2017/57 HD).*

REFERENCES

1. J. Hayashi, T. Horikawa, I. Takeda, K. Muroyama, F. N. Ani, *Carbon,* **40**, 2381 (2002).
2. B. Y. Jibril, R. S. Al-Maamari, G. Hegde, N. Al-Mandhary, O. Houache, *J. Anal. Appl. Pyrolysis,* **80,** 277 (2007).
3. H. Benaddi, T. J. Bandosz, J. Jagiello, J. A. Schwarz, J.N. Rouzaud, D. Legras, F. Bèguin, *Carbon,* **38,** 669 (2000).
4. K. Nakagawa, S. R. Mukai, K. Tamura, H. Tamon, *Chemical Engineering Research and Design,* **85,** 1331 (2007).
5. R. Ubago-Pérez, F. Carrasco-Marín, D. Fairén-Jiménez, C. Monero-Castilla, *Microporous and Mesoporous Materials,* **92,** 64 (2006).
6. P. Ariyadejwanich, W. Tanthapanichakoon, K. Nakagawa, S. R. Mukai, H. Tamon, *Carbon,* **41,** 157 (2003).
7. M. Shimada, T. Iida, K. Kawarada, Y. Chiba, T. Mamoto, T. Okayama, *J. Mater. Cycles Waste Manag*., **6**, 111 (2004).

8. F. Oguz Erdogan, *Analytical Letters,* **49,** 1079 (2016).
9. K. Fu, Q. Yue, B. Gao, Y. Wang, Q. Li, *Colloids and Surfaces A,* **529,** 842 (2017).
10. A. Niksiar, B. Nasernejad, *Biomass and Bioenergy,* **106,** 43 (2017).
11. A. B. Fadhil, *Energy Conversion and Management,* **133,** 307 (2017).
12. N. Arena, J. Lee, R. Clift, *Journal of Cleaner Production,* **125** ,68 (2016).
13. J. M. V. Nabais, C. E. C. Laginhas, P. J. M. Carrott, M. M. L. R. Carrott, *Fuel Processing Technology,* **92,** 234 (2011).
14. A. B. Fadhil, A. I. Ahmed, H. A. Salih, *Fuel,* **187,** 435 (2017).
15. S. S. Lam, R. K. Liew, Y. M. Wong, P. N. Y. Yek, N. L. Ma, C. L. Lee, H. A. Chase, *Journal of Cleaner Production,* **162,** 1376 (2017).
16. C. A. Philip, *J. Chem. Tech. Biotechnol*., **67,** 248 (1996).
17. J. Guo, A. C. Lua, *Microporous and Mesoporous Materials,* **32,** 111 (1999).
18. J. Hayashi, A. Kazehaya, K. Muroyama, A. P. Watkinson, *Carbon,* **38,** 1873 (2000).
19. T. Tay, S. Ucar, S. Karagöz, *Journal of Hazardous Materials,* **165,** 481 (2009).
20. T. H. Liou, *Chemical Engineering Journal,* **158,** 129 (2010).
21. R. Aravindhan, J. R. Rao, B. U. Nair, *Journal of Hazardous Materials,* **165,** 688 (2009).
22. M. F. González-Navarro, L. Giraldo, J. C. Moreno-Piraján, *Journal of Analytical and Applied Pyrolysis,* **107,** 82 (2014).
23. X. Tian, H. Ma, Z. Li, S. Yan, L. Ma, F. Yu, G. Wang, X. Guo, Y. Ma, C. Wong, *Journal of Power Sources,* **359**, 88 (2017).
24. A. S. Al-Rahbi, P. T. Williams, *Waste Management,* **49,** 188 (2016).
25. Y. Li, Q. Du, T. Liu, X. Peng, J. Wang, J. Sun, Y. Wang, S. Wu, Z. Wang, Y. Xia, L. Xia, *Chemical Engineering Research and Design,* **91,** 361 (2013).
26. Y. Yao, H. Li, J. Liu, X. Tan, J. Yu, Z. Peng, *Journal of Nanomaterials,* Art. ID 571745, (2014).
27. T. Erdogan, F. Oguz Erdogan, *Analytical Letters,* **49,** 917 (2016).
28. M. Roosta, M. Ghaedi, A. Daneshfar, S. Darafarin, R. Sahraei, M. K. Purkait, *Ultrasonics Sonochemistry,* **21,** 1441 (2014).
29. F. Oguz Erdogan, *Journal of Textiles and Engineering*, **107,** 181 (2017).
30. K. D. Belaid, S. Kacha, M. Kameche, Z. Derriche, *Journal of Environmental Chemical Engineering,* **1,** 496 (2013).
31. B. H. Hameed, A. A. Ahmad, N. Aziz, *Desalination,* **247,** 551 (2009).
32. T. Kou, Y. Wang, C. Zhang, J. Sun, Z. Zhang, *Chemical Engineering Journal,* **223,** 76 (2013).
33. L. C. Juang, C. C. Wang, C. K. Lee, *Chemosphere*, **64,** 1920 (2006).
34. C. O. Nweke, G. C. Okpokwasili, *International Journal of Biosciences,* **3,** 11 (2013).
35. Z. Huang, X. Wang, D. Yang, *Water Science and Engineering,* **8,** 226 (2015).
36. E. Rubín, P. Rogríguez, R. Herrero, M. E. Sastre de Vicente, *Journal of Chemical Technology and Biotechnology,* **81,** 1093 (2006).
37. Z. Emami, S. Azizian, *Journal of Analytical and Applied Pyrolysis,* **108,** 176 (2014).
38. M. R. Mafra, L. Igarashi-Mafra, D. R. Zuim, É. C. Vasques, M. A. Ferreira, *Brazilian Journal of Chemical Engineering,* **30,** 657 (2013).
39. P. S. Kumar, P. S. A. Fernando, R. T. Ahmed, R. Srinath, M. Priyadharshini, A. M. Vignesh, A. Thanjiappan, *Chemical Engineering Communications,* **201,** 1526 (2014).
40. M. Auta, B. H. Hameed, *Chemical Engineering Journal,* **198-199,** 219 (2012).
41. B. H. Hameed, *Journal of Hazardous Materials,* **161,** 753 (2009).
42. C. O. Nweke, G. C. Okpokwasili, *International Journal of Biosciences,* **3,** 11 (2013).
43. S. A. Kosa, G. Al-Zhrani, M. A. Salam, *Chemical Engineering Journal,* **181-182,** 159 (2012).
44. F. Oguz Erdogan, *Chemistry & Chemical Technology*, in press (2018).

СРАВНИТЕЛНО ИЗСЛЕДВАНЕ НА АДСОРБЦИЯТА НА СЪНСЕТ ЖЪЛТО БАГРИЛО ВЪРХУ АКТИВЕН ВЪГЛЕН ОТ КОСТИЛКИ НА ДРЕНКИ И ВЪРХУ ВЪГЛЕРОДНИ НАНОТРЪБИЧКИ

Ф. О. Ердоган*

Департамент по химия и технологии за химична обработка, Професионално училище на Коджаели, Университет на Коджаели, Коджаели, Турция

Постъпила на 13 декември, 2017; приета на 20 юли, 2018

(Резюме)

Целта на това изследване е да се произведе евтин активен въглен от костилки на дренки (*Cornus mas* L.) и да се сравни адсорбционното му отнасяне към хранителното багрило сънсет жълто FCF (SY) с това на търговски многостенни въглеродни нанотръбички. Активният въглен от костилки на дренки (AC) и търговските многостенни въглеродни нанотръбички (MWCNT) са охарактеризирани чрез N_2 адсорбционни изотерми и SEM. Адсорбцията на хранителното багрило SY върху AC и MWCNT е детайлно изследвана. Адсорбционният тест в статични условия показа, че степента на адсорбция на багрилото зависи от неговата концентрация, времето на контакт, температурата на разтвора и количеството адсорбент. Експерименталните данни за адсорбционното равновесие са сравнени с моделите на Лангмюир, Фройндлих, Темкин и DR и са определени параметрите на изотермния модел. Максималният адсорбционен капацитет за AC и MWCNT е определен съответно като 125.3 и 43.8 mg/g. Кинетичните данни съответстват на уравнения от псевдо-първи порядък, псевдо-втори порядък и Елович. Изчислени са скоростните константи. Установени са промените в термодинамичните параметри енталпия, ентропия и свободна енергия на Гибс. Показано е, че активният въглен, произведен от костилки на дренки, е подходящ за адсорбция на хранителното багрило SY и може да се използва като евтин и ефективен адсорбент за обработка на промишлени отпадни води.

Bulgarian Chemical Communications, Volume 50, Issue 4 (pp. 602 – 607) 2018

Kinetic study and modeling of Zn^{2+}removal from wastewater by adsorption onto multi-walled carbon nanotubes

H. Sadegh[1,*], R. Shakibaei Lalehloo[2], S. M. Seyed Arabi[2], M. Jalili[3], P. Chauhan[1]

[1] *West Pomeranian University of Technology, Szczecin, Faculty of Chemical Technology and Engineering, Szczecin, Poland*

[2] *Department of Chemistry, Karaj Branch, Islamic Azad University, Karaj, Iran*

[3] *Department of Chemistry, Shahr-e-Qods Branch, Islamic Azad University, Tehran, Iran*

Received, January 8, 2018; Revised, July 20, 2018

Adsorption methods for the removal of Zn^{2+} as a toxic heavy metal ion using multi-walled carbon nanotubes (MWCNTs) as an adsorbent are presented here. SEM and FTIR techniques were used for the characterization of the MWCNTs. The relationship between the optimization factors (adsorbent dosage, contact time and initial heavy metal ion concentration) and the adsorption properties of the MWCNTs was studied. The quantity of metals adsorbed during various time intervals is the base of kinetics of adsorption. A thorough investigation was done on the modeling of kinetic curves. The results of the adsorption kinetics study showed that the adsorption of Zn^{2+} fitted most closely to the pseudo-second-order model (R^2>0.999), and the adsorption equilibrium time was 55 min. The Langmuir isotherm model was used to fit the adsorption equilibrium data.

Keywords: Multi-walled carbon nanotubes; Adsorption; Kinetics; Isotherm; Zn^{2+}, Water treatment.

INTRODUCTION

Heavy metals are nowadays among the most important pollutants in surface and groundwater [1, 2]. Thus, the removal of such toxic materials from wastewater is becoming a crucial issue. To control this issue, many physical, chemical and biological technologies have been developed [3, 4]. Due to its high efficiency and economic consideration, adsorption process was reported to be the most suitable method to this purpose [5, 6]. In addition, adsorption does not result in secondary pollution by producing harmful substances during the process [7-10]. Some adsorbents such as zeolites, biomaterials, polymers, etc., have been extensively used for adsorption of toxic heavy metal ions [11-16]. Since the adsorption efficiency is mostly dependent on the adsorbent properties, therefore developing an effective adsorbent is of vital importance for the widely applications of adsorption in water treatment [17-19]. Therefore, development of more efficient adsorbents has attracted the attention of quite a large number of researchers. New adsorbents based on nanomaterials are used to remove heavy metal ions from wastewater and remove the traditional sorbents defects [20, 21]. Carbon nanotubes (CNTs) have attracted significant interdisciplinary interest on account of their exclusive physical and chemical properties; nonetheless, the hydrophobicity of CNTs may restrict some of their applications [22, 23]. Therefore, CNTs surface treatments with functional groups or nanoparticles leads to overcoming of their drawbacks toward some applications [24-27]. The aim of the present paper was to study the possibility of the removal of Zn^{2+} heavy metal ions by MWCNTs. A kinetic study according to three different models was applied. The reaction order and the rate constants were studied and calculated using batch studies.

EXPERIMENTAL

Materials

MWCNTs were obtained from NanoAmor Nanostructured & Amorphous Materials, Inc, USA. Chemical vapor deposition (CVD) method was used to prepare MWCNTs with purity of 95%, outer diameters of 50 nm, length in the range from 500 to 2000 nm and specific surface area of 40 m^2 g^{-1}. In addition, $ZnCl_2$ aqueous solutions with different concentrations were prepared and used as sources of Zn^{2+}. All other chemicals were purchased from Merck Inc, USA.

Samples Characterization

FTIR (Fourier transformation infrared spectroscopy) was used to examine the functional groups of the prepared materials using a Tensor 27, Bruker, Germany. Around 5 mg of the powder was homogenized with about 100 mg of KBr with an agate mortar and was pelletized before the measurement. The surface morphology characteristics of the montmorillonite particles were

* To whom all correspondence should be sent:
E-mail: hamid-sadegh@zut.edu.pl

observed by FESEM.

Adsorption Experiments

A stock Zn^{2+} solution (1000 mg L^{-1}) was prepared by dissolving $ZnCl_2$ into deionized water and diluting to prepare all synthetic fresh solutions used in the investigation. To find the optimum Zn^{2+} adsorption conditions and to study the adsorption in batch conditions, a 100 mL stoppered conical flask and a temperature-controlled shaker were used for the experiment. Dosage effects were studied in the range of 2–10 mg (initial concentration (C_o) of 20 mg L^{-1}, natural pH, 25 ºC, contact time of 1 h). The effect of contact time was studied in the time range of 1-60 min (20 mg L^{-1}, 10 mg, natural pH, 25 ºC). Adsorption equilibrium studies in a single system were carried out with initial concentrations ranging from 10 to 70 mg L^{-1}. Zn^{2+}concentrations were determined by GBC-932 atomic adsorption spectrophotometer (AAS, GBC, Australia). The adsorption capacity q_e (mg g^{-1}) which is the adsorbed amount of adsorbate per unit mass of the adsorbent at time t was calculated according to Eq. (1):

$$q_e = \frac{(C_o - C_e)V}{m} \qquad (1)$$

where, C_o and C_e (mg L^{-1}) are the initial and equilibrium Zn^{2+} concentrations, respectively. V (L) is the volume of adsorption solution and m (g) is the mass of adsorbent.

RESULTS AND DISCUSSION

Characterization of Adsorbent

The FTIR spectrum of the sample is shown in Fig. 1a. The band observed near 1580 cm^{-1} in both samples indicates presence of a cylinder-like carbon structure (rolled graphene sheet). The morphological characteristics of the MWCNTs were investigated by SEM and are shown in Fig. 1b.

Adsorption Studies

Effect of Dosage: Presence of satisfactory adsorbent amount is an important parameter to consider as it determines the number of free adsorption sites for a given initial concentration.

The experiments were carried out at 25 ºC (the MWCNTs dosage in the range of 2–10 mg, Zn^{2+} solution volume and concentration were 25 mL 20 mg·L^{-1}, respectively). Adsorption of ions increased rapidly with the increasing dosage of adsorbent, which due to the increase in the number of active sites with increased amount of MWCNTs, as shown in Fig. 2.

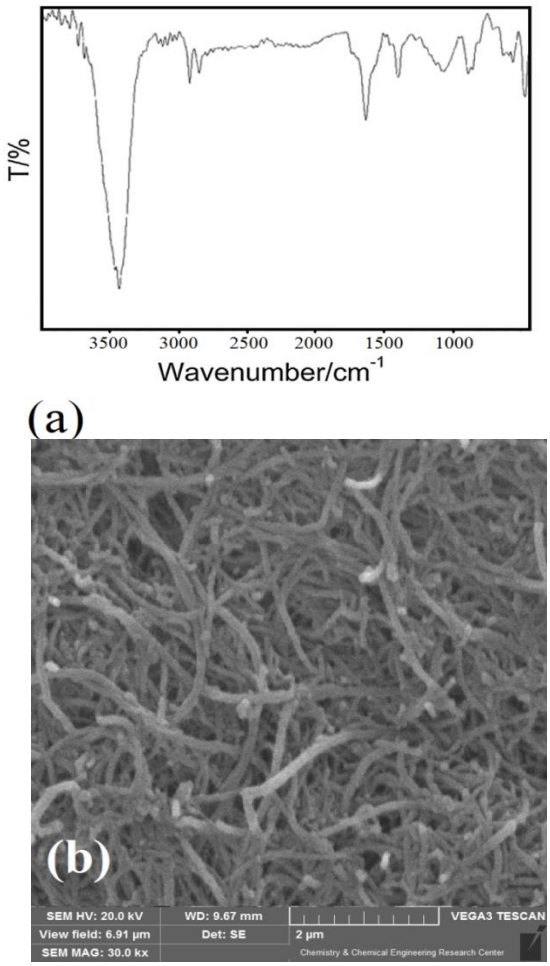

Fig. 1. FTIR spectrum (a) and SEM micrograph (b).

At 8 mg, the adsorption of Zn^{2+} reached equilibrium state. Considering the adsorption and practicality, 8 mg was selected as the optimum adsorbent dosage in the following experiments.

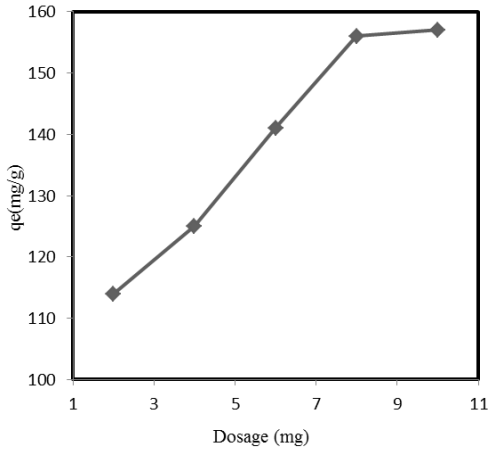

Fig. 2. Effect of adsorbent dosage (20 mg L^{-1}, natural pH, 25 ºC, 2 h).

Effect of Contact Time: One of the meaningful parameters in the design of economical wastewater treatment systems is the equilibrium time [28, 29].

The effect of contact time on the adsorption process was studied and evaluated. The investigation was executed with 8 mg of MWCNTs at natural pH and 25 ºC.

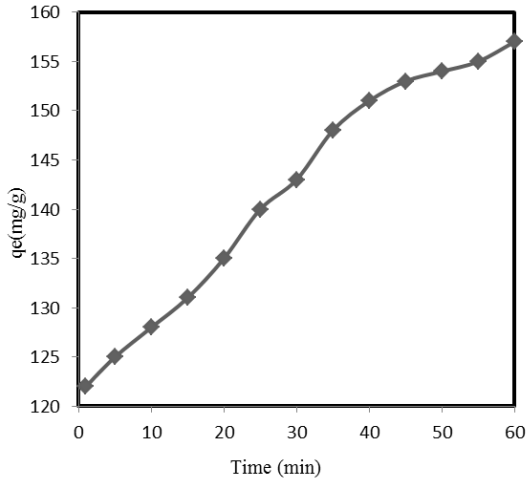

Fig. 3. Effect of contact time (20 mg L^{-1}, 10 mg, natural pH, 25 ºC).

From the results shown in Fig. 3 it is clear that the MWCNTs adsorbent exhibits a gradual increase in Zn^{2+} adsorption capacity with the increase in the reaction contact time. The metal adsorption capacity value was found to reach saturation after 55 min with maximum adsorption of Zn^{2+}. These findings refer to the binding processes of $Zn^{2+}$to the surface of MWCNTs adsorbent *via* two different steps [30]. The first is related to a linear and constant increase in the metal capacity while increasing the contact time from 1 to 55 min due to the possible occupation of the surface functional groups of the adsorbent by the target metal ion. The second step is directly related to the equilibrium and saturation conditions which require more than 55 min. Finally, this period was taken as the optimal contact time for the rest testing.

Adsorption Kinetics and Modeling: To study the kinetic mechanism that refers *to* the adsorption process, the data described in the "effect of contact time and effect of temperature" sections were used for further analysis. Different kinetic models *were* applied such as pseudo–first order, pseudo–second order and intraparticle diffusion to interpret the experimental data [31-35].

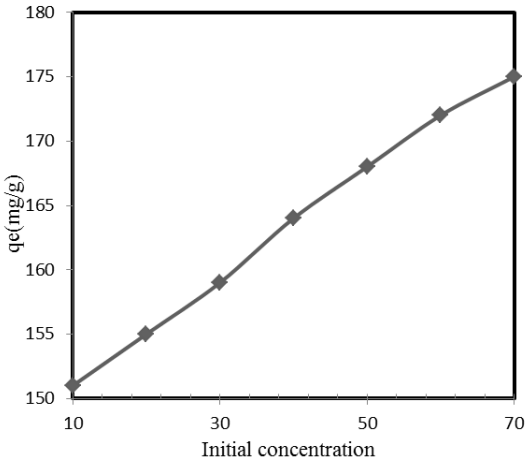

Fig. 4. Effect of initial concentration (10 mg, pH 2, 25 ºC, 60 min).

Table 1. Kinetic parameters of Zn^{2+} adsorption by MWCNTs

Model	Parameters	R^2
Pseudo–first order	q_e = 118.71 mg g^{-1} K_1 = 0.190 min^{-1}	$R_1^2 = 0.889$
Pseudo–second order	q_e = 92.9 mg g^{-1} K_2 = 0.035 g mg^{-1} min^{-1}	$R_2^2 = 0.999$
Intraparticle diffusion	k_p = 78.25 mg g^{-1} $min^{-1/2}$ C = 5.0856	$R_3^2 = 0.788$

A linear form of the pseudo–first order model could be given as:

$$\ln(q_e - q_t) = \ln(q_e) - k_1 t \qquad (2)$$

where, q_e and q_t are the amounts of ion adsorbed (mg g^{-1}) at equilibrium and time t, respectively. k_1 is the equilibrium rate constant (min^{-1}). The linear fit between the $\ln(q_e - q_t)$ and contact time (t) can show an approximation of pseudo–first order kinetics.

The linear form of the pseudo–second order model [33] can be expressed as follows:

$$\frac{t}{q_t} = \frac{1}{k_2 q_e^2} + (\frac{1}{q_e})t \qquad (3)$$

where, k_2 is pseudo–second order equilibrium rate constant (g mg^{-1} min^{-1}). The linear fit between the t/q_t and contact time (t) can show an approximation of pseudo–second order kinetics.

The intraparticle diffusion model was used to explore the possibility of intraparticle diffusion resistance affecting adsorption [36]:

$$q_t = k_p t^{1/2} + c \quad (4)$$

where, k_p is the intraparticle diffusion rate constant and c is the intercept which is related to the thickness of the boundary layer. According to this model, when intraparticle diffusion is involved in the adsorption process the plot should be linear and intraparticle diffusion is the rate controlling step if the line passes through the origin [37]. All kinetic parameters obtained from the experimental data fitting using the above mentioned equations are shown in Table 1. To best describe the adsorption process, it is noticeable from Table 1 that the very high value of correlation coefficients (> 0.999), and the good fit proves that the pseudo–second order model with good correlation is the best description. This suggests that the rate–limiting step of Zn^{2+} ion onto MWCNTs is chemisorption, where valency forces are involved *via* electrons sharing or exchange between the MWCNTs and the Zn^{2+} ions [38].

Adsorption Isotherms

In order to describe the interactive behavior of adsorbate and adsorbent, adsorption isotherms were used. To estimate the adsorption capacity (Q_o), the equilibrium data were fitted using Langmuir and Freundlich models [35, 36]. Below, we can see the mathematical description of these models, Eqs. ((5) and (6), respectively):

$$\frac{1}{Q_e} = \frac{1}{Q_o} + \left(\frac{1}{Q_o K_L}\right)\frac{1}{C_e} \quad (5)$$

$$\ln Q_e = \ln K_F + \frac{1}{n}\ln C_e \quad (6)$$

where, Q_e is the solid phase adsorbate equilibrium amount (mg g^{-1}); Q_o is the maximum adsorption capacity (following Langmuir monolayer adsorption technique) (mg g^{-1}); K_L is Langmuir constant (L mg^{-1}); *n* and K_F (mg g^{-1})(L mg^{-1}) are Freundlich constants which are related to the adsorption intensity and adsorption capacity, respectively. The values of *1/n* and K_F are found from the slope and intercept, respectively, of the linear plot of experimental data of $\ln Q_e$ *versus* $\ln C_e$. 1/n values show the different kinds of isotherm: not reversible (1/n = 0), favorable (0 < 1/n < 1) and unfavorable (1/n > 1) [38]. Langmuir isotherm numbers of K_L and Q_o can be obtained from the intercept and slope of the linear plot of $1/Q_e$ *vs.* $1/C_e$. Table 2 shows the adsorption isotherm for Zn^{2+} ion on MWCNTs surface.

From Table 2 one can see that Langmuir isotherm demonstrates a better fit of experimental data than Freundlich isotherm. Also, this proves that the surfaces of adsorbents are primarily built of heterogeneous adsorption patches [36] and lesser homogeneous patches [39]. which is The Freundlich constant n is a measure of adsorption intensity. From Table 2 it can be seen that the values of 1/n (adsorbent) were lower than 1, which shows high adsorption intensity [40]. Results show that MWCNTs surface is better in adsorption of Zn^{2+} ion. R_L, a dimensionless parameter is used to show the favorability of adsorption process of Zn^{2+} ion onto adsorbent surfaces. The mathematical definition of R_L is as follows:

$$R_L = \frac{1}{1+K_L C_O} \quad (7)$$

In terms of R_L, the adsorption process can be seen as irreversible ($R_L = 0$), favorable ($0 < R_L < 1$), linear ($R_L = 1$) or unfavorable ($R_L > 1$) [41-43]. From the results it was noticeable that in case of MWCNTs surface, the value of R_L for adsorption of Zn^{2+} ion was between 0 and 1. So, the adsorption of Zn^{2+} onto the adsorbent is favorable. MWCNTs has an adsorption capacity of about 93 mg g^{-1}.

Table 2. Fitting experimental data of Zn^{2+} adsorption to the equations of Langmuir and Freundlich.

Model	Parameters	R^2
Langmuir	$Q_o = 93$	0.999
	$K_L = 4.98$	
Freundlich	1/n = 0.611	0.998
	$K_F = 54.8$	

CONCLUSIONS

Multi-walled carbon nanotubes (MWCNTs) are an effective adsorbent for the removal of Zn^{2+} from aqueous solutions. Adsorption capacity depends on adsorbent dosage, contact time and initial metal ion concentration. Langmuir and Freundlich isotherms were used to determine the adsorption parameters and the data of equilibrium are best described by Langmuir model which gives the value of 93 mg g^{-1} as the maximum adsorption capacity. The adsorption process was studied kinetically and the obtained data were analyzed using the pseudo–first order, pseudo–second order, intraparticle diffusion models. Pseudo–second order was found to be the best correlation model based on the values of the correlation coefficient (R^2). Therefore, it can be concluded that the MWCNTs have potentiality and are a promising adsorbent for environmental management and water treatment due to their better efficiency and feasibility.

REFERENCES

1. C. Williams, D. Aderhold, R. Edyvean, *Water Res*., **32,** 216 (1998) .
2. K. Kadirvelu, K. Thamaraiselvi, C. Namasivayam, *Bioresour. Technol*., **76,** 63 (2001) .
3. V. Gupta, *J. Environ. Manage*., **90,** 2313 (2009) .
4. H. Sadegh, G. A. M. Ali, A. S. H. Makhlouf, K. F. Chong, N. S. Alharbi, S. Agarwal, V. K. Gupta, *J. Mol. Liq.*, **258**, 345 (2018).
5. S. M. Seyed Arabi, R. S. Lalehloo, M. R. T. B. Olyai, G. A. M. Ali, H. Sadegh, *Physica E Low Dimens. Syst. Nanostruct.* **106**, 150 (2019) .
6. H. H. Abdel Ghafar, G. A. M. Ali, O. A. Fouad, S. A. Makhlouf, *Desalin. Water Treat*., **53,** (2013) 2980.
7. A. Stafiej, K. Pyrzynska, *Sep. Purif. Technol*., **58,** 49 (2007) .
8. K. Zare, V. K. Gupta, O. Moradi, A. S. H. Makhlouf, M. Sillanpää, M. N. Nadagouda, H. Sadegh, R. Shahryari-ghoshekandi, A. Pal, Z.-J. Wang, *J. Nanostruct. Chem*., **5,** 227 (2015) .
9. S. Babel, T.A. Kurniawan, *J. Hazard. Mater*., **97,** 219 (2003) .
10. V. Gupta, H. Sadegh, M. Yari, R. Shahryari Ghoshekandi, B. Maazinejad, M. Chahardori, *Global J. Environ Sci. Manage*., **1,** 149 (2015) .
11. D. Sud, G. Mahajan, M. Kaur, *Bioresour. Technol*., **99,** 6017 (2008) .
12. D. W. O'Connell, C. Birkinshaw, T. F. O'Dwyer, *Bioresour. Technol*., **99,** 6709 (2008) .
13. W. W. Ngah, M. Hanafiah, *Bioresour. Technol*., **99,** 3935 (2008) .
14. F. Fu, Q. Wang, *J. Environ. Manage*., **92**, 407 (2011) .
15. S. E. Bailey, T. J. Olin, R. M. Bricka, D. D. Adrian, *Water Res*., **33,** 2469 (1999) .
16. S. Shin, J. Jang, *Chem. Commun*., **41,** 4230 (2007) .
17. O. Moradi, V. K. Gupta, S. Agarwal, I. Tyagi, M. Asif, A. S. H. Makhlouf, H. Sadegh, R. Shahryari-ghoshekandi, *J. Ind. Eng. Chem*., **28**, 294 (2015) .
18. V. K. Gupta, I. Tyagi, S. Agarwal, H. Sadegh, R. Shahryari-ghoshekandi, M. Yari, O. Yousefi-nejat, *J. Mol. Liq*., **206,** 129 (2015) .
19. H. Sadegh, R. Shahryari-ghoshekandi, I. Tyagi, S. Agarwal, V. K. Gupta, *J. Mol. Liq*., **207,** 21 (2015).
20. M. Hua, S. Zhang, B. Pan, W. Zhang, L. Lv, Q. Zhang, *J. Hazard. Mater*., **211,** 317 (2012) .
21. S.-H. Huang, D.-H. Chen, *J. Hazard. Mater*., **163,** 174 (2009) .
22. O. Moradi, H. Sadegh, R. Shahryari-ghoshekandi, M. Norouzi, Application of Carbon Nanotubes in Nanomedicine: New Medical Approach for Tomorrow. Handbook of Research on Diverse Applications of Nanotechnology in Biomedicine, Chemistry, and Engineering, 90, (2015) .
23. H. Sadegh, R. Shahryari-ghoshekandi, *Nanomed. J*., **2,** 231 (2015) .
24. H. Sadegh, R. Shahryari-ghoshekandi, A. Masjedi, Z. Mahmoodi, M. Kazemi, *Int. J. Nano Dimens*.,**7,** 109 (2016) .
25. J. L. Bahr, E. T. Mickelson, M. J. Bronikowski, R. E. Smalley, J. M. Tour, *Chem. Commun*., **2**, (2001) 193.
26. K. Zare, F. Najafi, H. Sadegh, *J. Nanostruct. Chem*., **3,** 1 (2013) .
27. H. Sadegh, R. Shahryari-ghoshekandi, M. Kazemi, *Int. Nano Lett*., **4,** 129 (2014) .
28. K. Zare, H. Sadegh, R. Shahryari-ghoshekandi, M. Asif, I. Tyagi, S. Agarwal, V.K. Gupta, *J. Mol. Liq*., **213,** 345 (2015) .
29. H. Sadegh, K. Zare, B. Maazinejad, R. Shahryari-ghoshekandi, I. Tyagi, S. Agarwal, V.K. Gupta, *J. Mol. Liq*., **215**, 221 (2016) .
30. M. Rajabi, B. Mirza, K. Mahanpoor, M. Mirjalili, F. Najafi, O. Moradi, H. Sadegh, R. Shahryari-ghoshekandi, M. Asif, I. Tyagi, S. Agarwal, V.K. Gupta, *J. Ind. Eng. Chem*., **34,** 130 (2016) .
31. V. Gupta, O. Moradi, I. Tyagi, S. Agarwal, H. Sadegh, R. Shahryari-ghoshekandi, A. Makhlouf, M. Goodarzi, A. Garshasbi, *Crit. Rev. Env. Sci. Technol*., **46**, 93 (2016) .
32. R. Shahryari-ghoshekandi, H. Sadegh, *Jordan J. Chem.*, **9,** 267 (2014) .
33. Y.-S. Ho, G. McKay, *Process Biochem*., **34,** 451 (1999) .
34. Y.-S. Ho, *J. Hazard. Mater*., **136,** 681 (2006) .
35. S. Agarwal, H. Sadegh, M. Monajjemi, A. S. Hamdy, G. A. Ali, A. O. Memar, R. Shahryari-ghoshekandi, I. Tyagi, V. K. Gupta, *J. Mol. Liq*., **218,** 191 (2016) .
36. K. Zare, H. Sadegh, R. Shahryari-ghoshekandi, B. Maazinejad, V. Ali, I. Tyagi, S. Agarwal, V. K. Gupta, *J. Mol. Liq*., **212,** 266 (2015) .
37. V. Gupta, I. Tyagi, H. Sadegh, R. Shahryari-Ghoshekandi, A. Makhlouf, B. Maazinejad, *Sci. Technol. Dev*., **34,** 195 (2015) .
38. H. Sadegh, R. Shahryari-ghoshekandi, S. Agarwal, I. Tyagi, M. Asif, V. K. Gupta, *J. Mol. Liq*., **206,** 151 (2015) .
39. A. S. Özcan, B. Erdem, A. Özcan, *Colloids Surf.*, A, **266,** 73 (2005).
40. W. Tsai, C. Lai, K. Hsien, *J. Colloid Interface Sci*., **263,** 29 (2003).
41. H. Kh. Moghaddam, M. Pakizeh, *J. Ind. Eng. Chem*., **21,** 221 (2015).
42. V. K. Gupta, S. Agarwal, A. K. Bharti, H. Sadegh, *J. Mol. Liq.* **230**, 667 (2017) .
43. V. K. Gupta, S. Agarwal, H. Sadegh, G. A. M. Ali, A. K. Bharti, A. S. Makhlouf, J. Mol. Liq., **237**, 466 (2017).

КИНЕТИЧНО ИЗСЛЕДВАНЕ И МОДЕЛИРАНЕ НА ОТСТРАНЯВАНЕТО НА Zn^{2+} ОТ ОТПАДНА ВОДА ЧРЕЗ АДСОРБЦИЯ ВЪРХУ МНОГОСТЕННИ ВЪГЛЕРОДНИ НАНОТРЪБИЧКИ

Х. Садег[1,*], Р. Шакибай Лалехоло [2], С. М. Сейд Араби[2], М. Джалили[3], П. Чаухан[1]

[1] Западно-Померански технологичен университет, Шчечин, Факултет по химична технология и инженерство, Шчечин, Полша

[2] Департамент по химия, Клон Карадж, Ислямски Азад университет, Карадж, , Иран

[3] Департамент по химия, Шахр-е-Кодс клон, Ислямски Азад университет, Техеран, Иран

Постъпила на 8 януари, 2018; коригирана на 20 юли, 2018

(Резюме)

Представени са адсорбционни методи за отстраняване на токсичния метален йон Zn^{2+} с адсорбент многостенни въглеродни нанотръбички (MWCNTs). SEM и FTIR методи са използвани за охарактеризиране на MWCNTs. Изучена е връзката между оптимизационните фактори (количество адсорбент, време на контакт и начална концентрация ва токсичния метален йон) и адсорбционните свойства на MWCNTs. Количеството метал, адсорбирано за различни интервали от време, е в основата на адсорбционната кинетика. Моделирани са кинетичните криви. Установено е, че адсорбцията на Zn^{2+} съответства на модел от псевдопърви порядък ($R^2 > 0.999$) и времето за достигане на адсорбционно равновесие е 55 min. Равновесните адсорбционни данни съответстват на изотермния модел на Langmuir.

Bulgarian Chemical Communications, Volume 50, Issue 4 (pp. 608 – 614) 2018

Synthesis, characterization and CO_2 adsorption of Fe(III)-based metal-organic framework

S. U. Rather*, A. Muhammad, A. A. Al-Zahrani, T. E. Youssef, L. A. Petrov

Department of Chemical and Materials Engineering, King Abdulaziz University, P.O. Box 80204, Jeddah 21589, Saudi Arabia

Received, April 17, 2018; Revised, August 7, 2018

Iron (III)-based metal-organic framework (Fe-MOF) was synthesized via solvothermal method utilizing tritopic bridging 1,3,5-Tris(4-carboxyphenyl) benzene as a linker between metal centers. Thermogravimetric analysis revealed that weight loss in the entire temperature range corresponds to loss of desorption of adsorbed gases from pores and cavities, removal of N, N-dimethyl formamide, and framework disintegration. Specific surface area was found to be 300 m^2/g and a very little rise in the isotherm at partial pressure > 0.2, indicates microporous character of the sample. Maximum CO_2 adsorption capacity of Fe-MOF sample measured at room temperature and partial pressure of 0.9 atm was found to be 3.0 wt.%. Temperature increase from 298 to 343 K decreases adsorption capacity is related to Le-Chatelier's Principle. Linearity of CO_2 adsorption in a Fe-MOF sample related to weak adsorption sites.

Keywords: Solvothermal, Metal-organic frameworks, Ligand, Surface area, Thermogravimetric analysis, Adsorption

INTRODUCTION

Anthropogenic carbon dioxide discharging from natural and manufactured sources need to mitigate for the sake of pollution free environment. For researchers, scientists and academicians worldwide, an intimidating task lies ahead to reduce greenhouse gases (GHGs) emission from various sources such as combustion of fossil fuels, electricity and heat sector, transportation, industrial processes, deforestation, commercial and residential places [1, 2]. Multiple programs, conferences, and seminars are held worldwide to make people aware about harmful effects of GHGs emission especially CO_2, a primary source of global warming. Combustion of fossil fuels and industrial processes are responsible for 65% of CO_2 emission worldwide. Moreover, combustion of fossil fuels such as coal, natural gas, and oil in USA alone produces 83% of GHGs emissions. Recently different type of methods are utilized to separate CO_2 from fossil fuel gas emissions and one of the main method to reduce CO_2 emission is adsorption [3, 4]. Physical and chemical adsorption methods are widely used to separate CO_2 from mixture [5, 6].

High selectivity, high porosity, tunable property, low cost, good mechanical strength, stable adsorption capacity post many cycles, and sufficient adsorption/desorption kinetic properties are mandatory parameters to adsorb CO_2 efficiently. Functionalized carbon materials, carbon-based nanomaterials, pyrogenic carbons, and carbon composites used as adsorbents for CO_2 capture at low temperature and moderate pressure [4, 7-10]. Zeolites also used for CO_2 adsorption owing to its unique high porous characteristics, open cavities in the form of channels and cages, and well-defined structures [11, 12]. Porous metal-organic frameworks (MOFs) also known as coordination polymer considered as promising adsorbent for CO_2 adsorption [13]. MOFs are blend of organic and inorganic mixture of metal ions or clusters coordinated to one or more than one type of ligands to form network type structures [14, 15]. MOFs display wide diversity and structural disparity in combination with lower topological restrictions on the formation of three-dimensional frameworks [16]. High surface area, permanent porosity, stability, and functionalization are unique characteristics of MOFs [17].

Excessive surface area and variable pore structure MOFs synthesized by solvothermal and non-solvothermal, microwave, electrochemical, mechanochemical, and sonochemical methods [14, 18-20]. For the preparation of 3D network type MOF structures, different kinds of metal or metal oxide (polyhedral) clusters with unique neutral, cationic, and anionic organic ligands with rigid backbones such as pyrazine, bipyridine, carboxylates, and imidazole are used [19]. Generally, for the preparation of various kinds of MOFs, heating a mixture of metal salt and organic ligands in a solvent such as water, ethanol, diethylformamide, and dimethylformamide routes are used [14, 20, 21]. Preparation of MOF-177 via solvothermal method by employing zinc acetate/zinc nitrate as a metal center and tritopic

* To whom all correspondence should be sent:
E-mail: rathersami@kau.edu.sa;
rathersami@gmail.com

organic ligand benzene tribenzoic acid (BTB) as a linker in the presence of solvent DEF/DMF are used [22, 23]. Furthermore, synthesis of MOF-39 by connecting zinc oxide metal centers by trigonal organic linker BTB are also prepared by solvothermal method [24].

In this report, convenient solvothermal method are utilized for the preparation of Fe(III)-based metal-organic framework (Fe-MOF) using a reaction involving iron nitrate nonahydrate metal salt as precursor and tritopic 1,3,5-Tris(4-carboxyphenyl) benzene as a linker. Thermal stability and surface area of Fe-MOF measured by thermogravimetric and nitrogen adsorption/desorption isotherms. The CO_2 adsorption capacity of Fe-MOF calculated at 25, 30, 40, 50, 60, 70°C and low pressure 0.0 to 0.9 bar using thermogravimetric analysis method.

EXPERIMENTAL

Synthesis of Iron-based Metal-Organic Framework (Fe-MOF)

Iron nitrate nonahydrate (99%), 1, 3, 5-tris (4-carboxyphenyl) benzene (>98%), ethanol (99.8%), N, N-dimethylformamide (99.8%), and chloroform (>99.5%) were purchased from Sigma-Aldrich and were used without further purification. The synthesis of Fe-MOF performed via solvothermal method. In a typical procedure, 0.270 g iron nitrate nonahydrate was dissolved in 25 ml ethanol, whereas 0.2 g 1,3,5-tris(4-carboxyphenyl) benzene was dissolved in 10 ml N, N-dimethylformamide (DMF). Mixture of above solutions transferred to teflon-lined autoclave and heated at 80°C for 3 days. The reaction mixture cooled slowly to RT and hereafter called as Fe-MOF. The resulting precipitate filtered, washed with DMF to separate some traces of unreacted reagent. Finally, DMF reacted sample washed many times with chloroform to reduce presence of DMF inside crystals. The sample was dried and stored within glove box under Ar atmosphere. Further experimental details of synthesis method presented elsewhere [25]. Fe-MOF was characterized using Fourier-transform infra-red (FT-IR) and scanning electron microscopy (SEM). Nitrogen adsorption performed at 77 K using Micromeritics ASAP 2000 instrument.

CO_2 adsorption capacity measurements of Fe-MOF sample performed by thermogravimetric analysis (TGA) (NETZSCH-Gerätebau GmbH, TG 209 F3) instrument. ~30 mg of Fe-MOF sample used in each CO_2 adsorption experiment. Prior to each adsorption, a sample was stationed in an alumina crucible fixed in TGA furnace and heated to 100°C (10°C/min.) in a flowing nitrogen (100 ml/min.) and retain at that temperature until a constant weight of sample was obtained. This process for continuing flowing nitrogen at 100°C for 1 h is to ensure the surface of Fe-MOF sample is clean prior commencing adsorption experiments. At constant RT, a gas mixture of 90% CO_2-10% He (100 ml/min.) was released into sample holder holding sample. The increase in weight perceived due to adsorption of CO_2 and preserved until equilibrium was established. Under these conditions, adsorption uptake of CO_2 was determined as the amount of CO_2 adsorbed in milligrams per gram of Fe-MOF (mg CO_2/g Fe-MOF). Adsorption data for other experiments obtained in a similar manner using helium as an inert carrier.

RESULTS AND DISCUSSION

Schematic illustration synthesis of Fe-MOF used to understand the structure of Fe-MOF presented in Fig.1. Iron nitrate an inorganic compound comprising of iron, nitrate and varying number of water molecules attached is used as a metal center (Fig. 1(a)) and 1,3,5-Tris(4-carboxyphenyl) benzene (H_3BTB), a tritopic bridging ligand acts as a linker between metal center (Fig. 1 (b)). One of the Fe^{3+} is coordinated to nine oxygen atoms, where seven of the coordinated oxygen atoms belongs to different BTB^{3-} ligands and two oxygen atoms belongs to terminal water molecules (Fig. 1(d)). Cross-sectional view of Fe-MOF generated from Fig.1 (c) and (d) displaying 1D porous channels between metal central layers (Fig. 1(e).

Thermal behavior of Fe-MOF calculated using thermogravimetric and differential thermal analysis (DTA). Fixed mass of sample independently heated in an inert atmosphere using a heating ramp of 10°C/min in the temperature range of 25 to 800°C. Fig. 2 (a) and (b) represents thermogravimetric and differential analysis profile of Fe-MOF. Visible continuous decrease in weight loss in the entire temperature range observed [26-29]. ~45.0 wt.% weight loss was observed in the temperature range of 50–250°C and can be attributed to desorption of adsorbed gases from their pores and cavities and loosely bound water molecules [30, 31]. Sample weight loss ~22.0 wt.% observed in the temperature range of 250-500°C corresponds to removal of guest molecules such as N, N dimethyl formamide and adsorbed water molecules from atmosphere. Moreover, above weight loss also indicates initiation of decomposition of Fe-MOF sample [25]. Pore and cavity texture further improved possibly by degassing at elevated temperature for a longer period. Weight loss ~15 wt.% above 500°C

indicates complete disintegration of framework including ligand BTB. The T_{max}, i.e. the temperature at which rate of losing water or adsorbed water molecules or guest molecules such as DMF or disintegration of MOF is maximum and is calculated from differential thermal analysis. The T_{max} for losing water, adsorbed water/guest molecules, and disintegration of MOF was 117, 470 and 704°C presented in Fig. 2 (b). Total weight loss observed in the entire temperature range is ~82 wt.% and remaining residue corresponds to oxides of metal center.

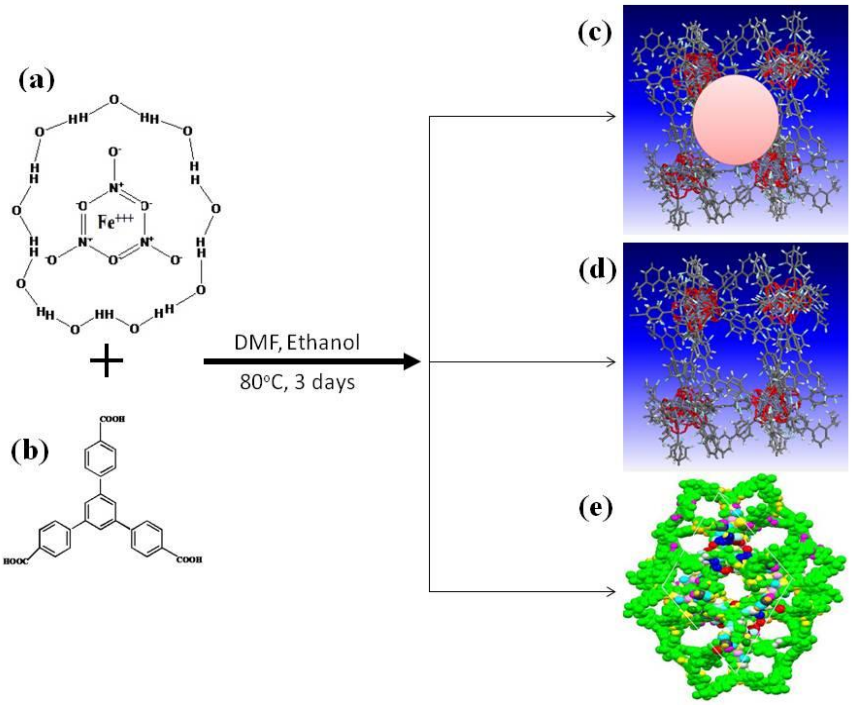

Fig. 1. Schematic illustration preparation method of Fe-MOF, where (a) iron nitrate nonahydrate metal salt as a precursor, (b) tritopic 4,4',4''-benzene-1,3,5-triyl-tribenzoic acid (H_3BTB) ligand as a linker, and (c) , (d) and (e) are three different structural forms of Fe-MOF.

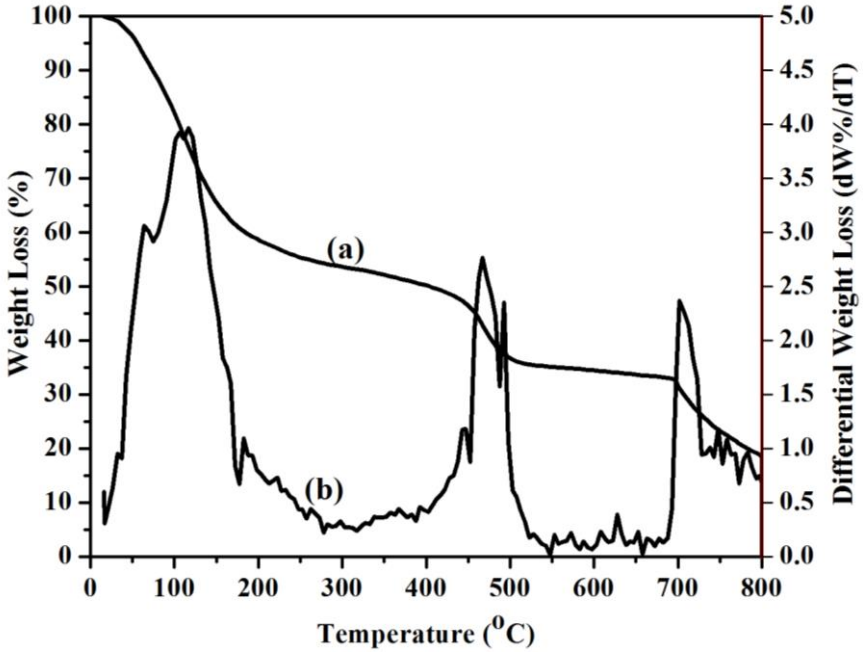

Fig. 2. Thermogravimetric and differential profiles of Fe-MOF, performed in an oxygen atmosphere using ramp rate 10°C/min.

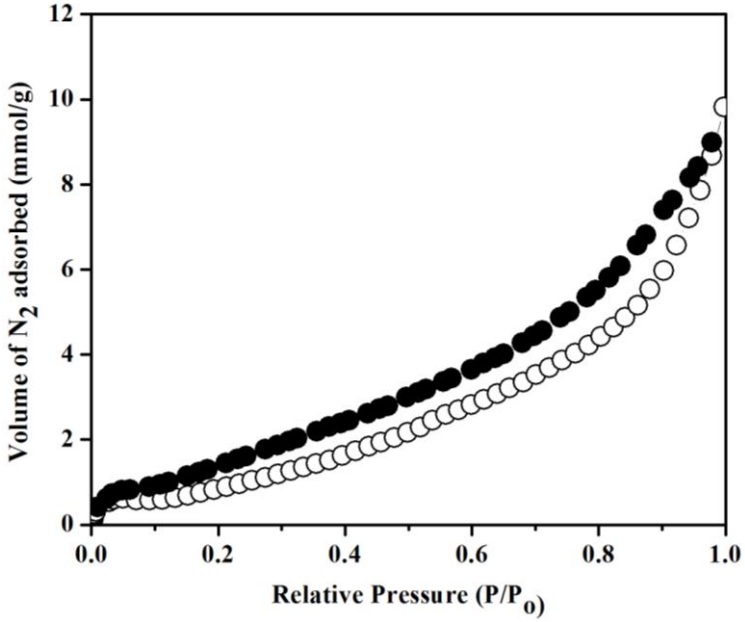

Fig. 3. Nitrogen adsorption/desorption isotherm of Fe-MOF recorded at 77K.

Brunauer–Emmett–Teller (BET) surface area and pore size distribution of sample measured from nitrogen adsorption/desorption profile using Micromeritics ASAP 2000 instrument. The nitrogen adsorption isotherm of Fe-MOF sample carried out by keeping the sample isothermal at 77 K. Fig. 3 presented nitrogen adsorption isotherm of sample. According to the IUPAC classification, the evolution of adsorption isotherm with increasing P/Po described as a type II isotherm indicating microporous structure of sample. There is a very little rise in the isotherm at partial pressure > 0.2, indicating very high microporous density. For relative pressure between 0.1 and 1.0, a gradual rise in the volume of the nitrogen adsorption observed. The specific surface area estimated from linear fit to the BET adsorption isotherm, for the relative pressure range P/Po 0.0 to 1.0 found to be 300 m^2/g.

FT-IR spectra of Fe-MOF synthesized by solvothermal method presented in Fig. 4. Several intense bands throughout the spectrum in agreement with the literature observed. Strong band that appears at 1400 cm^{-1} is assigned to symmetric (υ_s) stretching of C=O bond related to carboxylate group of ligand BTB and asymmetric (υ_{as}) stretching of same also existed at ~1600 cm^{-1} region. The C=C bond attributed to stretching vibrations of BTB linker appears at ~1500 cm^{-1} region. Small peaks visible at 1300-100 cm^{-1} region corresponds to in-plane bending vibrations of aromatic C-H bonds while as weak peaks appeared at 1000-800 cm^{-1} attributed to out of plane bending vibrations of C-H bonds. First overtone of in- and out of plane vibrations of C-H bonds of ligand BTB appears at ~1600-2000 cm^{-1}, whereas in- and out of plane vibrations of C-H bonds appears at ~2600-2100 cm^{-1}[32-34]. SEM images presented in Fig. 5 (a) and (b) indicates morphological characterization of Fe-MOF sample. Crystal structure images presented resembles trigonal lattices with average diameter of 6.76 μm.

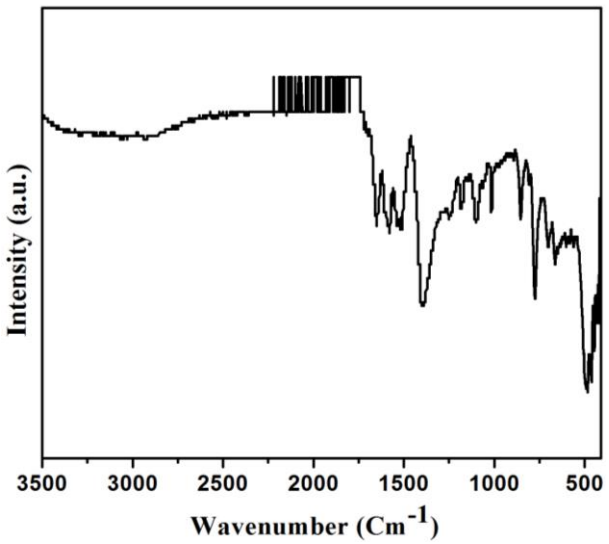

Fig. 4. Fourier-transform infrared (FTIR) spectra of Fe-MOF sample.

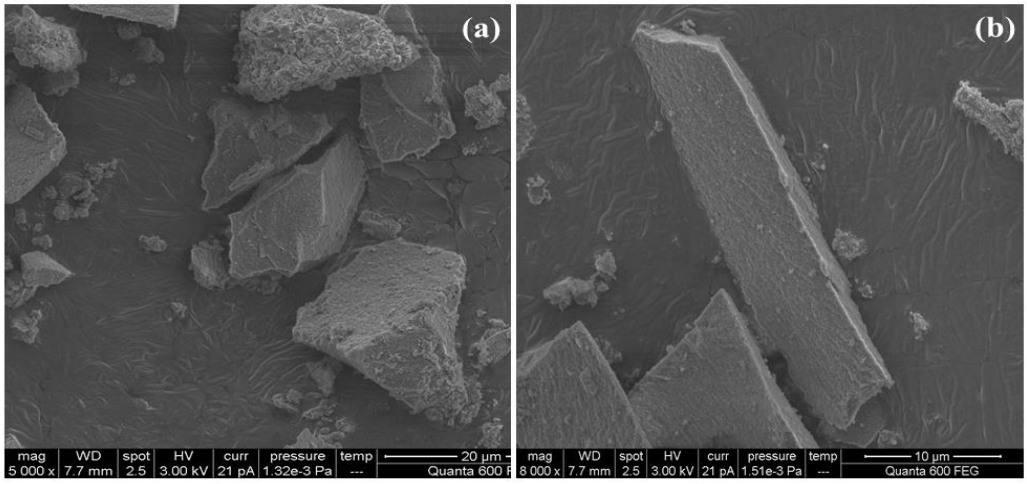

Fig. 5. Representative scanning electron microscope (SEM) images of Fe-MOF. The scale bar for (a) and (b) is 20 and 10 µm, respectively.

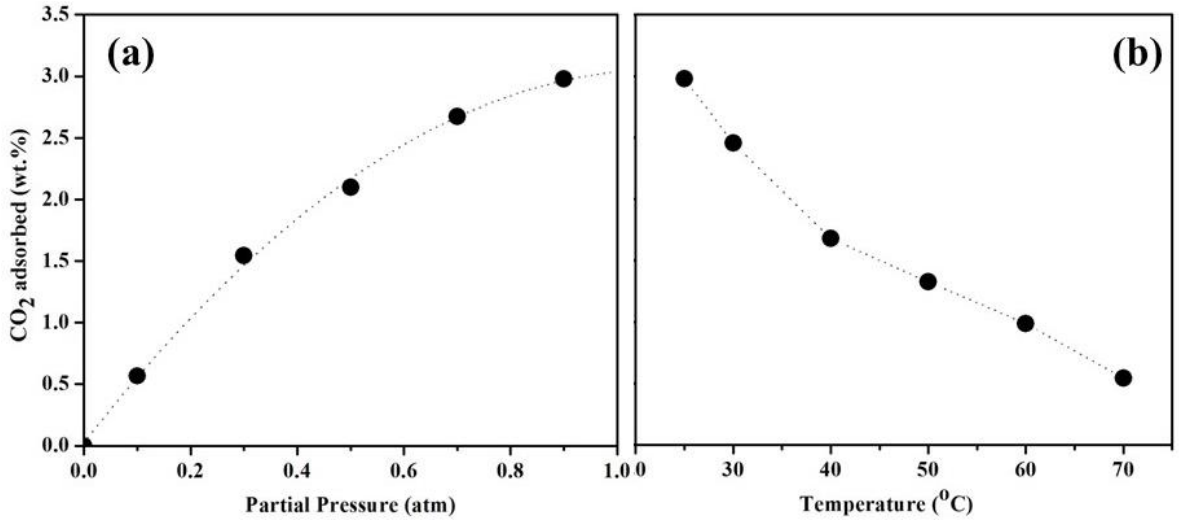

Fig. 6. (a) CO_2 adsorption capacity of Fe-MOF sample performed at 25°C and partial pressure range of 0.0 and 0.9 atm. (b) CO_2 adsorption of Fe-MOF sample performed at 25, 30, 40, 50, 60, and 70°C and pressure 0.9 atm.

Considering highly porous nature of Fe-MOF sample, CO_2 adsorption capacity measurements presented in Fig. 6 (a) and (b) performed at different temperatures and partial pressure range of 0.0 and 0.9 atm. Sample follows monotonous type CO_2 adsorption isotherm (type I) and adsorption is limited to few molecular layers only. At low pressure, gradual rise of CO_2 adsorption observed and at high pressure, linear adsorption indicating adsorption sites on Fe-MOF are weak and relatively homogeneous. Maximum CO_2 adsorption capacity of sample found to be ~3.0 wt.% at 298 K and partial pressure of 0.9 atm. The CO_2 adsorption capacity of our sample very low compared to adsorption literature data of various types of MOFs and reason may be poor BET surface area. Moreover, as far as high gas adsorption capacity is concerned, high surface area is mandatory. Temperature elevation from 25 to 70°C decreases CO_2 adsorption capacity of Fe-MOF (Fig. 6(b)). Furthermore, reduction of adsorption capacity with decreasing temperature is due to Le Chatelier's principle. The CO_2 adsorption capacity data obtained fitted to Langmuir adsorption isotherm to estimate maximum adsorption (q_m) and adsorption equilibrium constant (K) according to the Langmuir adsorption equation:

$$q_e = q_m \frac{Kp_e}{1 + Kp_e}$$

where p_e is the equilibrium partial pressure of CO_2. Polymath, a nonlinear regression software used to determine Langmuir equation parameters q_m, K, and correlation coefficient (R^2) as a statistical indicator of goodness of model prediction.

CONCLUSION

Fe-MOF synthesized by solvothermal method using tritopic ligand H_3BTB as a linker to study structural, thermal, morphological, and CO_2 adsorption properties. Thermal profile of Fe-MOF shows continuous weight loss in the entire temperature range of RT to 800ºC. Furthermore, weight reduction of sample corresponds to loss of loosely bound water molecules attached to metal center and ligands, within cavities and channels, adsorbed water molecules, guest molecules such as DMF and MOF disintegration. Specific surface area of Fe-MOF found to be 300 m^2/g and little rise in the isotherm at partial pressure > 0.2, indicating very high microporous density. The CO_2 adsorption capacity of Fe-MOF was found to be 3.0 wt.% at 298 K and partial pressure of 0.9 atm. Furthermore, CO_2 adsorption decreases as the temperature increases follows Le-Chatelier's Principle. The CO_2 adsorption capacity increases linearly with pressure indicating adsorption sites on sample are weak and relatively homogeneous.

Acknowledgements: *This project was funded by the Deanship of Scientific Research (DSR), King Abdulaziz University, Jeddah, under grant No. (1434/135/494). The authors, therefore, acknowledge with thanks DSR technical and financial support.*

REFERENCES

1. J. H. Edwards, *Catal. Today* **23**, 59 (1995).
2. M. R. Raupach, G. Marland, P. Ciais, C. Le Quere, J. G. Canadell, G. Klepper, C. B. Field, *Proc. Natl. Acad. Sci. U.S.A* **104**, 10288 (2007).
3. Z. Liang, M. Marshall, A. L. Chaffee, *Energ. Fuel*. **23**, 2785 (2009).
4. D. Cazorla-Amoro´s, J. Alcaniz-Monge, A. Linares-Solano, *Langmuir* **12**, 2820 (1996).
5. M. Ishibashi, H. Ota, N. Akutsu, S. Umeda, M. Tajika, J. Izumi, A. Yasutake, T. Kabata, Y. Kageyama, *Energy Convers. Mgrat.* **37**, 929 (1996).
6. Y. Liu, Y. Yang, Q. Sun, Z. Wang, B. Huang, Y. Dai, X. Qin, X. Zhang, *ACS Appl. Mater. Interfaces* **5**, 7654 (2013).
7. Z. Yong, V. Mata, A. E. Rodrigues, *Sep. Purif. Technol.* **26**, 195 (2002).
8. N. P. Wickramaratne, M. Jaroniec, *ACS Appl. Mater. Interfaces*, **5** 1849 (2013).
9. R. V. Siriwardane, M. S. Shen, E. P. Fisher, J. A. Poston, *Energ. Fuel.* **15**, 279 (2001).
10. F. Su, C. Lu, W. Cnen, H. Bai, J. F. Hwang, *Sci. Total Environ.* **407**, 3017 (2009).
11. P. D. Jadhav, R. V. Chatti, R. B. Biniwale, N. K. Labhsetwar, S. Devotta, S. S. Rayalu, *Energ. Fuel.* **21**, 3555 (2007).
12. D. Bonenfant, M. Kharoune, P. Niquette, M. Mimeault, R. Hausler, *Sci. Technol. Adv. Mater.* **9**, 013007 (2008).
13. P. L. Llewellyn, S. Bourrelly, C. Serre, A. Vimont, M. Daturi, L. Hamon, G. D. Weireld, J. S. Chang, D. Y. Hong, Y. K. Hwang, S. H. Jhung, G. Ferey, *Langmuir* **24**, 7245 (2008).
14. N. Stock, S. Biswas, *Chem. Rev.* **112**, 933 (2012).
15. S. L. James, *Chem. Soc. Rev.* **32**, 276 (2003).
16. J. L. C. Rowsell, O. M. Yaghi, *Micropor. Mesopor. Mat.* **73**, 3 (2004).
17. H. Furukawa, N. Ko, Y. B. Go, N. Aratani, S. B. Choi, E. Choi, A. Ö. Yazaydin, R. Q. Snurr, M. O'Keeffe, J. Kim, O. M. Yaghi1, *Science* **329**, 424 (2010).
18. Y. Sun, H. Zhou, *Sci. Technol. Adv. Mater.* **16**, 054202 (2015).
19. Y. R. Lee, J. Kim, W. S. Ahn, *Korean J. Chem. Eng.* **30**, 1667 (2013).
20. O. Shekhah, H. Wang, S. Kowarik, F. Schreiber, M. Paulus, M. Tolan, C. Sternemann, F. Evers, D. Zacher, R. A. Fischer, C. Woll, *J. Am. Chem. Soc.* **129**, 15118 (2007).
21. A. D. Burrows, K. Cassar, R. M. W. Friend, M. F. Mahon, S. P. Rigby, J. E. Warren, *Cryst. Eng. Comm.* **7**, 548 (2005).
22. S. Proch, J. Herrmannsdçrfer, R. Kempe, C. Kern, A. Jess, L. Seyfarth, J. Senker, *Chem. Eur. J.* **14**, 8204 (2008).
23. D. J. Tranchemontagne, J. R. Hunt, O. M. Yaghi, *Tetrahedron* **64**, 8553 (2008).
24. J. Kim, B. Chen, T. M. Reineke, H. Li, M. Eddaoudi, D. B. Moler, M. O′Keeffe, O. M. Yaghi, *J. Am. Chem. Soc.* **123**, 8239 (2001).
25. D. Saha, R. Zacharia, L. Lafi, D. Cossement, R. Chahine, *Chem. Eng. J.* **171**, 517 (2011).
26. A. R. Chowdhuri, D. Bhattachary, S. K. Sahu, *Dalton Trans.* **45**, 2963 (2016).
27. T. H. Chen, A. Schneemann, R. A. Fischer, S. M. Cohen, *Dalton Trans.* **45,** 3063 (2016).
28. P. V. Dau, L. R. Polanco, S. M. Cohen, *Dalton Trans.* **42**, 4013 (2013).
29. B. X. Dong, L. Chen, S. Y. Zhang, J. Ge, L. Song, H. Tian, Y. L. Teng, W. L. Liu, *Dalton Trans.* **44**, 1435 (2015).
30. J. Tang, M. Yang, W. Dong, M. Yang, H. Zhang, S. Fan, J. Wang, L. Tana, G. Wang, *RSC Adv.* **6**, 40106 (2016).
31. A. Tăbăcaru, S. Galli, C. Pettinari, N. Masciocchi, T. M. McDonald, J.R. Long, *Cryst. Eng. Comm.* **17**, 4992 (2015).
32. T. V. N. Thi, C. L. Luu, T. C. Hoang, T. Nguyen, T. H. Bui, P. H. D. Nguyen, T. P. P. Thi, *Adv. Nat. Sci.: Nanosci. Nanotechnol.* **4**, 035016 (2013).
33. D. Ge, J. Peng, G. Qu, H. Geng, Y. Deng, J. Wu, X. Cao, J. Zheng, H. Gu, *New J. Chem.* **40**, 9238 (2016).
34. S. He, Z. Li, J. Wang, P. Wen, J. Gao, L. Ma, Z. Yang, S. Yang, *RSC Adv.* **6**, 49478 (2016).

СИНТЕЗ, ОХАРАКТЕРИЗИРАНЕ И CO_2 АДСОРБЦИЯ ВЪРХУ МЕТАЛ-ОРГАНИЧНА МРЕЖА НА ОСНОВАТА НА Fe(III)

С. У. Ратер*, А. Мухамад, А. А. Ал-Захрани, Т. Е. Юсеф, Л. А. Петров

Департамент по инженерна химия и химия на материалите, Университет „Крал Абдулазиз", п.к. 80204, Джеда 21589, Саудитска Арабия

Постъпила на 17 април, 2018; коригирана на 7 август, 2018

(Резюме)

Метал-органична мрежа (MOF) на основата на Fe (III) е получена по солвотермичен метод с помощта на тритопичен мостов лиганд 1,3,5-трис (4-карбоксифенил) бензен като свързващо звено и хром като метал, образуващ вторична градивна част. Непрекъснатата загуба на тегло в цялата температурна област е свързана с загуба чрез десорбция на адсорбирани газове от порите и кухините, отстраняване на молекули-гости като N, N-диметилформамид (DMF) и дезинтеграция на мрежата. Специфичната площ от 420 m^2/g и рязкото нарастване на изотермата при парциално налягане >0.2 atm свидетелстват за микропорестия характер на пробата. Адсорбционният капацитет на Fe-MOF, измерен при 298 K и парциално налягане 0.9 atm, е 3.5 wt.%. Повишаването на температурата от 298 до 343 K понижава адсорбционния капацитет съгласно принципа на Le Chatelier. Адсорбцията на CO_2 нараства линейно с повишаване на налягането от 0 до 0.9 atm поради сравнително слабите адсорбционни центрове и тяхната хомогенност.

Bulgarian Chemical Communications, Volume 50, Issue 4 (pp. 615 – 620) 2018

Structural change of lignin in catalytic oxidation by Co(salen)

X.-F. Zhou[1,2,3,4,5,6,7*]

[1.] *Hunan Provincial Key Lab of Dark Tea and Jin-hua, Hunan City University, Yiyang, P.O. Box 413000, China*
[2.] *Guangzhou Key Laboratory of Environmental Catalysis and Pollution Control, School of Environmental Science and Engineering, Institute of Environmental Health and Pollution Control, Guangdong University of Technology, Guangzhou, P.O. Box 510006,China*
[3.] *Guangxi Key Laboratory of Chemistry and Engineering of Forest Products, Guangxi University For Nationalities, Nanning, P.O. Box 530006, China*
[4.] *Key Laboratory of Advanced Energy Materials Chemistry of Ministry of Education of China, Nankai University, Tianjin, P.O. Box 300071, China*
[5.] *Faculty of Chemical Engineering, Kunming University of Science and Technology, Kunming, P.O. Box 650500, China*
[6.] *Key Laboratory for Solid Waste Management and Environment Safety of Ministry of Education of China, Tsinghua University, Beijing, P.O. Box 100084, China*
[7.] *Key Laboratory of Pulp and Paper Science and Technology of Ministry of Education/Shandong Province, Qilu University of Technology, Jinan, P.O. Box 250353, China*

Received, April 27, 2018; Accepted, July 18, 2018

In order to improve the catalytic performance, Co(salen) catalysis was performed on Indulin lignin. The structural changes of the lignin during the biomimetic treatment were characterized by ^{13}C-NMR, HSQC and ^{31}P-NMR spectroscopy. As a result of the biomimetic treatment, a decrease of β-O-4, β-β and β-5 linkage was observed, especially a cleavage of β-O-4 linkage. The fact that the condensed substructures were significantly decomposed explained the lignin degradation in-deep. In addition to these changes, the proposed route was applied to the lignin oxidation by Co(salen) catalysis based on the subtraction of phenolic hydrogen atoms.

Keywords: Biomimetic catalysis; Indulin lignin; Co(salen); HSQC; ^{13}C and ^{31}P-NMR spectroscopy

INTRODUCTION

Lignin contains a variety of different C-C and C-O linkages, which is related to the physicochemical and degradable properties of lignin. In addition, many chemical reactions such as alkylation, oxidation or reduction and condensation occur in lignin conversion *via* carbonyl, aliphatic hydroxyl and other active functional groups [1]. Moreover, the C-C and C-O linkages are refractory to the degradation of lignin [2], and the S/G ratio in the lignin structure is characteristically an important factor affecting the degradability of lignin [3, 4]. In summary, the reactivity is related to its lignin structure.

In recent years, scientists have made great efforts in catalytic oxidation of lignin, for example, biomimetic catalysts were used to oxidize lignin. M(salen) complex is a biomimetic catalyst, which has both enzymatic and chemical catalytic activity. Some studies have demonstrated the potential of M(salen) as a catalyst in lignin oxidation [5-7]. The activity was affected by the oxygen species in the catalytic system of M(salen). Compared with the binuclear peroxo-complex, the mononuclear superoxo-complex showed a strong catalytic activity in capturing phenolic hydrogen atoms from the substrates [8, 9]. Carmen *et al.* [10] found that the phenoxy cobalt radicals correlated with the formation of the oxidation products and the conversion rates of the substrates.

The reaction properties of lignin have yet to be further explored due to the complex mechanism involved. In addition, biomimetic catalysis has not been practically utilized in lignin conversion because the mechanism is still not clear. Therefore, it is necessary to find out the reaction mechanism of the biomimetic oxidation of lignin. In this paper, Co(salen) was applied to catalyze the oxidation of lignin. The structure of lignin was analyzed by ^{13}C-NMR, 2D HSQC NMR and ^{31}P-NMR. This may be a useful study for providing a mechanistic insight into the application of a biomimetic catalyst in lignin transformation.

Materials and methods

Indulin lignin: Indulin lignin was purchased from Sigma-Aldrich. It was an alkaline lignin derived from pine.

Catalytic oxidation of lignin by Co(salen): The treatment was carried out at 90 °C in a 1 L pressure reactor for 3 h. Typical processing conditions were as follows: 1g of Indulin lignin, 0.1 % dosage of Co(salen) (based on lignin), 1:1 molar ratio of pyridine to Co(salen), 0.5 MPa oxygen pressure,

* To whom all correspondence should be sent:
E-mail: lgdx602@sina.com

100 ml deionized water. After filtration, the residue was dissolved in tetrahydrofuran and filtered. The filtrate was evaporated in vacuum to obtain the residual lignin.

NMR analysis: The NMR analyses of the lignin samples were performed using DMSO-d6 as a solvent on the Bruker DRX500 MHz spectrometer. The frequency of 101.39 MHz was used for the quantitative ^{13}C-NMR with an inverse-gated decoupling sequence, 90° pulse angle. ^{31}P-NMR spectra were obtained after derivatization of the lignin with 2-chloro-4,4,5,5-tetramethyl-1,3,2-dioxaphospholane (TMDP) using cyclohexanol as internal standard. 2D HSQC NMR spectra were recorded using a standard Bruker pulse sequence with a 90° pulse, 0.12 s acquisition time, 1.3 s pulse delay, and a $^{1}J_{C\text{-}H}$ of 143 Hz. The quantitative analysis of the lignin functional groups by ^{13}C- and ^{31}P-NMR had a standard deviation of ~3.0 % and ~1.2 %, respectively.

RESULTS AND DISCUSSION

Quantitative ^{13}C-NMR analysis

The structure of the lignin samples was elucidated by ^{13}C-NMR before and after treatment with Co(salen). The quantitative determination was performed for different lignin moieties using the integral region of δ 162.3-102.7 ppm as a reference of six aromatic carbons [11].

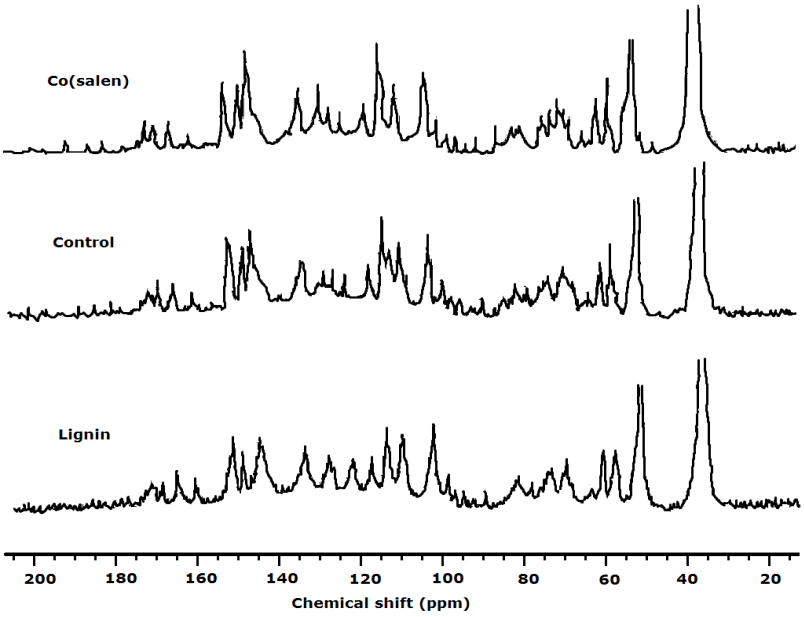

Figure 1. Quantitative ^{13}C-NMR spectra of the lignin samples.

Table 1. Content of functional groups by ^{13}C-NMR analysis.

Chemical shift (ppm)	Assignment	Amount (Ar)		
		Lignin	Control	Co(salen)
182.7-180.6	C=O in spirodienone structure	0.03	0.05	0.08
173.2-168.1	C=O in phenyl-COOR	0.24	0.28	0.35
167.7-165.8	C=O in conjugated phenyl-COOR	0.12	0.17	0.23
162.3-157.6	C_4 in p-hydroxyphenyl structure	0.02	0.04	0.07
155.2-141.7	C_3/C_4 in guaiacyl structure, C_3/C_5 in syringyl structure	1.57	1.72	2.13
140.4-122.8	C_1 in guaiacyl, syringyl, and p-hydroxyphenyl structure C_4 in syringyl structure, C_2/C_6 in p-hydroxyphenyl structure	2.26	2.05	1.68
122.6-118.3	C_6 in guaiacyl structure	0.38	0.47	0.71
116.5-112.6	C_5 in guaiacyl structure, C_3/C_5 in p-hydroxyphenyl structure	0.92	0.76	0.42
112.6-110.3	C_2 in guaiacyl structure	0.35	0.48	0.73
108.5-102.7	C_2/C_6 in syringyl structure	0.83	0.74	0.54
90.4-77.8	C_β in β-O-4, C_α in β-5 and β-β	0.81	0.62	0.33
65.2-61.7	C_γ in β-5 and β-O-4 with C_α=O in guaiacyl and syringyl structure	0.42	0.31	0.16
61.3-56.6	C_γ in β-O-4 structure without C_α=O	0.46	0.32	0.17
58.4-56.9	methoxyl group	0.84	0.64	0.37
52.7-51.3	C_β in β-β and C_β in β-5 structure	0.17	0.12	0.06

The spectra are presented in Figure 1, and the data are summarized in Table 1 [12, 13]. It is observed that the biomimetic treatment resulted inconsiderable changes in recovered lignin structure. The peak at δ 160 ppm confirmed the presence of p-hydroxy phenyl (H) units. The units of guaiacyl (G) and syringyl (S) in the lignin were evidenced by the chemical shifts between *δ* 125.6-110.3 and *δ* 108.5-102.7 ppm, respectively. Rencoret *et al.* [14] have reported that wood lignins are mainly composed of syringyl and guaiacyl units. The S/G ratio was found to decrease from 0.76 to 0.46 after the treatment with Co(salen). It was noticed that after the treatment the content of β-β and β-5 linkages decreased according to the amount per C_6 by the integration of C_β at *δ* 51.3-52.7 ppm. The β-O-4 linkages in lignin without C_α=O were quantified based on the C_γ at *δ* 56.6-61.3 ppm. There was about 34 % decrease after the biomimetic treatment compared to the control.

HSQC NMR analysis

HSQC NMR was applied to analyze the lignin structure before and after the biomimetic treatment by Co(salen). The results are shown in Table 2 [15, 16]. In HSQC NMR analysis, the spectrum is usually divided into high-field (0-50 ppm/0-3 ppm), aliphatic (50-100 ppm/3-6 ppm) and aromatic region (100-150 ppm/6-9 ppm). On the whole, the strength of the peaks decreased after the lignin was treated with Co(salen), which was the result of lignin degradation, as shown in Table 2. After the lignin was catalytically treated with Co(salen), the peak intensity of the guaiacyl, syringyl and p-hydroxyphenyl structures in the HSQC spectra decreased, indicating the degradation of these structural units in the biomimetic oxidation of lignin. Moreover, HSQC also confirmed the results obtained by ^{13}C-NMR analysis, in which the linkages of β-O-4, β-β, β-5 and methoxyl group were cleaved. The decrease in the content of methoxyl groups may be due to the degradation of syringyl structure and the demethylation of methoxyl groups. In addition, the α-5 structure in lignin (39.6-39.5 ppm/2.26-2.85 ppm) was found to decompose by the biomimetic oxidation. The functional groups at the side chains were oxidized according to the peak intensity, such as -CH_3 in aliphatic structure (13.6-19.2 ppm/0.76 ppm-0.84 ppm), -CH═CH- in guaiacyl structure (127.4 ppm/7.33 ppm), resulting in an increase in carbonyl content in the lignin (24.3-24.6 ppm/1.23-1.62 ppm, 37.3 ppm/1.98 ppm, 38.5 ppm/2.04 ppm, 73.5 ppm/3.26, 119.7 ppm/7.38 ppm).

Table 2. Analysis of functional groups by HSQC.

Chemical shift (ppm)		Functional group	Signal		
			Lignin	Control	Co(salen)
13.6-19.2	0.76~0.84	-CH_3 in aliphatic structure	s	w	vw
24.3-24.6	1.23-1.62	-CO-CH_3	vw	w	s
37.3	1.98	-CH_2-CH_2-COOH	vw	w	s
38.5	2.04	-CO-CH_2-CH_3, -CO-CH_2-COOH	vw	w	s
39.6-39.5	2.26-2.85	C_α-H in α-5 structure	s	w	vw
55.7	3.16	C_γ-H in β-β structure	s	w	vw
73.5	3.26	Ph-OCH_2-COOH	vw	w	s
59.6-61.3	3.35-3.57	C_γ-H in β-O-4 structure	s	w	vw
55.4	3.73	-OCH_3	s	w	vw
92.4-93.2	3.94-4.35	C_β-H in β-O-4 structure	s	w	vw
101.8	4.25	C_1-H in carbohydrate structure	s	w	vw
93.2-93.4	4.42-4.46	C_β-H in β-β structure	s	w	vw
71.6	4.65	C_α-H in threo β-O-4 structure	s	w	vw
71.6	4.88	C_α-H in erythro β-O-4 structure	s	w	vw
92.6	5.06	C_β-H in β-5 structure	s	w	vw
114.6-115.3	6.43-6.52	C_2-H in quinoid structure	vw	w	s
104.3	6.76	$C_{2/6}$-H in syringyl structure	s	w	vw
128.3	6.84	C-H in coniferol structure	s	w	vw
7.7	6.94	C_2-H in guaiacyl structure	s	w	vw
118.5-119.4	6.74~6.85	C_6-H in guaiacyl structure	s	w	vw
119.7	7.38	C_6-H in guaiacyl structure containing C=O	vw	w	s
114.5-115.6	6.89~7.14	C_5-H in guaiacyl structure	s	w	vw
142.7	7.44	C_6-H in quinoid structure	vw	w	s
128.3	7.05	$C_{2/6}$-H in p-hydroxyl phenyl structure	s	w	vw
127.4	7.33	-CH═CH- in guaiacyl structure	s	w	vw

s, strong; w, weak; vw, very weak.

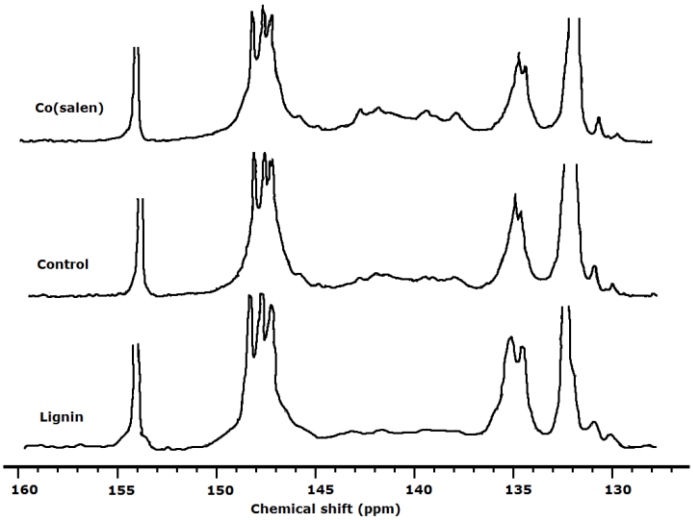

Figure 2. Quantitative ^{31}P-NMR spectra of the lignin samples.

Table 3. Content of functional groups by ^{31}P-NMR analysis.

Chemical shift (ppm)	Functional group	Content (mmol/g)		
		Lignin	Control	Co(salen) catalysis
154.3-153.6	Internal standard	-	-	-
149.5-145.4	Aliphatic hydroxyl groups	1.57	1.23	1.06
144.2-140.4	Condensed phenolic hydroxyl groups	0.62	0.36	0.17
143.3-142.2	Phenolic hydroxyl groups in syringyl structure	0.25	0.38	0.52
140.4-138.7	Phenolic hydroxyl groups in guaiacyl structure	0.16	0.29	0.36
138.6-137.3	p-Phenolic hydroxyl groups	0.13	0.25	0.42
136.2-133.4	Hydroxyl groups in carboxyl groups	0.14	0.48	0.73

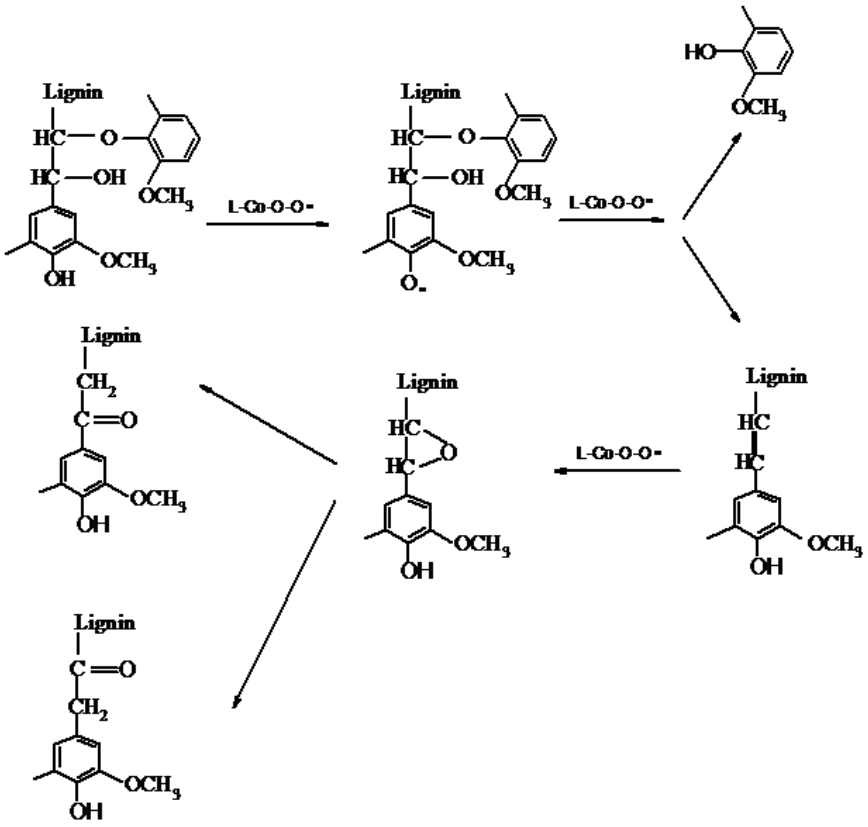

Figure 3. Representative pathways of lignin depolymerization by Co(salen).

Quantitative ^{31}P-NMR analysis

The quantitative ^{31}P-NMR analysis was used to determine the hydroxyl groups in order to elucidate the lignin oxidation. The spectra are presented in Figure 2, and the hydroxyl content is shown in Table 3 [17]. The data clearly illustrated that the most prominent ones in the lignin were aliphatic hydroxyl groups, which was in line with the report by Pu *et al*. [18] that the major hydroxyl groups in the wood lignin were in the aliphatic regions.

After biomimetic treatment, the content of the aliphatic hydroxyl groups decreased from 1.23 mmol/g to 1.06 mmol/g due to the oxidation at the side chains in the lignin, which was confirmed by the increase in the content of the carboxyl groups (136.2-133.4 ppm). The content of the condensed phenolic hydroxyl groups decreased from 0.36 mmol/g to 0.17 mmol/g, indicating that the condensed type substructures in the lignin were obviously degraded. In addition, the data shown in Table 3 suggest that the phenolic hydroxyl content of the syringyl, guaiacyl and p-hydroxyphenyl substructures in the Co(salen)-treated lignin increased when compared with the control. This was due to the cleavage of β-O-4 linkage leading to an increase in phenolic hydroxyl groups. As shown in Figure 1, the superoxocobalt complex initiated the reaction by subtraction of phenolic hydrogen atoms, leading to the cleavage of β-O-4 linkage. Further oxidation at the side-chain gave carbonyl groups [19, 20].

CONCLUSIONS

In accordance with the lignin transformation, in this study the structure of Indulin lignin in the biomimetic treatment with Co(salen) was examined by ^{13}C, ^{31}P-NMR and HSQC. During the biomimetic catalysis, the structural behavior of the lignin significantly changed. It was observed that the cleavage of β-O-4 linkage resulted in an increase in phenolic hydroxyl groups by the treatment. The side chains in the lignin were oxidized. Furthermore, the content of the units wasobserved to decrease in the guaiacyl, syringyl and p-hydroxyphenyl substructure as a result of the biomimetic treatment.

Acknowledgements: *This work was supported by the Open Research Foundation of Hunan Provincial Key Lab of Dark Tea and Jin-hua of Hunan City University (HC6120), the Open Research Foundation of Guangzhou Key Laboratory of Environmental Catalysis and Pollution Control of Guangdong University of Technology (GKLECPC-11), the Open Research Foundation of Guangxi Key Laboratory of Chemistry and Engineering of Forest Products of Guangxi University for Nationalities (GXFC17-18-03), the Open Research Foundation of Key Laboratory of Advanced Energy Materials Chemistry of Ministry of Education of China of Nankai University (111 project, B12015), the National Natural Science Foundation of China (21766015), the Open Research Foundation of Key Laboratory for Solid Waste Management and Environment Safety of Ministry of Education of China of Tsinghua University (SWMES 2017-09), and the Open Research Foundation of Key Laboratory of Pulp and Paper Science and Technology of Ministry of Education/Shandong Province of Qilu University of Technology (KF2015011).*

REFERENCES

1. L. S. Kocheva, A. P. Karmanov, Y. A. Karmanova, *Russ. Chem. Bull.*, **63**(9), 2036 (2014).
2. X. Pan, J. F. Kadla, K. Ehara, N. Gilkes, J.N. Saddler, *J. Agr. Food Chem.*, **54,** 5806 (2006).
3. A. Arshanitsa, J. Ponomarenko, T. Dizhbite, A. Andersone, R. J. A. Gosselink, J. V. D. Putten, M. Lauberts, G. Telysheva, *J. Anal. Appl. Pyrol.*, **103**(9), 78 (2013).
4. W. Gong, Z. Xiang, F. Ye, G. Zhao, *Ind. Crop. Prod.*, **91,** 340 (2016).
5. F. Masarin, M. Norambuena, H.O.R. Ramires, B.J. Demuner, P.C. Pavan, A. Ferraz, *J. Chem. Technol. Biotechnol.*, **91(5),** 1422 (2016).
6. S. Sonar, K. Ambrose, A. D. Hendsbee, J. D. Masuda, R. D. Singer, *Can. J. Chem.*, **90**(1), 60 (2012).
7. J. Zeng, C. G. Yoo, F. Wang, X. Pan, W. Vermerris, Z. Tong, *ChemSusChem*, **8**(5), 861 (2015).
8. E. C. Niederhoff, J. H. Timmon, A. E. Martell, *Chem. Rev.*, **84**(2), 137 (1984).
9. T. Elder, J. J. Bozell, *Holzforschung*, **50**(1), 24 (1996).
10. C. Carmen, O. Marco, P. Luca, B. Rindone, R. Scotti, J. Sipila, F. Morazzoni, *J. Chem. Soc. Dalton Trans.*, 3007 (2002).
11. L. Oliveira, D. V. Evtuguin, N. Cordeiro, A. J. D. Silvestre, A. M. S. Silva, I. C. Torres, *J. Agr. Food Chem.*, **54**(7), 2598 (2006).
12. K.M. Holtman, H.M. Chang, H. Jameel, J.F. Kadla, *J. Wood Chem. Technol*., **26,** 21 (2006).
13. M. S. Jahan, S. P. Mun, *J. Wood Chem. Technol*., **27,** 83 (2007).
14. J.P. Encores, P.A. Gutiérrez, A.T. Martínez, J.C. Delrío, *J. Agr. Food Chem.*, **63**(2), 603 (2015).
15. N. Fukagawa, G. Meshitsuka, A. Ishizu, *J. Chem. Technol.*, **11**(3), 373 (1991).
16. T. Khimoto, A. Ueki, H. Tamori, Y. Uraki, M. Ubukata, *Holzforschung*, **58**(4), 355 **(**2004).
17. Z. Michael, R. Arthur, *Holzforschung*, **55**(3), 283 (2001).
18. Y. Pu, S. Cao, A.J. Ragauskas, *Energy Environ. Sci.*, **4**(9), 3154 (2011).
19. I. Kuźniarska-Biernacka, M. A. Carvalho, S. B. Rasmussen, M. A. Bañares, K. Biernacki, A. L.

Metaphase, A. G. Rolo, A. M. Fonseca, I.C. Neves, *Eur. J. Inorg. Chem*., 5408 (2013).

20. M. J. Jia, A. Seifert, W. R. Thiel, *Chem. Mat.*, **15,** 2174 (2003).

СТРУКТУРНИ ПРОМЕНИ В ЛИГНИН ПРИ КАТАЛИТИЧНО ОКИСЛЕНИЕ С Co(САЛЕН)

Кс.-Ф. Жоу[1,2,3,4,5,6*]

[1.] *Главна лаборатория по тъмен чай и Jin-hua на провинция Хунан, Университет на Хунан, Иянг, п.к. 413000, Китай*

[2.] *Главна лаборатория на Гуанджоу по екологичен катализ и контрол на замърсяването, Училище по екологична наука и инженерство, Гуандонски технологичен университет, Гуанджоу, п.к. 510006, Китай*

[3.] *Главна лаборатория на Гуанкси по химия и горско инженерство, Университет на Гуанкси за националностите, Нанинг, п.к. 530006, Китай*

[4.] *Главна лаборатория по химия на материали за енергия на Министерството на образованието на Китай, Университет на Нанкай, Тянджин, п.к. 300071, Китай*

[5.] *Факултет по инженерна химия, Кунмински научен и технологичен университет, Кунмин, п.к. 650500, Китай*

[5.] *Главна лаборатория по управление на твърди отпадъци и екологична безопасност на Министерството на образованието на Китай, Пекин, п.к. 100084, Китай*

[6.] *Главна лаборатория по хартиена обработка на Министерството на образованието на провинция Шандон, Технологичен университет на Килу, Джинан, п.к. 250353, Китай*

Постъпила на 27 април, 2018; приета на 18 юли, 2018

(Резюме)

За подобряване на ефективността на катализа при окислението на ингулин лигнин е използван Co(сален). Структурните промени на лигнина при биомиметичната обработка са проследени чрез ^{13}C-NMR, HSQC и ^{31}P-NMR спектроскопия. В резултат на биомиметичната обработка е установено скъсяване на връзките β-O-4, β-β и β-5, и по-специално, разцепване на β-O-4 връзката. Фактът, че кондензираните субструктури значително се разлагат, обяснява дълбочинната деградация на лигнина. В допълнение на тези промени, предложеният механизъм е приложен към окислението на лигнин, катализирано с Co(сален) чрез отстраняване на фенолни водородни атоми.

Bulgarian Chemical Communications, Volume 50, Issue 4 (pp. 621 – 630) 2018

Effect of heat absorption on Cu-water based magneto-nanofluid over an impulsively moving ramped temperature plate

M. R. Mishra[1], S. M. Hussain[1*], R. Sharma[2], G. S. Seth[3]

[1]*Department of Mathematics, O. P. Jindal University, Raigarh, India*
[2]*Department of Mathematics, GITAM, Bangaluru, India*
[3]*Department of Applied Mathematics, Indian Institute of Technology (ISM), Dhanbad, India*

Received, July 18, 2017; Revised, August 6, 2018

The aim of the present paper is to explore the effects of heat absorption on a transient free convective boundary-layer flow of an electrically conducting, viscous and incompressible magneto-nanofluid over an impulsively moving vertical ramped temperature plate. Water-based nanofluids with added nanoparticles of titanium oxide, aluminium oxide and copper are taken into account. The mathematical model of the problem is obtained using the model of nanoparticle volume fraction. The governing model is solved analytically by making use of Laplace transform technique. The expressions for nanofluid velocity, nanofluid temperature, skin friction and Nusselt number were obtained for both the cases of ramped and isothermal conditions. The effects of various physical parameters on the nanofluid velocity and nanofluid temperature are shown by various graphs whereas the numerical values of skin friction and Nusselt number are presented in tables. The numerical results of the problem were compared for both ramped and isothermal conditions and it is observed that the numerical values in case of isothermal conditions are lower in magnitude as compared to ramped conditions.

Keywords: Nanofluid, Free convection, Heat absorption, Ramped temperature

INTRODUCTION

The study of nanofluids has attracted several researchers due to their huge applications in real life problems and industries. Initially, the term nanofluid, pioneered by Choi [1], refers to a suspension of nanoparticles having diameter less than 100 nm in a base fluid such as water, ethylene glycol, etc. Normally, conventional base fluids do not have an adequate thermal conductivity for many practical applications. Therefore, to augment the thermal conductivity of the base fluid, metal nanoparticles having higher thermal conductivity than the conventional base fluid are added to the fluid. Nanofluids being a mixture of nanoparticles and a base fluid are an innovative type of energy transport fluid and their novel property makes them tremendously useful in different processes of heat transfer including microelectronics, automobiles, hybrid-powered engines, fuel cells, domestic refrigerator, nuclear reactor coolants, pharmaceutical processes, etc. Choi [1] was the first who pointed out that the thermal conductivity of a base fluid can be radically improved by uniform dispersion of nano-sized particles into a fluid. This concept prompted many researchers towards nanofluids, and abundant studies, analyzing the thermal properties of nanofluids, have been worked out. Keblinski *et al*. [2] explored the possible mechanism for the augmentation of thermal conductivity of the fluid by a uniform suspension of nano-sized particles in the fluid. Buongiorno [3] proposed a non-homogeneous equilibrium model which states that the thermal conductivity of a fluid can be significantly enhanced due to the presence of Brownian diffusion and thermophoretic diffusion effects of nanoparticles. Remarkable research studies reporting the improvement in the thermal conductivity of fluids due to a suspension of nanoparticles and its frequent applications have been presented by Jang and Choi [4], Daungthongsuk and Wongwises [5], Seyyedi *et al*. [6], Rashidi *et al*. [7], Garoosi *et al*. [8,9] and Malvandi and Ganji [10,11].

The hydromagnetic nanofluids possess both liquid and magnetic characteristics and are known to have enthralling relevance to magneto-optical wavelength filters, ink float separation, optical switches, optical gratings, nonlinear optical materials, etc. The magneto-nanofluids have wide applications in drug delivery for cancer treatment as they play a significant role in guiding the drug particles up the blood stream to a tumor because the magnetic nanoparticles are known to be more adhesive to tumor cells than to non-malignant cells. The magneto-nanofluids are also known to have applications in the treatment of hyperthermia, contrast enhancement in magnetic resonance imaging and magnetic cell separation. Following this, Sheikholeslami *et al*. [12-14] reported their

* To whom all correspondence should be sent:
E-mail: hussain.modassir@yahoo.com

investigations on the problems of MHD convective flow of nanofluids considering different geometries and configurations. Sheikholeslami and Ganji [15] theoretically analyzed the problem of hydromagnetic flow in a permeable channel infused with nanofluid. They concluded that due to the increasing values of Reynolds number and nanoparticle volume fraction the nanofluid velocity boundary-layer thickness shrinks whereas it amplifies with the augment of Hartmann number. Recently, Hayat *et al*. [16] examined the unsteady hydromagnetic two-dimensional squeezing flow of nanofluids confined between two parallel walls under the influence of Brownian motion and thermophoresis effects. More recently, Dhanai *et al*. [17] investigated the influence of thermal slip on hydromagnetic mixed convective flow of nanofluid with heat transfer along an inclined cylinder taking into account the effects of thermophoresis, Brownian motion and viscous dissipation. They concluded that an increase in mass transfer parameter leads to a raise in the rate of heat transfer whereas it reduces due to thermal slip parameter. The heat generation/absorption has an important impact on the heat transfer characteristics in the various physical phenomena involved in the industry such as dissociating fluids in packed-bed reactors, post accident heat removal, fire and combustion, underground disposal of radioactive waste material, storage of food stuffs, etc. This encouraged many researchers to undertake the investigation of hydromagnetic convective flow over bodies with different geometries under the influence of heat generation/absorption. Some relevant studies dealing with the influence of heat generation or absorption have been reported by Acharya and Goldstein [18], Vajravelu and Nayfeh [19], Chamkha [20], Leea *et al*. [21], Sheikh and Abbas [22], Mehmood and Saleem [23], Mondal *et al*. [24] and Nandkyeolyar *et al*. [25]. Hamad and Pop [26] investigated the unsteady free convective nanofluid flow over an oscillatory moving vertical permeable flat plate under the influence of constant heat source and magnetic field in a rotating frame of reference. Chamkha and Aly [27] studied the two-dimensional steady hydromagnetic free convective boundary-layer nanofluid flow of an incompressible pure base fluid suspended with nanoparticles over semi-infinite vertical permeable plate in the presence of magnetic field, heat generation or absorption, thermophoresis and Brownian diffusion effects. The analysis of MHD free convective flow of Al_2O_3 -water based nanofluid in an open cavity considering uniform thermal boundary condition in the presence of uniform heat absorption/generation was performed by Mahmoudi *et al*. [28].

In all the aforesaid studies, the solutions were analyzed by considering simplified conditions, where velocity and temperature at the plate are continuous and defined. But, numerous problems of practical interest require the velocity and temperature to satisfy non-uniform, discontinuous or arbitrary conditions at the plate. Following this, several researchers, namely, Chandran *et al*. [29], Seth *et al*. [30-32], Nandkyeolyar *et al*. [33,34] and Hussain *et al*. [35] studied the problems of convective flow past a moving plate considering the ramped temperature. Khalid *et al*. [36] obtained the exact solution for a natural convective flow of a nanofluid past an oscillating moving vertical plate with ramped temperature, using the Laplace transform technique. Hussain *et al*. [37] explored the combined effects of Hall current and rotation on a natural convective flow with heat transfer over an accelerated moving ramped temperature in the presence of heat absorption and homogenous chemical reaction employing the Laplace transform technique. Recently, Hussain *et al*. [38,39] discussed the impact of thermal radiation on the magneto free convective nanofluid over a moving uniformly accelerated ramped temperature plate with and without considering Hall effects. Subsequently, Sharma *et al*. [40] extended this problem in a rotating medium by making use of Laplace transform technique.

Objective of the present research work is to analyze the consequence of heat absorption on the natural convective flow of an incompressible, viscous and electrically conducting magneto-nanofluid over an impulsively moving ramped temperature plate. It is expected that the present findings will be useful in biological and physical sciences, transportation, electronics cooling, environment and national security.

MATHEMATICAL ANALYSIS

Formulation of problem and its solution

In the present study, we considered unsteady hydromagnetic natural convective flow of an electrically conducting, viscous and incompressible nanofluid over an impulsive moving vertical infinite plate. The coordinate system is chosen as follows: x'-axis is considered along the length of the plate in upward direction and y'-axis is normal to the plane of plate. A uniform transverse magnetic field B_0 is applied in a direction which is parallel to y'-axis.

Table 1. Thermophysical properties of base fluid and nanoparticles [38]

	ρ $\left(\mathrm{kg/m^3}\right)$	c_p $\left(\mathrm{J/kgK}\right)$	k $\left(\mathrm{W/mK}\right)$	$\beta\times10^5$ $\left(K^{-1}\right)$	ϕ	σ $\left(\mathrm{S/m}\right)$
Water (Base fluid)	997.1	4179	0.613	21	0.00	5.5×10^{-6}
Cu (Copper)	8933	385	401	1.67	0.05	59.6×10^{6}
Al_2O_3 (Alumina)	3970	765	40	0.85	0.15	35×10^{6}
TiO_2 (Titanium oxide)	4250	686.2	8.9538	0.90	0.20	2.6×10^{6}

The fluid and plate are at rest and are maintained at a uniform temperature α'_∞ at time $t'\le 0$. At time $t'>0$, the plate starts moving in x'-direction with uniform velocity U_0 in its own plane. The temperature of the plate is raised or lowered to $\alpha'_\infty+(\alpha'_w-\alpha'_\infty)t'/t_0$ when $0<t'\le t_0$ and it is maintained at uniform temperature α'_w when $t'>t_0$ (t_0 being characteristic time). The schematic diagram of the model is presented in Fig. 1. The water-based nanofluid is considered which contain three types of nanoparticles: Cu, Al_2O_3 and TiO_2. The nanoparticles are assumed to have uniform shape and size. Moreover, it is also assumed that both the base fluid and the nanoparticles are in thermal equilibrium state and no slip takes place between them. The thermophysical properties of base fluid and nanoparticles are given in Table 1. The plate is considered to be of infinite extent in x' and z' directions and is electrically non-conducting so all physical quantities except pressure are functions of y' and t' only. Since the magnetic Reynolds number of the flow is taken to be very small, the induced magnetic field is neglected so that the magnetic field $\vec{B}\equiv(0,B_0,0)$. No electric field is applied, so the electric field due to polarization of charges is negligible; that is, $\vec{E}\equiv(0,0,0)$. This corresponds to the case where no energy is added or extracted from the fluid by electrical means.

Under the assumptions made above and Boussinesq approximation, the governing equations for natural convective flow of an electrically conducting, viscous and incompressible magneto-nanofluid taking into account the effects of heat absorption are given by:

$$\rho_{nf}\frac{\partial U}{\partial t'}=\mu_{nf}\frac{\partial^2 U}{\partial y'^2}-\sigma_{nf}B_0^2U+g\left(\rho\beta\right)_{nf}\left(\alpha'-\alpha'_\infty\right), \quad (1)$$

$$\frac{\partial \alpha'}{\partial t'}=\frac{k_{nf}}{\left(\rho c_p\right)_{nf}}\frac{\partial^2\alpha'}{\partial y'^2}-\frac{Q_0}{\left(\rho c_p\right)_{nf}}(\alpha'-\alpha'_\infty), \quad (2)$$

where

U, α', ρ_{nf}, μ_{nf}, σ_{nf}, g, β_{nf}, $\left(\rho c_p\right)_{nf}$, Q_0 and k_{nf} are: component of nanofluid velocity in x'-direction, temperature of the nanofluid, density of the nanofluid, dynamic viscosity of the nanofluid, electrical conductivity of the nanofluid, acceleration due to gravity, thermal expansion coefficient of the nanofluid, heat capacitance of the nanofluid, heat absorption coefficient and thermal conductivity of the nanofluid, respectively.

Initial and boundary conditions for the nanofluid flow problem are:

$$\left.\begin{aligned}&U=0,\ \alpha'=\alpha'_\infty \text{ for } y'\ge 0 \text{ and } t'\le 0,\\ &U=U_0 \text{ at } y'=0 \text{ for } t'>0,\\ &\alpha'=\alpha'_\infty+\left(\alpha'_w-\alpha'_\infty\right)t'/t_0 \text{ at } y'=0 \text{ for } 0<t'\le t_0,\\ &\alpha'=\alpha'_w \text{ at } y'=0 \text{ for } t'>t_0,\\ &U\to 0,\ \alpha'\to\alpha'_\infty \text{ as } y'\to\infty \text{ for } t'>0.\end{aligned}\right\} \quad (3)$$

For the nanofluids, the expressions for ρ_{nf}, μ_{nf}, σ_{nf}, $\left(\rho\beta\right)_{nf}$ and $\left(\rho c_p\right)_{nf}$ are given as:

$$\left.\begin{aligned}&\rho_{nf}=(1-\phi)\rho_f+\phi\rho_s,\ \mu_{nf}=\mu_f(1-\phi)^{-2.5},\\ &\left(\rho\beta\right)_{nf}=(1-\phi)\left(\rho\beta\right)_f+\phi\left(\rho\beta\right)_s,\\ &\left(\rho c_p\right)_{nf}=(1-\phi)\left(\rho c_p\right)_f+\phi\left(\rho c_p\right)_s,\\ &\sigma_{nf}=\sigma_f\left[1+\frac{3(\sigma-1)\phi}{(\sigma+2)-(\sigma-1)\phi}\right],\ \sigma=\frac{\sigma_s}{\sigma_f},\end{aligned}\right\} \quad (4)$$

where

ϕ, ρ_f, ρ_s, μ_f, β_f, β_s, $\left(\rho c_p\right)_f$, $\left(\rho c_p\right)_s$, σ_f and σ_s are: solid volume fraction of nanoparticle, density of the base fluid, density of the nanoparticle, viscosity of the base fluid, thermal expansion coefficient of the base fluid, thermal expansion coefficient of the nanoparticle, heat capacitance of the base fluid, heat capacitance of the nanoparticle, electrical conductivity of the base fluid and electrical conductivity of the nanoparticle, respectively. The expressions presented in equation (4) are limited to spherical nanoparticles, and are not valid for other shapes of nanoparticles. The model for effective thermal conductivity of the nanofluid, i.e., k_{nf} for the spherical nanoparticles, given by Hamilton and Crosser model followed by Oztop and Abu-Nada [38], is expressed as:

$$k_{nf}=k_f\left[\frac{k_s+2k_f-2\phi\left(k_f-k_s\right)}{k_s+2k_f+\phi\left(k_f-k_s\right)}\right], \quad (5)$$

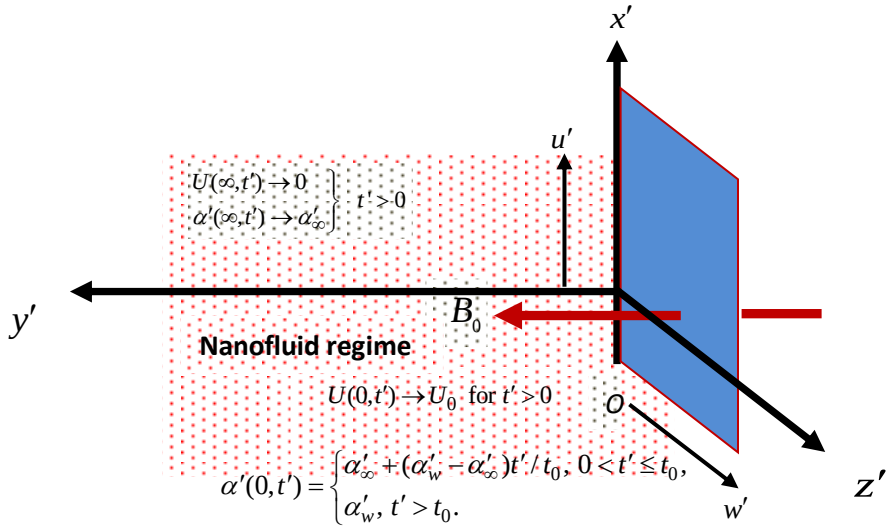

Fig. 1. Schematic diagram of the model

where k_f is the thermal conductivity of the base fluid and k_s is the thermal conductivity of the nanoparticles.

In order to convert the equations (1)-(3) in dimensionless form, now we introduce the following non-dimensional variables and parameters:

$$y=\frac{y'}{U_0 t_0}, u=\frac{U}{U_0}, t=\frac{t'}{t_0}, \alpha=\frac{\alpha'-\alpha'_\infty}{\alpha'_w-\alpha'_\infty}. \tag{6}$$

Equations (1) and (2), in dimensionless form, reduce to:

$$\frac{\partial u}{\partial t}=K_1\frac{\partial^2 u}{\partial y^2}-K_2 M^2 u+K_3 G_r\alpha, \tag{7}$$

$$\frac{\partial \alpha}{\partial t}=\frac{1}{K_5}\frac{\partial^2 \alpha}{\partial y^2}-K_6\alpha, \tag{8}$$

where,

$$\left.\begin{aligned}
&\lambda_1=\left[(1-\phi)+\phi\left(\frac{\rho_s}{\rho_f}\right)\right],\ \lambda_2=\left[1+\frac{3(\sigma-1)\phi}{(\sigma+2)-(\sigma-1)\phi}\right],\ \sigma=\frac{\sigma_s}{\sigma_f},\\
&\lambda_3=\left[(1-\phi)+\phi\frac{(\rho\beta)_s}{(\rho\beta)_f}\right],\ \lambda_4=\left[(1-\phi)+\phi\frac{(\rho c_p)_s}{(\rho c_p)_f}\right], Q=\frac{\upsilon_f Q_0}{(\rho c_p)_f U_0^2}\\
&K_1=\frac{1}{(1-\phi)^{2.5}\lambda_1},\ K_2=\frac{\lambda_2}{\lambda_1},\ K_3=\frac{\lambda_3}{\lambda_1},\ K_4=\frac{k_{nf}}{k_f},\ K_5=\frac{P_r}{K_4}, K_6=\frac{Q}{\lambda_4}\\
&M=\frac{\sigma_f B_0^2\upsilon_f}{\rho_f U_0^2}, G_r=\left[\frac{g\beta_f\upsilon_f(\alpha'_w-\alpha'_\infty)}{U_0^3}\right],\quad P_r=\frac{(\rho\upsilon c_p)_f}{k_f}.
\end{aligned}\right\} \tag{9}$$

$$\left.\begin{aligned}
&u=0,\ \alpha=0 \text{ for } y\geq 0 \text{ and } t\leq 0,\\
&u=1 \text{ at } y=0 \text{ for } t>0,\\
&\alpha=t \text{ at } y=0 \text{ for } 0<t\leq 1,\\
&\alpha=1 \text{ at } y=0 \text{ for } t>1,\\
&u\to 0,\ \alpha\to 0 \text{ as } y\to\infty \text{ for } t>0.
\end{aligned}\right\} \tag{10}$$

The characteristic time t_0 may be defined according to the non-dimensional process mentioned above as $t_0=\upsilon_f/U_0^2$, where U_0 is characteristic velocity.

The initial and boundary conditions (3) in dimensionless form reduce to:

$$u(y,t)=\frac{1}{2}g(y,t)+\lambda_3\left[f_1(y,t)-H(t-1)f_1(y,t-1)\right], \tag{11}$$

$$\alpha(y,t)=\alpha_1(y,t)-H(t-1)\,\alpha_1(y,t-1), \tag{12}$$

where,

$$g(y,t)=\left[e^{y\sqrt{\lambda_1\lambda_2}}erfc\left(\sqrt{\lambda_2}t+\frac{y}{2}\sqrt{\frac{\lambda_1}{t}}\right)+e^{-y\sqrt{\lambda_1\lambda_2}}erfc\left(-\sqrt{\lambda_2}t+\frac{y}{2}\sqrt{\frac{\lambda_1}{t}}\right)\right], \tag{13}$$

$$\alpha_1(y,t)=\frac{1}{2}\left[\left(t+\frac{y}{2}\sqrt{\frac{K_5}{K_6}}\right)e^{y\sqrt{K_5K_6}}erfc\left(\sqrt{K_6}t+\frac{y}{2}\sqrt{\frac{K_5}{t}}\right)+\left(t-\frac{y}{2}\sqrt{\frac{K_5}{K_6}}\right)e^{-y\sqrt{K_5K_6}}erfc\left(-\sqrt{K_6}t+\frac{y}{2}\sqrt{\frac{K_5}{t}}\right)\right], \tag{14}$$

$$f_1(y,t)=\frac{e^{\lambda_4 t}}{2\lambda_4^{\,2}}\Bigg[e^{y\sqrt{\lambda_1(\lambda_2+\lambda_4)}}erfc\left(\sqrt{(\lambda_2+\lambda_4)t}+\frac{y}{2}\sqrt{\frac{\lambda_1}{t}}\right)+e^{-y\sqrt{\lambda_1(\lambda_2+\lambda_4)}}erf\left(-\sqrt{(\lambda_2+\lambda_4)t}+\frac{y}{2}\sqrt{\frac{\lambda_1}{t}}\right)$$
$$-e^{y\sqrt{K_5(K_6+\lambda_4)}}erf\left(\sqrt{(K_6+\lambda_4)t}+\frac{y}{2}\sqrt{\frac{K_5}{t}}\right)-e^{-y\sqrt{K_5(K_6+\lambda_4)}}erf\left(-\sqrt{(K_6+\lambda_4)t}+\frac{y}{2}\sqrt{\frac{K_5}{t}}\right)\Bigg]$$
$$-\frac{1}{2\lambda_4}\Bigg[\left\{\frac{1}{\lambda_4}+\left(t+\frac{y}{2}\sqrt{\frac{\lambda_1}{\lambda_2}}\right)\right\}\left\{e^{y\sqrt{\lambda_1\lambda_2}}erf\left(\sqrt{\lambda_2 t}+\frac{y}{2}\sqrt{\frac{\lambda_1}{t}}\right)\right\}$$
$$+\left\{\frac{1}{\lambda_4}+\left(t-\frac{y}{2}\sqrt{\frac{\lambda_1}{\lambda_2}}\right)\right\}\left\{e^{-y\sqrt{\lambda_1\lambda_2}}erf\left(-\sqrt{\lambda_2 t}+\frac{y}{2}\sqrt{\frac{\lambda_1}{t}}\right)\right\}$$
$$-\left\{\frac{1}{\lambda_4}+\left(t+\frac{y}{2}\sqrt{\frac{K_5}{K_6}}\right)\right\}\left\{e^{y\sqrt{K_5K_6}}erf\left(\sqrt{K_6 t}+\frac{y}{2}\sqrt{\frac{K_5}{t}}\right)\right\}$$
$$-\left\{\frac{1}{\lambda_4}+\left(t-\frac{y}{2}\sqrt{\frac{K_5}{6K_2}}\right)\right\}\left\{e^{-y\sqrt{K_5K_6}}erf\left(-\sqrt{K_6 t}+\frac{y}{2}\sqrt{\frac{K_5}{t}}\right)\right\}\Bigg]. \qquad (15)$$

Here $H(t-1)$ and $erfc(x)$ are Heaviside step and complementary error functions, respectively.

Solution for the case of isothermal plate

The expressions (11) to (15) represent the solution for nanofluid velocity and temperature for the time-dependent natural convective flow of electrically conducting, viscous and incompressible magneto-nanofluids over an impulsively moving vertical ramped temperature plate under the influence of heat absorption. In order to analyze the effect of ramped temperature on the flow-field, it is worthwhile to compare such a flow with the one near an impulsively moving vertical uniform temperature plate. Owing to the assumptions made in the initial and boundary condition (10), the equations (7) and (8) are solved analytically with the help of Laplace transform technique and the exact solutions for nanofluid velocity $u(y,t)$ and nanofluid temperature $\alpha(y,t)$ are obtained as aforesaid, the solutions for nanofluid velocity and temperature for natural convective magneto-nanofluids flow over an impulsively moving vertical plate with isothermal condition are obtained and are expressed in the following forms:

$$u(y,t)=\frac{1}{2}\left[e^{y\sqrt{\lambda_1\lambda_2}}erfc\left(\sqrt{\lambda_2 t}+\frac{y}{2}\sqrt{\frac{\lambda_1}{t}}\right)+e^{-y\sqrt{\lambda_1\lambda_2}}erfc\left(-\sqrt{\lambda_2 t}+\frac{y}{2}\sqrt{\frac{\lambda_1}{t}}\right)\right]$$
$$+\frac{\lambda_3}{\lambda_4}\Bigg[\frac{e^{\lambda_4 t}}{2}\left\{e^{y\sqrt{\lambda_1(\lambda_2+\lambda_4)}}erfc\left(\sqrt{(\lambda_2+\lambda_4)t}+\frac{y}{2}\sqrt{\frac{\lambda_1}{t}}\right)+e^{-y\sqrt{\lambda_1(\lambda_2+\lambda_4)}}erfc\left(-\sqrt{(\lambda_2+\lambda_4)t}+\frac{y}{2}\sqrt{\frac{\lambda_1}{t}}\right)\right.$$
$$\left.-e^{y\sqrt{K_5(K_6+\lambda_4)}}erfc\left(\sqrt{(K_6+\lambda_4)t}+\frac{y}{2}\sqrt{\frac{K_5}{t}}\right)-e^{-y\sqrt{K_5(K_6+\lambda_4)}}erfc\left(-\sqrt{(K_6+\lambda_4)t}+\frac{y}{2}\sqrt{\frac{K_5}{t}}\right)\right\}\Bigg]$$
$$-\frac{\lambda_3}{\lambda_4}\Bigg[\frac{1}{2}\left\{e^{y\sqrt{\lambda_1\lambda_2}}erfc\left(\sqrt{\lambda_2 t}+\frac{y}{2}\sqrt{\frac{\lambda_1}{t}}\right)+e^{-y\sqrt{\lambda_1\lambda_2}}erfc\left(-\sqrt{\lambda_2 t}+\frac{y}{2}\sqrt{\frac{\lambda_1}{t}}\right)\right.$$
$$\left.-e^{y\sqrt{K_5K_6}}erfc\left(\sqrt{K_6 t}+\frac{y}{2}\sqrt{\frac{K_5}{t}}\right)+e^{-y\sqrt{K_5K_6}}erfc\left(-\sqrt{K_6 t}+\frac{y}{2}\sqrt{\frac{K_5}{t}}\right)\right\}\Bigg], \qquad (16)$$

$$\alpha(y,t)=\frac{1}{2}\left[e^{y\sqrt{K_5K_6}}erfc\left(\sqrt{K_6 t}+\frac{y}{2}\sqrt{\frac{K_5}{t}}\right)+e^{-y\sqrt{K_5K_6}}erfc\left(-\sqrt{K_6 t}+\frac{y}{2}\sqrt{\frac{K_5}{t}}\right)\right]. \qquad (17)$$

Skin friction and Nusselt number

The expressions for Nusselt number *Nu*, which measures the rate of heat transfer at the plate and skin friction τ, which measures the shear stress at the plate are presented in the following forms for both ramped and isothermal conditions:

For a ramped temperature plate:

$$Nu = -\frac{1}{2}\left[\left(\sqrt{\frac{K_5}{K_6}} + 2t\sqrt{K_5K_6}\right)\left\{erfc(\sqrt{K_6 t}) - 1\right\} - 2\sqrt{\frac{K_5}{t\pi}}\, e^{-K_6 t}\right] - \frac{1}{2}H(t-1)\left[\left(\sqrt{\frac{K_5}{K_6}} + 2(t-1)\sqrt{K_5K_6}\right)\left\{erfc(\sqrt{K_6(t-1)}) - 1\right\} - 2\sqrt{\frac{K_5}{(t-1)\pi}}\, e^{-K_6(t-1)}\right], \quad (18)$$

$$\tau = \sqrt{a_1 a_2}\left\{erfc(\sqrt{a_2 t}) - 1\right\} - \sqrt{\frac{a_1}{t\pi}}\, e^{-a_2 t} + a_3\left[f_2(t) - H(t-1) f_2(t-1)\right], \quad (19)$$

$$f_2(t) = \frac{e^{a_4 t}}{a_4}\left[\sqrt{a_1(a_2 + a_4)}\left\{erfc\left(\sqrt{(a_2 + a_4)t}\right) - 1\right\} - \sqrt{K_5(K_6 + a_4)}\left\{erfc\left(\sqrt{(K_6 + a_4)t}\right) - 1\right\} - \sqrt{\frac{a_1}{t\pi}}\, e^{-(\lambda_2 + \lambda_4)t} + \sqrt{\frac{K_5}{t\pi}}\, e^{-(K_6 + a_4)t}\right]$$

where,

$$-\frac{1}{2a_4}\left[\sqrt{\frac{a_1}{a_2}}\left\{erfc\left(\sqrt{a_2 t}\right) - 1\right\} + \left(\frac{1}{a_4} + t\right)\sqrt{a_1 a_2}\, 2\left\{erfc\left(\sqrt{a_2 t}\right) - 1\right\} - \left(\frac{1}{a_4} + t\right)\sqrt{\frac{a_1}{t\pi}}\, 2e^{-a_2 t} + \sqrt{\frac{K_5}{K_6}}\left\{erfc\left(\sqrt{K_6 t}\right) - 1\right\} + \left(\frac{1}{a_4} + t\right)\sqrt{K_5 K_6}\, 2\left\{erfc\left(\sqrt{K_6 t}\right) - 1\right\} - \left(\frac{1}{a_4} + t\right)\sqrt{\frac{K_5}{t\pi}}\, 2e^{-K_6 t}\right],$$

$$a_1 = \frac{1}{K_1},\ a_2 = MK_2,\ a_3 = \frac{G_r \cdot a_1 \cdot K_3}{K_5 - a_1} \text{ and } a_4 = \frac{K_5 \cdot K_6 + a_1 \cdot a_2}{K_5 - a_1}.$$

For an isothermal temperature plate,

$$Nu = \sqrt{\frac{K_5}{t\pi}}\, e^{-K_6 t} - \sqrt{K_5 K_6}\left\{erfc(\sqrt{K_6 t}) - 1\right\}, \quad (20)$$

$$\tau = \left[\sqrt{a_1 a_2}\left\{erfc\left(\sqrt{a_2 t}\right) - 1\right\} - \sqrt{\frac{a_1}{t\pi}}\, e^{-a_2 t}\right] + \frac{a_3}{a_4}\left[e^{a_4 t}\left\{\sqrt{a_1(a_2 + a_4)}\left\{erfc\left(\sqrt{(a_2 + a_4)t}\right) - 1\right\} - \sqrt{\frac{a_1}{t\pi}}\, e^{-(a_2 + a_4)t} - \sqrt{K_5(K_6 + a_4)}\left\{erfc\left(\sqrt{(K_6 + a_4)t}\right) - 1\right\} - \sqrt{\frac{K_5}{t\pi}}\, e^{-(K_6 + a_4)t}\right\}\right]$$

$$-\frac{a_3}{a_4}\left[\sqrt{a_1 a_2}\left\{erfc\left(\sqrt{a_2 t}\right) - 1\right\} - \sqrt{\frac{a_1}{t\pi}}\, e^{-a_2 t} - \sqrt{K_5 K_6}\left\{erfc\left(\sqrt{K_6 t}\right) - 1\right\} + \sqrt{\frac{K_5}{t\pi}}\, e^{-K_6 t}\right]. \quad (21)$$

RESULTS AND DISCUSSION

In order to emphasize the effects of various physical parameters on the flow-fluid, the numerical computations were performed and numerical results for the nanofluid velocity and temperature were described with the help of various graphs. For the engineering aspects, the numerical values of skin friction and Nusselt number are presented in different tables. Three distinct types of water-based nanofluids with nanoparticles of copper (Cu), aluminum oxide (Al_2O_3) and titanium oxide (TiO_2) were taken into account. The numerical values of copper-water based nanofluid velocity $u(y,t)$, computed from the analytical solutions reported in this paper are shown by different graphs against the boundary layer coordinate y in Figs. 2-6 for different values of magnetic parameter M, heat absorption parameter Q, Grashof number G_r, nanoparticle volume fraction ϕ and time t taking Prandtl number $P_r = 6.2$. The values of ϕ are considered in the range $0 < \phi \le 0.25$. In addition, the spherical nanoparticles with thermal conductivity and their dynamic viscosity are given in Table 1. The values of other physical parameters are shown in the respective figures. It can be observed from Figs. 2 and 3 that the nanofluid velocity gets reduced due to reduced magnetic and heat absorption parameters M and Q, respectively. This may be endorsed to the fact that the existence of magnetic field in the presence of an electrically conducting nanofluid generates a resistive type of body force, termed as Lorentz force which has a tendency to impede the motion of a fluid in the boundary layer region. Fig. 4 shows that augmentation in G_r results in significant rise in the nanofluid velocity which is

persistent to the fact that the Grashof number G_r behaves as a gratifying pressure gradient which accelerates the nanofluid velocity in the entire boundary layer region. It can be seen from Fig. 5 that the volume fraction of nanoparticle ϕ slows down the nanofluid velocity near the proximity of the plate while it has an annulment consequence away from the moving plate.

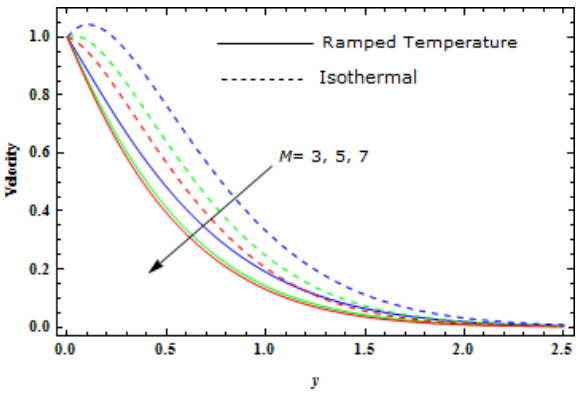

Fig. 2. Effect of M on velocity profiles

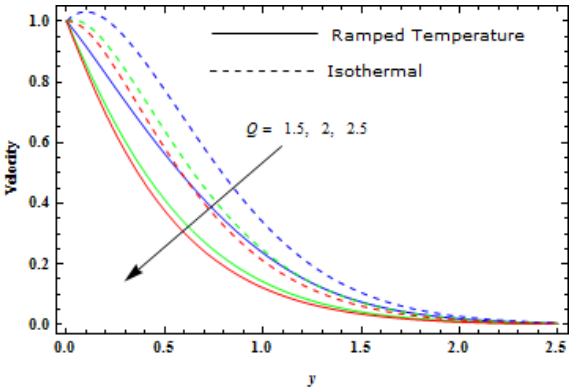

Fig. 3. Effect of Q on velocity profiles.

This happens due to the reason that the increasing value of volume fraction of nanoparticle reduces the thermal conductivity of the fluid, which in turn causes the thickness of the boundary layer to reduce and the viscosity to increase, thereby reducing the nanofluid velocity in the proximity of the moving plate. Fig. 6 reveals that as time passes, the fluid velocity gets accelerated. The consequences of heat absorption parameter Q, nanoparticle volume fraction ϕ and time t on copper-water based temperature profiles are shown in Figs. 7-9, taking Prandtl number $P_r = 6.2$. In Fig. 7 it is observed that as heat absorption parameter gradually increases, a significant reduction results in the nanofluid temperature for both ramped and isothermal conditions. From Figs. 8 and 9 it is evident that the nanofluid temperature rises with the increase of nanoparticle volume fraction ϕ and time t for both ramped and isothermal conditions. Physically, it is described as the nanoparticles volume fraction has a tendency to raise the nanofluid temperature throughout the boundary layer region; also nanofluid temperature gets increased with the progress of time for both ramped and isothermal cases.

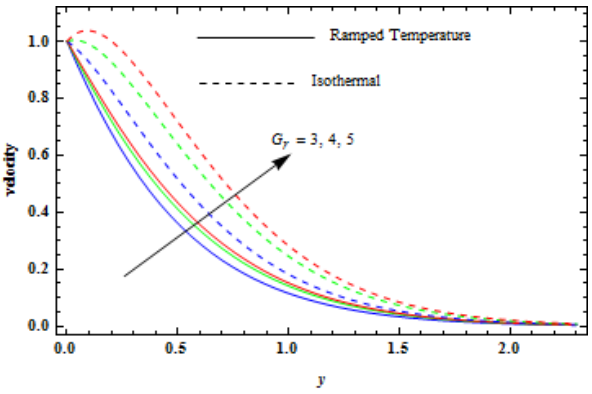

Fig. 4. Effect of G_r on velocity profiles.

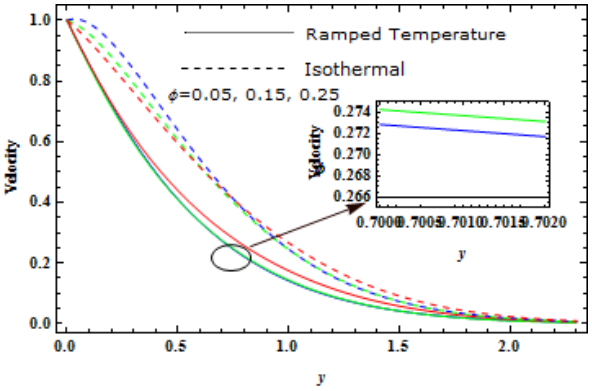

Fig. 5. Effect of ϕ on velocity profiles.

The comparison of nanofluid temperature profiles in the case of isothermal and ramped conditions for different nanofluids with nanoparticles of Cu, Al_2O_3 and TiO_2 is depicted in Fig. 10. It is seen from Fig. 10 that for both isothermal and ramped conditions, the temperature of TiO_2-water based nanofluid is higher in magnitude followed by the temperature of Al_2O_3-water and Cu-water based nanofluids.

The numerical values of skin friction τ for both cases of ramped and isothermal temperature plates considering the copper-water based nanofluid, evaluated from equations (19) and (21) are given in Table 2 for different values of M, G_r, ϕ, Q and t keeping Prandtl number $P_r = 6.2$.

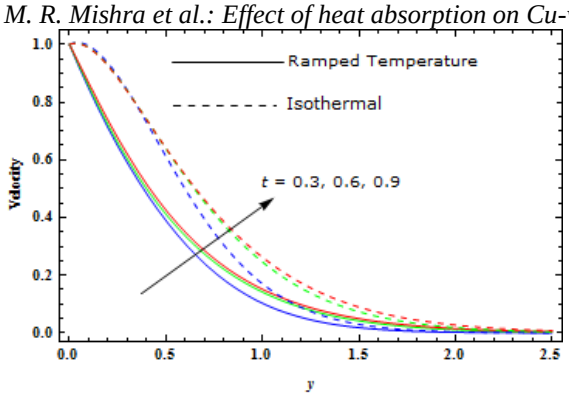

Fig. 6. Effect of t on velocity profiles.

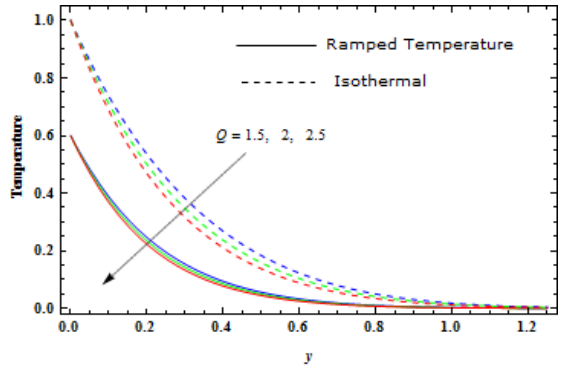

Fig. 7. Effect of Q on temperature profiles.

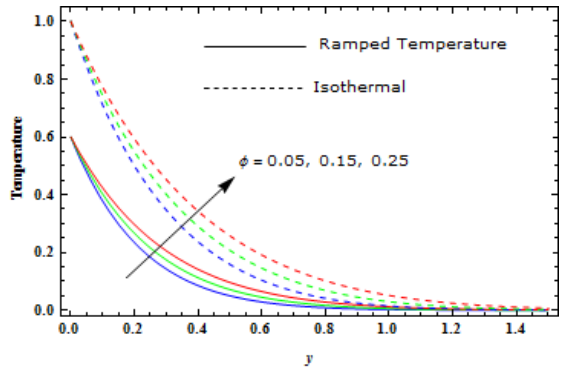

Fig. 8. Effect of ϕ on velocity profiles.

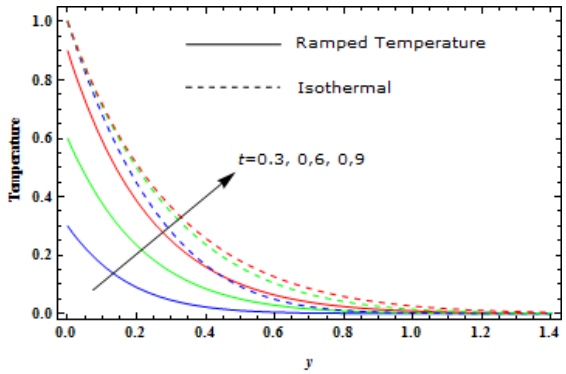

Fig. 9. Effect of t on temperature profiles.

It follows from Table 2 that the shear stress increases due to the increase of M, G_r, ϕ, Q and t. This infers that magnetic field, thermal buoyancy force, volume fraction of nanoparticle, heat absorption parameter have tendency to increase the shear stress at the plate, also it gets augmented as time passes for both ramped and isothermal conditions.

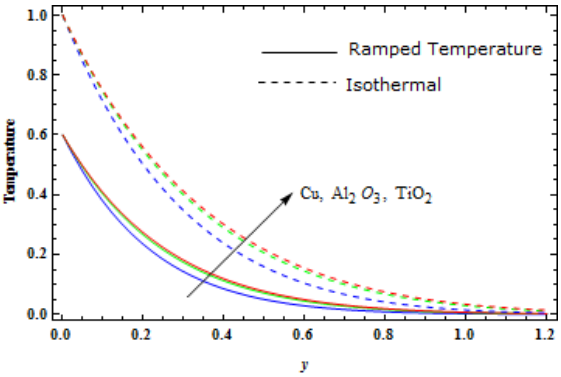

Fig. 10. Comparison of temperature profiles for different nanofluids.

It is reckoned from Table 3 that the Nusselt number Nu for both ramped and isothermal conditions, increases for increasing value of Q and decreases with the increase of ϕ, whereas for the ramped case it increases and decreases for isothermal case with the increase in t. This suggests that for both cases of ramped and isothermal conditions, the rate of heat transfer at the plate gets raised with the augmentation of heat absorption parameter whereas the volume fraction of nanoparticles has an adverse effect on it. As time passes the rate of heat transfer gets improved for the ramped case whereas it gets reduced for the isothermal case.

Validation of the obtained results

The obtained results were validated by comparing the nanofluid velocity profiles with the results obtained by Khalid *et al*. [36] considering similar assumptions but in the absence of magnetic field and heat absorption. This comparison demonstrates an excellent conformity of our results as it is revealed from Fig. 11.

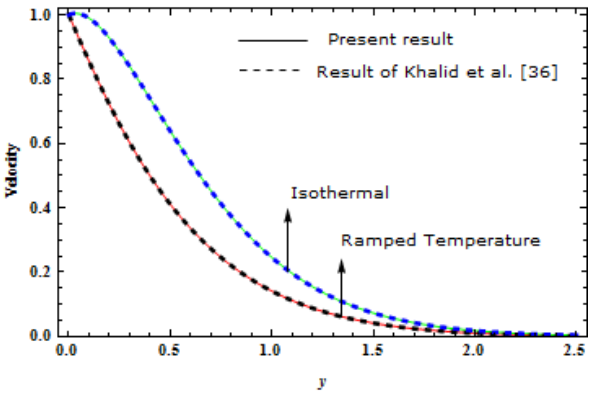

Fig. 11. Comparison of nanofluid velocity profiles in the present work considering $M=Q=0$ with those obtained by Khalid *et al*. [36] when ω =0

Table 2. Skin friction τ for Cu-water based nanofluid when $P_r = 6.2$

M	G_r	ϕ	Q	t	τ for ramped temperature	τ for isothermal plate
3	4	0.05	2	0.6	6.15463	5.80615
5	4	0.05	2	0.6	6.29641	6.14205
7	4	0.05	2	0.6	6.58365	6.58457
5	**3**	0.05	2	0.6	4.99342	4.82386
5	**4**	0.05	2	0.6	6.29641	6.14205
5	**5**	0.05	2	0.6	7.59940	7.46024
5	4	**0.05**	2	0.6	6.29641	6.14205
5	4	**0.15**	2	0.6	9.81332	9.37154
5	4	**0.25**	2	0.6	19.1638	18.7232
5	4	0.05	**1.5**	0.6	4.32815	4.35649
5	4	0.05	**2**	0.6	6.29641	6.14205
5	4	0.05	**2.5**	0.6	8.98351	8.71207
5	4	0.05	2	**0.3**	3.52347	2.84424
5	4	0.05	2	**0.6**	6.29641	6.14205
5	4	0.05	2	**0.9**	17.8309	17.7829

Table 3. Nusselt number Nm for Cu-water based nanofluid

ϕ	Q	T	Nu for ramped temperature	Nu for isothermal plate
0.05	2	0.6	2.94341	3.38195
0.15	2	0.6	2.54640	2.94062
0.25	2	0.6	2.21385	2.56973
0.05	**1.5**	0.6	2.84580	3.00798
0.05	**2**	0.6	2.94341	3.38195
0.05	**2.5**	0.6	3.05186	3.72975
0.05	2	**0.3**	2.60289	3.68166
0.05	2	**0.6**	2.94341	3.38195
0.05	2	**0.9**	3.76742	3.31097

CONCLUSIONS

The exact solution of the governing equations was obtained by using Laplace transform technique to explore the consequences of various relevant parameters on the natural convective flow of an incompressible, viscous and electrically conducting magneto-nanofluid over an impulsively moving ramped temperature plate. The important findings are summarized below for both the cases of ramped temperature and isothermal plates:

(i) The existence of magnetic field in the presence of an electrically conducting nanofluid generates a resistive type of body force, which has a tendency to impede the motion of fluid in the boundary layer region.

(ii) The thermal buoyancy force behaves as a gratifying pressure gradient which accelerates nanofluid velocity in the regime of boundary layer.

(iii) The increasing value of the volume fraction of nanoparticles reduces the thermal conductivity of fluid, which in turn reduces the thickness of the boundary layer and increases the viscosity of fluid and as result the nanofluid velocity gets reduced in the proximity of the moving plate. The nanofluid velocity gets accelerated with progress of time.

(iv) Heat absorption has a tendency to decrease the nanofluid temperature whereas the nanoparticle volume fraction has a tendency to enhance the nanofluid temperature. As time progresses the nanofluid temperature is enhanced.

(v) Magnetic field, thermal buoyancy force, volume fraction of nanoparticles and heat absorption parameter have a tendency to increase the shear stress at the plate.

(vi) The rate of heat transfer at the plate gets raised with the augmentation of heat absorption parameter whereas the volume fraction of nanoparticles has an adverse effect on it. As time passes, the rate of heat transfer gets improved for the ramped case whereas it gets reduced for the isothermal case.

REFERENCES

1. S. U. S. Choi, *ASME FED 231/MD*, **66**, 99 (1995).
2. P. Keblinski, S.R. Phillpot, S.U.S. Choi, J.A. Eastman, *Int. J. Heat Mass Transf*., **42**, 855 (2002).
3. J. Buongiorno, *J. Heat Transf*., **128**, 240 (2006).
4. S. P. Jang, S. U. S. Choi, *J. Heat Transf*., **129**, 617 (2007)

5. W. Daungthongsuk, S. Wongwises, *Renew. & Sust. Energy Reviews*, **11**, 797 (2007).
6. S. M. Seyyedi, H. Bararnia, D. D. Ganji, M. Gorji-Bandpy, S. Soleimani, *Int. J. Thermal Sci*., **61**, 1 (2012).
7. M. M. Rashidi, E. Momoniat, M. Ferdows, A. Basiriparsa, *Math. Prob. Eng*., (Article ID 239082) (2014).
8. F. Garoosi, G. Bagheri, M. M. Rashidi, *Powder Tech*., **275**, 239 (2015).
9. F. Garoosi, B. Rohani, M. M. Rashidi, *Powder Tech*., **275**, 304 (2015).
10. A. Malvandi, D. D. Ganji, *Adv. Powder Tech*., **25**, 1369 (2014).
11. A. Malvandi, D. D. Ganji, *Particuology*, **24**, 113 (2016).
12. M. Sheikholeslami, M. Hatami, D. D. Ganji, *Powder Tech.*, **246**, 327 (2013).
13. M. Sheikholeslami, M. Gorji-Bandpy, R. Ellahi, A. Zeeshan, *J. Magnetism Magnetic Materials*, **369**, 69 (2014).
14. M. Sheikholeslami, M. Gorji-Bandpy, D. D. Ganji, *J. Taiwan Inst. Chem. Engineers*, **45**, 1204 (2014).
15. M. Sheikholeslami, D. D. Ganji, *Scientia Iranica B*, **21**, 203 (2014).
16. T. Hayat, T. Muhammad, A. Qayyum, A. Alsaedi, M. Mustafa, *J. Molecular Liquids*, **213**, 179 (2016).
17. R. Dhanai, P. Rana, L. Kumar, *Powder Tech*., **288**, 140 (2016).
18. S. Acharya, R. J. Goldstein, *J. Heat Transf.*, **107**, 855 (1985).
19. K. Vajravelu, J. Nayfeh, *Int. Commun. Heat Mass Transf.*, **19**, 701 (1992).
20. A. J. Chamkha, *Numer. Heat Transf.*, **32**, 853 (1997).
21. J. K. Lee, J. Koo, H. Hong, Y. T. Kang, *Int. J. Refrigeration*, **33,** 269 (2010).
22. M. Sheikh, Z. Abbas, *J. Magnetism and Magnetic Materials*, **396**, 204 (2015).
23. A. Mehmood, M. Saleem Iqbal, *J. Molecular Liq.*, **224**, 1326 (2016).
24. H. Mondal, P. De, S. Chatterjee, P. Sibanda, P. K. Roy, *J. Nanofluids*, **6,** 189 (2017).
25. R. Nandkeolyar, P. K. Kameswaran, S. Shaw, P. Sibanda, *J. Heat Transf.*, **136**, 122001 (2014).
26. M. A. A. Hamad, I. Pop, *Heat Mass Transf.*, **47**, 1517 (2011).
27. A. J. Chamkha, A. M. Aly, *Chem. Eng. Comm.*, **198**, 425 (2011).
28. A. Mahmoudi, I. Mejri, M. A. Abbassi, A. Omri, *Powder Tech.*, **269**, 275 (2015).
29. P. Chandran, N.C. Sacheeti, A.K. Singh, *Heat Mass Transf.*, **41**, 459 (2005).
30. G. S. Seth, M. S. Ansari, R. Nandkeolyar, *Heat Mass Transf.*, **47**, 551 (2011).
31. G. S. Seth, S. M. Hussain, S. Sarkar, *J. Porous Media*, **17(1)**, 67 (2014).
32. G. S. Seth, S. Sarkar, S. M. Hussain, G. K. Mahato, *J. Appl. Fluid Mech.*, **8(1)**, 159 (2015).
33. R. Nandkeolyar, G. S. Seth, O. D. Makinde, P. Sibanda, M. S. Ansari, *ASME J. Appl. Mech.*, **80**, 061003 (2013).
34. R. Nandkeolyar, M. Das, H. Pattnayak, *J. Orissa Mathematical Soc.*, **32**, 15 (2013).
35. S. M. Hussain, J. Jain, G. S. Seth, *Bull. Chem. Comm.*, **48(4)**, 659 (2016).
36. A. Khalid, I. Khan, S. Shafie, *The Europ. Physical J. – Plus*, **130**, 57 (2015).
37. S.M. Hussain, J. Jain, G. S. Seth, M. M. Rashidi, *J. Magnetism Magnetic Materials*, **422**, 112 (2017).
38. S. M. Hussain, R. Sharma, M. K. Mishra, G. S. Seth, *J. Nanofluid*, **6,** 840 (2017).
39. S. M. Hussain, J. Jain, G. S. Seth, M. M. Rashidi, *Scientia Iranica B*, **25**, 1243 (2018).
40. R. Sharma, S. M. Hussain, H. Joshi, G. S. Seth, *Diffusion Foundations*, **11**, 129 (2017).
41. H. F. Oztop, E. Abu-Nada, *Int. J. Heat Fluid Flow*, **29**, 1326 (2008).

ВЛИЯНИЕ НА АБСОРБЦИЯТА НА ТОПЛИНА ВЪРХУ МЕД-СЪДЪРЖАЩ МАГНИТО-НАНОФЛУИД НАД ИМПУЛСНО ДВИЖЕЩА СЕ ПЛАСТИНА С ПРОМЕНЯЩА СЕ ТЕМПЕРАТУРА

М. Р. Мишра[1], С. М. Хусаин[1*], Р. Шарма[2], Г. С. Сет[3]

[1] Департамент по математика, Университет О. П. Джиндал, Райгар, Индия

[2] Департамент по математика, GITAM, Бангалуру, Индия

[3] Департамент по приложна математика, Индийски институт по технология (ISM), Дханбад, Индия

Постъпила на 18 юли, 2017; коригирана на 6 август, 2018

(Резюме)

Изследвано е влиянието на абсорбцията на топлина върху транзиентния свободен конвективен поток на граничния слой на електропроводима, вискозна и несвиваема магнито-нанотечност над импулсно движеща се вертикална пластина с променлива температура. Използвана е нанотечност на основата на вода с добавени наночастици от титанов оксид, алуминиев оксид и мед. Математическият модел е получен с използване на модела на обемната фракция на наночастиците. Управляващият модел е решен аналитично с помощта на трансформационната техника на Laplace. Изразите за скоростта и температурата на течността, повърхностното триене и числото на Nusselt са получени за случаите на променяща се и на постоянна температура. Влиянието на различните физични параметри върху скоростта на нанотечността е илюстрирано графично, а числените стойности на повърхностното триене и числото на Nusselt **с**а представени в таблици. Получените резултати при променяща се и при постоянна температура са сравнени и е установено, че стойностите при изотермни условия са по-ниски от тези при променлива температура.

Bulgarian Chemical Communications, Volume 50, Issue 4 (pp. 631 – 637) 2018

Heat transfer performance of stainless steel, mild steel and aluminium target plate for various configurations of impinging air jet

K. Jeyajothi, P. Kalaichelvi*

Department of Chemical Engineering, National Institute of Technology, Tiruchirappalli-620015, Tamil Nadu, India

Received, July 17, 2018; Revised, August 3, 2018

In spite of several studies carried out on jet impingement on a plane surface, this work describes a new approach of comparing the heat transfer characteristics when three different materials are used as a target. The heated target plates are made up of stainless steel, mild steel and aluminium and are kept at different heights (2 to 8 mm) from a nozzle with diameter ranging from 0.5 to 3 mm. Measurements were done at the stagnation point using air jets with velocity of 6.4 and 9.2 m/s. The major characteristics of a jet impinging on a plane could be shown by straightforward experiments like spreading over method. Nusselt number was calculated for various values of jet Reynolds number and it was observed that adequate cooling of the plate is attained and enhanced with an increase in Reynolds number. It was also noted that the placement of the target is critical for optimum performance in practical applications. The increment in air velocity and Reynolds number improved heat transfer while increment in nozzle height decreased the performance at the stagnation point. Furthermore, three new reliable empirical correlations were established using the experiments performed.

Keywords: Impinging air jet, Target plate material, Round nozzle, Stagnation Nusselt number, Empirical correlation.

INTRODUCTION

Impinging jets, which are gas or liquid released with specific flow direction towards or over a target surface, provide efficient means for energy and mass transfer in many modern industrial processes. Some heat transfer applications of impinging jets includes stock material cooling, electronic components cooling, material forming, defogging of heated optical surfaces, internal cooling of turbine blades, heat treatment and cooling of critical machine parts [1]. They can be found in equipment involving heating, cooling or drying units, pulverisation, food processing, annealing of materials, building ventilation and cleaning operations. Removal of small particulates from surfaces and drying are some typical examples for mass transfer applications. Heat transfer due to impingement and abrasion caused due to landing and take-off jet devices were also studied [2–4].

The mechanism and structure of impinging jets should be understood to find the suitable methods of predicting jet performance. Optimized design of these kinds of installations need in-depth idea on the jet structure. Two-dimensional incompressible laminar slot air jet impingement on isothermally heated surface was studied for 100 ≤ Reynolds number (Re_D) ≤ 400 with different ratios of separation distance (nozzle-to-target plane distance) and jet width ranging from 1 to 8 mm to develop correlations between boundary layer thickness and stagnation Nusselt number (Nu_s) with respect to Re_D and separation distance [5]. Another experimental study of heat transfer behaviour of a confined slot laminar jet impingement has been performed for $190 \leq Re_D \leq 1537$ [6]. Investigation on the rate of cooling of a surface, due to the effect of multi-jet array, revealed an intense periodic oscillation in the Nusselt number (Nu) streamwise profile for different array spacing when the distance between the target plate and jet is fixed [7]. The peak in heat transfer coefficient increased by keeping smaller jet-to-plate spacing and diminished at larger spacing when the jet applied was cross flow [8]. In studies on an impinging square jet through cross flow, formation of vortices was noticed and their number, strength and location depended on the jet-to-cross flow velocity and on the jet-to-plate spacing [9]. Operation of jet at cross flow also has been reported to reduce Nu by 60% [10]. Protrusions on the confinement surface resistricted the jet inlet interaction with exhaust flow while enhancing heat transfer rates [11]. Studies on various other types of jets including elliptical jets, liquid jets and isothermal gas and flame jets were also reported [12–14]. Apart from experimental works, theoretical or empirical analysis and various types of computational methods were applied for studying impinging jets [15–17].

The main goal of the study is to determine and suggest the best performing plate material for achieving the best heat transfer characteristics out of

* To whom all correspondence should be sent:
E-mail: kalai@nitt.edu

the three selected target plates labelled as SS (stainless steel), MS (mild steel) and AL (aluminium). No such comparison of heat transfer characteristics of target material for impinging air jet was found in the literature and this work is the first attempt in that aspect. Operating configuration was optimized using different input parameters like air jet velocities, nozzle diameters, nozzle heights from target surface and Reynolds number and the outcome performance was measured in terms of Nu. Only few studies were performed on analysis of the combined effect of such input parameters. Therefore, this study would be a significant contribution to the heat transfer research on the air jet impingement.

Only stagnation point was considered for this study because our preliminary studies at different locations determining stagnation, local and average heat transfer coefficients showed that at the stagnation point, a maximum heat transfer occurred giving high Nu (data not shown). This study intended: (1) to examine the flow properties of the jet; (2) to explore the effect of Reynolds number and nozzle distance from stagnation point; (3) to develop empirical correlation of Nu_S for all three materials and (4) to validate the results from experiments with the theoretical values.

EXPERIMENTAL

Experimentation setup

The setup used for the experimentation consisted of three major components, *viz*., air supply system, heated target plate and monitoring instrumentation. Fig. 1 elucidates the schematics of the major components of the setup. The working fluid (air) is compressed through the compressor (CEC model A829, 7 kg/cm^2, 760 rpm, 120 L capacity with single-phase induction motor, Prv-15 model pressure with air filters, regulator, bypass valve and a pressure gauge with 0-14 kg/cm^2 range). Then, the air is passed through a flowmeter (RG-05 model glass tube rotameter with pressure rating of 40 bar and range 0-100 Lpm) to a flexible tube at the end of the air supply system which is connected to a duct and a round-edged nozzle is fitted to this duct. As per the experimental configuration, the nozzle with corresponding dimension is used at the end of the duct. A Kapton heater (vari-volt type 10-p capacity 10A) with a uniform heating element (3950 W/m^2) inserted in an insulator assembly was used to heat the target plate. The power supplied was monitored by employing a voltmeter, measuring the potential difference and an ammeter, measuring the current flow. A digital anemometer (Lutron model: AM-4201) and a mercury thermometer were used to measure the air jet velocity and temperature, respectively. The target was placed perpendicularly to the axis of the impinging jet. The spacing height between the nozzle and the plate was adjusted by a moving support, which facilitated vertical and horizontal movements. The air jet from the nozzle impinged normally onto the center of the heated target and a precisely calibrated K-type thermocouple was used to record the plate surface temperature.

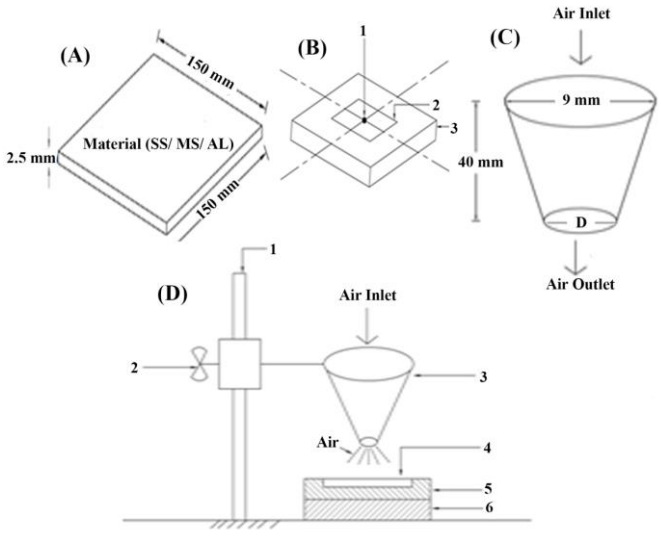

Fig. 1. (**A**) Target plate (**B**) Plate insulator heater box [1–Stagnation point, 2–Target plate, 3–Fire brick chamber with Kapton heater] (**C**) Nozzle element [D–0.5 to 3 mm] (**D**) Experimental arrangement [1–Stand, 2–Height adjusting clamp, 3–Jet nozzle, 4–Target surface, 5–Heating chamber, 6–Base]

Experimental procedure

Experiments were carried out for different nozzle diameters (D) and various nozzle-to-plate distances at two air flow velocities (v) (as shown in Table. 1). The air supply from the compressor was controlled by the flowmeter to vary the air velocity. Heating by the heater and cooling due to impinging jet occurred simultaneously. A steady state condition was achieved when the heat loss by convection from the top surface of the plate equals the heat conducted to the top surface of the heated plate. After the steady state was achieved for 45 min, the surface temperature of the plate was recorded. A total of 108 measurements were made with the thermocouple installed for measuring the local temperatures of the heated target surface. The measurements for all experiments were performed in a symmetric mode and the acquisition of all experimental data was at a steady state. The configuration used in this study is compared to some of the impinging jet configurations from the existing literature in Table 2.

Estimation of heat transfer characteristics

The characteristics of heat transfer were deduced by converting the temperature data into heat transfer information. The stagnation heat transfer coefficients were determined to calculate the removal of heat from the test surface and to obtain an accurate convective heat flux [6]. Reynolds number was calculated with the air flow parameters using Eq. 1.

$$Re_D = \frac{D \times v \times \rho}{\mu} \qquad (1)$$

where, μ is the viscosity of air; ρ is the denisity of air.

At the steady state conditions, the stagnation heat transfer coefficient (h_S) was derived for the plate with thickness of 2.5 mm at the center of the plate (i.e., distance (x) from the target plate center = 0). By combining the Fourier's law with the Newton's law of cooling (Eq. 2), the local convective heat transfer at the stagnation point was derived by Eq. 3 and the stagnation Nusselt number (Nu_S) was calculated from Eq. 4.

$$-KA \left.\frac{dT}{dx}\right|_{x=2.5} = hA\,(T_w - T_a) \qquad (2)$$

$$h_S = \frac{2.5 \times q}{(T_{w,x} - T_a)} \qquad (3)$$

where, A is the surface area of the plate; K is the thermal conductivity of air; $T_{w,x}$ is the temperature of the wall at a distance x; T_a is the temperature of the air; T_w is the temperature of the wall; h is the heat transfer coefficient; q is the convective heat flux on the top of the plate.

$$Nu_S = \frac{h_S \times D}{K} \quad \text{at x =0} \qquad (4)$$

Table 1. Operational parameters

Parameter	Range
Nozzle diameter	0.5, 1.0, 1.5, 2.0, 2.5 and 3.0 mm
Height of nozzle above the plate	2, 4 and 8 mm
Air velocity	6.4 and 9.2 m/s
Reynolds number	192.61 to 1661.26
Target plate thickness	2.5 mm

Table 2. Comparison of experimental configurations

References	D (mm)	H/D	Re_D	Nozzle geometry	Target plate
Chou and Hung [5]	1, 1.5	1-8	100-400	RN	SS
Lin *et al.* [6]	5	1-20	190-1537	OP	SS
Rady and Arquis [11]	1, 1.5	1-4	250, 500	CN	SS
Arjocu and Liburdy [12]	0.5, 1.5	1-6	300, 1500	SA	AL
Morris *et al.* [13]	3.18, 6.35	1-4	8500-13000	CN	SS
Meola [21]	2-12	1.6-20	200-100000	RN, RectO	SS
Mahgoub [22]	2.7-11	11	10^5 - 10^6	RectO	AL
Present study	0.5-3	0.67-16	192.61-1661.26	R-LTN	SS,MS,AL

Abbreviations: SA=square array, OP=jet orifice plate, R-LTN=round long-throat nozzle, CN= circular nozzle, RN=round nozzle, RectO=rectangular opening, SS=stainless steel, MS=mild steel, AL=aluminium

Uncertainty analysis

The uncertainty in Nusselt number was predisposed mostly by the determination of heat flux and wall temperature. The surface heat flux was affected by the difference in the plate dimensions that was claimed in the supplier description to be less than ±7% of the normal value. The uncertaintiy in the values measured by a calibrated flow meter was ±0.5% and that of the thermocouple was ±0.75%. The Nusselt number uncertainty was acknowledged to be optional and stretched from 4.5 to 10.43% [18]. Thus, the cumulative uncertainty was found to be <9%, which is well within the acceptable limits (±15%) [14,19] in experimental data.

RESULTS AND DISCUSSION

The foremost inflection of the present study is heat transfer characteristics at the stagnation point of an unconfined jet on three different target materials. A sequence of experimental trials was conducted to discover the flow and heat transfer characteristics with the selected jet configurations having three different nozzle heights (H) above the plate for each plate material. This set of experiments was repeated with each of the 6 nozzles (with D = 0.5 to 3 mm) leading to 54 performance outcomes for each of the two air velocities. The effect of nozzle height or nozzle-to-plate distance on Nu_S for the various nozzle diameters is compared in Figs. 2 and 3 for the three target materials (SS, MS and AL), where v = 6.4 and 9.2 m/s, respectively. It is seen that the Nu_S increased with increase in the velocity for every nozzle, while the Nu_S decreased as the height increased. The decrease in Nu_S was more rapid when H was increased from 2 to 4 mm. This may be mainly due to the reduction of air flow as the distance between nozzle and plate was increased [6]. This effect was witnessed because of higher air flow dispersion. At lower height, the air flow was confined at the impinging point and hence, the heat transfer was higher at lower heights. Therefore, the height with maximum heat transfer (2 mm) was considered for further calculations. Among the three materials, SS showed high Nu_S values while AL had the least Nu_S values. When $H \leq 4$ mm, the Nu_S of the materials where close to each other for $D \leq 1.5$ mm. As D increased above 1.5 mm, SS and MS had nearer Nu_S, and AL had a notably lower Nu_S. Thus, the low heat transfer ability of AL is clearly evident. The Reynolds number varies according to nozzle diameter and the air jet velocities on which it is dependent. Re_D values calculated for this study ranged from laminar to transient regime. The effects of Re_D on Nu_S when H = 2 mm and v = 9.2 m/s were compared for the target materials in Fig. 4, which reveals that the Nu_S values were higher for higher Re_D. As the Re_D increased, the Nu_S distribution became slightly convex. The comparable trend of increase or decrease in the Nu_S with change of materials was perceptible. It is further inferred that the bigger the nozzle diameter, the higher is Nu_S because of the higher Re_D associated with the larger nozzles [6]. Moreover, the smaller nozzle could have delivered a lower quantity of air compared to that of the bigger nozzle. This, in turn, has affected the Nu_S and subsequently, the heat transfer characteristics. Flow resistance with the smaller nozzle was yet another factor affecting the Nu_S.

The heat transfer coefficient condensed in dimensionless form as Nu could be related to the Reynolds number according to Eq. 5 [20], which conveys that the ratio of total heat transfer corresponding to conductive heat transfer is proportional to the momentum flux:

$$Nu \propto Re_D^{\,a} \tag{5}$$

where, α is the power law constant and its value ranges from 0.5 to 0.99 in the experiments depending on the range of Reynolds number.

Meola [21] and Mahgoub [22] investigated various power law equations at the stagnation zone and stated that the Nusselt numbers could be correlated in the following form:

$$Nu = C_1 Re_D^{\,C_2} \tag{6}$$

where, C_1 and C_2 are empirical constants obtained from experimental data. In particular, the heat transfer near to the stagnation point may be computed according to Eq. 6 for the laminar and transient regime ($276.88 \geq Re_D \leq 1661.26$ at a velocity of 9.2 m/s) by calculating the correlation factors from Fig. 4 for all 3 materials, and the data sets are reduced to Eqs.7 (SS), 8 (MS) and 9 (AL). Their corresponding correlation coefficient (R^2) values are 0.995, 0.993 and 0.961, respectively.

$$Nu_S = 0.425\, Re_D^{\,0.892} \tag{7}$$

$$Nu_S = 0.393\, Re_D^{\,0.891} \tag{8}$$

$$Nu_S = 0.527\, Re_D^{\,0.805} \tag{9}$$

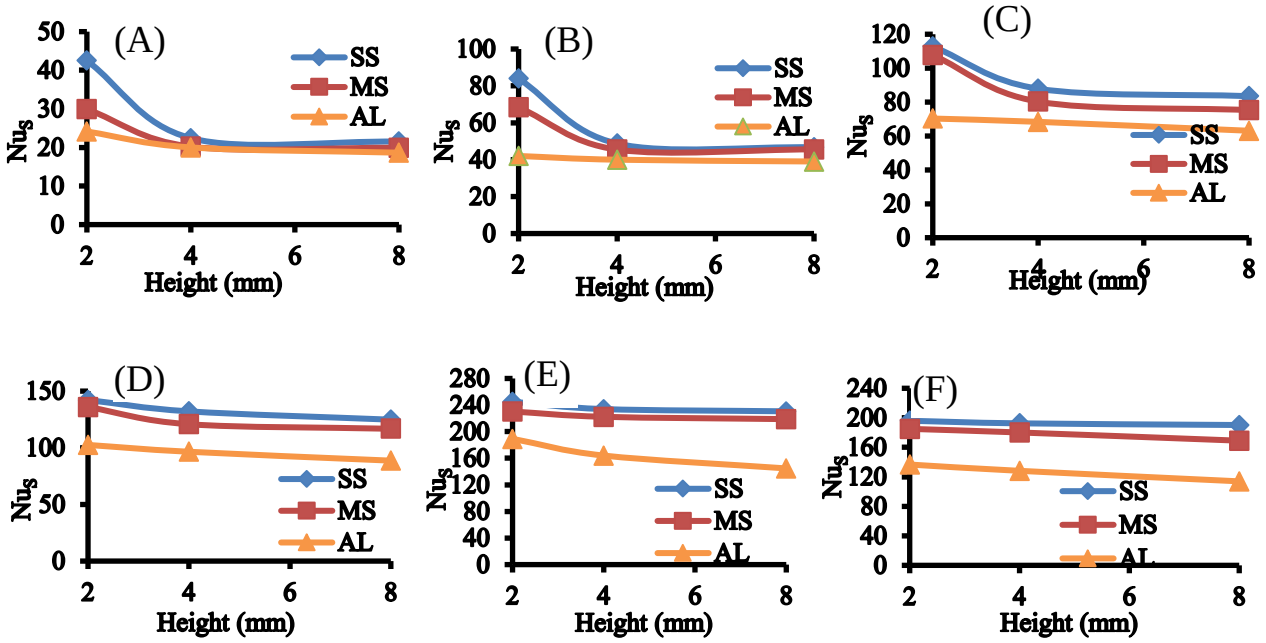

Fig. 2. Effect of nozzle height (H) on the Nu_S at air velocity (v) of 6.4 m/s for various nozzle diameters (**A**) 0.5 mm; (**B**) 1 mm; (**C**) 1.5 mm; (**D**) 2 mm; (**E**) 2.5 mm; (**F**) 3 mm

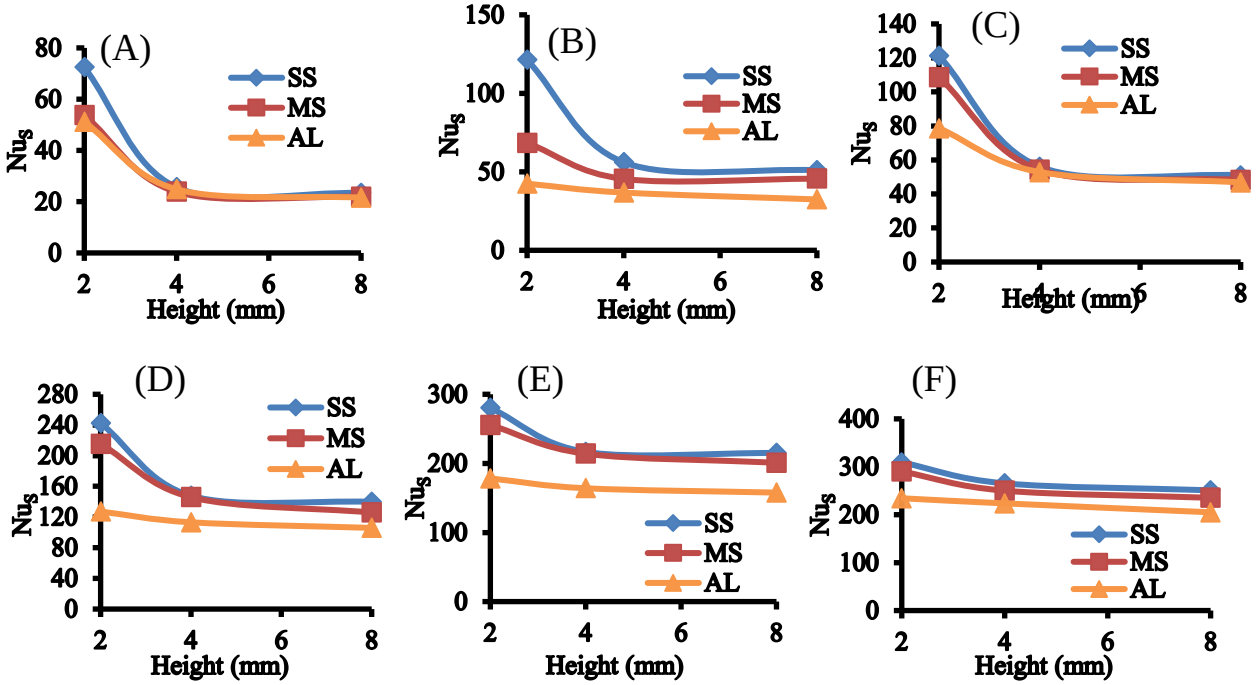

Fig. 3. Effect of nozzle height (H) on the Nu_S at air velocity (v) of 9.2 m/s for various nozzle diameters (**A**) 0.5 mm; (**B**) 1 mm; (**C**) 1.5 mm; (**D**) 2 mm; (**E**) 2.5 mm; (**F**) 3 mm.

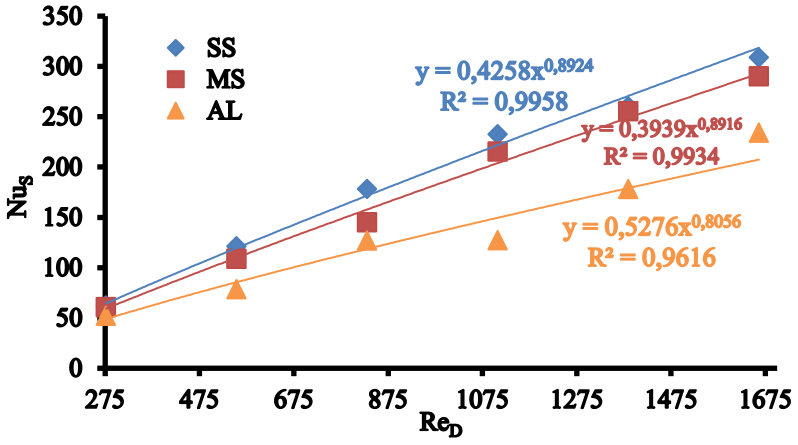

Fig. 4. Relationship between Re_D and the maximum Nu_S obtained (when H = 2 mm and v = 9.2 m/s)

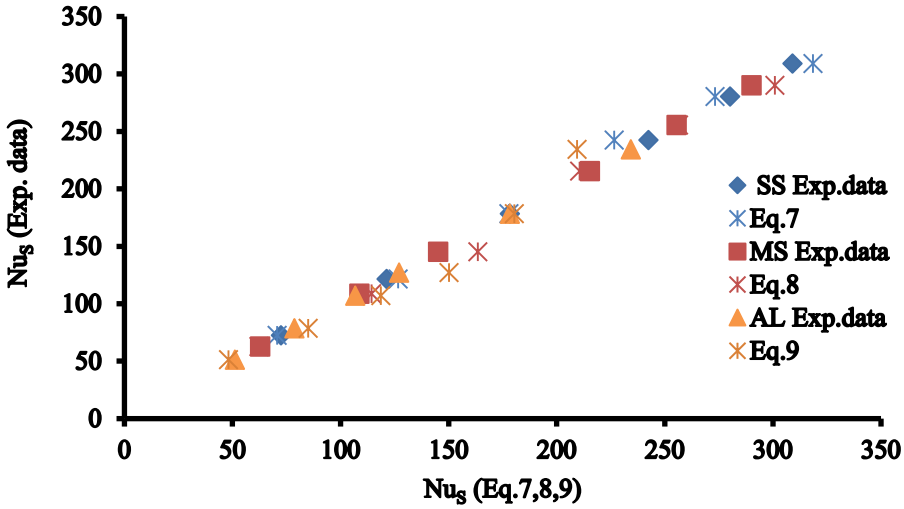

Fig. 5. Validation of experimental (Exp.) Nu_S data against empirical Nu_S data obtained from Eqs. 7, 8 and 9.

The Nu_S values obtained from these empirical correlations were plotted against the experimental values in Fig. 5. One could observe that the experimental values are closer to the empirical values derived from Eqs. 7, 8 and 9. The average deviation between the experimental and predicted values for SS, MS and AL were found to be 3.17%, 4.17% and 9.16%, respectively, and these deviations are well within the permissible error of 15% [6]. Thus, the empirical correlations developed in this study were validated and the best performing material among the three was SS.

CONCLUSIONS

Effects of forced convection heat transfer over three different horizontal flat plates in the stagnation region were investigated with an impinging air jet. The experiments carried out for different values of nozzle diameter, flow velocity, and nozzle height revealed that the stagnation Nusselt number is at the peak for the least nozzle location height for all nozzles albeit the variations in nozzle diameter and air velocity. Higher air velocity with increased Reynols number yielded better heat transfer performance. A new empirical correlation was derived for each target material and the predicted values were validated against the experimental data. Stainless steel plate showed evidently better heat transfer ability under the experimental conditions of this study.

REFERENCES

1. J. Ferrari, N. Lior, J. Slycke, *J. Mater. Process. Technol.*, **136**, 190 (2003).
2. H. Martin, *Adv. Heat Transfer*, **13**, 1 (1977).
3. K. Jambunathan, E. Lai, M. A. Moss, B. L. Button, *Int. J. Heat Fluid Flow*, **13**, 106 (1992).
4. C. D. Donaldson, R. S. Snedeker, *J. Fluid Mech.*, **45**, 281 (1971).
5. Y. J. Chou, Y. H. Hung, *J. Heat Transfer*, **16**, 479 (1994).
6. Z. H. Lin, Y. J. Chou, Y. H. Hung, *Int. J. Heat Mass Transfer*, **40**, 1095 (1997).
7. I. Sezai, L. B. Y. Aldabbagh, in: The effect of jet-to-jet spacing on the cooling performance of impinging

jet arrays, Proc. 3rd Int. Conf. Comput. Heat Mass Transfer, Banff, Canada, 2003, p. 26.
8. R. J. Goldstein, A. I. Behbahani, *Int. J. Heat Mass Transfer*, **25**, 1377 (1982).
9. L. B. Y. Aldabbagh, I. Sezai, A. A. Mohamad, *J. Heat Transfer*, **125**, 243 (2003).
10. S. Al-Sanea, *Int. J. Heat Mass Transfer*, **35**, 2502 (1992).
11. M. Rady, E. Arquis, *Appl. Therm. Eng.*, **26**, 1310 (2006).
12. S. C. Arjocu, J. A. Liburdy, *J. Heat Transfer*, **122**, 240 (2000).
13. G. K. Morris, S. V. Garimella, R. S. Amano, *J. Heat Transfer*, **118**, 562 (1996).
14. R. Viskanta, *Exp. Therm. Fluid Sci.*, **6**, 111 (1993).
15. S. J. Downs, E. H. James, *ASME*, 87-HT-35 (1987).
16. S. Polat, B. Huang, A. S. Mujumdar, W. J. M. Douglas, *Annu. Rev. Numer. Fluid Mech. Heat Transfer*, **2**, 157 (1989).
17. F. F. Grinstein, E. Gutmark, T. Parr, *Phys. Fluids*, **7**, 148 (1995).
18. R. J. Moffat, *J. Fluid Sci.*, **1**, 3 (1988).
19. C. F. Ma, Q. Zheng, H. Sun, K. Wu, K. Horii, *Exp. Therm Fluid Sci.*, **17**, 238 (1998).
20. J. N. B. Livingood, P. Hrycak, Lewis Research Centre, NASA TM X-2778, (1973).
21. C. Meola, *Heat Transfer Eng.*, **30**, 221 (2009).
22. S. E. Mahgoub, *Ain Shams Eng. J.*, **4**, 605 (2013).

ЕФЕКТИВНОСТ НА ТОПЛОПРЕНОСА НА ПЛАСТИНИ ОТ НЕРЪЖДАЕМА СТОМАНА, МЕКА СТОМАНА И АЛУМИНИЙ ЗА РАЗЛИЧНИ КОНФИГУРАЦИИ НА УДАРНА ВЪЗДУШНА ДЮЗА

К. Джеяджоти, П. Калайчелви*

Департамент по инженерна химия, Национален технологичен институт, Тиручирапали- 620015, Тамил Наду, Индия

Постъпила на 17 юли, 2018; коригирана на 3 август, 2018

(Резюме)

Описан е нов подход за сравняване на характеристиките на топлопренос при ударна струя върху равна повърхност от различен материал. Нагреваемите пластини са изготвени от неръждаема стомана, мека стомана и алуминий и са разположени на различни разстояния (от 2 до 8 mm) от дюзата с диаметър от 0.5 до 3 mm. Измерванията са проведени при точката на стагнация с използване на въздушна струя със скорост от 6.4 и 9.2 m/s. Основните характеристики на струйния удар върху повърхността могат да се илюстрират чрез прост експеримент, например, по метода на разпространението. Числото на Nusselt е пресметнато за различни стойности на струйното число на Reynolds и е установено, че се постига адекватно охлаждане на пластината, което се подобрява с нарастване на числото на Reynolds. Установено е също, че позицията на пластината е критична за оптималната ефективност при практическо приложение. Повишаването на скоростта на въздуха и на числото на Reynolds води до подобряване на топлопреноса, докато повишаването на височината на дюзата влошава ефективността в точката на стагнация. На основата на проведените експерименти са намерени три нови корелации.

Bulgarian Chemical Communications, Volume 50, Issue 4, (pp. 638 – 646) 2018

Study of 4-chlorophenol biological treatment using yeast and mold isolated from industrial and petroleum wastewaters (Imam Khomeini Port, Mahshahr)

A. Alirezaei[1], M. Bayat[1*], M. Alimohmmadi[2], S. Hashemi[3]

[1]*Department of Microbiology, Science and Research branch, Islamic Azad University, Tehran, Iran*
[2] *Department of Environmental Health Engineering , School of Public Health, Tehran University of Medical Science, Tehran, Iran*
[3]*Department of Medical Parasitology and Mycology, School of Public Health, Tehran University of Medical Science, Tehran, Iran*

Received November 23, 2017; Revised February 15, 2018

Phenolic derivatives are some of the most toxic pollutants in the environment. Chlorophenols are the most toxic pollutants of water and wastewater. Since 4-chlorophenol is a highly soluble compound in water, it is abundantly found in water and wastewater. Because of high costs, high energy consumption and in some cases environmental inconsistency of the chemical and biological removal methods, biochemical decomposition of 4-chlorophenol is very important. In the present study, 13 strains of bacteria and 6 strains of yeast and mold were purified and isolated from Shahid Tondgooyan wastewater treatment plant (Imam Khomeini Port, Mahshahr), which lasted about 15 days. Then, the ability of each microorganism isolated in the presence of 100 ppm of 4-chlorophenol was studied and two microbial species suitable for TY_1 and TY_2 were selected for use in a mixed microbial culture. 4-Chlorophenol decomposition was performed in the presence of 100 ppm of 4-chlorophenol. In this research, one of the most important factors affecting 4-chlorophenol degradation by mixed microbial culture including glucose concentration with 2 and 5 g/l was investigated. After examination, the microbial species suitable for TY_1 and TY_2 were able to completely remove 100 ppm of 4-chlorophenol, so that the TY_1 strain was removed completely after 45 h and the TY_2 strain after 21 h. Using a mixture of TY_1 and TY_2 strains (50/50) in the presence of 2 g/l of glucose, 100 ppm of 4-chlorophenol were completely removed after 18 h. Based on the 18SrRNA gene sequence analysis, the molecular identification of the two superior strains was carried out, both belonging to the genus *Trichosporon*. Considering the high potential of *Trichosporon* species, including their potential applications in increasing oil recovery and eliminating pollutants, it would be hoped that the further exploration of strains characteristics and the search for new native strains could play a crucial role in the application of native strains in the oil industry.

Keywords: Chlorophenol wastewater treatment, Shahid Tondgooyan, *Trichosporon*, Eliminating pollutants

INTRODUCTION

With the development of societies and the creation of different technologies and industries, despite the diminution of many human problems, several other problems have been added. One of the most important issues that have arisen with the emergence of new industries is the loss of environmental resources and pollution of the environment, including water and soil, by various chemical pollutants from the output of various industries. One of the most important human goals in recent decades was protecting the environment against the growing trend of pollution. Water resources are some of the most important biological resources and protecting and cleaning them from pollutants are among the most important tasks. Phenol and phenolic derivatives are considered among the most significant pollutants in the environment by the Environmental Protection Agency [1]. These compounds are used in several industrial processes for the production of chemicals such as pesticides, explosives, drugs, textiles, paints and resins. Phenolic compounds are produced not only from human activities, but also naturally by the decomposition of leaves and wood. As a result, these materials are found in soils and sediments, and often lead to contamination of groundwater and wastewater [2, 3].

Due to the high toxicity of these compounds and the pathogenic properties of some of them, various methods have been used to remove and analyze these toxic compounds, among which biodegradation methods are some of the most effective and easy methods for the removal and decomposition of this type of pollutants. In these methods, microorganisms are used as a decomposing agent of toxic compounds.

The origin of environmental pollution with chlorophenols

Chlorophenols are abundant in urban sewage, industrial outlets and waterways, which creates serious health risks for humans due to high toxicity.

* To whom all correspondence should be sent:
E-mail: Dr_mansour_bayat@yahoo.com

Meanwhile, due to their relatively high solubility in water, these compounds easily move in different water environments and pollute groundwater [3, 4]. Because of the stability and resistance of chlorophenols, these materials are not only found in surface and underground waters, but also in soils and sediments [4]. Also, the stability of these compounds in wastewater treatment systems and their mixtures with other chemicals that can be consumed by microorganisms also disrupt the decomposition and removal of these chemicals [5, 6].

The wastewater from these activities with varying concentrations of chlorophenols inhibits the microorganisms that reduce the chemical oxygen demand (COD) and also prevent the use of nitrogen and phosphorus [5].

Conventional methods for the removal of chlorophenols from the environment

There are various methods for the removal and decomposition of chlorophenols, which can be referred to as physical, chemical and biological methods. There are other methods, such as burning and incineration and landfilling, which are the oldest methods for removing pollutants. Different absorption methods, washing with gas and liquid phase, solvent extraction in solid and liquid phase, chemical oxidation, electrochemical methods, catalytic methods using photocatalytic and sonochemical degradation and enzymatic methods are some physical and chemical methods for removal of chlorophenols in the solid phase like soils and sediments, and in the liquid phase, such as water and wastewater. These methods are subject to serious limitations. High costs, hazardous and harmful by-products, disposal of chemical reagents and solvents in the environment and recontamination of environment are among the limitations of these methods [6].

Biodegradation of chlorophenols and effective microorganisms

Today, the biodegradation of aromatic compounds by microorganisms is of particular interest. Many microbial species, including bacteria and fungi, can remove chlorophenols as the only carbon source. Due to the use of decomposing microorganisms in chlorophenols biodegradation, the microbial cultures are classified into two main groups, which are discussed below.

Pure microbial cultures

There are many microorganisms, including bacteria and fungi that can remove chlorophenols. In Table 1, a list of aerobic chlorophenol biodegrading microorganisms is presented as the only carbon source [7, 8].

Mixed microbial cultures

Mixed microbial culture is a group of different species of microorganisms that act as a population together. Examples of microbial collections are found in active sludge ponds; biofilms such as those found in trickling filters and also in various soil ecosystems. Mixed cultures have been used in fermentation processes, such as food fermentation and alcohol production, production of yogurt and cheese, as well as in wastewater and contaminated water treatment from very old times.

In microbial collections, organisms work together in a complex system, all of which utilize each other's activities in the population. For example, microbial collections are more efficient in complex organic waste degradation than single species or even mixtures mixed with microorganisms and with a greater variety of metabolic capabilities [9, 10].

MATERIALS AND METHODS

General stages of the project

- Sampling
- Stages of phenol degrading microorganism culture
- Isolation of molds and yeast phenol decomposing fungi
- Measuring chlorophenol removal
- Determining the identity of selected fungi
- Molecular identification of superior strains

Nutrient and mineral culture media

The culture media used in this study can be used for the isolation of fungi from bacteria which are sabouraud dextrose agar (SDA), sabouraud dextrose agar with chloramphenicol (SC) and potato dextrose agar (PDA). In the next step, for the final purification of yeast from mold, specific culture media, such as yeast peptone agar (YPG) and malt agar extract (YM) were used.

Mineral salt medium (MSM) and trace elements used in enrichment and biodegradation of pollutants are shown in Tables 2 and 3 [12]. 4-Clorophenol of 98% purity, used in experiments, was purchased from Merck Group in Germany. Table 4 presents the 4-chlorophenol specifications. Due to the growth of microorganisms in 4-chlorophenol mineral environments, glucose was used as a substrate for growth supplement or primary substrate in the enrichment and recovery phases of the wastewater. In cases where glucose supplement substrate was added to the environment, its concentration was considered 2 and 5 g/l [13].

Table 1. List of chlorophenols and their degrading microorganisms [11]

Microorganisms	Chlorophenols
Desulfovibrio dechloracetivorans (ATCC700921), *Alcaligenes sp.*, *Ralstonia sp.*, *Azotobacter sp.*, *P. putida*, *Cystobacteri sp.*, *P.cepacia*	2-Chlorophenol
Desulfomonile tiedjei	3-Chlorophenol
P. putida, *Comamonas testosteroni JH5*, *P.cepacia*, *Rulstonie eutropha*, *Alcaligenes sp.*, *Azotobacter sp.*, *Ralstonia sp.*, *Candida tropicalis*, *Fusarium flocciferium* *Penicillium*, *Aspergillus*, *Graphium*, *Phanerochaete*, *Fusarium sp.*	4-Chlorophenol
Desulfitobacterium dehalogenans, *Desulformonile tiediei*, *Ralstonia sp.*, *Clostridium sp.* *Burkholderia cepacia*, *P. pickettii* (DTP0606).	2,4 Dichlorophenol
Desulfomonile tiedjei, *Desulfovibrio dechloracetivorans*	2,5 Dichlorophenol
Desulfitobacterium dehalogenans(JW/IU-DC1), *Mycobacterium chlophenolicum*, *P.cepacia* *Azotobacter sp.*, *P.pickettii* (DTP0606), *Desulforibrio dechloracetivorans*, *Ralstonia sp.*	2,6 Dichlorophenol

Microbial cultures

Since the main objective of the study was the elimination of 4-chlorophenol by native microorganisms, the wastewater treatment unit was used as a source of microbial isolation. The wastewater and sludge used in these experiments were prepared from different parts of the Shahid Tondgooyan Wastewater Treatment Plant (Fig. 1)

Pre-treatment of microbial source and selection of microorganisms

Due to the increased ability to remove pollutants by microorganisms in wastewater and sludge, a series of 4-chlorophenol pollutant adaptation and enrichment was performed on it as follows.

Adaptation of sludge and wastewater of Shahid Tondgooyan Petrochemical Plant

Since the microorganisms of the wastewater at first had a negligible growth, the adaptation operation was done in presence of auxiliary substrates on the sludge and wastewater to enhance the ability to remove and then isolate the microbial species. Aeration was done each time to work with the wastewater and to activate its microorganisms [14, 15].

Fig. 1. Sampling location

Table 2. Specifications of mineral salt media used in the experiments [16]

Mineral salt	NH_4NO_3	$MgSO_4.7H_2O$	$CaCl_2.2H_2O$	$KHPO_4$	KH_2PO_4
Salt concentration (g/L)	0.5	0.2	0.02	0.5	0.5

Table 3. Specifications of trace elements used in the experiments [16]

Trace elements	$MnSO_4.H_2O$	$FeSO_4.7H_2O$	$CuSO_4.5H_2O$	$ZnSO_4.7H_2O$	$NaMoO_4$	$CoCl_2.7H_2O$
Salt concentration (g/L)	0.025	0.15	0.025	0.02	0.034	0.053

Table 4. Specifications of 4-chlorophenol used in the experiments

Molecular formula	Molecular mass (g/mol)	Density (g/cm^3)	Melting point (°C)	Boiling point (°C)	% Purity
C_6H_5OCl	128.56	306.1	45-43	220	98

To initiate the experiments, salt culture medium and trace elements salt solution was used. To strengthen the wastewater and sludge samples and the necessity of existence of a stimulus substrate for

the growth of microorganisms along with toxic contamination of 4-chlorophenol, 2 and 5 g/l glucose were also used.

Adaptation was performed in 5 stages for 60 days. In each stage, 10% of the previous culture was transferred to the fresh mineral culture medium containing pollutants [16]. Finally, the microorganism was separated from the final habituation stage. The pollutant concentration used at each stage of the various habituation operations varied from low to high and finally was 100 ppm.

Isolation and purification of microorganisms

After performing the habituation and enrichment on sludge and effluent and ensuring the removal of 4-chlorophenol by it at the applied concentration range, purification of microbial culture was done by culturing the microorganisms obtained from the last enrichment step on plates containing PDA and using streaking technique.

Isolation of phenol-decomposing mold and yeast fungi

After enhancement of microbial strains, sabouraud dextrose agar (SDA), sabouraud dextrose agar with chloramphenicol (SC) and potato dextrose agar (PDA) were used to isolate fungi from bacteria. In the next step, the yeast strains from mold from specific culture media, such as yeast peptone agar (YPG), malt agar extract (YM) were used for the final purification. Then, each of the pure colonies was examined macroscopically and microscopically.

4-Chlorophenol biodegradation using isolated microorganisms

To perform 4-chlorophenol biodegradation tests, all decomposition tests were first performed on pure microbial species and then, after obtaining the desired results, the main experiments were carried out on a mixed microbial culture. All experiments in this section were carried out under operating conditions of 30 °C, 200 rpm in 100 ml Erlenmeyer flasks in replicate [17].

Biodegradation using single microbial species

After purification and separation of the species obtained from the habituation and the enrichment of wastewater and sludge, biodegradation was first done on single species.

The 4-chlorophenol biodegradation experiments were performed using microorganisms isolated from the enrichment phase in the presence of 100 ppm of 4-chlorophenol. Also, the effects of glucose concentration as growth supplement substrate were investigated at 2 and 5 g/l on 4-chlorophenol biodegradation [17, 18].

4-Chlorophenol biodegradation using mixed microbial culture

At this stage, a mixture of isolated microorganisms from the enrichment phases on sludge and wastewater was used as a mixed microbial culture, which is described below.

In this part of the experiments, a mixture of isolated microorganisms was used as a mixed microbial culture. The experiments were conducted as follows: after ensuring the 4-chlorophenol decomposition by isolated species from the enrichment stages, subsequent experiments were carried out using a mixed culture of isolated microbial species. All experiments were carried out at a concentration of 100 ppm of 4-chlorophenol and 2g/l of glucose [18-20].

Molecular identification of superior strains

A. Extracting genomic DNA from isolated strains: Direct extraction of DNA of isolated strains was carried out using a phenol-chloroform method from a solid and liquid medium.

B. Quantitative analysis of DNA: A quantitative analysis is performed on each sample using a biophotometer. Each sample was studied at a dilution of 1:50 in water and in the absorption of 230/260, 280/260.

C. Identification of fungal strains by direct PCR method based on the sequence of ITS area.

D. Universal primers: Most fungi were identified using the ITS area. In this study, universal strains primers (ITS1 and ITS4) were used to identify the selected strains [21, 22].

Microbial source pre-treatment experiments

After performing a series of adaptation experiments (5 stages for 60 days) and enrichment (5 stages for 15 days), on the sludge and effluent, the selected microorganisms were purified and isolated for 4-chlorophenol biodegradation.

RESULTS

Isolation of microorganisms

In this study, sabouraud dextrose agar (SDA), sabouraud dextrose agar with chloramphenicol (SC) and potato dextrose agar (PDA) were used to isolate the fungi from bacteria. In the next step, for the final purification of yeast strains from mold, specific culture media such as yeast peptone agar (YPG) and malt agar extract (YM) were used.

After adaptation and enrichment of the collected samples and purification of strains, a total of 19

bacterial species (13 strains of bacteria and 6 strains of yeast and mold) were isolated and purified, which were morphologically examined (Table 5). Fig. 2 shows the macroscopic forms (observation) and Fig.3 shows the microscopic forms of the isolated strains.

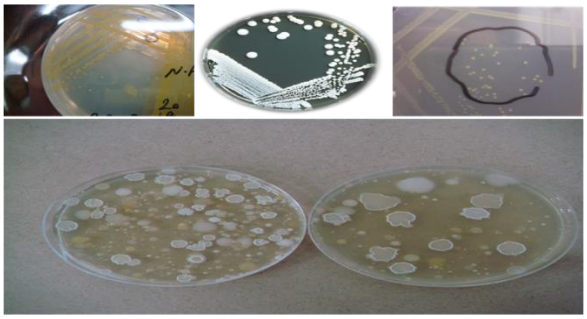

Fig. 2. Macroscopic observations of the isolated microorganisms.

Finally, 2 microbial strains in screening showed the best results in 4-chlorophenol biodegradation. Using microscopic and macroscopic observations and biochemical tests, it was shown that TY_1 and TY_2 strains isolated from the reversible wastewaters are a yeast species.

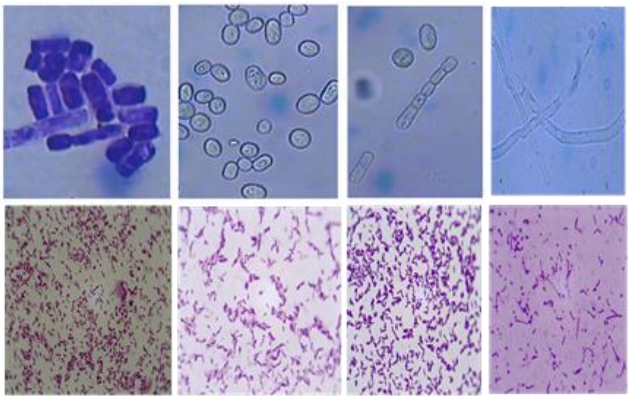

Fig. 3. Microscopic observations of isolated microorganisms

4-Chlorophenol degradation using TY_1 isolated microorganism

After examining the apparent form of the TY_1 isolated microorganism, the microorganism growth curve was examined and drawn up. In Fig. 4 the cellular growth curve of the TY_1 isolated microorganism is shown.

After examining the growth conditions and selecting the end of the logarithmic phase of growth as an appropriate age for microbial inoculation, the 4-chlorophenol 100 ppm decomposition was performed by TY_1 microbial species. In Fig. 5 the 4-chlorophenol biodegradation process is shown in terms of time by TY_1 isolated microorganism. The TY_1 microorganism is capable of completely degrading 100 ppm of 4-chlorophenol in about 45 h.

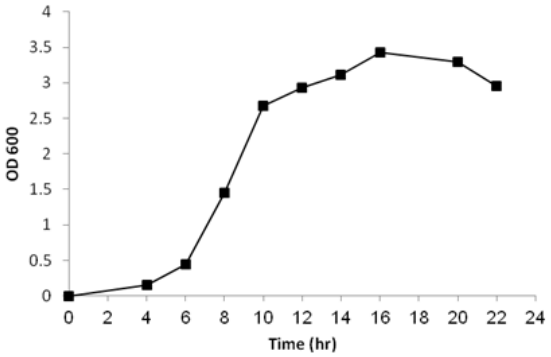

Fig. 4. TY_1 isolated microorganism growth curve

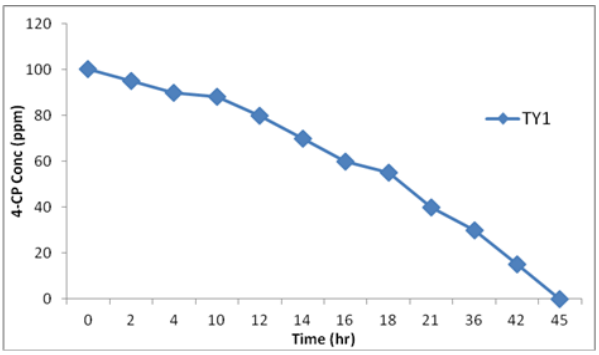

Fig. 5. Changes in 4-chlorophenol concentration with time by TY_1 isolated microorganism.

4-Chlorophenol degradation using TY_2 isolated microorganism

After examining the appearance of the TY_2 species, the microorganism growth curve was examined and drawn up. Fig. 6 shows the TY_2 isolated microorganism growth curve. After examining the growth conditions and selecting the end of the growth logarithmic phase as an appropriate age for microbial inoculant, the 100 ppm 4-chlorophenol degradation was performed by TY_2 microbial species. Fig. 7 shows the 4-chlorophenol biodegradation process in TY_2 isolated microorganism as a function of time. The TY_2 microorganism is capable of completely degrading 100 ppm of 4-chlorophenol in about 21 h. This microbial species is a superior microorganism among microorganisms isolated from wastewater, which is able to remove 4-chlorophenol in the shortest time compared with other isolated microbial species.

Table 5. Microscopic form and isolation site of isolated strains

Isolation site	Microscope form	Sample
Storage tank (interstitial water)	Gram negative bacilli	TB_1
Location of oil drainage of reservoirs to return to the refinery system	Gram positive bacilli	TB_2
Oil storage tank	Gram positive bacilli	TB_3
Oil storage tank	Gram positive coco-bacillus	TB_4
Storage tank	Gram positive bacilli	TB_5
Accumulated oil sludge	Gram positive coco-bacillus	TB_6
Accumulated oil sludge	Gram positive bacilli	TB_7
Total refinery effluent flow	Gram negative bacilli	TB_8
Total refinery effluent flow	Gram positive bacilli	TB_9
Total refinery effluent flow	Gram negative bacilli	TB_{10}
Total refinery effluent flow	Gram negative bacilli	TB_{11}
Total refinery effluent flow	Gram positive bacilli	TB_{12}
Total refinery effluent flow	Gram positive bacilli	TB_{13}
Total refinery effluent flow	Yeast	TY_1
Total refinery effluent flow	Yeast	TY_2
Total refinery effluent flow	Yeast	TY_3
Total refinery effluent flow	Mold	TY_4
Total refinery effluent flow	Mold	TY_5
Total refinery effluent flow	Yeast	TY_6

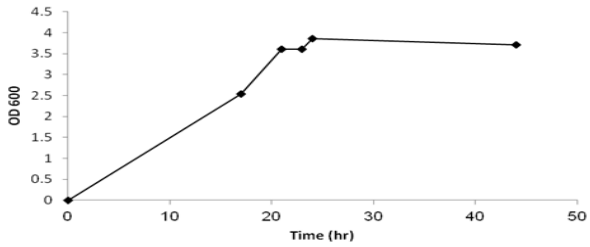

Fig. 6. Growth curve of TY_2 isolated microorganism

4-Chlorophenol degradation using TY_1TY_2 mixed microbial culture

After isolation of wastewater microorganisms, purification and performing removal tests, two microbial species TY_1TY_2 were available for examination of 4-chlorophenyl elimination experiments.

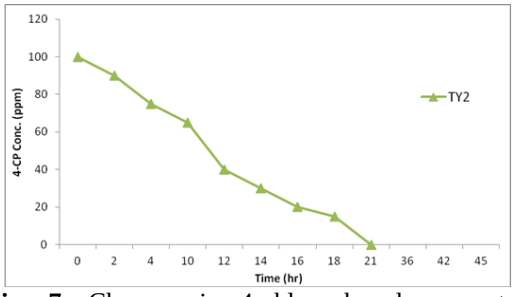

Fig. 7. Changes in 4-chlorophenol concentration *versus* time by isolated microorganism TY_2

Biodegradation experiments were done using mixed culture with two TY_1TY_2 microorganisms (50/50 TY_1TY_2) in the presence of 100 ppm of 4-chlorophenol and 2g/l of glucose as supplementary substrate. In these experiments, 4-chlorophenol degradation by the mixed culture and by the single species was compared. Fig. 8 shows the changes in the biomass growth of pure cultures and mixed microbial culture in the presence of 100 ppm of 4-chlorophenol and 2 g/l of glucose as supplementary substrate. The two TY_1TY_2 microbial species were able to completely degrade 100 ppm of 4-chlorophenol in approximately 18 h.

Fig. 9 shows the changes in the concentration of 4-chlorophenol during the process of degradation by single and mixed microbial culture.

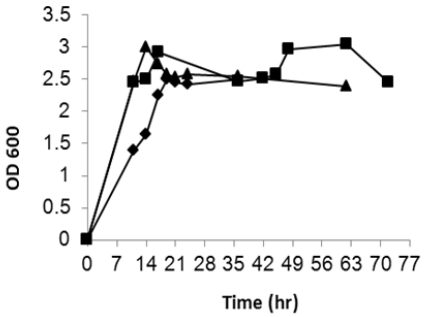

Fig. 8. Comparison of cell mass growth in the 4-chlorophenol degradation process using mixed and pure culture of two microbial species (TY_2:♦, TY_1:■, TY_1TY_2:▲)

Effect of carbon source concentration in pollutant degradation

Considering that the enrichment operation was done in presence of 2 g/l of glucose and the microbial species were isolated at this concentration, additional examination of the degradation was performed with glucose concentration of 5 g/l, because the high concentration of the primary substrate can be a deterrent to 4-chlorophenol degradation and one of the important factors in the removal of pollutants. The primary effect of glucose as the primary substrate is on the growth of existing microorganisms, so at higher concentrations, we will necessarily have further growth of the biomass. In Fig. 10, 4-chlorophenol degradation at two glucose concentrations of 2 and 5 g/l at different times is shown. It is concluded that the concentration of 2 g/l of glucose was sooner consumed and resulted in the elimination of 4-chlorophenol in a shorter time.

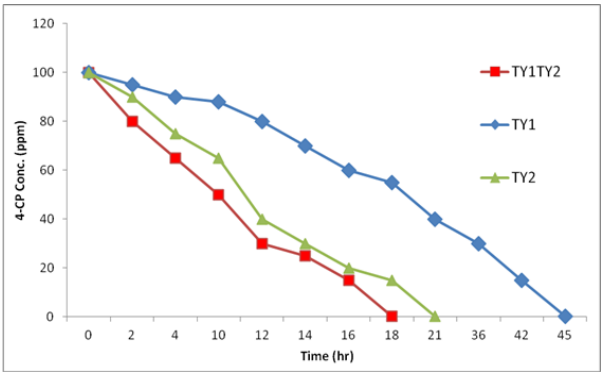

Fig. 9. Comparison of changes in 4-chlorophenol concentration in the 4-chlorophenol degradation process using mixed and pure culture of the two species TY_1 and TY_2 (TY_2:▲, TY_1:♦, TY_1TY_2:■)

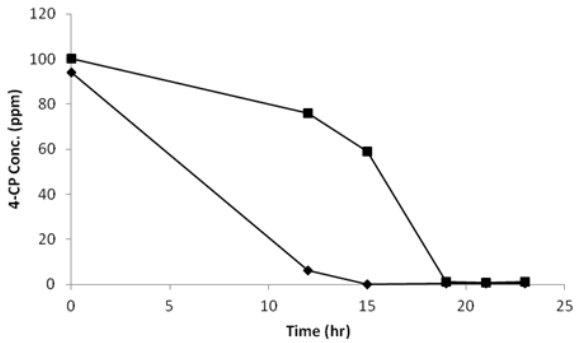

Fig. 10. 4-Chlorophenol changes over time in different concentrations of glucose by TY_1TY_2 (50:50) mixed culture in presence of 100 ppm of 4-chlorophenol (♦: 2 g/l glucose concentration, ■: 5 g/l of glucose concentration)

Molecular identification of selected strains

At first, 2 genomic DNA were extracted from selected yeasts (TY_1 and TY_2), which provided the best results in 4-chlorophenol biodegradation, and then part of their 18srRNA gene sequence was reproduced using universal primers and PCR method. In the next step, the PCR product, 2 selected strains, with a size of 1000-100, were taken on a 1% agarose gel and a specific strip of about 530 bp was observed from the 18SrRNA gene on the gel (Fig. 11).

Results of the molecular identification of selected strains

The next step was to determine the identity and molecular identification of isolated strains. Based on the sequences obtained, using the BLAST software on the NCBI website, they were compared with the NCBI reported sequences, and the closest microbial species was extracted from the NCBI gene data bank. The results show that strains TY_1 and TY_2 also exhibited the highest similarity (99%) to genus *Trichosporon.*

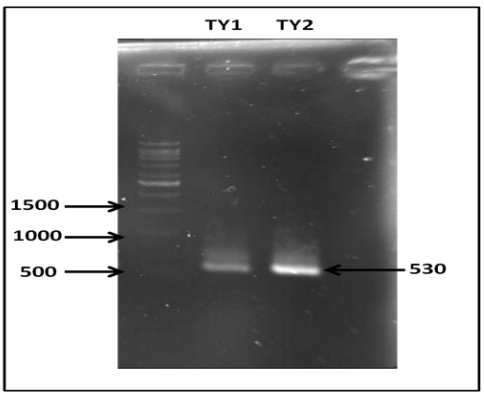

Fig. 11. Electrophoresis of PCR products of 18S rRNA gene of selected strains

DISCUSSION

Comparison of biodegradation performance by mixed culture and pure microbial culture

From the obtained results of the experiments, it seems that the mixed microbial culture acts as an isolated single species, TY_2, so that the elimination time in both TY_2 microbial culture and TY_1TY_2 mixed culture is approximately the same. The complete removal time of 100 ppm 4-chlorophenol by TY_2 strain was 21 h, and the complete removal time of 100 ppm 4-chlorophenol by mixed culture TY_1TY_2 in presence of 2 g/l glucose was about 18 h.

In a study by Puhakka *et al*. (1995), mixed culture performance composed of three isolated microbial species was the same as the function of each of them alone [23]. In another study by Sahinkaya and Dilek (2007), the data (specific rate of removal of 2,4-dichlorophenol) showed that the yield of pure cultures isolated from mixed

cultivation in 30 ppm of 2,4-dichlorophenol was much better than that of mixed habituated culture [24].

In any case, the results of mixed microbial culture should be examined on a more detailed scale. In Table 6, the effect of mixed culture and pure microorganisms in 4-chlorophenol degradation is compared.

CONCLUSIONS

In the present study, microorganisms capable of biodegradation of 4-chlorophenol were first isolated and purified using adaptation and enrichment operations on wastewater and sludge. Due to the increased ability of wastewater and sludge microorganisms in using 4-chlorophenol as the only source of energy and carbon in all experiments, 5 g/l of glucose was used as supplementary substrate. The enrichment and habituation operations lasted for about 60 days, and the microbial species obtained from the last stages of adaptation and enrichment operations were purified and isolated by doing several linear cultures. The results showed that the adaptation and enrichment of the microorganisms in the petrochemical sludge and wastewater of the Tondgooyan Unit was very effective in increasing 4-chlorophenol biodegradation.

After examining the growth process of all isolated species, by examining the elimination by them in the mineral microbial culture, isolated microbial species, suitable microorganisms for the 4-chlorophenol biodegradation were selected. In the following, 4-chlorophenol biodegradation tests were performed by selected microorganisms and a mixed culture, and the behavior of single and mixed microbial culture was compared. The results showed that the mixed microbial culture was not significantly different from pure microbial species, but the mixed culture would probably show this difference in the metabolic path of 4-chlorophenol degradation.

In the final stage of the experiments, the effect of the initial concentration of glucose with two concentrations of 2 and 5 g/l was considered as a supplementary substrate. The results indicated that with increasing 4-chlorophenol concentration, its degradation time would be longer, but higher glucose concentration, despite the higher growth of microorganisms in its presence, had an inhibitory effect on the microbial culture in 4-chlorophenol degradation.

Table 6. Comparison of biodegradation performance by mixed culture of the present study with other researchers

Scholar	Microbial culture	Concentration of 4-chlorophenol (ppm)	Substrate of growth supplement	Removal time (h)	Removal return (%)
Sahinkaya *et al*., 2005 [24]	Enriched mixed culture	300	Peptone	50	100
Yang *et al*., 2008 [13]	Isolated microorganism	100	Glucose or sodium acetate	96	100
Lee *et al*., 2007 [12]	Enriched mixed culture	50	Glucose	40	100
Wang *et al*., 1999 [25]	*P. putida*	200	Glucose	30	100
Lima *et al*., 2004 [26]	Algae collection	50	-	120	100
This research	Microbial mixed culture	100	Glucose (2g/l)	18	100
This research	Microbial mixed culture	100	Glucose (5g/l)	20	80

REFERENCES

1. I. P. Solyanikova, L. A. Golovleva, G. K. Skryabin, *J. Environ. Sci. Health, Part B*, **39**, 333 (2005).
2. N. V. Pradeep, S. Anupama, K. Navya, H. N. Shalini, M. Idris, U. S. Hampannavar, *Appl. Water Sci*., **5,**105 (2015).
3. C. Zhang, L. Fu, Zh. Xu, H. Xiong, D. Zhou, M. Huo, *Environ. Sci. Pollution Res.*, **24**, 24725 (2017).
4. A. M. Santana, Z. S. Ferrera, M. E. T. Padron, J. J. S. Rodriguez, *Molecules*, **14**, 298 (2009).
5. P. M. Armenante, D. Kafkewitz, C. J. Lewandowski Jou, *Water Research*, **33** (3), 681 (1998).
6. A. Farrell, B. Quilty, *Water Research*, **36**, 2443 (2002).
7. A. Tarighian, G. Hill, J. Headley, S. Pedras, Enhancement of 4-chlorophenol biodegradation using glucose, *Clean Technol. Environ. Policy*, **5**, 61 (2003).

8. V. M. Monsalvo, A. F. Mohedano, J. A. Casas, J. J. Rodriguez, *Bioresearch Technol.*, **100**, 4572 (2009).
9. N. Chamkouri, S. Khodadoust, F. Ghalavandi, *J. Chromat. Sci.*, **53**, 1720 (2015).
10. W. Gaufeng, X. Hong, J. Mei, *Chem. Technol. College*, **6**, 67 (2004).
11. H. Muftah, E. Naas, A. Hussein, H.A. Mousa, M. E. Gamal, Microbial Degradation of Chlorophenols, Springer International Publishing Switzerland, S.N. Singh (ed.), Microbe-Induced Degradation of Pesticides, Environmental Science and Engineering, 2017, p. 23.
12. C. Y. Lee, Y. Pu Lee, *World J. Microb. Biotechnol.*, **23**, 383 (2007).
13. C. F. Yang, C. M. Lee, *Biodegradation*, **19**, 329 (2008).
14. P. Saravanan, K. Pakshirajan, P. Saha, *Bioresource Technol.*, **99**, 205 (2008).
15. N. Chamkouri, A. Niazi, V. Zare-Shahabadi, *Spectrochim. Acta - Part A: Molecular and Biomolecular Spectroscopy*, **156**, 105 (2016).
16. W. S. El-Sayed, M. Ismaei, F. El-Beih, *Austr. J. Basic .Appl. Sci.*, **3**, 776 (2009).
17. A. Farrell, B. Quilty, *Biodegradation*, **10**, 353 (1999).
18. Y. Herrera, A. I. Okoh, L. Alvarez, N. Robledo, M. R. Trejo-Hernandez, *World J. Microb. Biotechnol.*, **24**, 55 (2008).
19. H. Zouari, M. Labat, S. Sayadi, *Bioresource Technol.*, **84**, 145 (2002).
20. I. Hiroaki, *Int. J. Genetics Genomics*, **3**, 20 (2015).
21. H. A. Raja, A. N. Miller, C. J. Pearce, N. H. Oberlies, *J. Natural Products*, **80**, 756 (2017).
22. M. Norazah, *Recent Advances*, **2**, 11 (2011).
23. J. A. Puhakka, R. P. Herwig, P. M. Koro, G. V. Wolfe, J. F. Ferguson, *Appl. Microbial Biotechnol.*, **42**, 951 (1995).
24. E. Sahinkaya, F. B. Dilek, *J. Biotechnol.*, **127**, 716 (2007).
25. S. J. Wang, K. C. Loh, *Biodegradation*, **10**, 261 (1999).
26. A. A. C. Lima, M. F. J. Raposo, P. M. L. Castro, R. M. Morais, , *Water Research*, **38**, 97 (2004).

ИЗСЛЕДВАНЕ НА БИОЛОГИЧНАТА ОБРАБОТКА НА 4-ХЛОРОФЕНОЛ С МАЯ И ПЛЕСЕН ОТ ИНДУСТРИАЛНИ И ПЕТРОЛНИ ОТПАДНИ ВОДИ (ПРИСТАНИЩЕ „ИМАМ ХОМЕЙНИ“ МАХШАХР)

А. Алирезаеи[1], М. Баят[1*], М. Алимохамади[2], С. Хашеми[3]

[1] *Департамент по микробиология, Научен и изследователски клон, Ислямски Азад университет, Техеран, Иран*

[2] *Департамент по екологично здравно инженерство, Училище за публично здраве, Техерански университет по медицина, Техеран, Иран*

[3] *Департамент по медицинска паразитология и микология, Училище за публично здраве, Техерански университет по медицина, Техеран, Иран*

Постъпила на 23 ноември, 2017 г.; коригирана на 15 февруари, 2018 г.

(Резюме)

Фенолните производни са едни от най-токсичните замърсители на околната среда, а хлорофенолите са най.токсичните замърсители във води и отпадни води. 4-Хлорофенолът е много добре разтворим във вода и поради това е широко разпространен в природни и отпадни води. Тъй-като химичните и биологичните методи за очистване на водите са с висока стойност и енергоемкост, а в някои случаи са вредни за околната среда, в настоящата работа е изследвано биохимичното разлагане на 4-хлорфенол. 13 бактериални щама и 6 щама от мая и плесен са пречистени и изолирани от завода за обработка на отпадна вода „Шахид Тондгоян“ (пристанище „Имам Хомейни“ Махшахр) в продължение на 15 дни. Изучени са свойствата на всеки микроорганизъм, изолиран в присъствие на 100 ppm 4-хлорофенол и два микробиални вида, TY_1 и TY_2, са избрани за използване като смесена микробиална култура. Изучено е влиянието на един от най-важните фактори върху разлагането на 4-хлорофенола със смесена микробиална култура - концентрацията на глюкоза (2 и 5 g/l). Установено е, че микробиалните видове TY_1 и TY_2, отстраняват напълно 100 ppm 4-хлорофенол, като щамът TY_1 отстранява напълно след 45 h, а щамът TY_2 след 21 h. С използване на смес от TY_1 и TY_2 щамове (50/50) в присъствие на 2 g/l глюкоза, 100 ppm 4-хлорофенол се отстранява напълно за 18 h. На основата на анализа на 18SrRNA генна секвенция е проведена молекулна идентификация на двата най-добри щама, които принадлежат към вида *Trichosporon*. Имайки пред вид високия потенциал на вида *Trichosporon*, включително за повишаване на добива на петрол и отстраняване на замърсителите се очаква, че по-нататъшните изследвания на подходящи щамове и търсенето на нови природни щамове може да играе решаваща роля за прилагането на природни щамове в петролната индустрия.

Bulgarian Chemical Communications, Volume 50, Number 4 (pp. 647 – 654) 2018

Research on protective method of ship electrostatic field based on metal polarization control

Wang Xiangjun, Liu Yi*, Liu Dehong

School of Electrical Engineering, Naval University of Engineering, 430033, China

Received April 21, 2018; Accepted July 28, 2018

There is the electrochemical corrosion among different metals of the ship in the seawater, of which the foremost is the electrochemical corrosion between the steel hull and the bronze propeller. In this electrochemical corrosion process, the hull is the electrochemical corrosion anode, and the propeller is the electrochemical corrosion cathode. Besides, the corrosion current from the hull to the propeller current would generate around the ship. The corrosion current would form an electrostatic field in the seawater, and field signal is easily detected by the mine and detection equipment, which can bring a great threat to the ships. In this paper, based on the research on the metal polarization curve, the potential balance method combining the anode polarization of the hull and the cathodic polarization of the propeller is proposed, to make the potential difference reduce to 0V. At this point, the corrosion current can be also greatly reduced, and the associated underwater electric field can also be eliminated. It is demonstrated that the proposed method can reduce the underwater electrostatic field indeed, and the electric field protection effect is obvious.

Keywords: Cathodic polarization; Anodic polarization; Tafair formula; Polarization potential; Electrostatic field protection

1. INTRODUCTION

The ships are in service in seawater, of which different underwater metallic materials (such as hull, propeller, rudder, bulb, etc.) have different electrode potentials. For instance, the electrode potential of a commonly used marine steel plate is -0.64 V, and the potential of the copper propeller is -0.32 V. The present domestic ships are mainly shaft through ships, of which the propeller-shaft and the hull are in the electrical connection state [1]. In terms of the shaft through structure, the electrochemical corrosion between the propeller and the hull is inevitable, and a certain potential difference is maintained in the seawater. The potential difference forms a primary battery generating stable corrosion current via the conductive seawater, thus a steady state electric field is established. This macro-corrosion battery with complex structure is one of major origins of the underwater electric field generated by ships, of which the voltage is determined by the materials and the depolarization strength [2, 3].

In terms of China's ships, the sacrificial anode and the impressed current cathodic protection methods are adopted to protect the hull from corrosion. However, both of aforementioned methods would increase the strength of the electric field around the ship and reduce the ship stealth [4, 5].

According to some projections, the total sacrificial anode protection current intensity of a medium-sized ship can reach hundreds or even thousands of amps. Due to the great intensity of the protection current, the strong electrostatic field around the ships can be generated even if the electrodes are closer to each other.

There are few auxiliary auxiliaries in the impressed current cathodic protection system, and the protection current density is generally greater than the sacrificial anode indicators (such as 10 ~ 60mA/m of the the painting hull), and therefore the stronger electric field would be generated around the ship hull [6]

The shaft cutting technology applied to the Russian ships make the propeller and the hull form a direct electrical connection state without the macroaxis, which greatly reduces the corrosion current, and the underwater electric field around the ship is reduced thereby. The China's present macoraxis manufacturing level determines that shaft cutting state can be achieved, and therefore China's ships cannot use Russia's electric field protection methods for reference. Based on this background, it is very necessary to propose an active protection method that is suitable for homemade ships, which not only can protect the hull from corrosion, but also can reduce the strength of the underwater electric field around the ships.

* To whom all correspondence should be sent:
E-mail: liuyi8888a@163.com

2. THE ANODE POLARIZATION AND CATHODIC POLARIZATION POTENTIAL VARIATION LAW OF HULL-PROPELLER

Each metal in the seawater has a ceatian electrode potential: the metal surface partial ions would be affected by the water polar molecule in the process of contacting with the electrolyte solution, and a "double electrode layer" would generate at the interface, causing the potential difference between the metal and seawater. The metal with different electrode potentials in the electrolyte solution can form a corrosion current loop when there is an external electrical connection, which results in the occurrence of electrochemical corrosion [7]. In this process, the electrode where an oxidation reaction (lose electrons) is performed is referred to as an anode, and the electrode where a reduction reaction (obtain electrons) is performed is referred to as a cathode. As shown in Figure.1, in the process of ship's electrochemical corrosion, the steel hull (electrode potential is negative) is the anode of electrochemical corrosion, and the bronze propeller (electrode potential is positive) is the cathode of electrochemical corrosion [8].

The corrosion current flows from the hull to the propeller in the seawater, and the ship's electrostatic field is formed. As a result of the propeller rotation, the contact resistance between the hull and the propeller changes periodically, and the modulated corrosion current generates a periodically varying shaft-frequency electric field. Therefore, the ship's corrosion current is the main source of the ship's electrostatic field and the shaft-frequency electric field [9].

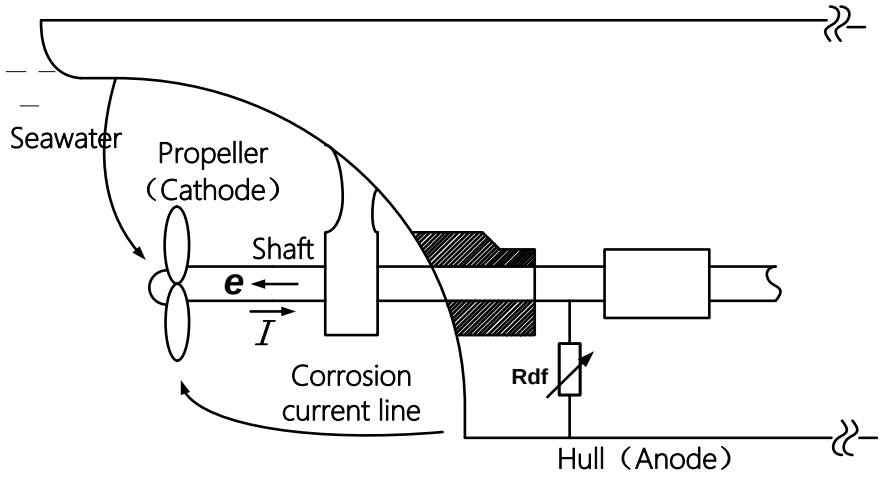

Fig.1. Schematic diagram of electrochemical corrosion of naval vessels.

In the process of the aforementioned metal electrochemical corrosion, the corrosion current would cause the electrons to move, and the electrode polarization would occur in the hull and the propeller: the electrons on the hull (anode) would flow into the propeller (cathode) through the main axis, resulting in a decrease in the electric charge density of the electric double layer on the hull, while the charge density of the electric double layer on the propeller would increase [10].

In this way, the potential of the anode (hull) gradually moves in the positive direction (anode polarization), and the potential of the cathode (propeller) gradually moves in the negative direction (cathode polarization). In the process of polarization, the potential difference between the hull and the propeller is gradually reduced, and the corrosion current in the circuit is gradually reduced. The polarization causes the electrochemical corrosion to slow down. However, the degree of the natural electrode polarization to reduce electrochemical corrosion is relatively weak, and electrochemical corrosion cannot be eliminated [11].

If the electrode polarization can be controlled artificially to decrease the potential difference between the hull and the propeller to 0V, the potential balance would be realized; the corrosion current would disappear, and the associated underwater electric field would also be eliminated. The potential polarization balance is shown in Figure 2.

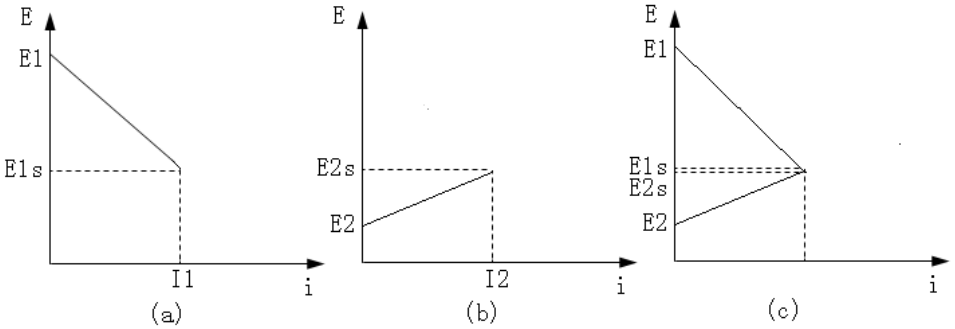

Fig.2. Potential balance polarization diagram. (a) propeller cathodic polarization; (b) Hull anodic polarization; (c) potential balance)

The polarization reaction of the metal electrode can be expressed by the Tafel formula:

$$I = I_a - |I_c| = I_{0,a} \exp(\frac{E - E_{e,a}}{\beta_a}) - I_{0,c} \exp(-\frac{E - E_{e,c}}{\beta_c}) \quad (1)$$

Where I is polarization current density, $I_{0,a}$ and $I_{0,c}$ are exchange current density of metal anodic dissolution reaction and cathodic reduction reaction respectively. $E_{e,a}$ and $E_{e,c}$ are balance potentials of metal anodic dissolution reaction and cathodic reduction reaction respectively; β_a and β_c are Tafel slopes of metal anodic dissolution reaction and cathodic reduction reaction respectively.

In the case of I=0, the metal does not produce polarization reaction, and its potential is the metal corrosion potential E_{corr}. At this time, the absolute value of the current density of the metal anode reaction is equal to the absolute value of the current density of the cathode reaction, which is also equal to the metal average corrosion current density I_{corr}:

$$I_{0,a} \exp(\frac{E_{corr} - E_{e,a}}{\beta_a}) = I_{0,c} \exp(-\frac{E_{corr} - E_{e,c}}{\beta_c}) = I_{corr} \quad (2)$$

Based on the Eq.(1) and Eq.(2), the Eq.(3) can be obtained as follows:

$$I = I_{corr}[\exp(\frac{E - E_{corr}}{\beta_a}) - \exp(-\frac{E - E_{corr}}{\beta_c})] \quad (3)$$

The Eq.(3) is the *E*-*I* curve (polarization curve) equation of the corrosion metal electrode. The E_{corr} is assumed as the origin of axis E, and then the coordinates of E axis is changed to ΔE:

$$\Delta E = E - E_{corr} \quad (4)$$

In fact, ΔE is the metal polarization potential value after polarization based on the corrosion potential. In the case of ΔE=0, there is no polarization reaction about metal; ΔE>0: the metal is subjected to anodic polarization reaction; $\Delta E < 0$: the metal is subjected to cathodic polarization reaction.

Based on the Eq.(3) and Eq.(4), the following formula can be obtained through the further mathematical operation:

$$I = I_{corr}[\exp(\frac{\Delta E}{\beta_a}) - \exp(-\frac{\Delta E}{\beta_c})] \quad (5)$$

In the process of metal cathodic polarization, the polarization rate is not only determined by the electrochemical process on the metal surface, but also the depolarization diffusion process in the solution. In this case, the relationship between the absolute value of cathode current density and electrode potential is:

$$|I_c| = \left(1 - \frac{|I_c|}{I_L}\right) I_{0,c} \exp(-\frac{E - E_{e,c}}{\beta_c}) \quad (6)$$

Where I_L is the absolute value of the diffusion current density of the cathode reaction. In the case of $E = E_{corr}$, the Eq.(7) can be deduced from the Eq.(4) and Eq.(6):

$$|I_c| = \frac{I_{corr} \exp(-\frac{\Delta E}{\beta_c})}{1 - \frac{I_{corr}}{I_L}[1 - \exp(-\frac{\Delta E}{\beta_c})]} \quad (7)$$

Then, the metal polarization equation considering depolarization diffusion process can be obtained as follows:

$$I = I_{corr}\left\{\exp(\frac{\Delta E}{\beta_a}) - \frac{I_{corr} \exp(-\frac{\Delta E}{\beta_c})}{1 - \frac{I_{corr}}{I_L}[1 - \exp(-\frac{\Delta E}{\beta_c})]}\right\} \quad (8)$$

The polarization experiment is performed on a certain type of high-strength steel for marine, to compare the experimental results with the theoretically calculated Tafir curve, which is shown in Fig.3.

From Fig.3, it is can be learned that the polarization curve is basically consistent with the theoretical Tafel curve. As a result, the Tafir formula can be used as the basis for the research on the polarization of the hull and propeller.

3. POTENTIAL BALANCE ELECTRIC FIELD PROTECTION EXPERIMENTAL COUNTER DESIGN

On the basis of theoretical research, the electric field protection experimental prototype is developed, which is based on the potential balance principle [12]. By means of the auxiliary electrodes arranged at different parts of hull, the anodic polarization is performed to the hull, and cathodic polarization is performed to the propeller, to ensure that the potential difference between the hull and propeller keeps constant at 0V. Fig.4 presents the design principle of the electric field protection experimental prototype [13].

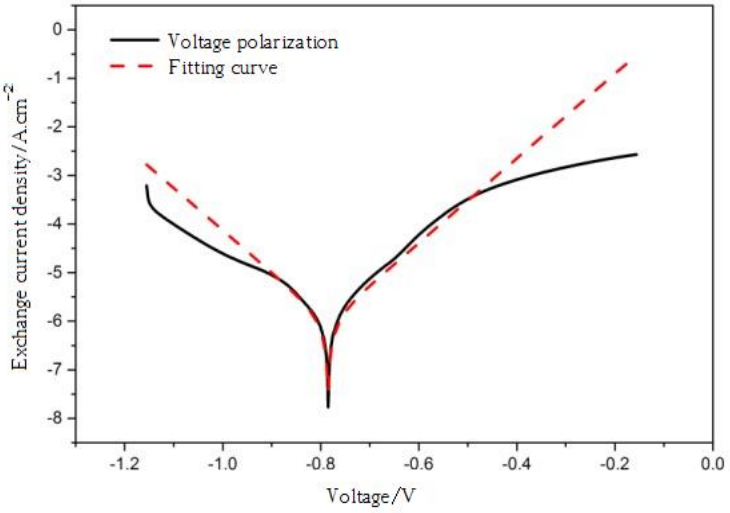

Fig.3. Fitting of polarization curve and Tafir curve of high strength steel of ship.

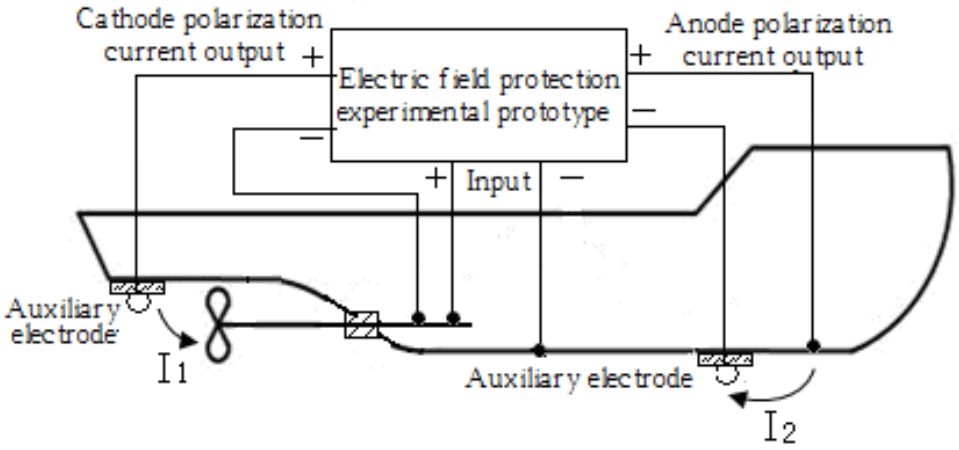

Fig.4. Design schematic diagram of experimental prototype for electric field protection.

The potential difference between the hull and the propeller is used as the control signal, to control the anodic polarization current and the cathodic polarization current outputting from the electric field protection prototype. When the potentials of propeller and hull are close, the corrosion current would disappear, and the underwater electric field would eliminate [14, 15].

The operating principle of the electric field protection experimental prototype is presented as follows:

The potentiometric signal of the main axis relative to the hull flows from the contact brush device to input port of the electric field protection test prototype, and two sets of current would output from the controlled port of the electric field protection prototype: 1, The anode polarization current flows from the hull to the suxiliary electrode through the sea, which will flow back to the electric field protection test prototype finally; 2, The cathode polarization current flows from the auxiliary electrode to the propeller through the sea, which will flow back to the electric field protection test prototype through the main axis .

The electric field protection experimental prototype composition diagram is shown in Figure 5, which mainly contains the following parts:(1) Potential detection device; (2) Polarization current output control device; (3) Controllable constant current source (4) Polarization current output electrode.

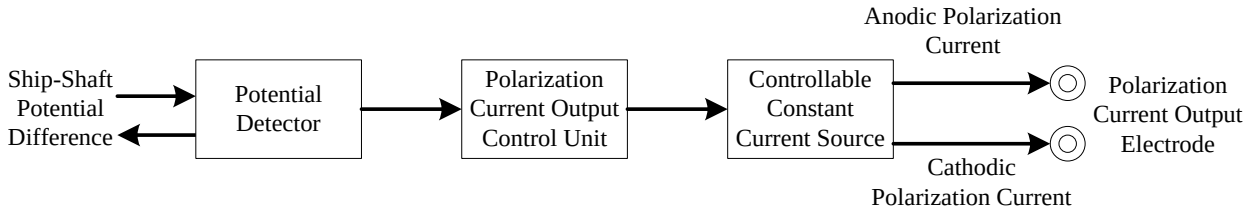

Fig.5. The composition diagram of electric field protection experiment prototype.

4. EXPERIMENTAL STUDY ON UNDERWATER ELECTROSTATIC FIELD PROTECTION OF SHIP MODEL POTENTIAL BALANCE

4.1 Experimental program

The ship model potential balance and electromagnetic field protection experiment is based on the simultaneous anodic polarization of the hull and cathodic polarization of the propeller, which can make the potential difference between the hull and the propeller equal zero, to measure the change of the electric field around the ship model. The experiment is based on two cases of propeller rotating or not, to obtain electric field measurement data before and after performing electrostatic field protection, which is used to measure the protection effectiveness.

4.2.Experimental preparation

The experiment is carried out in a non-magnetic electric field pool, and the length, width and depth of the pond are set to 8 m, 5 m and 1.5 m respectively. The experimental sea water with depth of 0.6m is poured into the pool, combined with the industrial salt to make the conductivity of the sea water equal 3.8s/m.

A set of Ag-AgCl electrodes with three-component are placed at the bottom of the pool, to measure the electric field values of Ex, Ey and Ez, and calculate the electric field module values. The immersion time of electric field sensor is set to 24 hours.

Based on the ship model drag device, the experimental ship model is expected to be in uniform motion state in the experimental pool, and the three-component electric field sensor would measure the passing characteristic curve of the experimental ship model.

4.3.Experimental Results

The experimental process is based on the ship model's forward and backward uniform movement in the experimental pool with the length of 8 meters. Given that the confidentiality of experimental data, the electric field values of given graphics have been treated, which would not affect the judgment of the electrostatic field protection effect after adopting the potential balance electrostatic field protection method.

According to the characteristics of the underwater electrostatic field of the ship, the electric field module value |E| contains the three components of the electric field value, which can reflect the protective effect more accurately, so that the electric field module |E| can be used as the evaluation criteria.

The electrostatic field protection experiment in the case of non-rotating propeller. In the case of propellers not rotating, the three-component electric field values before and after adopting potential balance protection method are used for experimental verification, and the variation of |E| is presented as Fig.6 shows. The ordinate in the Fig.6 is the processed electric field value, the abscissa represents time, the upper right corner is the curve explaining, and the number is the time of measurement.

The electrostatic field value and module value of each component as well as the protective effect are shown in Table 1.

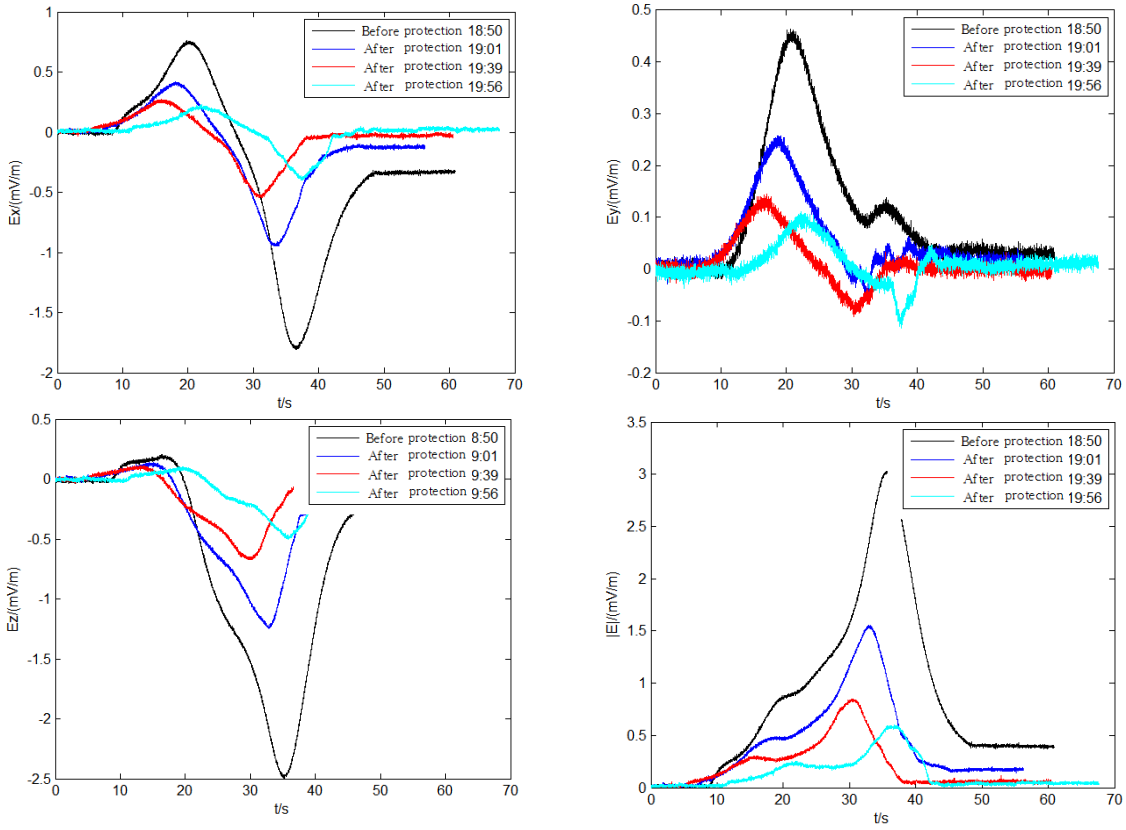

Fig.6. The propeller does not rotate, electrostatic field values of natural corrosion and invisible.

Table 1. The propeller does not rotate, electrostatic field value of ship model and its protective effect.

Time	18:50	19:01	19:39	19:56
Ex (Peak-to-Peak Value)	2.57	1.37	0.82	0.63
Ex(Decreasing Proportion)(%)		46.73	68.00	75.57
Ey(Peak-to-Peak Value)	0.48	0.31	0.24	0.22
Ey (Decreasing Proportion) (%)		34.85	51.04	53.53
Ez(Peak-to-Peak Value)	2.70	1.38	0.79	0.61
Ez(Decreasing Proportion) (%)		48.76	70.78	77.57
|E|(Peak-to-Peak Value)	3.03	1.55	0.85	0.60
|E| (Decreasing Proportion) (%)		48.67	71.94	80.22

There are some analysis from the aforementioned experimental results

1) Based on the electrostatic field protection method with potential balance, three components of the electric field values and electric field model values at the same test point have been significantly reduced. Once the potential balance protection test prototype is initiated, the electric field modulus |E| would be reduced by 48%; after one hour of polarization, the electric field modulus |E| would be reduced by 80%, and the protective effect is demonstrated;

2) The electric field three-component and module characteristic curve dose not change after adopting the electrostatic field protection method with potential balance, which shows that the method would not change the electrostatic field distribution characteristic of the ship model, but only reduces the numerical value.

3) From Fig.5, it can be concluded that the longer the polarization is applied, the better the electrostatic field is. The reason for the aforementioned phenomenon is that the polarization is a dynamic variation process, and it would take some time to reach the dynamic equilibrium state, which is in accordance with the theoretical analysis results.

The electrostatic field protection experiment in the case of propeller rotating (v=100r/min). In the case of propellers rotating with velocity of 100

r/min (to simulate the actual navigational status of ships), the three-component electric field values before and after adopting potential balance protection method are used for experimental verification, and the variation of |E| is presented as Fig.6 shows.

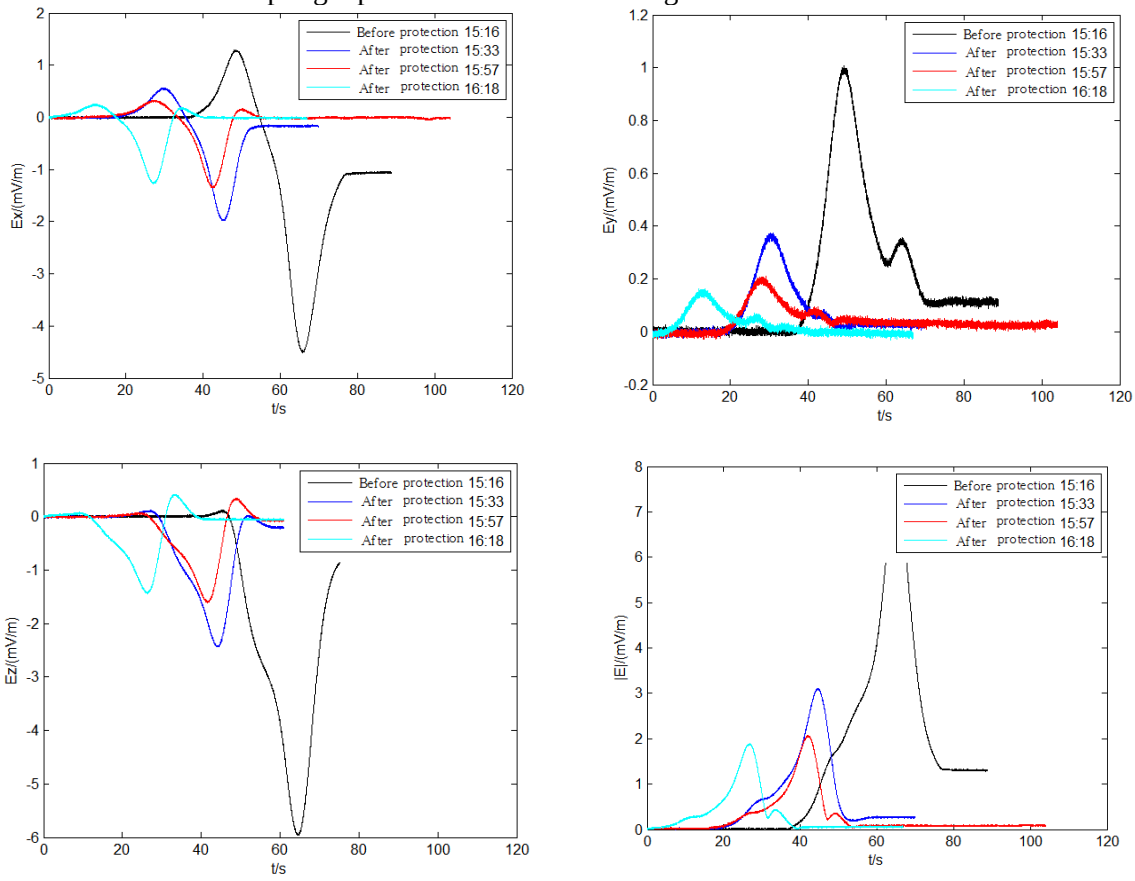

Fig.7. Propeller speed is 100r/min, electrostatic field values of natural corrosion and invisible.

Table 2. The propeller speed is 100r/min, electrostatic field value of ship model and its protective effect

Time	15:16	15:33	15:57	16:18
Ex (Peak-to-Peak Value)	5.80	2.55	1.68	1.53
Ex(Decreasing Proportion)(%)		56.00	70.99	73.70
Ey(Peak-to-Peak Value)	1.03	0.40	0.24	0.19
Ey (Decreasing Proportion) (%)		60.89	76.56	81.23
Ez(Peak-to-Peak Value)	6.09	2.56	1.95	1.86
Ez(Decreasing Proportion) (%)		57.93	67.89	69.52
|E|(Peak-to-Peak Value)	7.38	3.10	2.07	1.90
|E| (Decreasing Proportion) (%)		57.97	71.94	74.33

There are some analysis from the aforementioned experimental results

1) Based on the electrostatic field protection method with potential balance, three components of the electric field values and electric field model values at the same test point have been significantly reduced. Once the potential balance protection test prototype is initiated, the electric field modulus |E| would be reduced by 57%; after one hour of polarization, the electric field modulus |E| would be reduced by 74%, and the protective effect is demonstrated;

2) The electric field three-component and module characteristic curve dose not change after adopting the electrostatic field protection method with potential balance; there is only some difference between the start time of measuring and ship model moving, which makes each curve has a certain translation on the time axis.

3) From Fig.7, it can be concluded that the longer the polarization is applied, the better the electrostatic field is.

4) The final protective effect of the experiment in the case of propeller rotating is only 74%, which is worse than the protective effect in the case of propeller not rotating. The reasons for the experimental results are presented as follows: After propeller rotating, the propeller cathodic polarization process is more complicated due to the periodic change of the contact resistance near the propeller; As a result of the simultaneous opening of the axial frequency protection equipment, the additional axial frequency protection current would generate between the shaft and shell, which make has an effect on the polarization process

5. CONCLUSION

On the basis of research on the hull-propeller metal polarization law, the naval vessel electric field protection method based on the potential balance is proposed in this study. Then, the experimental prototype is designed to carry on the electrostatic field protection experiment in the experimental pool, and the experimental results are analyzed further. Finally, the electric field protection control method is analyzed.

The experimental results show that the ship model electrostatic field can be reduced by more than 70% based on the proposed method, and the electrostatic field protection effect is demonstrated. In addition, once the axial frequency electric field protection device is initiated, the electrostatic field protection effect would get worse, and how to strike a balance would be the focus of further study.

It is noted that the method of controlling the polarization current level to achieve a better potential balance is the key to achieve the electric field protection. In the further study, it is considered to lay out the reference electrode to achieve polarization current controlling, of which signal can be used to judge the potential balance state.

Acknowledgement. The authors are grateful for the support provided fort his study by the National Natural Science Foundation of China (NSFC-41476153).

REFERENCES

1. Gong S., Lu X., *J. Naval Univ. Eng*., **2**, 1 (2008).
2. Li .J., Bao Z.H., Gong S.G., Hu P., Wu J.H., Xing S.H., *J. Naval Univ. Eng*., **23**, 67 (2011).
3. Cao Y., Ji D, Zhu W.B., *Ship Sci. Technol.*, **37**, 69 (2015).
4. Zang Y., Yue R., Li P., *Ship Sci. Technol*., **34**, 11 (2012).
5. Liu Y., Wang X.J., *Total Corrosion Control*, 31, 38 (2017).
6. F.C. Walsh, G. Kear, A.H. Nahle,. *Corrosion Sci*., **123,** 1 (2017).
7. Wang H., Yang K., Zheng K., *J. Electromagn. Waves Appl.*, **29**, 858 (2015).
8. Ji D.,Wang X.J.,Liu Y.,Liu D.H., *J. Sichuan Ordn*., **35**, 4 (2014).
9. Wu Z.Q., Zhu X.H., Li B., *Sensor & Transducers*, **186,** 161 (2015).
10. I. Danaee, M.N. Khomami, A.A. Attar, *J. Materials Sci. Techno*l., **29**, 89 (2013).
11. Sun J.Z., Jiang H.L., Xia Z.S., *Appl. Mech. Materials. Trans Tech Publications*, **602,** 2649 (2014).
12. Jiang H.L., Zhang H.P., Xia Z.S., *Appl. Mech. Materials. Trans Tech Publications*, **563**, 333 (2014).
13. Zhang H.P., Chen X.G., Ao C.Y., *Appl. Mech. Materials. Trans Tech Publications*, **527**, 172 (2014).
14. Jia Y., Jiang R., Gong S., *Acta Armamentarii*, **5**, 11 (2013).
15. Jia Y., Jiang R., Gong S., *J. Shanghai Jiaotong Univ.,* **7,** 3 (2013).

ИЗСЛЕДВАНЕ НА ЗАЩИТЕН МЕТОД ОТ ЕЛЕКТРОСТАТИЧНОТО ПОЛЕ НА КОРАБИ, ОСНОВАН НА ПОЛЯРИЗАЦИОННИЯ КОНТРОЛ НА МЕТАЛИТЕ

Ван Сянгджун, Лю И*, Лю Дехонг

Училище по електро-инженерство, Морски инженерен университет, Китай

Постъпила на 21 април, 2018 г.; приета на 28 юли, 2018 г.

Известна е електрохимичната корозия сред различните метали при корабите в морска вода, като най-значителна е тази между стоманения корпус и бронзовото витло. При този електрохимичен корозионен процес корпусът е анод, а витлото – катод. При това се генерира корозионен ток, а заедно с това и електростатично поле в морската вода, което лесно се открива от мини и откриващи съоръжения, които са голяма заплаха за корабите. В настоящата работа е предложен метод за изравняване на потенциалите между корпуса и витлото, основан на кривите на поляризация на металите и комбинирайки анодната и катодната поляризацията. По този начин корозионният ток силно се намалява, а свързаното с него подводно електрично поле може също да се елиминира. Показано е, че с предложения метод се намалява подводното електрично поле, а защитният ефект срещу корозия е очевиден.

Bulgarian Chemical Communications, Volume 50, Issue 4 (pp. 655 – 671) 2018

Optimizing final product properties and Ziegler-Natta catalyst performance with and without hydrogen in propylene polymerization by kinetic modeling

Gh. H. Varshouee[1], A. Heydarinasab[1*] A. Vaziri[1], B. Roozbahani[2]

[1] *Department of Chemical Engineering, Tehran Science and Research Branch, Islamic Azad University, Tehran, Iran*

[2] *Department of Chemical and Biomolecular Engineering, Research Associates of Rice University, USA*

Received, December 4, 2017; Revised, August 2, 2018

Kinetics of propylene polymerization with its unique complexity has the key role on final product properties, but is heavily influenced by the hydrogen amount. Hydrogen, as chain-transfer agent, gives rise to a reduction of the average molecular weight of the polymer and directly affects the final product properties; and on the other hand, based on some theories up to a certain amount causes an increase followed by a decrease in the number of active sites. Therefore, this dual hydrogen behavior must be optimized. To date, no adequate kinetic model has been developed to predict and optimize this behavior and to simultaneously calculate the vital indices of final product properties such as melt flow index, number/weight average molecular weight, and polydispersity index. In addition to determining of the indices, by using the model some vital kinetic parameters such as activation energy, initial rate of reaction and deactivation constant can be easily calculated. The proposed model in this study was coded in MATLAB/SIMULINK software by using the polymer moment balance approach having in mind the dormant site theory as the most credible theory at the moment. The model was validated by comparison with lab experimental data and an agreement within the acceptable range of error was shown. Finally, the optimum reaction temperature and the optimum hydrogen amount according to the used catalyst were obtained as 70°C and 18 mg hydrogen in this study.

Keywords: Mathematical modeling, Propylene polymerization, Kinetic study, Hydrogen response, Population balance, Dormant site theory.

INTRODUCTION

Production of polypropylene (PP) is a multi-billion business, yielding more than 60 million metric tons of the polymer. Between 2005 and 2010, the average annual growth rate of polypropylene production has been about 6.5%/yr. Global polypropylene production capacity is expected to grow by 4.2%/yr from 2010 onwards [1]. With a view to the different applications of the polymer, different molecular weight distributions and final product properties are required; consequently, accurate control of the polymerization process is essential for adjusting appropriate final product properties. Hydrogen, as chain transfer agent, is one of the most important affecting factors on the reaction kinetics and final product properties. Up to now, despite of disputing on the role of hydrogen upon the polymerization, there is no validated mathematical model able to predict the kinetics and the end product simultaneously.

To date, most articles published in the field of polypropylene polymerization modeling have been concerned with heat and mass transfer inside the slurry polymer particles [2-4], or based on the mechanism of reaction and how multigrain particle grow according to [5-7]. Other studies have only concentrated on loop reactors [8,9] and fluidized-bed reactors (FBRs) [10,11], namely bulk and gas phase polymerization that are not applicable to a slurry reactor. As regards rate profiles of propylene polymerization, the first article on liquid phase (i.e. bulk polymerization, no slurry) was published by Samson *et al.* [12] and a number of other authors investigated the hydrogen effect on the kinetics [13-15].

Al-haj *et al*. [15] have observed a hydrogen effect on the profile of the polymerization curve of propylene polymerization in a liquid pool. Their research work was based on experimental results and did not provide a mathematical model. In relation to investigating hydrogen effect during propylene polymerization, many experimental studies have been carried out, but the results of these studies have been ambiguous and even contradictory. This means that the introduction of hydrogen gas during propylene homo-polymerization with Ziegler-Natta catalysts affects the polymerization rate, which can decrease, increase, or remain unaffected (Albizzati *et al*.) [16].

Guastalla & Gianinni, [17] showed that the initial rate of propylene polymerization reaches

* To whom all correspondence should be sent:
E-mail: a.heidarinasab@srbiau.ac.ir

asymptotically about 2.5 times the activity without hydrogen as hydrogen partial pressure is increased, whereas the deactivation rate decreases. Spitz *et al*. [18] found that low hydrogen concentrations in the reactor cause an enhancement of the rate profile; higher hydrogen levels lowered activity and increased deactivation. Rishina *et al*. [19] showed that there is a similar activation effect of hydrogen and found that the effect is reversible. Many researchers reported a similar hydrogen activation effect for different catalyst types and polymerization media [11,19-23]. Contrary to these findings, Soga & Siona [24] found that for $TiCl_4/MgCl_3/Al(C_2H_5)_3$/ethyl benzoate, the propylene polymerization rate decreases with increasing hydrogen partial pressure. According to the authors this is due to the slow addition of the monomer to the catalyst-hydrogen bond formed in the step of chain transfer to hydrogen. Similarly, Kahnnan *et al*. [25] made the conclusion that using a prepolymerized $TiCl_3/Et_2AlCl$ catalyst system, hydrogen not only has no effect on the polymerization rate for low hydrogen concentrations but the rate of polymerization decreases at a high hydrogen concentration; because adsorbed hydrogen lowers the effective monomer concentration near the catalytically active sites. Van Putten [10] pointed out that when hydrogen mole fraction exceeds the value of 0.011, gas-phase propylene polymerization rate starts to decrease. However, when hydrogen concentration is between 0 and 0.011?, a considerable increase in the polymerization rate is observed. According to the author, the decrease in the polymerization rate is due to the slow addition of the monomer to the catalyst-hydrogen bond formed in the step of chain transfer to hydrogen. The author further modeled the polymerization rate and the quasi-single site termination probability as a function of hydrogen-to-propylene molar ratio based on the dormant site theory [15]. Nevertheless, up to now, disputing continues. Luo *et al*. (2013) have modeled loop propylene polymerization reactors in bulk media [26]. The model focused on commercial reactor variables without paying attention to kinetics and final product properties. Next year, another paper has been published on modeling multi-scale PP properties, but in an FBR reactor [27]. In 2016, Seong *el al*. simulated liquid polypropylene polymerization reactors based on Spheripol technology [28]. Although they have paid attention to some final product properties such as average molecular weight and polydispersity, it was not suitable for kinetic study and predicting final product properties.

By means of profile polymerization rate operating conditions, the constancy of the reactor system and quality control of final product can be investigated and indicated, in particular, while hydrogen exists in the reactor system. Given that the effect of hydrogen on the reactor is still vague, a validated model of profile polymerization rate that could correctly predict the system is inevitable. Despite the importance of the matter, a few investigations have been devoted to this subject and no validated model was presented.

The aim of this work is to present a validated model for predicting profile polymerization rate, the effect of hydrogen concentration on profile rate, calculating the model of fraction activated sites catalyst *via* hydrogen concentration and determining important kinetic parameters such as (Ea, Ep, Rp0, Kd). In addition, the model is capable of calculating the most important final product indices, such as melt flow index (MFI), number average molecular weight (Mn), weight average molecular weight (Mw) and polydispersity index (PDI). In addition, the other purpose of this paper is to reveal the effect of hydrogen content on the fraction of activated catalyst sites during polymerization. The model was implemented in a MATLAB/SIMULINK environment and was validated with experimental data in slurry polymerization and the hydrogen response on the kinetic reaction was investigated. The global errors between the model outputs and experimental data are in an acceptable range.

EXPERIMENTAL

Materials

The 4th generation of spherical $MgCl_2$ supported Ziegler-Natta catalyst containing 3.6 wt% of Ti and diisobutyl phthalate (DIBP) as internal donor was supplied by Südchemie, Germany. Triethylaluminium (TEA of 98% purity) from Merck, Germany, diluted in n-heptane, used as co-catalyst and the so-called external donor (cyclohexyl methyl dimethoxy silane) were purchased from Merck and were used without further purification. Polymer grade propylene was provided by Shazand Petrochemical, Iran and was used as received. Hydrogen and nitrogen used were of >99.999% purity. Nitrogen was further purified by passing over beds of absorbents.

Polymer synthesis

In this study, slurry homopolymerization was carried out in heptane medium. Polymerization reactor was a 1L stainless steel vessel manufactured by Büchi Co.; polymerization set-up was designed

in order to conduct slurry polymerization in one vessel. A schematic diagram of the polymerization set-up is shown in Fig 1. A high pressure N_2 line was used to transfer liquid monomer and catalytic system into the reactor.

Catalyst system was injected to the reactor through a stainless steel cylinder in N_2 atmosphere. All gases were online purified by passing through three purification trains (containing molecular sieves) in a series. The individual gases were then filtered and the flow of each reactant was measured and controlled with a mass flow controller manufactured by Brooks.

Experimental R_p-t curves were recorded, the molecular weights of products were measured by gel permeation chromatography (GPC), employing an Agilent PL-220 model with TSK columns at 155°C using 1,2,4-trichlorobenzene as a solvent. The GPC was calibrated with narrow molecular weight distribution polystyrene standard as a reference. MFI of samples were evaluated according to ASTM 1238 at a temperature of 230ºC and load of 2.16 kg.

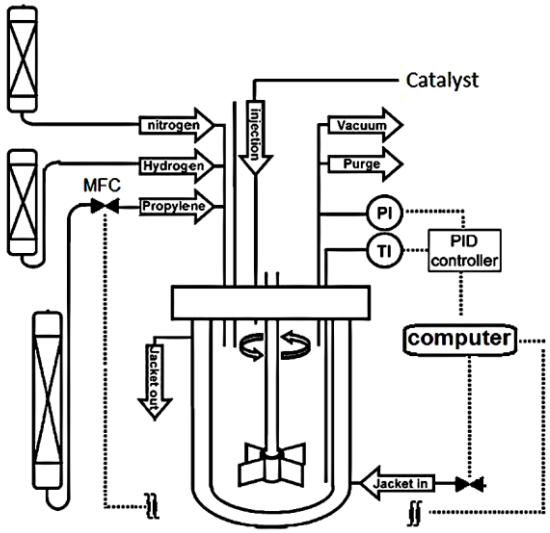

Figure 1. Simplified scheme of the reactor system.

Polymerization procedure

A typical polymerization procedure consisted of reactor preparation, polymerization and discharge. Details are as follows:

Firstly, the reactor was flushed with nitrogen gas at 90°C for 1 h and the reactor temperature was reduced to 20°C, then purged with propylene gas for 15 min. Afterwards, 500 ml of heptane as a solvent was introduced to the reactor; all inputs and outputs of the reactor were closed and stirring at 200 rpm for 5 min was performed for solvent degassing using a vacuum pump. Subsequently, hydrogen was entered to the reactor (based on recipe conditions), then propylene was introduced to the reactor according to controller program, then the reactor was heated up to equilibrium thermodynamic conditions (T=70°C, Pr = 7.5 bar), finally the reactor was ready for catalyst injection to start polymerization. Injecting catalyst to the reactor was carried out under pressure *via* an injection system during polymerization time (two hours) at constant temperature and pressure, that is to say, the reaction was executed under isothermal and isobaric reactor conditions. Data were collected every five seconds.

It is worth mentioning that catalyst preparation should be done according to recipe in a glove box in a nitrogen atmosphere 20 min before injection to the reactor. After each experiment, the resulting polymer was dried under ambient conditions in a laboratory hood for 24 h.

Modeling description

Assumptions: The following modeling assumptions were considered:

1. It was supposed that propylene polymerization was carried out in an amorphous phase and amorphous phase concentrations during polypropylene polymerization were at the thermodynamic equilibrium conditions obeying Sanchez and Lacombe Equation (SLE) [29] for calculating the amount of X, the hydrogen molar ratio Eq (52).
2. It was assumed that $\gamma_1 = \gamma_2 = \cdots = \gamma_{NC}$, where γ is equilibrium constant and NC is number of solvent in slurry phase components.
3. The reaction temperature, pressure and monomer concentration were kept constant during the polymerization process.
4. The resistances of both mass and heat transfer and the diffusion effect of the reactants were ignored.
5. It was assumed that the propagation constant is independent of the length of the growing polymer chain.
6. "Dormant sites theory" for activating catalyst by hydrogen concentration was used [15].

Formulation

As olefin polymerization kinetics with Ziegler-Natta catalysts might be fairly complicated, to date, several reaction steps have been proposed in the literature [9,10,12,18]. However, the most comprehensive steps were proposed by Zacca [9]. The ODE mass balance equations used in the model are (1)-(4). Since the model is a semi-batch process and constant monomer concentration during the polymerization is assumed, the input and output terms (Q_f and Q_0) are eliminated, then the terms of η and ζ are meaningless for our study.

The concentration variations with time used in he modeling are as follows:

$$C_j = C_H, C_A, C_E, C_{Mi}, C_B, C_S, C_T, C_{cat}, P_0^k, \mu_0^k, \mu_1^k, \lambda_0^k, \lambda_1^k, \lambda_2^k$$

The basic kinetic model used in this work is a simplified kinetic mechanism based on Zacca proposal [9] for semi-batch polymerization.

$$\frac{dC_{j,R}}{dt} = [\frac{Q_f C_{j,f}}{V_R}]_{feed\,(input)} - [\frac{(\eta/\zeta) Q_0 C_{j,R}}{V_R}]_{output} + R_j \qquad (1)$$

$$C_{j,R} = \frac{Mole \quad of \; j}{Total \quad Volume} \qquad \text{for j= 1,2,....,NC} \qquad (2)$$

$$\eta_j = \frac{C_{j,a}}{C_{j,l}} \qquad \text{for j= 1,2,....,NC} \qquad (3)$$

$$\zeta_j = \frac{C_{j,o}}{C_{j,R}} = \frac{\rho_0}{\rho_R} \cdot D_f \qquad \text{where :} \qquad (\eta/\zeta) = \begin{cases} \eta & for \quad liquid \quad phase \quad components \\ \zeta & for \quad solid \quad phase \quad components \end{cases} \qquad (4)$$

Therefore, in this work, our model is based on twelve of the most important reactions R5-16 and according to the dormant sites theory [15] the reactions R17-20 for hydrogen response model, as shown below:

Reaction Step	Component	Reaction	Rate Equation	Reaction No
Site activation	Hydrogen	$C_p + H_2 \rightarrow P_0^K$	$R_{aH}^K = k_{aH}^k C_p C_{H,a}^{O_{aH}^K}$	(5) R_1
	Al-alkyl	$C_p + A \rightarrow P_0^K + B$	$R_{aA}^K = k_{aA}^k C_p C_{A,a}^{O_{aA}^K}$	(6) R_2
	Monomer *i*	$C_p + M_i \rightarrow P_0^K + M_i$	$R_{aMi}^K = k_{aMi}^k C_p C_{Mi}^{O_{aMi}^K}$	(7) R_3
Chain initiation	Monomer *i*	$P_0^k + M_i \rightarrow P_{\delta_i,i}^K$	$R_{P0i}^K = k_{P0i}^k P_0^K C_{M_i,a}$	(8) R_4
Chain propagation	Monomer *j*	$P_{n,i}^K + M_j \xrightarrow{Kp} P_{n+\delta_j,j}^K$	$R_{Pji}^K = k_{Pji}^k P_{n,j}^K C_{M_j,a}$	(9) R_5
Chain transfer	Hydrogen	$P_{n,i}^K + H_2 \xrightarrow{Kh} P_0^K + D_n^k$	$R_{cHi}^{K,n} = k_{cHi}^k P_{n,i}^K C_{H,a}^{O_{cHi}^K}$	(10) R_6
	Monomer *j*	$P_{n,i}^K + M_j \xrightarrow{Km} P_{\delta_j,j}^K + D_n^k$	$R_{cM_{ji}}^{K,n} = k_{cM_{ji}}^k P_{n,i}^K C_{j,a}^{O_{cMj,i}^K}$	(11) R_7
Site deactivation	Hydrogen	$P_{n,i}^K + H_2 \rightarrow C_d + D_n^k$	$R_{aHi}^{K,n} = k_{dH}^k P_{n,i}^K C_{H,a}^{O_{dH}^K}$	(12) R_8
		$P_0^K + H_2 \rightarrow C_d$	$R_{dH0}^K = k_{dH}^k P_0^K C_{H,a}^{O_{dH}^K}$	(13) R_9
	Al-alkyl	$P_{n,i}^K + A \rightarrow C_d + D_n^k$	$R_{dAi}^{K,n} = k_{dA}^k P_{n,i}^K C_{A,a}^{O_{dA}^K}$	(14) R_{10}
	Spontaneous	$P_{n,i}^K \rightarrow C_d + D_n^k$	$R_{dSpi}^{K,n} = k_{dSp}^k P_{n,i}^K$	(15) R_{11}
		$P_0^K \rightarrow C_d$	$R_{dSp0}^K = k_{dSp}^k P_0^K$	(16) R_{12}

Using dormant sites theory [15]:

Dormant site formation	$C_j + M \xrightarrow{K_s} S_{j+1}$	(17) R_{17}
Dormant sites reactivation by H_2	$S_j + H_2 \xrightarrow{K_{reh}} C_0 + D_j$	(18) R_{18}
Reactivation of dormant sites by monomer	$S_j + M \xrightarrow{K_p} S_{j+1}$	(19) R_{19}
Deactivation	$C_j \xrightarrow{K_d} D_j$	(20) R_{20}

The component rate equation [9] used in the model is as follows:

Hydrogen $$R_H = -\sum_{K=1}^{Ns}[R_{aH}^k + R_{rH}^k + R_{dH0}^k + \sum_{i=1}^{Nm}\sum_{n=\delta_i}^{\infty}(R_{cHi}^{k,n} + R_{dHi}^{k,n})] \quad (21)$$

Co-catalyst $$R_A = -\sum_{K=1}^{Ns}[R_{aA}^k + R_{dA0}^k + \sum_{i=1}^{Nm}\sum_{n=\delta_i}^{\infty}R_{dAi}^{k,n}] - R_{eA} \quad (22)$$

Electron donor $$R_E = -\sum_{K=1}^{Ns}[R_{dE0}^k + \sum_{\substack{l=1\\l\neq K}}^{Ns}R_{tE0}^{kl} + \sum_{i=1}^{Nm}\sum_{n=\delta i}^{\infty}(\sum_{\substack{l=1\\l\neq K}}^{Ns}(R_{tEi}^{lk,n} + R_{dEi}^{k,n})] - R_{eE} \quad (23)$$

Poison $$R_X = -\sum_{K=1}^{Ns}[R_{dX0}^k + \sum_{i=1}^{Nm}\sum_{n=\delta_i}^{\infty}R_{dXi}^{k,n}] - R_{eE} - R_{eA} \quad (24)$$

Potential sites $$R_{Cp} = -\sum_{K=1}^{Ns}(R_{aH}^k + R_{aA}^k + R_{aSp}^k + \sum_{i=1}^{Nm}R_{aM_i}^k) \quad (25)$$

Vacant sites $$R_{P_0^k} = R_{aH}^k + R_{aA}^k + R_{aSp}^k + \sum_{i=1}^{Nm}R_{aMi}^k + R_{rH}^k - R_{dH0}^k - R_{dE0}^k - R_{aA0}^k - R_{dSp0}^k - R_{dX0}^k - \sum_{j=1}^{Nm}R_{p0j}^k + \sum_{i=1}^{Nm}\sum_{n=\delta i}^{\infty}(R_{cHi}^{k,n} + R_{cSpi}^{k,n}) + \sum_{i=1}^{Nm}\sum_{\substack{l=1\\l\neq K}}^{Ns}\sum_{n=\delta i}^{\infty}(R_{tEi}^{lk,n} + R_{tSpi}^{lk,n})] + \sum_{\substack{l=1\\l\neq K}}^{NS}(R_{tE0}^{lk} + R_{tSp0}^{lk} - R_{tE0}^{kl} - R_{tSp0}^{kl}) \quad (26)$$

Dead sites $$R_{Cd} = \sum_{K=1}^{Ns}[(R_{dH0}^k + R_{dE0}^k + R_{aA0}^k + R_{dX0}^k + R_{aSp0}^k - R_{rH}^k) + \sum_{i=1}^{Nm}\sum_{n=\delta i}^{\infty}(R_{dHi}^{k,n} + R_{dEi}^{k,n} + R_{dAi}^{k,n} + R_{dXi}^{k,n} + R_{dSpi}^{k,n})] \quad (27)$$

Monomer $$R_{Mi} = -\sum_{K=1}^{Ns}[R_{P0i}^k + \sum_{j=1}^{Nm}\sum_{n=\delta i}^{\infty}(R_{Pij}^{k,n} + R_{cMi,j}^{k,n})] \quad (28)$$

Moments equations:

The moments equations for slurry polymerization of PP are presented:

Live polymer $$R_{P_{n,i}^k} = \delta(n-\delta_i)[R_{P0i}^k + \sum_{j=1}^{Nm}\sum_{m=\delta i}^{\infty}R_{cMi,j}^{k,m}] + \sum_{j=1}^{Nm}k_{pij}^k C_{Mi,a}P_{n-\delta_i,j}^k - \sum_{j=1}^{Nm}k_{pij}^k C_{Mj,a}P_{n,i}^k - \alpha_i^k P_{n,i}^k \quad (29)$$

Dead polymer $$R_{D_{n,}^k} = \sum_{i=1}^{Nm}\alpha_i^k P_{n,i}^i \quad \text{where} \quad (30)$$

$$\alpha_i^k = k_{cHi}^k C_{H,a}^{O_{cHi}^k} + k_{cSpi}^k + \sum_{j=1}^{Nm}k_{cMj,i}^k C_{Mj,a} + \sum_{\substack{l=1\\l\neq K}}^{Ns}(k_{tEi}^{kl}C_{E,a}^{O_{tE}^{kl}} + k_{tSpi}^{kl}) + k_{dHi}^k C_{H,a}^{O_{dH}^k} + k_{dAi}^k C_{A,a}^{O_{dA}^k} + k_{dEi}^k C_{E,a}^{O_{dE}^k} + k_{dXi}^k C_{X,a}^{O_{dX}^k} + k_{dSpi}^k$$

Live moment $$\mu_{\delta_i,i}^k = \sum_{n=1}^{\infty}n^{\delta_i}P_{n,i}^k \quad (31)$$

Bulk moment $$\lambda_{\delta_i}^k = \sum_{n=\delta_i}^{\infty}(\sum_{i=1}^{Nm}P_{n,i}^k + D_n^k) \quad (32)$$

Zero-order live polymer moments $$R_{\mu_{0,i}^K} = R_{P0i}^k + \sum_{j=1}^{Nm}k_{cM_i,j}^k C_{Mi,a}\mu_{0,J}^k - \alpha_i^k\mu_{0,J}^k + \sum_{j=1}^{Nm}[k_{pij}^k C_{Mi,a}\mu_{0,J}^k - k_{pji}^k C_{Mj,a}\mu_{0,i}^k] \quad (33)$$

First-order live polymer moments $$R_{\mu_{\delta l}^K} = \sum_{i=1}^{Nm}\delta(i-l)[R_{P0i}^k + \sum_{j=1}^{Nm}k_{cM_i,j}^k C_{Mi,a}\mu_{0,J}^k] - \sum_{i=1}^{Nm}\alpha_i^k\mu_{\delta_l,i}^k + \sum_{i=1}^{Nm}\sum_{j=1}^{Nm}k_{pij}^k C_{Mi,a}\delta(i-1)\mu_{0,i}^k \quad (34)$$

Zero-order bulk polymer moments $$R_{\lambda_0^K} = \sum_{i=1}^{Nm}[R_{P0i}^k + \sum_{j=1}^{Nm}k_{cM_i,j}^k C_{Mi,a}\mu_{0,J}^k] \quad (35)$$

First-order bulk polymer moments $$R_{\lambda_{\delta l}^K} = \sum_{i=1}^{Nm}\delta(i-l)[R_{P0i}^k + \sum_{j=1}^{Nm}k_{cM_i,j}^k C_{Mi,a}\mu_{0,J}^k] + \sum_{i=1}^{Nm}\sum_{j=1}^{Nm}\delta(i-1)k_{pij}^k C_{Mi,a}\mu_{0,J}^k \quad (36)$$

Second-order bulk polymer moments $$R_{\lambda_2} = \sum_{K=1}^{Ns}\sum_{j=1}^{Nm}[R_{P0i}^k + \sum_{i=1}^{Nm}k_{cMj,i}^k C_{Mj,a}\mu_{0,i}^k] + \sum_{k=1}^{Ns}\sum_{i=1}^{Nm}\sum_{j=1}^{Nm}k_{pji}^k C_{Mj,a}(\mu_{0,i}^k + 2\mu_{1,i}^k) \quad (37)$$

The basic polymer properties, called end-use properties, are four items: number average molecular weight (Mn), weight average molecular weight (Mw), melt flow index (MFI) and polydispersity index (PDI).

The equations used in the model are as follows [9]:

$$\overline{M_n} = \sum_{K=1}^{Ns}\sum_{i=1}^{Nm} \frac{\lambda_{\delta_i}^k}{\lambda_0^k}\overline{M_i} \quad (38)$$

$$\overline{M_w} = \lambda_2 \cdot \sum_{k=1}^{Ns} \lambda_0^k \overline{M_n} \Big/ \left(\sum_{K=1}^{Ns}\sum_{i=1}^{Nm} \lambda_{\delta_i}^k\right)^2 \quad (39)$$

Then: $$DPI = \frac{\overline{M_w}}{\overline{M_n}} \quad (40)$$

As the melt flow index is a function of molecular weight, the power-law-type equation below is suggested. Parameters a and b are calculated by fitting appropriate experimental data, it will be discussed later.

$$R_p = R_{p0} \bullet \exp(-k_d \circ t) \quad (41)$$

Determination of the kinetic parameters

A typical polymerization rate profile (Figs. 6 and 7) is comprised of two areas; (I) initial polymerization start up zone, (II) quasi-steady-state zone [15].

Each zone has a significant meaning in kinetic analysis; detailed discussions of these issues have undergone a considerable debate and are not repeated here for the sake of brevity.

Pater *et al*. [13] and some other researchers [14, 15] have shown that the rate of polymerization at isothermal conditions can be described as a first-order process in monomer concentration and the deactivation of the catalyst as a first-order process in the number of active sites. The following equations are used:

$$R_p = K_p C_m C^* \quad (42)$$

$$\frac{dC^*}{dt} = -K_d C^* \quad (43)$$

Combination and integration for isothermal conditions leads then to the following expression that is often used in the literature to describe the time dependent rate of polymerization:

$$R_p = R_{p0} \bullet \exp(-k_d \circ t) \quad (44)$$

So, for finding R_p at isothermal conditions, two parameters, namely R_{p0} and k_d should be obtained. R_{p0} and k_d are determined graphically by the profile of the polymerization rate curve, as shown in Fig. 2. These parameters depend on reaction temperature, hence according to Arrhenius equation, we have:

$$R_p = R_{p0} \bullet \exp(-\frac{E_a}{R.T}) \quad (45)$$

$$k_d = k_{d0} \cdot \exp(\frac{-E_{a,d}}{RT}) \quad (46)$$

Here, R_{p0} is the initial reaction rate, k_d the deactivation constant, $E_{a,d}$ the activation energy for the lumped deactivation reaction, t shows time, and T indicates the temperature. So it could be calculated from the profile of the rate curve of polymerization (t=0).

Since the rate of polymerization depends on temperature, having R_{p0} at different temperatures by using Arrhenius equation, the activation energy of any type of catalyst is easily predictable (as shown by the typical curve in Fig. 2).

Two very important issues should be considered about the activation energy of the Z-N catalyst: (1) it is independent of the hydrogen concentration [15] and (2) it is an intrinsic property of any catalyst and thus can be expected to differ from one type to another.

Yield of the polymerization can be calculated by integrating the rate.

$$Y_{calc} = \int_0^t R_P \cdot dt \quad (47)$$

Amount of Y_{calc} is exactly equal to the area under the profile curve. If this value is multiplied by the weight of catalyst, the produced polymer will be obtained in each batch. Experimentally, the yield is measured by weighing the dry product of batch polymerization. But in fact, much more monomers (consumed monomer) are entered to the reactor, that a part of them are reacted and the other part have remained as unconverted monomer in liquid and gas phases. The model is capable of directly calculating yield and consumed monomer. By plotting the natural logarithm of the reaction rate *versus* polymerization time, a linear fit can be made where the slope of the fit line is k_d, and the intercept is R_{p0}. Fig. 2 illustrates the method.

Hydrogen effect and dormant sites theory to determine k_p

Propagation reaction is the most important reaction in polymerization. Accordingly, determining the value of constant (K_P) and activation energy (E_p) is inevitable for modeling. Before proceeding with discussions in this regard, it is necessary to understand dormant sites theory and the role of hydrogen in polymerization.

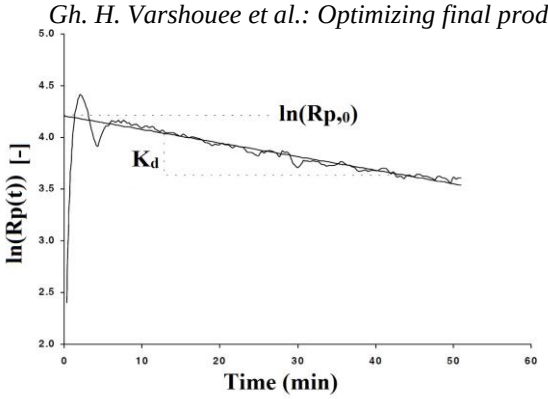

Figure 2. Determination of initial reaction rate R_{p0} and deactivation constant k_d.

Hydrogen always acts as a chain transfer agent during olefin polymerization; when the hydrogen concentration increases, the molecular weight of the polyolefin decreases. On the other hand, the effect of hydrogen on catalyst activity during olefin polymerization is less predictable and varies depending on the type of catalyst, monomer, and donor systems. For instance, hydrogen generally reduces the polymerization rate of ethylene and increases the polymerization rate of propylene when high-activity $TiCl_4/MgCl_2$ catalysts are used (Shaffer and Ray [4]). On the other hand, the effect of hydrogen on catalyst activity during olefin polymerization is less predictable and varies depending on the type of catalyst, monomer, and donor systems. For instance, hydrogen generally reduces the polymerization rate of ethylene and increases the polymerization rate of propylene when high-activity $TiCl_4/MgCl_2$ catalysts are used. So it is concluded that the hydrogen effect depends on two factors: (i) nature of catalyst system and (ii) monomer type. So far, three theories have been suggested to account for the increase in the value of the polymerization rate caused by hydrogen.

Theory 1: Increase in the number of active sites theory.

Theory 2: Change in oxidation states theory.

Theory 3: Dormant sites theory.

The former two theories have been discussed and rejected in the open literature [24,18] and are not repeated here for the sake of brevity.

According to the third, strongest theory so far, the hydrogen effect is illustrated in this statement. Since a propylene molecule is asymmetric with respect to the double bond, it has been suggested that monomers may insert at the catalyst site in four distinct arrangements (head to tail, tail to tail, tail to head and head to head).

Growing chains have two positions of dealing with other monomers (position 1-2 and position 2-1). If the growing chain reacts with position 2-1 of propylene, a “dormant site“ will be created, as shown in Fig. 4. Dormant sites are the drawback of propylene polymerization. Busico *et al.*, (1993) [30] have measured the distributions of end groups in polypropylene in the presence of hydrogen and have suggested that if the propylene molecule inserts in the 2-1 mode, the rate of propagation is reduced due to steric hindrance by the Ti atom. These results are supported by the end group analysis done by Chadwick *et al.* [31].

According to the dormant sites theory, increasing the hydrogen concentration decreases the concentration of dormant sites. The modeling of reaction kinetics and molecular weight is based on the dormant site mechanism (Weickert, 2002 [15]). A "quasi-single-site" model is applied to explain the average behavior of the active sites. In addition, it is assumed that all active sites have the same average rate constants. The chain transfer with co-catalysts is neglected and a quasi steady state is assumed for dormant sites.

This means that according to the dormant sites theory, the reactions $R_{9\text{-}11}$ and $R_{17\text{-}20}$ are the effective reactions on hydrogen response. Using the long chain hypothesis in addition to the assumptions mentioned earlier, the kinetics of Z-N catalysts can be described as a first-order function of both monomer concentration, C_m, and the concentration of active sites, C using a lumped propagation constant K_p .

$$R_p=K_p.C.C_m \tag{48}$$

In reality, the active sites are more or less covered by the polymer produced. The actual catalyst site concentration is between the maximum concentration of active sites C_{max}, and the concentration of dormant sites Cs:

$$C= C_{max} - C_S \tag{49}$$

The concentration of the dormant sites can be calculated assuming the quasi-steady-state:

$$R_S = 0 = K_s.C.C_m - K_{reh}.C_s.C_{H2} - K_{rem}.C_s.C_m \tag{50}$$

K_s, K_{reh} and K_{rem} are rate constants for dormant sites formation, dormant sites reactivation by hydrogen and monomer reactions respectively. So by rearranging these equations, it is concluded that:

$$C_s = \frac{K_s.C}{K_{reh}.X + K_{rem}} \tag{51}$$

where X is the hydrogen molar ratio defined as:

$$X = \frac{C_{H2}}{C_m} \tag{52}$$

Combining Equations (49) and (51) leads to:

$$C = \frac{C_{\max}.(1+K_1.X)}{1+K_2+K_1X} \quad (53)$$

with

$$K_1 = \frac{K_{reh}}{K_{rem}};\ K_2 = \frac{K_s}{K_{rem}} \quad (54)$$

Based on this derivation, Equation (43) can be described as a function of three parameters, k_1, k_2 and k_p:

$$R_p = \frac{K_p.C_m.C_{\max}.(K_1.X+1)}{1+K_1.X+K_2} \quad (55)$$

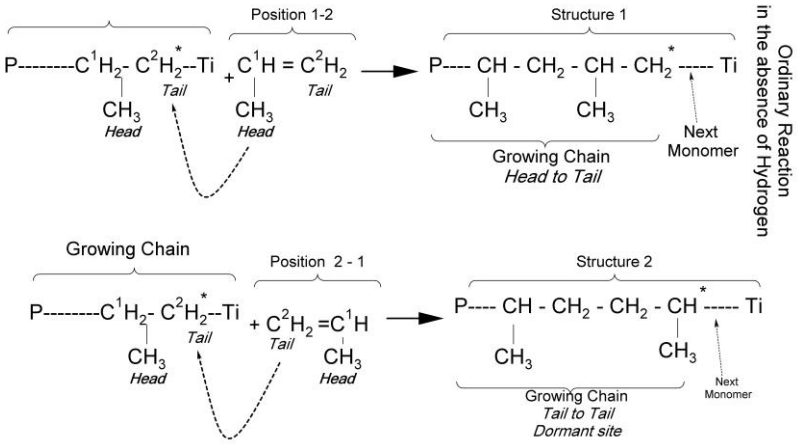

Figure 3. Dormant site generation

Equation (55) can be rewritten as:

$$R_p = K_p.C_{\max}.C_m.f_{H_2} \quad (56)$$

with the hydrogen-dependent function f_{H2} defined as:

$$f_{H_2} = \frac{1+K_1.X}{1+K_2+K_1.X} \quad (57)$$

The parameter f_{H2} represents the fraction of active sites in system. In the absence of hydrogen X = 0, and f_{H2} has a minimum value. This means that the active sites of catalyst are at minimum level in the polymerization system. Consequently, if $f_{H2,max}$ = 1, 100 % of the catalyst sites are active in the reaction.

Equation (57) has three parameters to be determined, namely k_p, k_1, and k_2 The fit is done in two steps, in the first step the value of (k_p/(l +k2)) is obtained, then the values of k_1 and k_2 are estimated. The first step: As the active sites of the catalyst are heterogeneous, the calculated k_P is an average value. This value is determined using the experiments without hydrogen, runs 1, 2 and 3. When no hydrogen is used in the experiments, Eq (55) can be rewritten as:

For X=0 (no hydrogen)

$$R'_{p_0} = \frac{K'_p}{1+K_2}.\rho_m \quad (58)$$

where R'_{p_0} [mol/l sec] and R_{p_0} [kg/g_{cat}.h], and with rearrangement we have:

$$R_{p_0} = \frac{R'_{p_0}}{\rho_m} = \frac{K_p'}{1+K_2} \quad (59)$$

Based on these results, the dependency of (k_p/l +k_2) on reaction temperature has the following form:

$$K_p = K_{p_0}.(1+K_2).\exp(-\frac{E_p}{R.T}) \quad (60)$$

Then we have:

$$Ln(\frac{R_{p_0}}{\rho_m}) = Ln(\frac{K_p}{1+K_2}) = Ln(K_{p_0}) - \frac{E_p}{R.T} \quad (61)$$

Here ρ_m is the monomer density. The Arrhenius plot for (k_p/l+k_2), Fig. 9, shows an excellent fit with linear correlation coefficient (R^2) of 0.9967.

MODELING ALGORITHM

Fig. 4 presents the algorithm of the model solution in a MATLAB/SIMULINK environment. It is composed of two parts; main-program (named "Runsim") and subroutine (function file).

In this study, as in the available literature [8,9], the initially guessed kinetic constants were applied to the model and afterward were adjusted and the exact values were determined for the polymerization according to the set-up (experimental data) by the iterative methodology, as shown in Fig. 5.

RESULTS AND DISCUSSION

Comparison of the model outputs and experimental results in different conditions is summarized in Table 1. The model was validated by experimental data (as shown in Fig. 6(a) in the absence of hydrogen at different temperatures and in Fig. 7 at a constant reactor temperature (70ºC) with different hydrogen concentrations). As it can be seen, the experimental results and model outputs were within an acceptable margin of errors. The margin of errors was determined by:

1. Global error that is the summation of truncation, method and round off error;
2. Personal and measurement equipment errors;
3. Selection of Equation of state.
4. Errors resulting from assumptions.

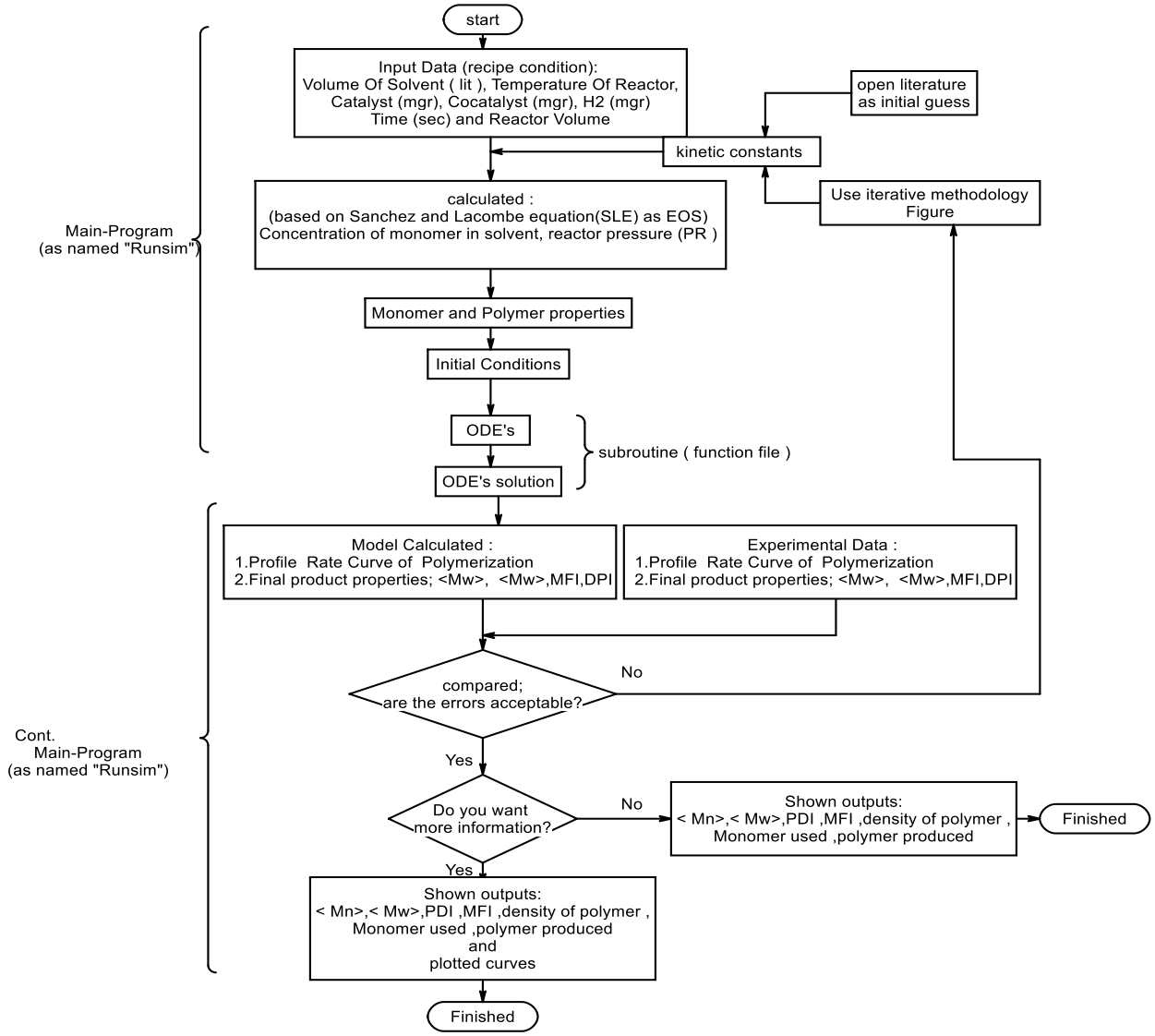

Figure 4. The general algorithm modeling in this work

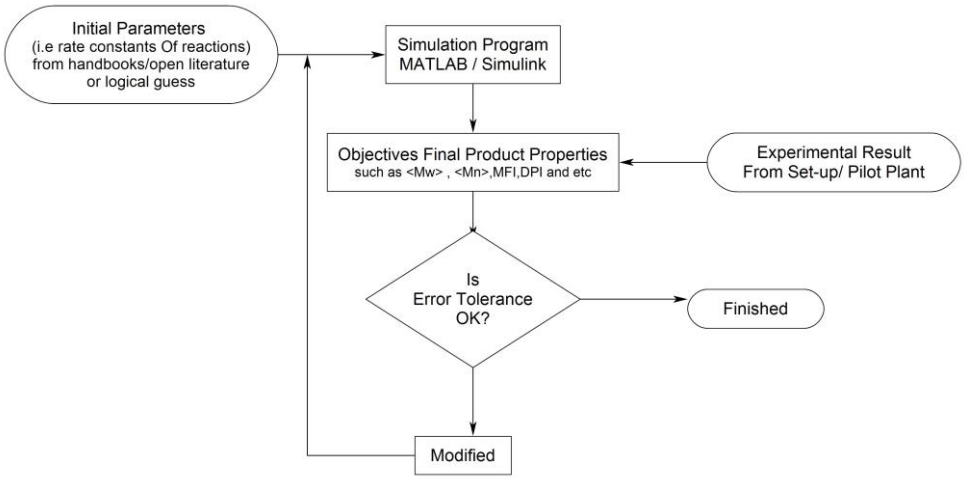

Figure 5. The iterative methodology used to adjust kinetic parameters (constants) in this work.

Table 1. Summarized polymerization recipe; Model and experimental output results

Recipe					Results (Experimental / Model)							
Run No.	T (°C)	H2 (mg)	Catalyst (mg)		Y (gram)	Rp0	Kd (1/hr)	< Mn >	< Mw >	PDI	MFI	ρ (Kg/m^3)
1	65	0	20	Exp. R[1]	63.29	5.01	1.42	210259	863057	4.1	0.75	
				Mod. R[2]	65.13	5.19	1.42	205570	834523	4.06	0.81	589.44
2	70	0	20	Exp. R	72.66	6.5	1.95	304642	1104374	3.63	0.42	
				Mod. R	76.4	7.46	1.98	323780	1214440	3.75	0.33	619.37
3	75	0	20	Exp. R	63.07	8.85	2.04	236154	1124367	4.76	0.4	
				Mod. R	67.25	8.92	2.13	270243	1178300	4.36	0.36	614.62
4	70	183	10	Exp. R	81.33	11.24	2.27	29962	144192	4.81	37	
				Mod. R	88.4	11.43	2.3	32812.7	148874	4.54	36.99562	637.11
5	70	274	10	Exp. R	74.61	11.02	2.05	24016	116939	4.87	62	
				Mod. R	76.81	11.2	2.35	24981.1	123303	4.94	61.98627	620.01
6[6]	70	2000[5]	10	Exp. R								
				Mod. R	64.92	9.34	2.81	9952.25	70163.4	7.06		
7[7]	70	2500[8]	10	Exp. R								
				Mod. R	61.26	8.74	2.97	8353.86	61651.5	7.38		

X: Hydrogen molar ratio calculated by Aspen Software polymer software based on SLE (SOE). [1] Experimental result, [2] Model result, [3] 18 mg H_2 is equivalent to 0.00466 molar ratio X, [4] 27 mg H_2 is equivalent to 0.00703 molar ratio X, [5]2000 mg H_2 is equivalent to 0.0206 molar ratio X, [6] Mathematically calculated. But in fact, this product is off or wax grade, [7] 2500 mg H_2 is equivalent to 0.0243 molar ratio X, [8] Mathematically calculated. But in fact, this product is off or wax grade.

After validating the model, the data of runs 6 and 7 come from model for checking the performance of model and calculating some kinetic parameters such as K_1 for Eq (57) to modeling f_{H2}. The results of the model are in line with what was expected.

The results of Table 1 demonstrated that in the absence of hydrogen, the polymerization rate increased up to 70°C and then decreased at 75°C.

This claim can be verified by investigating the yield of products because the polymerization rate has a direct impact on the yield. Meanwhile, increasing reaction temperature leads to increased deactivation constant (K_d) of the catalyst (Table 1). Accordingly, this event is an important constraint of the reaction. Deactivation of the used catalyst as a function of temperature can be interpreted by Fig. 6 (b) and (c). From Fig. 6 (b) it can be seen that the rate of polymerization at the highest temperature (75°C) sharply increases to the peak in the initial zone, then rapidly drops to point A (about half an hour after beginning the reaction). Hence forward the rate gradually decreases until one hour after starting polymerization and hereafter, it is in a steady condition. So it is concluded that, in the first half hour of the reaction, the catalyst loses most of its activities and after one hour, its activity is at the least possible. This event is not very favorable, and it is a drawback of the process conditions. The profile rate of polymerization at 70°C is the most favorable one, since firstly, it provides the highest yield, and secondly, the catalyst deactivation rate is more acceptable than the other. Therefore it is concluded that 70°C is the optimum reactor temperature. The decrease in polymer yield at the higher temperature is due to catalyst deactivation ether by overreduction of the catalyst sites or *via* an alkylation process with the Lewis base [12].

In order to investigate the effect of variable hydrogen concentration on the profile polymerization rate, Fig. 7 was plotted at the optimum reactor temperature (70°C). To verify the performance of the model, Fig. 7 compares the experiment with the model profile polymerization rate. It is seen that each of both profile rates in same conditions have a fairly good consistence with each other in an acceptable margin of error. The error margin of the final product properties such as Mw, DPI and MFI between model output results and experimental data is acceptable as well (*cf.* Table 1). Accordingly, it is concluded that the model is validated.

It is worth mentioning that according to Arrhenius equation, Ea is dependent on temperature and independent on hydrogen concentration [15]. Therefore, activation energy was calculated by Eq (45) and Fig. 8. It is notable that the activation energy obtained in this work is in line with the open literature data as shown in Table 2. From Fig. 9, the constants of equation (41) could be estimated for predicting MFI by average MW.

Since the most reactions in the polymerization belong to propagation reactions, as expected, the overall activation energy Ea should be very close to the propagation activation energy Ep. Therefore, with calculating and comparing Ep with Ea at least error, it could be a criterion of the accuracy and validity of the model.

Ep was calculated by means of dormant site generation theory using Eq (61) and plotting in Figure 8. The figure shows an excellent fit with linear correlation coefficient (R^2) of 0.9967. Then, from the slope of the line in Fig 10, Ep is obtained. It is interesting to note that comparing Ea and Ep , the difference is only 4% error (Table 3). This is another reason that the model was well enough validated. In addition, the dormant site generation theory is accurately justified by the profile curve rate of propylene polymerization.

In this respect, Al-haj *et al.* (2007), using experimentally method in liquid pool media, have calculated Ea and Ep with approximately 12.82% error (*cf.* table 2). Therefore, this error difference has a significant effect on the subsequent calculations such as R_{p0}, K_1 and K_2 (summarized in Table 3).

Using the dormant theory, equation (57) is obtained. On the other hand, K_1 and K_2 can be estimated using the output of the model and Fig. 8. The equation predicts the fraction of the catalyst active sites *via* hydrogen molar ratio (X). For instance, if there is no hydrogen in the polymerization system (X=0), only 10% of the potential of the catalyst is active, and about 90% of it is laid down and unused (Fig. 9 a). The impact of this issue on Y and R_{p0} is exactly clear and the model is able to predict that (*cf.* Fig. 6 b,c,d,e,f and table 1). Then, by slightly increasing hydrogen content such as X=0.00466, the fraction of activated sites of the catalyst rapidly increases (85.5%) (Figs. 7 and 11 a). But the increasing hydrogen content caused an increase in the deactivation constant K_d (Fig. 11 c). This is not desirable due to the quick deactivation of the catalyst. On the other hand, the increasing hydrogen content has an inverse effect on R_{p0} and Y, in other words, it may lead to changing final product properties and even producing off grade or wax product (Fig. 11 b and d).

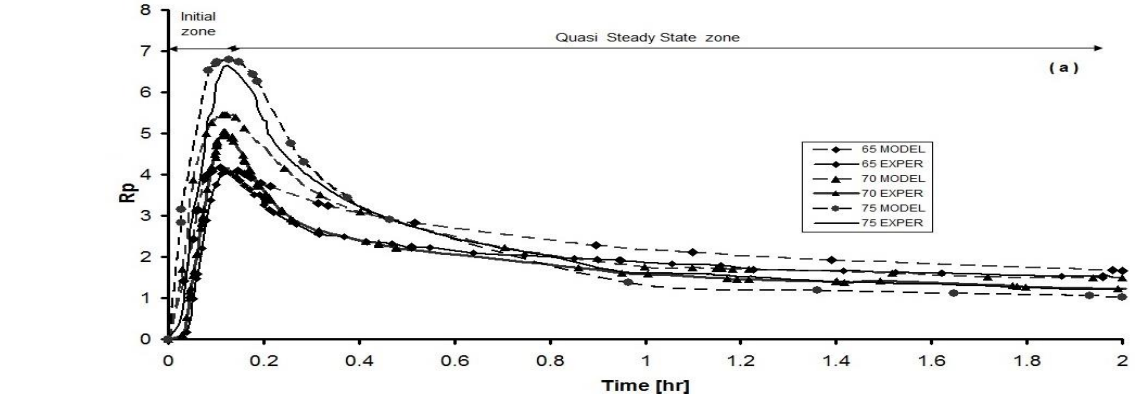
Initial zone
Quasi Steady State zone
(a)
65 MODEL
65 EXPER
70 MODEL
70 EXPER
75 MODEL
75 EXPER
Rp
Time [hr]

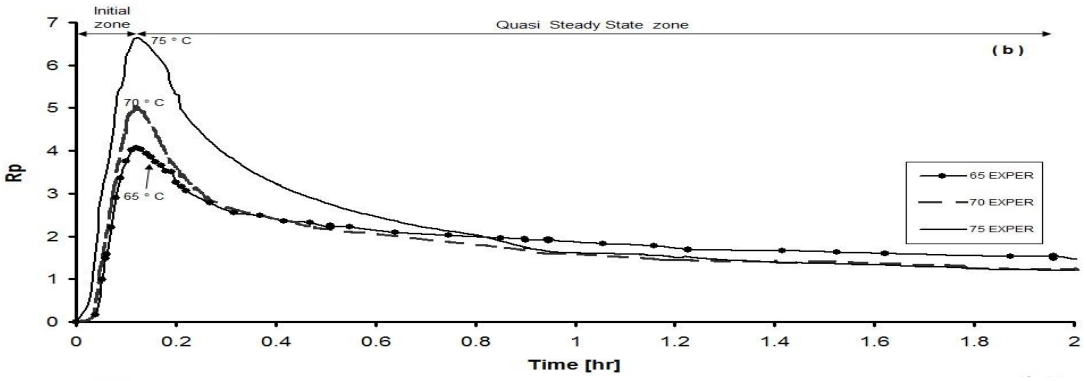
Initial zone
Quasi Steady State zone
(b)
75 ° C
70 ° C
65 ° C
65 EXPER
70 EXPER
75 EXPER
Rp
Time [hr]

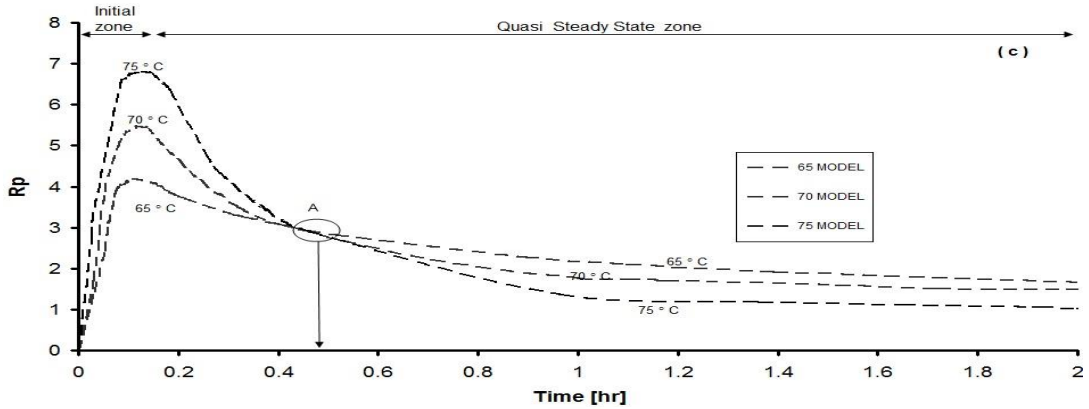
Initial zone
Quasi Steady State zone
(c)
75 ° C
70 ° C
65 ° C
A
65 MODEL
70 MODEL
75 MODEL
Rp
Time [hr]

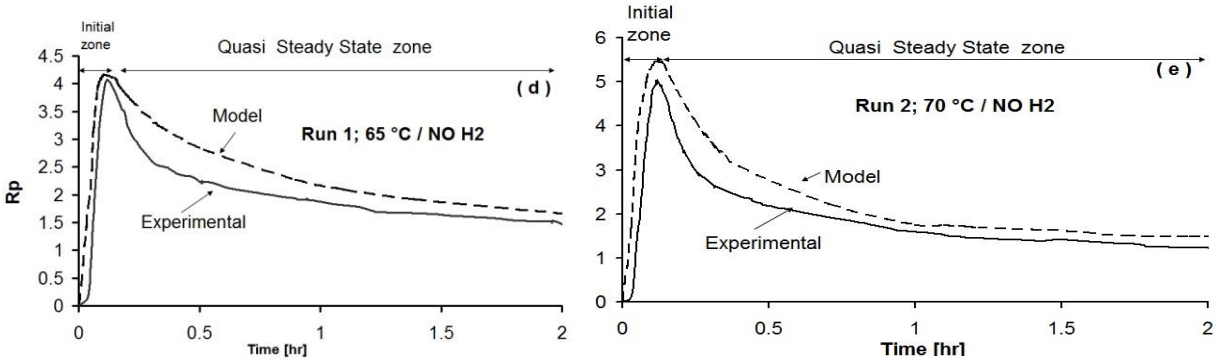
Initial zone
Quasi Steady State zone
(d)
Model
Run 1; 65 °C / NO H2
Experimental
Rp
Time [hr]
Initial zone
Quasi Steady State zone
(e)
Run 2; 70 °C / NO H2
Model
Experimental
Time [hr]

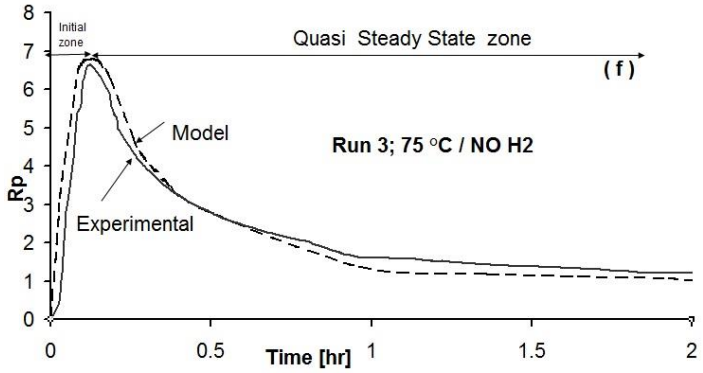

Figure 6. Comparison of experimental and model profile rate in the absence of hydrogen at different temperatures. (a) comparison of model and experimental altogether; (b) comparison of all experimental runs (1,2,3) altogether; (c) comparison of all model runs (1,2,3) altogether; (d) comparison of model and experimental run 1; (e) comparison of model and experimental run 2; (f) comparison of model and experimental run 3.

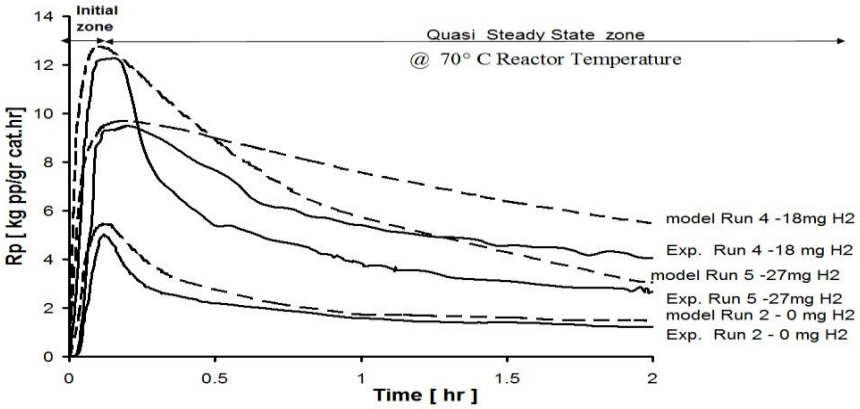

Figure 7. Comparison of experimental and model profile rate in the presence of different hydrogen concentrations at a constant temperature of 70°C.

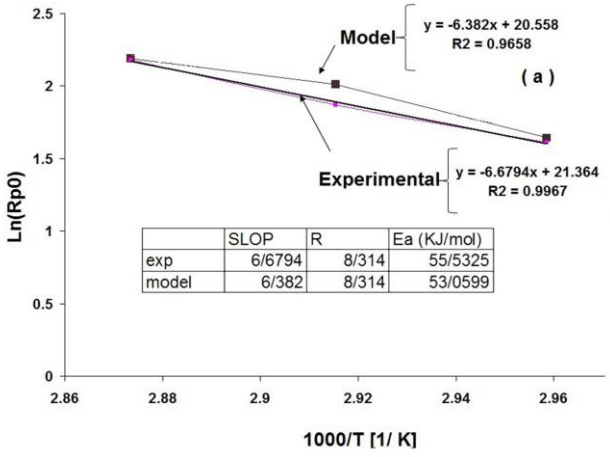

Figure 8. Obtaining Ea by Arrhenius plot of the initial polymerization rates R_{p0} at different temperatures

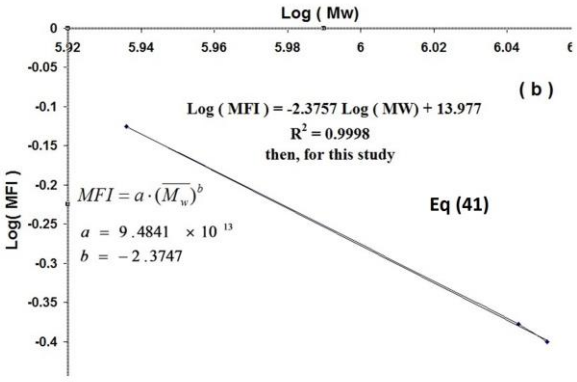

Figure 9. Obtaining constants of eq (42), relation of Mw with MFI

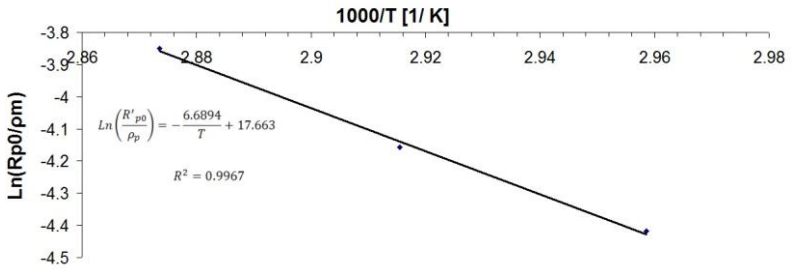

Figure 10. Calculation of propagation constant by using Eq (61)

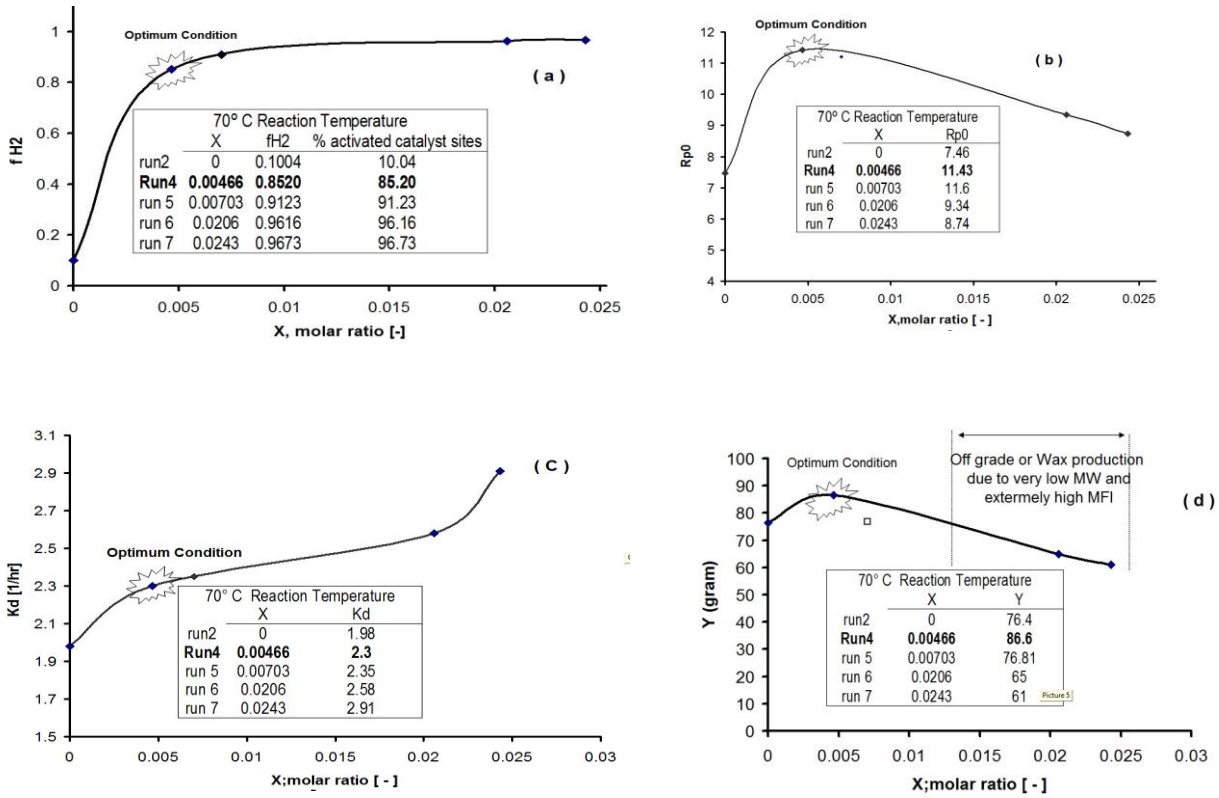

Figure 11. Effect of various hydrogen concentrations on the kinetic parameters: (a) f_{H2};(b) R_{p0}; (C) K_d; (d) Yield

Table 2. Comparison of reported activation energies (Ea) in propylene polymerization systems.

Worker	Catalyst System	Phase	Ea, (KJ/mol)	Reference
Yuan *et. al.*	δ-$TiCl_3$. 1/3 $AlCl_3$ /DEAC	Slurry	53.9	32
Soares *et. al.*	$TiCl_3$/DEAC	Slurry	57.7	20
Al-haj *et al.*	$MgCl_2$/$TiCl_4$/phthalate/silane/TEA	Liq. pool	58.6	15
This work (ave)	$MgCl_2$/$TiCl_4$/phthalate/silane/TEA	Slurry	55.53	*This paper Exp.*
This work (ave)	$MgCl_2$/$TiCl_4$/phthalate/silane/TEA	Slurry	53.05	*This paper Model.*

CONCLUSION

In this paper, a validated mathematical model based on moment approach for an isothermal slurry polymerization of propylene with Ziegler-Natta catalysts is presented that is able to calculate the most important indices of end used product, such as melt flow index (MFI) , number average molecular weight (Mn), weight average molecular weight (Mw) and polydispersity index (PDI), and hydrogen response of the propylene polymerization system.

The model output was in good agreement with experimental results and revealed that there was an optimum temperature (70°C) and hydrogen concentration (18 mg) to achieve maximum amount of polymer yield. At the optimum temperature the PDI was at minimum, indicating optimum dispersity of the polymer chains. In absence of hydrogen, an increase in temperature led to reduction of molecular weight and enhancement of MFI. The activation energy did not depend on the presence or absence of hydrogen and hydrogen

concentration. The model could be able to predict deactivation constant of a unknown catalyst in the presence or absence of hydrogen in the polymerization system.

Table 3. Comparison of kinetic constants in this work with literature data.

	Condition	Overall Ea [kJ/mol]	Ep [kJ/mol]	Err. %	K_{p_0} $[m^3 / gr_{cat}.hr]$	$K_{2[-]}$
Al-haj *et al*. [15] Slurry-bulk	Liquid pool	58.6	67.22	12.82	6.41×10^8	8.02
	$K_1 = -32.2\cdot T^2 + 2.26\cdot T - 3.86\times10^6$					
	Catalyst system: $MgCl_2/TiCl_4$/phthalate/silane/TEA					
This work	Slurry in heptane	53.0599	55.61	4.5	4.69×10^6	8.97
	$K_1 = -1.529\cdot T^2 + 555.24\cdot T - 4.226\times10^6$					
	Catalyst system: $MgCl_2/TiCl_4$/phthalate/silane/TEA					

Notation:

C	total active site concentration, kgmol/m^3
C_d	dead-site concentration, kgmol/m^3
Cj	component *j* bulk concentration, kgmol/m^3
	component *j* concentration at amorphous polymer phase
Cj, a	(effective concentration), kgmol/m^3
Cj,f	component *j* concentration at feed stream, kgmol/ m^3
Cj,l	liquid-phase concentration of component *j*, kgmol/ m^3
Cj,R	concentration into the reactor, kgmol/ m^3
Ck	type *k* active specie concentration, kgmol/m^3
Cp	potential site concentration, kgmol/m3
CP_w	cooling water specific heat, J/kgK
Df	discharge factor
$Dk\,n$	dead polymer chain concentration with ***n*** monomers originated from site *k*, kgmol/m^3
DPI	polydispersity index
K	two-site equilibrium constant, kgmol^{-1}
Kr,ik	kinetic constant for reaction *r* with end-group *i* and site *k*
mC_3, f	monomer feed flow rate, kg/s
mC_{AT}, f	catalyst feed flow rate, kg/s
MFI	melt flow index, gr/10 min
Mj	component *j* molecular weight, kg/kgmol
Mn	number average molecular weight for bulk polymer, kg/kgmol
Mw	mass average molecular weight, kg/kgmol
N	vector containing the number of each monomer in a polymer chain
NC	number of liquid-phase components

Greek letters

γj	equilibrium constant for *j* component between liquid phase and amorphous polymer phase
ξ	ratio between solid-phase components concentration at reactor output flow and into reactor
η	ratio between liquid-phase components concentration at reactor output flow and into reactor
χ	volume fraction of monomer in the amorphous polymer phase
ρl	liquid-phase density, kg m^3

REFERENCES

1. S. L. Bell, A private report by the Process Economics Program, SRI Consulting, IHS Inc., PEP Report 128E, September, 2011
2. A. G. M. Neto, J. C. Pinto, Steady-state modeling of slurry and bulk propylene polymerizations, *Chem. Eng. Sci*., **56**, 4043 (2001).
3. T. F. Mckenna, J. Dupuy, R. Spitz, Modeling of transfer phenomena on heterogeneous Ziegler catalysts: Differences between theory and experiment in olefin polymerization, an introduction, *Appl. Polym. Sci*., **57**, 371 (1995).
4. W. K. A. Shaffer, W. H. Ray, Polymerization of olefins through heterogeneous catalysis. XVIII. A kinetic explanation for unusual effects, *Appl. Polym. Sci*., **65**, 1053 (1997).
5. P. Sarkar, S. K. Gupta, Steady state simulation of continuous -flow stirred - tank slurry propylene polymerization reactors, *Polym. Eng. Sci.,* **32**, 732 (1992).
6. P. Sarkar, S. K. Gupta, Dynamic simulation of propylene polymerization in continuous flow stirred tank reactors**,** *Polym. Eng. Sci.,* **33**, 368 (1993).
7. P. Sarkar**,** S. K. Gupta, Modelling of propylene polymerization in an isothermal slurry reactor, *Polymer*, **32** (15), 2842 (1991).
8. Zh. H. Luo, Y. Zheng, Z. K. Cao, S. H. Wen, Mathematical modeling of the molecular weight distribution of polypropylene produced in a loop reactor**,** *Polymer Engineering and Science*, **47** (10), 1643 (2007).
9. A. S. Reginato, J. J. Zacca, A. R. Secchi, Modeling and simulation of propylene polymerization in nonideal loop reactors, *AIChE Journal*, **49** (10), 2642 (2003).
10. I. van Putten, Polypropylene Polymerization in A Circulating Slugging Fluidized Bed Reactor, PhD thesis, Enschede, University of Twente, 2004.
11. C. Chatzidoukas, J. D. Perkins, E. N. Pistikopoulos, C. Kiparissides, Optimal grade transition and selection of closed-loop controllers in a gas-phase

olefin polymerization fluidized bed reactor; *Chemical Engineering Science*, **58**, 3643 (2003).
12. J. J. C. Samson, J. B. Bosman, G. Weickert, K. R. Westerterp, Liquid-phase polymerization of propylene with a highly active Ziegler-Natta catalyst. Influence of hydrogen, co-catalyst, and electron donor on reaction kinetics. *Journal of Polymer Science: Part A: Polymer Chemistry*, **37**, 219 (1999.
13. J. T. M. Pater, G. Weickert, W. P. M. van Swaaij, Polymerization of liquid propylene with a fourth generation ziegler-natta catalyst: influence of temperature, hydrogen, monomer concentration, and prepolymerization method on polymerization kinetics, *Journal of Applied Polymer Science*, **87**, 1421 (2003).
14. F. Shimizu, J. T. M. Pater, W. P. M. van Swaaij, G. Weickert, Kinetic study of a highly active MgCl2-supported Ziegler-Natta catalyst in liquid pool propylene polymerization. II. The influence of alkyl aluminum and alkoxysilane on catalyst activation and deactivation. *Journal of Applied Polymer Science*, **83**, 2669 (2002).
15. A. M. Al-haj, B. Betlem, B. Roffel, G. Weickert, Hydrogen response in liquid propylene polymerization: towards a generalized model, *AIChE Journal*, **52** (5) ,1866 (2006).
16. E. Albizzati, U. Gianinni, G. Collina, L. Noristi, L. Resconi, Polypropylene Handbook, Catalysts and Polymerizations, E. Moore (ed.), Chap. 3, Carl Hanser Verlag, 1996, p. 11.
17. G. Guastalla, U. Gianinni, The Influence of hydrogen on the polymerization of propylene and ethylene with an MgCl2 supported catalyst. *Makromol. Chem., Rapid Commun.* **4**,519 (1983).
18. R. Spitz, P. Masson, C. Bobichon, A. Guyot, Activation of propene polymerization by hydrogen for improved MgCl2-supported Ziegler-Natta catalysts, *Makromol. Chem.*, **190**, 717 (1989).
19. L. A. Rishina, E. I. Vizen, L. N. Sosnovskaja, F. S. Dyachkovsky, Study of the effect of hydrogen in propylene polymerization with MgCl2 supported Ziegler-Natta catalysts. Part 1, Kinetics of Polymerization, *European Polymer Journal*, **30** (11), 1309 (1994).
20. J. B. P. Soares, A. Hamielec, Kinetics of propylene polymerization with a non-supported heterogeneous Ziegler-Natta catalyst-effect of hydrogen on rate of polymerization, stereoregularity, and molecular weight distribution, *Polymer*, **37** (20), 4607 (1996).
21. G. C. Han-Adebekun, M. Hamba, W. H. Ray, kinetic study of gas phase olefin polymerization with a TiCl4/ MgCl2 catalyst. I. Effect of polymerization conditions. *Journal of Polymer Science: Part A: Polymer Chemistry*, **35**, 2063 (1997).
22. H. Mori, M. Endo, M. Terano, Deviation of hydrogen response during propylene polymerization with various Ziegler-Natta catalysts, *Journal of Molecular Catalysis A*, 211 (1999).
23. G. B. Meier, G. Weickert, W. P. M. van Swaaij, Gas-phase polymerization of propylene: reaction kinetics and molecular weight distribution, *Journal of Polymer Science*: *Part A: Polymer Chemistry* **39**(4), 500 (2001).
24. K. Soga, T. Siano, Effect of hydrogen on the molecular weight of polypropylene with Ziegler-Natta catalysts. *Polymer Bulletin*, **8**, 261 (1982).
25. , R. Kahrman, M. Erdogan, T. Bilgic, Polymerization of propylene using a prepolymerized high-active Ziegler-Natta catalyst. I. Kinetic studies. *Journal of Applied Polymer Science*, **60**, 333 (1996).
26. X.F. Yang, T. Zheng, L.M. Che, Zh.H. Luo, A dynamically distributed reactor model for identifying the flow fields in industrial loop propylene polymerization reactors, *J. Appl. Polym. Sci*., 4302 (2013).
27. Y.-P. Zhua, Zh.-H. Luoa, J. Xiaoc, Multi-scale product property model of polypropylene produced in a FBR: From chemical process engineering to product engineering, *Computers and Chemical Engineering*, **71**, 39 (2014).
28. Sh. H. Kim, S. W. Baek, J. Ch. Lee, W. J. Lee, S. U. Hong , M. Oh, Dynamic simulation of liquid polymerization reactors in Sheripol process for polypropylene, *Journal of Industrial and Engineering Chemistry*, **33**,298 (2016).
29. G. M. N. Costa, S. Kislansky, L. C. Oliveira, F. L. P. Pessoa, S. A. B. Vieira de Melo, M. Embiruc, Modeling of solid–liquid equilibrium for polyethylene and polypropylene solutions with equations of state, *Journal of Applied Polymer Science*, **121**, 1832 (2010).
30. V. Busico, R. Cipullo, P. Corradini, Ziegler-Natta oligomerization of 1-alkenes: A Catalyst's "Fingerprint", 1. *Macromolecular Chemistry and Physics* **194**, 1079 (1993).
31. J. C. Chadwick, A. Miedema, O. Sudmeijer, Hydrogen Activation in Propene Polymerization with MgCl2 Supported Ziegler-Natta Catalysts: The Effect of the External Donor. *Macromolecular Chemistry and Physics*, **195,** 167 (1994).
32. H. G. Yuan, T. W. Taylor, K. Y. Choi, W. H. Ray, Polymerization of olefins through heterogeneous catalysis. 1. Low pressure propylene polymerization in slurry with Ziegler-Natta catalysts, *Journal of Applied Polymer Science*, **27**, 1691 (1982).

ОПТИМИЗИРАНЕ НА СВОЙСТВАТА НА КРАЙНИЯ ПРОДУКТ И ЕФЕКТИВНОСТ НА ЦИГЛЕР-НАТА КАТАЛИЗАТОР В ПРИСЪСТВИЕ И ОТСЪСТВИЕ НА ВОДОРОД ПРИ ПОЛИМЕРИЗАЦИЯТА НА ПРОПИЛЕН ЧРЕЗ КИНЕТИЧНО МОДЕЛИРАНЕ

Г. Х. Варшуе[1], А. Хейдаринасаб[1*] А. Вазири[1], Б. Розбахани[2]

[1] Департамент по инженерна химия, Техерански научен и изследователски клон, Ислямски Азад университет, Техеран, Иран

[2] Департамент по химична и биомолекулярна техника, Изследователски партньор на университета "Райс", САЩ

Постъпила на 4 декември, 2017; коригирана на 2 август, 2018

(Резюме)

С уникалната си сложност, кинетиката на полимеризацията има определящо влияние върху свойствата на крайния продукт, но силно се влияе от количеството на водород. Водородът, като агент на прехвърлянето на веригата, води до намаляване на средното молекулно тегло на полимера и директно влияе върху свойствата на крайния продукт; от друга страна, на основата на някои теории, води до известно нарастване на броя на активните центрове, последвано от намаляване. Следователно, това двойствено отнасяне трябва да се оптимизира. Досега не е разработен адекватен кинетичен модел за предсказване и оптимизиране на това отнасяне и за изчисляване на важните индекси на крайните продукти като индекс на потока на стопилката, бройно/средно молекулно тегло, индекс на полидисперсност. Освен определянето на тези индекси, чрез използване на модела могат да се изчислят някои основни кинетични параметри като активираща енергия, първоначална скорост на реакцията и константа на деактивация. Предлаганият в тази работа модел е кодиран в MATLAB/SIMULINK софтуер с използване на подхода за полимерен моментен баланс, основаващ се на теорията за спящите центрове като най-достоверна теория до момента. Моделът е валидиран чрез сравняване с лабораторни експериментални данни, като е установено съвпадение в рамките на приемливата грешка. Намерени са оптималната реакционна температура (70°C) и оптималното количество водород (18 mg) в съответствие с използвания катализатор.

Abbas A.R., Misbah M., Riaz M.A., Hanif M., Suleman, Gull Y., Kinetic and equilibrium modeling of the removal of Cr (VI) ions by chemically treated *Zea mays* (Corn) cob from aqueous solutions……7
Abbaspour H., See Bakhshi et al……...374
Abd-Elsabour M., See Rageh et al……198
Abo-Bakr A. M., See Rageh et al……..198
Abou-Krisha M. M., See Rageh et al……198
Afqir M., Tachafine A., Fasquelle D., Elaatmani M., Carru J.-C., Zegzouti A., Daoud M., Sol-gel hydrothermal preparation of $Bi_4Ti_3O_{12}$ ceramic.....429
Ahmad T., See Liaqat et al…….....….37
Akhmedov İ.M., See Naghiyev et al.....568
Al-Degs Y., See Gergov et al……265
Al-Ghamdi A., See Al-Sehemi et al……..484
Alimohmmad M., Alirezaei et al……..638
Alin A., See Gergov et al……..265
Alirezaei A., Bayat M., Alimohmmad M., Hashemi S., Study of chlorophenol biological treatment using yeast and mold isolated from industrial and petroleum wastewaters (isolated from the petrochemical wastewater of Imam Khomeini Port (Mahshahr))……638
Al-Jafshar N. M., See Naglah et al……351
Al-Khodir F.A.I., New chelation products of thorium(IV) and cerium(III) with diclofenac and paracetamol analgesic drugs: Synthesis, spectroscopic, thermal stability, antimicrobial activities investigations…. 208
Al-Otifi J. S., See Naglah et al……..351
Al-Sehemi A.G., Al-Ghamdi A., Dishovsky N.T., Malinova P. A., Atanasov N.T., Atanasova G. L. Comparison of properties of natural rubber composites with hybrid fillers containing different modifying phase and their applicability in flexible antennas……...484
Al-Wasidi A. S., See Naglah et al……351
Al-Zahrani A.A., See Rather et al……608
Angelov K.N., See Ivanov et al……..…….89
Angelov K.N., See Ivanov et al……..…….94
Apostolov A.A., See Pashkouleva et al…….524
Arpadjan S., See Voyslavov et al……..417
Arshad M., See Ishaque et al…….368
Arslan F., See Arslan et al. …….……..…16
Arslan H., Şenarslan D., Çevrimli B.S., Zengin H., Uzun D., Arslan F., Preparation of carbon paste electrode containing polyaniline-activated carbon composite for amperometric detection of phenol …….....…..16
Asadov K.A., See Naghiyev et al.....568
Asgarova A.R., See Naghiyev et al.....568
Ashraf M., See Liaqat et al…….....….37
Aslan E., Kürkçü Ö.K., Edge harmonic index of carbon nanocones and an algorithm ……...478
Atanasov N.T., See Al-Sehemi et al……..484
Atanasova G. L., See Al-Sehemi et al……...484
Atanassov A.N., See Borisova et al.....423
Avramova I.A., Radoykova T.Hr., Valchev I.V., Mehandjiev D.R., X-ray photoelectron spectroscopy investigations of lignocellulosic materials……...411
Bai H. L., Zhang D. J., Meng F. L., Fan Y., Zhang P., A metal-organic framework of Co(II): synthesis and supercapacitive properties……...433
Bakhshi S., Abbaspour H., Saeidisar S., Study of phytochemical changes, enzymatic and antioxidant activity of two halophyte plants: Salsola dendroides Pall and Limonium reniforme (Girard) Lincz in different seasons …….374
Bakir T., See Sayiner et al.....398
Balashev K. T., See Chanachev et al……..…...223
Basheva Zh.T., See Sassykova et al……82
Bayat M., See Alirezaei et al……638
Bayat M., See Vaseghi et al.....383
Bibi Y., See Ishaque et al……..368
Blaskov V., Stambolova I., Dimitrov L., Shipochka M., Stoyanova D., Eliyas A., Nanosized Zn_2SnO_4 powders synthesized by coprecipitation and consecutive hydrothermal treatment in two different alkaline media……..…58
Borisova L.H., Kiryakova D.S., Atanassov A.N., Transformation from α- to β-phase in vinylidene fluoride–hexafluoropropylene copolymer nano-composites prepared by co-precipitation method…423
Borovanska I., See Pashkouleva et al……524
Cai H.S., See Pang et al…….161
Canlıca M., Co, Ni, Cu phthalocyanines with tetra substituted bisbenzimide……..294
Carru J.-C., See Afqir et al……429
Çevrimli B.S., See Arslan et al. …….……....16
Chanachev Al. S., Simeonova S. S., Georgiev P. D., Ivanova Tz. N., Petrova S. D., Balashev K. T., Characterization by atomic force microscopy of gold nanoparticles functionalized with azocasein for protease colorimetric enzyme assay ……...223
Chauhan P., See Sadegh et al……602
Chen J.G., See Zhan et al…….....334
Chen M.Q., See Li et al…….494
Chen Z.G., See Zhan et al…….334
Cui G.T., Wang Z.C., Wang X.B., Wang X., Gao J.Q., Effect of boron and boron-nickel on low-temperature impact toughness of hot-rolled Nb-added HSLA H-beams.....145
Danova S.T., See Hristoskova et al……...459
Daoud M., See Afqir et al……..429
Denev P.N., See Ognyanov et al……..…530
Deniz N. G., See Gokmen et al……445
Dimitrijević S., Rajčić Vujasinović M., Dimitrijević St., Trumić B., Ivanović A., Stability of gold complex based on mercaptotriazole in acid and neutral media……..……..…50
Dimitrijević St., See Dimitrijević et al…….……..50
Dimitrijević V. D., See Krstić et al……...237
Dimitrov L., See Blaskov et al……..…..58
Dimitrov M.V., See Popova et al……..405
Dinesh B., See Pedda Kasim et al……363
Dirim S.N., See Talih et al……467
Dishovsky N.T., See Al-Sehemi et al……484
Docheva M.H., Popova V.T., Ivanova T.A., Nikolova V.V., Hristeva T.H., Nikolov N.N., Polyphenol content and

antioxidant activity of aqueous/methanol extracts from different tobacco species (*Nicotiana*)…….....553
Doggar M. Gh., See Ur-Rehman et al……...254
Đorđević D. M., See Krstić et al……...237
Dospatliev L., Ivanova M., Lacheva M., Radoukova T., *Morchella esculenta* (L.) growing in Bulgaria: chemical profile and hazard index……...538
Elaatmani M., See Afqir et al……429
Elezović N.M., See Takić et al.....243
Eliyas A., See Blaskov et al…… ……...58
Epifano F., See Fiorito et al……...189
Erdogan F.O., Comparative study of sunset yellow dye adsorption onto cornelian cherry stones-based activated carbon and carbon nanotube...……..592
Ertik O., See Sacan et al……119
Esmaeili E., Shafiei F., QSAR study on the physico-chemical parameters of barbiturates by using topological indices and MLR method……44
Fallah H., See Mohammadi et al……...111
Fan Y., See Bai et al……...433
Fang J.J., See Pang et al……161
Fasquelle D., See Afqir et al……..429
Feng G., See Yao et al……...228
Feng L., See Zhan et al……..334
Fiorito S., Epifano F., Preziuso F., Taddeo V. A., Genovese S., Waste waters of milk and cheese processing as an efficient promoter for the synthesis of 1,8-dioxo-octahydroxanthenes……..……...189
Fu Ch.Y., See Guo et al……....171
Ganji D. D., See Gerdroodbary et al……298
Gao J.Q., See Cui et al……..145
Gao T.Z., See Pang et al……161
Gao Zh.X., See Guo et al……...171
Genovese S., See Fiorito et al……....189
Georgiev P. D., See Chanachev et al……..……..223
Georgiev Y.N., See Ognyanov et al……..530
Gerdroodbary M.B., Ganji D. D., Taeibi-Rahni M., Vakilipour Sh., Moradi R., Application of direct simulation Monte Carlo for development of micro gas sensor ……..298
Gergov G., Alin A., Katsarov P., Simeonov V., Yankov D., Al-Degs Y., Net analyte signal-based methods for the simultaneous determination of paracetamol, propyphenazone and caffeine by UV spectrophotometry.....265
Ghauri M., See Ur-Rehman et al……...254
Ghorannevis M., See Vaseghi et al.....383
Gokmen Z., Deniz N. G., Onan M. E., Sayil C., Synthesis and spectral properties of new piperazine derivatives and a structural study ……..445
Gomathi V., Selvameena R., Crystal structure of 4-amino-N-pyrimidin-2-ylbenzenesulfonamide……...33
Grudeva V. V., See Papanov et al.....502
Gull Y., See Abbas et al. ……..7
Guo H.Y., Gao Zh.X., Fu Ch.Y., Luo Y., Xia D.P., Experimental study on the feasibility of reducing coal dust by alkaline solution …….……..….171
Gurbanov A.V., See Naghiyev et al.....568
Guseynov E.Z., See Naghiyev et al.....568
Hanif M., See Abbas et al……..…7
Hao R.T., See Yang et al……...324
Hao R.T., See Yang et al……...329
Haq A.U., See Liaqat et al……..….37
Hashemi S., Alirezaei et al……638
Hashemi S., See Vaseghi et al.....383
Hassanabadi A., See Khaleghdadi et al……194
Hassani A.H., See Rahbari et al.....124
Heydarinasab A., See Varshouee et al……655
Hodzhova M.M., See Ognyanov et al……...530
Hozzein W. N., See Naglah et al……...351
Hristeva T.H., See Docheva et al……...553
Hristoskova S.P., Yocheva L.D., Yankov D.S., Danova S.T., Newly characterized butyrate producing *Clostridium* sp. strain 4a1, isolated from chickpea beans (*Cicer arietinum* L.) ……..459
Hristov H., Nedyalkova M., Simeonov V., Insight into polymer-borate hybrid films - structural approach..281
Huang W.X., Wei Z.Z., Niu G.Y., Zhang Y.J, Shao H.F., Effects of sodium polyacrylate and potassium polymer on growth and physiological characteristics of different flue-cured tobaccos……...315
Hussain S.M., See Mishra et al……..…..…….....621
Imran M., See Liaqat et al……...….37
Ipci Y., See Sacan et al……..…119
Ishaque M., Bibi Y., Qayyum A., Khalid Rafiq M., Arshad M., Saqlan Naqvi S. M., Nisa S., Jenks M. A., Antioxidant potential, total phenolic and flavonoid contents of three culinary medicinal plant species of Lesser Hamalya, Pakistan ..……368
Ivanov K. V., See Papanov et al.....502
Ivanov O.D., Ralev Y.I., Todorov P.V., Popov I.P., Angelov K.N., Pérez-Díaz J.L., Kuneva M.K., Laboratory system for artificial fog generation with controlled number and size distribution of droplets……..……89
Ivanov O.D., Ralev Y.I., Todorov P.V., Popov I.P., Pérez-Díaz J.L., Kuneva M.K., System for generation of fogs with controlled impurities .....……..…...……94
Ivanova M., See Dospatliev et al.....538
Ivanova St. D., See Papanov et al.....502
Ivanova St.A., See Popova et al……405
Ivanova T.A., See Docheva et al……...553
Ivanova Tz. N., See Chanachev et al……..…..223
Ivanović A., See Dimitrijević et al…….……....50
Jaffery M. H., See Ur-Rehman et al……..254
Jalili M., See Sadegh et al……602
Jamil F., See Ur-Rehman et al……...254
Javid A.H., See Rahbari et al..... 124
Jenks M. A., See Ishaque et al……...368
Jeyajothi K., Kalaichelvi P., Heat transfer performance of stainless steel, mild steel and aluminium target plate for various configurations of impinging air jet……631
Kabasakal L., See Sacan et al……119
Kahveci B., See Menteşe et al……...218
Kalaichelvi P., See Jeyajothi et al……631
Kalykberdyev M.K., See Sassykova et al……..…82
Kandemirli F., See Sayiner et al.....398
Kara I., Chemical analysis of components in burned and unburned propellant powders ……204
Karadjova V., See Velkov et al……452
Katsarov P., See Gergov et al……265
Khabnadideh S., See Zamani et al……517

Khaleghdadi M., Hassanabadi A., One-pot three-component synthesis of 3-[(aryl)-arylsulfanyl-methyl]-4-hydroxy-6-methylpyran-2-one ……...194
Khalid Rafiq M., See Ishaque et al……368
Khalilov A.N., See Naghiyev et al.....568
Khanlarkhani A., See Parvizi et al……286
Khurram M.Sh., See Ur-Rehman et al……..254
Kirilova-Doneva M., See Pashkouleva et al……..524
Kiryakova D.S., See Borisova et al.....423
Kolikov K.H., See Minkov et al……..……63
Koumanova B.K., See Lavrova-Popova et al.....274
Krastev I.N., See Valkova et al…….560
Kratchanova M.G., See Ognyanov et al……530
Krishna M. S. R., See Pedda Kasim et al……..363
Krstić I. M., See Krstić et al……..237
Krstić N. S., Nikolić R. S., Dimitrijević V. D., Đorđević D. M., Stanković M. N., Krstić I. M., Nikolić M. G., Lactic acid and M(II) d-metals (Cu, Co, Mn, Cd) milli- and micro- quantities interaction: FTIR and ESI-MS analysis……..237
Kumar M., Rattan G., Prasad R., Promotional effect of Au on γ-Al_2O_3 supported cobalt based catalyst for total oxidation of methane ……..437
Kuneva M.K., See Ivanov et al……..……89
Kuneva M.K., See Ivanov et al……..……94
Kürkçü Ö.K., See Aslan et al……478
Lacheva M., See Dospatliev et al.....538
Lakshmi Sahitya U., See Pedda Kasim et al…….....363
Lavrova-Popova S.I., Yaneva Z.L., Koumanova B.K., Study on copper ions adsorption from aqueous solution by Emeraldine…....……..…274
Le P.T.Q., Nguyen V.M., Effect of polyphenol extract from *Polygonum multiflorum* Thunb. root on the storage of minced red tilapia (*Oreochromis* sp.)……...545
Li G., See Qin et al.....151
Li J., See Shang et al……133
Li M.C., See Yang et al…….324
Li M.C., See Yang et al…….329
Li X. L., See Qin et al.....151
Li Y. J., See Qin et al 151
Li Y.M., Ni W.M., Chen M.Q., Zhou Z., Yang Y. Q., Preparation of Fe_3O_4/TiO_2 composite and its application in photocatalysis of organic pollutants……..494
Li Z.B., See Zhan et al……...334
Liaqat M., Mahmud T., Imran M., Ashraf M., Haq A.U., Muddassar M., Ahmad T., Synthesis, characterization and biological activities of a novel Mannich base 2-[(3, 4-dimethoxyphenyl)(pyrrolidin-1-yl)methyl] cyclopentanone and its complexes with Cu(II), Co(II), Ni(II) and Fe(II) ions.……...……..…37
Liu D., See Wang et al……..641
Liu F.L., See Pang et al……..161
Liu Y., See Wang et al……..641
Liu Y.F., See Pang et al……..161
Luo Y., See Guo et al……...171
Mahanpoor K., See Shokri et al. ……....27
Maharramov A.M, See Naghiyev et al.....568
Mahmud T., See Liaqat et al……...37
Malinova P. A., See Al-Sehemi et al…….484
Mamedov I.G., See Naghiyev et al.....568
Mammadova G.Z., See Naghiyev et al.....568
Manev E.D., See Minkov et al……63
Massenova A.T., See Sassykova et al……..…82
Mehandjiev D.R., See Avramova et al……..411
Mehrgan M.R., See Rahbari et al.....124
Memon Sh.A., See Ur-Rehman et al…….254
Meng F. L., See Bai et al……...433
Meng L.F., See Wu et al.....306
Menteşe E., Yılmaz F., Kahveci B., A new green protocol for the synthesis of 2-substituted perimidines from hydrazones under catalyst- and solvent-free conditions…….218
Minkov I.L., Manev E.D., Sazdanova S.V., Kolikov K.H., Effect of controlled volume variation on the osmotic rate in aqueous solutions……63
Misbah M., See Abbas et al. ……..……...7
Mishra M.R., Hussain S.M., Sharma R., Seth G. S., Effect of heat absorption on Cu-water based magneto-nanofluid over an impulsively moving ramped temperature plate……621
Moazzez Dizgarani Sh., See Nikoofar et al.....100
Mohammadi A., Fallah H., Shahouzehi B., Najafipour H., Effect of LXR agonist T0901317 and miR-33inhibitor on SIRT1-AMPK and circulating HDL-C levels…111
Moradi R., See Gerdroodbary et al……298
Muddassar M., See Liaqat et al……...37
Muhammad A., See Rather et al……608
Mukhtar H., See Mushtaq et al……..575
Mukhtar H., See Mushtaq et al……...584
Mushtaq A., Mukhtar H., Shariff A.M., Effect of MEA on the performance of polysulfone/polyvinyl acetate blend membranes……..……..584
Mushtaq A., Mukhtar H., Shariff A.M., Synthesis and characterization of polymeric blend membranes enhanced by monoethanolamine for CO_2/CH_4 separation…….575
Naghiyev F.N., Maharramov A.M., Akhmedov İ.M., Asadov K.A., Khalilov A.N., Gurbanov A.V., Mammadova G.Z., Asgarova A.R., Guseynov E.Z., Mamedov I.G., One-pot synthesis of substituted imino- and imidazopyridines under catalyst-free conditions…….568
Naglah A. M., Al-Wasidi A. S., Al-Jafshar N. M., Al-Otifi J. S., Refat M. S., Hozzein W. N., Synthesis, characterization and antioxidant measurements of selenium (IV) complexes with some amino acids – binuclearcomplexes..……...351
Najafipour H., See Mohammadi et al……111
Nedyalkova M., See Hristov et al……..281
Nguyen V.M., See Le et al……...545
Ni W.M., See Li et al…….494
Nikolić M. G., See Krstić et al……..…237
Nikolić R. S., See Krstić et al……237
Nikolov N.N., See Docheva et al……..553
Nikolova V.V., See Docheva et al……..553
Nikoofar K., Moazzez Dizgarani Sh., HNO_3 immobilized on nano SiO_2: A novel efficient heterogeneous catalytic system for the synthesis of 2-substituted oxazolines, imidazolines, thiazolines, and 2-aryl-1H-benzimidazoles under solvent-free conditions ……100

Nisa S., See Ishaque et al……. 368
Niu G.Y., See Huang et al…….315
Nosrati A.C., See Vaseghi et al.....383
Nurakhmetova M., See Sassykova et al……..……82
Oancea S., See Răcuciu et al…….393
Ognyanov M.H., Hodzhova M.M., Petkova N.T., Denev P.N., Georgiev Y.N., Kratchanova M.G., Isolation and characterization of plant cell wall material from rose hip fruits……...530
Onan M. E., See Gokmen et al……..445
Paliulis D., See Seniūnaitė et al…….……...74
Palizdar Y., See Parvizi et al…….286
Paneva S.S., See Rizov et al……..250
Pang H.C., Fang J.J., Liu Y.F., Cai H.S., Liu F.L., Gao T.Z., Isotope signatures and hydrochemistry as tools in assessing nitrate source in shallow aquifer of Hebei, China…….……..……161
Papanov S. I., Petkova Ek. G., Ivanov K. V., Ivanova St. D., Grudeva V. V., Analytical characteristics of wild and cultivated strawberries (spring & autumn harvests) of Southern Bulgaria & Northern Greece……..502
Parvizi B., Khanlarkhani A., Palizdar Y., Nonlinear predictive control based on artificial neural network model for pilot reformer plant: Approach for ratio control…….…….286
Pashkouleva D., Kirilova-Doneva M., Borovanska I., Apostolov A.A., Degradation of partially absorbable surgical mesh: a chemical and mechanical study…524
Pedda Kasim D., Suneetha P., Krishna M. S. R., Dinesh B., Sri Deepthi R., Lakshmi Sahitya U., Identification of volatile compounds from maize aeral parts infested by *Chilo partellus* (swine hoe) using GC-MS analysis..……..……...363
Peng W.Y., See Zhan et al…….334
Pérez-Díaz J.L., See Ivanov et al……89
Pérez-Díaz J.L., See Ivanov et al……94
Petkov V., See Tsanova-Savova et al……..69
Petkova Ek. G., See Papanov et al.....502
Petkova N.T., See Ognyanov et al…….530
Petrov L.A., See Rather et al…….608
Petrova S. D., See Chanachev et al……...223
Popov I.P., See Ivanov et al……89
Popov I.P., See Ivanov et al……94
Popova T.M., Ivanova St.A., Dimitrov M.V., Characterization and drug release from extended-release matrix pellets with montelukast sodium…..405
Popova V.T., See Docheva et al…….553
Prasad R., See Kumar et al……437
Preziuso F., See Fiorito et al…….....189
Qayyum A., See Ishaque et al……...368
Qin F. X., Wei C. F., Wang Z. K., Li G., Li X. L., Li Y. J., Arsenate and arsenite removal by Fe-modified activated carbon supported nano-TiO_2: influence factors and adsorption effect……151
Răcuciu M., Oancea S., Impact of 50 Hz magnetic field on the content of polyphenolic compounds from blackberries…….393
Radoukova T., See Dospatliev et al.....538
Radoykova T.Hr., See Avramova et al……..411
Rafiq S., See Ur-Rehman et al……..254
Rageh H. M., Abou-Krisha M. M., Abo-Bakr A. M., Abd-Elsabour M., Detection limit and electrochemical behavior of maleic acid on a platinum electrode…198
Rahbari K., Hassani A.H., Mehrgan M.R., Javid A.H., Evaluating the process efficiency of industrial wastewater treatment plants using data envelopment analysis approach case study: Khuzestan steel company treatment plant ……124
Rajčić Vujasinović M., See Dimitrijević et al……50
Rakhmetova A.T., See Sassykova et al……...…82
Ralev Y.I., See Ivanov et al……89
Ralev Y.I., See Ivanov et al……94
Rather S.U., Muhammad A., Al-Zahrani A.A., Youssef T.E., Petrov L.A., Synthesis, characterization and CO_2 adsorption of Cr(III)-based metal-organic framework……608
Rattan G., See Kumar et al……437
Refat M. S., See Naglah et al……...351
Rezaei Z., See Zamani et al……...517
Riaz M.A., See Abbas et al. …….…....7
Ribarova F., See Tsanova-Savova et al……..69
Rizov T.N., Paneva S.S., Determination of fluoride in toothpaste and in mouthwash products by GC/FID/HS……..250
Roozbahani B., See Varshouee et al……655
Sacan O., Ertik O., Ipci Y., Kabasakal L., Sener G., Yanardag R., Protective effect of chard extract on glycoprotein compounds and enzyme activities in streptozotocin-induced hyperglycemic rat lungs 119
Sadegh H., Shahryari-ghoshekandi R., Jalili M., Chauhan P., Kinetic study and modeling of Zn^{2+}removal from wastewater by adsorption onto multi-walled carbon nanotubes…….....602
Saeidisar S., See Bakhshi et al……..374
Saqlan Naqvi S. M., See Ishaque et al……..368
Sassykova L.R., Basheva Zh.T., Kalykberdyev M.K., Nurakhmetova M., Massenova Rakhmetova A.T.,, The selective catalytic reactions for improvement K.S. of characteristics of gasolines….....82
Sayil C., See Gokmen et al……445
Sayiner H. S., Bakir T., Kandemirli F., Voltammetric and theoretical study of the interaction of ceftriaxone with phenylalanine……...398
Sazdanova S.V., See Minkov et al……..……63
Selvameena R., See Gomathi et al…..…….……33
Şenarslan D., See Arslan et al. …….……..…16
Sener G., See Sacan et al……...119
Seniūnaitė J., Vaiškūnaitė R., Paliulis D., Coffee grounds as low-cost adsorbent for the removal of copper (II) and lead (II) from aqueous solutions ……74
Seth G. S., See Mishra et al…….....621
Shafiei F., See Esmaeili et al…….……..44
Shahouzehi B., See Mohammadi et al…….....111
Shahryari-ghoshekandi R., See Sadegh et al……602
Shang L., Li J., Zhao Sh., Tian Y., Zhang Zh., Zhang L., Study on intrinsic sulfidation of iron oxides and oxidation behavior of sulfidation products ……...……..…133
Shao A.J., Wang S.W., Sun D.Y., A prediction model for equilibrium adsorption capacity of the saline soil in the estuary region of Yangtze River …...……141

Shao H.F., See Huang et al……315
Shariff A.M., See Mushtaq et al……575
Shariff A.M., See Mushtaq et al……584
Sharma R., See Mishra et al……..621
Shipochka M., See Blaskov et al……..…58
Shokri A., Employing reverse osmosis for the removal of ortho-toluidine from wastewater……..…..21
Shokri A., Mahanpoor K., Using UV/ZnO process for degradation of Acid red 283 in synthetic wastewater……27
Simeonov V., See Gergov et al……265
Simeonov V., See Hristov et al……281
Simeonov V., See Voyslavov et al……417
Simeonova S. S., See Chanachev et al……..223
Song G.L, See Yang et al……..324
Song G.L., See Yang et al……..329
Sri Deepthi R., See Pedda Kasim et al……..363
Stambolova I., See Blaskov et al……....58
Stanković M. N., See Krstić et al……..237
Stoyanova D., See Blaskov et al……..…58
Suleman M., See Abbas et al. ……..7
Sun D.Y., See Shao et al……..……..141
Suneetha P., See Pedda Kasim et al……..363
Suo G.Q., See Zhan et al……...334
Tachafine A., See Afqir et al……429
Taddeo V. A., See Fiorito et al……..189
Taeibi-Rahni M., See Gerdroodbary et al…….298
Takić L.M., Todorović B.Ž., Zdravković A.S., Elezović N.M., Živković N.V., Correlation analysis of physicochemical parameters of the ecological status: a case study of Ibar River (Serbia) ……243
Talih M., Dirim S.N., Determination of the drying characteristics of cherry laurel (*Laurocerasus officinalis* Roem.) puree in a freeze-dryer……..…467
Tang L., See Yao et al……..228
Tian Y., See Shang et al……133
Todorov P.V., See Ivanov et al……..……89
Todorov P.V., See Ivanov et al……..……94
Todorović B.Ž., See Takić et al.....243
Trumić B., See Dimitrijević et al…….……...…50
Tsakovski S., See Voyslavov et al……417
Tsanova-Savova S., Ribarova F., Petkov V., Quercetin content and ratios to total flavonols and total flavonoids in Bulgarian fruits and vegetables……..69
Tsekova D., See Velkov et al……452
Ur-Rehman M., Khurram M.Sh., Rafiq S., Memon Sh.A., Ghauri M., Jamil F., Jaffery M. H., Doggar M. Gh., Modeling of organic Rankine cycle for suitable working fluid in HYSYS for power generation in Pakistan ….....254
Uzun D., See Arslan et al. ……..16
Vaiškūnaitė R., See Seniūnaitė et al……74
Vakilipour Sh., See Gerdroodbary et al…….298
Valchev I.V., See Avramova et al……411
Valkova T.T., Krastev I.N., Instabilities during electrochemical deposition of Sn-Co alloys from gluconate/sulphate electrolyte……560
Varshouee Gh. H., Heydarinasab A. Vaziri, A., Roozbahani B., Optimizing final product properties and Ziegler-Natta catalyst performance with and without hydrogen in propylene polymerization by kinetic modeling……655
Vaseghi N., Bayat M., Nosrati A.C., Ghorannevis M., Hashemi S., ·Evaluation of the plasma jet effects on the citrinin and ochratoxin A producing species of the genus Penicillium……....…....383
Vaziri A., See Varshouee et al……655
Velkov Zh., Tsekova D., Karadjova V., Vezenkov L., Molecular modeling of galanthamine derivatives comprising peptide moiety: methods, targets and accuracy of results ……..452
Vezenkov L., See Velkov et al……..……452
Voyslavov Ts., Tsakovski S., Simeonov V., Arpadjan S., The effect of iron and manganese oxyhydroxide soil fraction on occurence of Cr(VI)……..417
Wang S.W., See Shao et al……141
Wang X., Liu Y., Liu D., Research on protective method of ship electrostatic field based on metal polarization control……..641
Wang X., See Cui et al…….....145
Wang X.B., See Cui et al……...145
Wang Y.D., See Zhan et al……334
Wang Z. K., See Qin et al.....151
Wang Z.C., See Cui et al……...145
Wei C. F., See Qin et al.....151
Wei Z.Z., See Huang et al……315
Wu H.Z., Meng L.F., Cloud point extraction combined with flame atomic absorption spectrometry for analysis of trace silver nanoparticles in environmental waters …….306
X.J. Hou, See Zhan et al……334
Xia D.P., See Guo et al…….....171
Xu L., See Yao et al……..228
Yanardag R., See Sacan et al……119
Yaneva Z.L., See Lavrova-Popova et al.....274
Yang H.G., Hao R.T., Li M.C., Song G.L., A novel all-thin-film electrochromic device for modulating optical transmittance …….....329
Yang H.G., Zhang J.D., Li M.C., Hao R.T., Song G.L, Effects of deposition pressure on Cu_2ZnSnS_4 films prepared by one-step sputtering with quaternary target …….324
Yang Y. Q., See Li et al……494
Yang Y.L., See Zhan et al……334
Yankov D., See Gergov et al……265
Yankov D.S., See Hristoskova et al……..459
Yao Sh., Xu L., Feng G., Tang L., Optimization scheme for a typical longitudinal three-level Rankine cycle cold energy power generation system for recycling liquid gas …….228
Yılmaz F., See Menteşe et al……218
Yocheva L. D., See Hristoskova et al……459
Youssef T.E., See Rather et al……...608
Zamani L., Rezaei Z., Khabnadideh S. Improved synthesis of fluconazole by using nano-SSA as a green catalyst…….517
Zdravković A.S., See Takić et al.....243
Zegzouti A., See Afqir et al……...429
Zengin H., See Arslan et al. …….……..16
Zhan S., Yang Y.L., Peng W.Y., Chen J.G., Li Z.B., X.J. Hou, Feng L., Suo G.Q., Chen Z.G., Zou J., Wang

Y.D., Thickness dependence of internal stress in electrodeposited nano-twinned copper……..……..334
Zhang D. J., See Bai et al……..433
Zhang J.D., See Yang et al……324
Zhang L., See Shang et al……..…133
Zhang P., See Bai et al……...433
Zhang Y.J, See Huang et al……...315
Zhang Zh., See Shang et al……133
Zhao Sh., See Shang et al……..133
Zhou X.-F., Structural change of lignin in catalytic oxidation by Co(salen)…….615
Zhou Z., See Li et al……..494
Živković N.V., See Takić et al.....243
Zou J., See Zhan et al……334

АВТОРСКИ УКАЗАТЕЛ

Або-Бакр А. М., виж Радех и др.....203
Абд-Елсабур М., виж Радех и др.....203
Ал-Кодир Ф.А.И., Нови хелатни продукти на торий(IV) и церий(III) с аналгетичните лекарства диклофенак и парацетамол: синтез и изследване на спектроскопските характери-стики, термичната стабилност и антимикроби-алната активност …….....217
Ал-Васиди А.С., виж Наглах и др.....362
Ал-Дегс И., виж Гергов и др.....273
Ал-Джафшар Н.М., виж Наглах и др.....362
Алин А., виж Гергов и др…….....273
Ал-Отифи Дж.С., виж Наглах и др.....362
Ангелов К.Н., виж Иванов и др.....93
Аршад М., виж Ишак и др.....373
Афкир М., Ташафин А., Фаскел Д., Елатмани М., Карю Ж.-С., Зегзути А., Дауд М., Зол-гел хидротермално получаване на $Bi_4Ti_3O_{12}$ керамика.....……432
Ахмад Т., виж Лакат и др.....43
Абаспур Х., виж Бакши и др.....382
Абу-Криша М. М., виж Радех и др.....203
Аврамова И.А., Радойкова Т.Хр., Вълчев И.В., Механджиев Д.Р., Изследване на лигно-целулозни материали посредством рентгенова фото-електронна спектроскопия.....416
Арпаджан С., виж Воиславов и др.....422
Арслан Ф., виж Арслан и др.....20
Арслан Х., Шенарслан Д., Чеврimли Б.С., Зенгин Х., Узун Д., Арслан Ф., Приготвяне на въглероден пастообразен електрод, съдържащ полианилин-активиран въглероден композит за амперометрично определяне на фенол.……20
Атанасов А.Н., виж Борисова и др.....428
Бакир Т., виж Сайнер и др.....404
Бакши С., Абаспур Х., Саедисар С., Изследване на фитохимичните промени, ензимната и анти-оксидантната активност на две халофитни растения - *Salsola dendroides Pall.* и *Limonium reniforme (Girard*) Lincz през различните сезони.....382
Балашев К., виж Чаначев и др.....227
Башева Ж.Т., виж Сасикова и др.....88
Баят М., виж Алирезаеи и др.....646
Баят М., виж Вазеги и др.....392
Биби Я., виж Ишак и др.....373
Блъсков В., Стамболова И., Димитров Л., Шипочка М., Стоянова Д., Елияс Ал., Нано-размерни прахове от Zn_2SnO_4, синтезирани чрез съутаяване и последователно хидротермично третиране в две различни алкални среди……62
Борисова Л.Х., Кирякова Д.С., Атанасов А.Н., Трансформация на α- в β- фаза при винилиденфлуорид-хексафлуоропропиленови съ-полимерни композити, получени по метода на съутаяването.....428
Боровanska И., виж Пашкулева и др.....529
Вазеги Н., Баят М., Носрати А.Х., Гораневис М., Хашеми С., Влияние на плазмените реактивни ефекти върху Цитринин- и Охратоксин А-произвеждащите форми на *Penicillium*.....392
Вазири А., виж Варшуе и др.....671
Вайшкунайте Р., виж Сенюнайте и др.....81
Вакилипур Ш., виж Гердроодбари и др.....305
Ван С., Лю И., Лю Д., Изследване на защитен метод от електростатичното поле на кораби, основан на поляризационния контрол на металите. 648
Варшуе Г.Х., Хейдаринасаб А., Вазири А., Розбахани Б., Оптимизиране на свойствата на крайния продукт и ефективност на Циглер-Ната катализатор в присъствие и отсъствие на водород при полимеризацията на пропилен чрез кинетично моделиране.....671
Везенков Л., виж Велков и др.....458
Велков Ж., Цекова Д., Караджова В., Везенков Л., Молекулно моделиране на производни на галантамин, съдържащи пептидна част……..458
Воиславов Ц., Цаковски С., Симеонов В., Арпаджан С., Влияние на почвената фракция, съдържаща железни и манганови оксихидроксиди, върху наличието на Cr(VI).....422
Вълкова Т.Т., Кръстев И.Н., Нестабилности при електрохимичното отлагане на Sn-Co сплави из глюконатно-сулфатен електролит.....567
Вълчев И.В., виж Аврамова и др.....416
Ганджи Д.Д., виж Гердроодбари и др.....305
Гао Т., виж Панг и др.....170
Гао Дж.С., виж Куи и др.....150
Гао Ж., виж Гуо и др.....175
Гаури М., виж Ур-Рехман и др.....264
Георгиев Й. Н., виж Огнянов и др.....537
Георгиев П., виж Чаначев и др.....227
Гергов Г., Алин А., Кацаров П., Симеонов В., Янков Д., Ал-Дегс И., Методи, основаващи се на нетния сигнал на аналита за едновременно определяне на парацетамол, пропифеназон и кафеин чрез УВ спектрофотометрия …….....273
Гердроодбари М.Б., Ганджи Д.Д., Таеиби-Рахни М., Вакилипур Ш., Моради Р., Приложение на директна Монте Карло симулация за разработване на микро газов сензор …….....305
Гокмен З., Дениз Н.Г., Онан М.Е., Саил Ц., Синтез и спектрални свойства на нови пиперазинови производни и структурен анализ ……..…...451
Гомати В., Селвамеена Р., Кристална структура на 4-амино-N-пиримидин-2-илбензенсулфонамид…..36
Гораневис М., виж Вазеги и др.....392
Гуо Х., Гао Ж., Фу Ч., Луо И., Ксиа Д., Експериментално изследване на възможностите за намаляване на въглищния прах с помощта на алкален разтвор …….....175
Гурбанов А.В., виж Нагиев и др.....574
Гусейнов Е.З., виж Нагиев и др.....574
Дауд М., виж Афкир и др.....432
Денев П. Н., виж Огнянов и др.....537
Дениз Н.Г., виж Гокмен и др.....451
Джавид А.Х., виж Рахбари и др. 132
Джалили М., виж Садег и др.....607

Джамил Ф., виж Ур-Рехман и др.....264
Джан Дж.Д., виж Ян и др.....328
Джан И.Дж., виж Хуан и др.....323
Джан С., Ян И.Л., Пън У. И., Чън Дж.Г., Ли З.Б., Хоу Кс.Дж., Фън Л., Суо Г.К., Чен З.Г., Зоу Дж., Уан И.Д., Зависимост на вътрешното напрежение от дебелината на електроотложени двойни медни кристали …….....338
Джанлъджа М., Фталоцианини на Co, Ni и Cu с тетразаместен бисбензимид ….....297
Джафери М.Х., виж Ур-Рехман и др.....264
Дженкс М.А., виж Ишак и др.....373
Дженовезе С., виж Фиорито и др.....193
Джеяджоти К., Калайчелви П., Ефективност на топлопреноса на пластини от неръждаема стомана, мека стомана и алуминий за различни конфигурации на ударна въздушна дюза.....637
Джорджевич Д.М., виж Кръстич и др.....242
Дизгарани Ш. М., виж Никоофар и др.....110
Дизгарани Ш.М., виж Никоофар и др.....15
Димитриевич В.Д., виж Кръстич и др.....242
Димитриевич С., Райчич Вуясинович М., Димитриевич Ст., Трумич Б., Иванович А., Стабилност на златен комплекс с меркаптотриазол в кисела и неутрална среда.....57
Димитриевич Ст., виж Димитриевич и др.....57
Димитров М.В., виж Попова и др.....410
Димитров Л., виж Блъсков и др.....62
Динеш Б., виж Педа Касим и др.....367
Догар, М.Г., виж Ур-Рехман и др.....264
Доспатлиев Л., Иванова М., Лачева М., Радукова Ц., Растеж на обикновената смръчкула в България: химически профил и здравен риск.....544
Дочева М.Х., Попова В.Т., Иванова Т.А., Николова В.В., Христева Ц.Х., Николов Н.Н., Полифеноли и антиоксидантна активност на водно-метанолни екстракти от различни видове тютюни ……...559
Елезович Н. М., виж Такич и др.....249
Елияс Ал., виж Блъсков и др.....62
Епифано Ф., виж Фиорито и др.....193
Жанг Ж., виж Шанг и др.....140
Жао Ш., виж Шанг и др.....140
Живкович Н.В., виж Такич и др.....249
Жоу Кс.-Ф., Структурни промени в лигнин при каталитично окисление с Co(сален).....620
Замани Л., Резаеи З., Кабнадидех С., Подобрен синтез на флуконазол с използване на наносилика-сярна киселина като „зелен” катализатор.....523
Здравкович А. С., виж Такич и др.....249
Зегзути А., виж Афкир и др.....432
Зенгин Х., виж Арслан и др.....20
Зоу Дж., виж Джан и др.....338
Иванов О.Д., Ралев Я.И., Тодоров П., Попов Й.П., Перес-Диас Х.Л., Кънева М.К., Система за генериране на мъгла с контролирани примеси.....99
Иванов О.Д., Ралев Я.И., Тодоров П.В., Попов Й.П., Ангелов К.Н., Перес-Диас Х.Л., Кънева М.К., Лабораторна система за генериране на изкуствена мъгла с контролирани брой и диаметър на капките.....93
Иванова М., виж Доспатлиев и др.....544
Иванова Ст.А., виж Попова и др.....410
Иванова Т.А., виж Дочева и др.....559
Иванова Цв., виж Чаначев и др.....227
Иванович А., виж Димитриевич и др.....57
Имран М., виж Лакат и др.....43
Ипчи И., виж Сакан и др.....123
Ишак М., Биби Я., Кайум А., Халид-Рафик М., Аршад М., Саклан Накви С. М., Низа С., Дженкс М.А., Антиоксидантен потенциал, общо съдържание на феноли и флавоноиди в три вида кулинарни растения в Лесер Хамалия, Пакистан.....373
Йълмаз Ф., виж Ментеше и др.....222
Кабасакал Л., виж Сакан и др.....123
Кабнадидех С., виж Замани и др.....523
Кайум А., виж Ишак и др.....373
Калегади М., Хасанабади А., Едностадиен трикомпонентен синтез на 3-[(арил)-арилсулфанил-метил]-4-хидрокси-6-метилпиран-2-он ……..197
Кара И., Химичен анализ на компонентите в изгорели и недоизгорели горивни прахове……207
Караджова В., виж Велков и др.....458
Карю Ж.-С., виж Афкир и др.....432
Кахведжи Б., виж Ментеше и др.....222
Кацаров П., виж Гергов и др.....273
Кин Ф., Уей Ч., Уанг Ж., Ли Г., Ли Кс., Ли И., Извличане на арсенат и арсенит с помощта на нано-TiO_2 нанесен върху модифициран с желязо активен въглен: влияещи фактори и адсорбционен ефект ….....160
Коликов К. Х., виж Минков и др.....68
Крачанова М. Г., виж Огнянов и др.....537
Кришна М.С.Р., виж Педа Касим и др.....367
Кръстич И.М., виж Кръстич и др.....242
Кръстич Н.С., Николич Р.С., Димитриевич В.Д., Джорджевич Д.М., Станкович М.Н., Кръстич И.М., Николич М.Г., Изследване на взаимодействието между млечна киселина и M(II) d-метали (Cu, Co, Mn, Cd) на милиграмово и микрограмово ниво чрез FTIR и ESI-MS анализ….....242
Ксиа Д., виж Гуо и др.....175
Куи Г.Т., Уанг З.К., Уанг Кс.Б., Уанг Кс., Гао Дж.С., Влияние на бор и бор-никел върху якостта на удар на горещо валцувани ниско легирани греди с висока якост, съдържащи добавен ниобий …….....150
Лаврова-Попова С. И., Янева З. Л., Хлебаров Г. И., Куманова Б. К., Изследване на адсорбцията на медни йони от воден разтвор с използване на Емералдин.....280
Лакшми Сахитиа У., виж Педа Касим и др.....367
Лачева М., виж Доспатлиев и др.....544
Ле П. Т. К., Нгуен В. М., Влияние на полифенолов екстракт от корени на *Polygonum Multiflorum* Thunb. върху съхранението на нарязана червена тилапия (*Oreochromis* sp.).....552
Ли М.Ц., виж Ян и др.....328
Ли М.Ц., виж Ян и др.....333
Ли Г., виж Кин и др.....160
Ли Дж., виж Шанг и др.....140
Ли З.Б., виж Джан и др.....338

Ли И., виж Кин и др.....160
Ли Кс., виж Кин и др.....160
Лиакат М., Махмуд Т., Имран М., Ашраф М., Хак А.У., Мудасар М., Ахмад Т., Синтез, охарактеризиране и биологична активност на нова Манихова база 2-[(3, 4-диметоксифенил) (пиролидин-1-ил)метил]циклопентанон и комплексите му с Cu(II), Co(II), Ni(II) и Fe(II) йони ….....43
Лиу И., виж Панг и др.....170
Лиу Ф., виж Панг и др.....170
Луо И., виж Гуо и др.....175
Лю Д., виж Ван и др.....648
Манев Е. Д., виж Минков и др.....68
Маханпоор К., виж Шокри и др.....32
Махмуд Т., виж Лакат и др.....43
Мемон Ш.А., виж Ур-Рехман и др.....264
Мерган М.Р., виж Рахбари и др. 132
Механджиев Д.Р., виж Аврамова и др.....416
Моради Р., виж Гердроодбари и др.....305
Мохаммади А., Фаллах Х., Шахузехи Б., Наджафипур Х., Влияние на LXR агонист T0901317 и miR-33 инхибитор на SIRT1-AMPK и циркулиращи HDL-C нива …….....118
Нагиев Ф.Н., Махарамов А.М., Ахмедов И.М., Асадов К.А., Халилов А.Н., Гурбанов А.В., Мамадова Г.З., Асгарова А.Р., Гусейнов Е.З., Мамедов И.Г. Едностадиен синтез на заместени имино- и имидазопиридини в отсъствие на катализатор.....574
Наглах А.М., Ал-Васиди А.С., Ал-Джафшар Н.М., Ал-Отифи Дж.С., Рефат М.С., Хоцеин У.Н., Синтез, охарактеризиране и антиоксидантна активност на комплекси на селен (IV) с някои аминокиселини – бинуклеарни комплекси …….....362
Наджафипур Х., виж Мохаммади и др.....118
Нгуен В. М., виж Ле и др.....552
Недялкова М., виж Христов и др.....285
Низа С., виж Ишак и др.....373
Николич М.Г., виж Кръстич и др.....242
Николич Р.С., виж Кръстич и др.....242
Николов Н.Н., виж Дочева и др.....559
Николова В.В., виж Дочева и др.....559
Никоофар К., Дизгарани Ш. М., HNO_3 имобилизирана върху нано SIO_2: нова ефективна хетерогенна каталитична система за синтез на 2-заместени оксазолини, имидазолини, тиазолини и 2-арил-1H-бензимидазоли в отсъствие на разтворител.....110
Никоофар К., Дизгарани Ш.М., HNO_3 имобилизирана върху нано SiO_2: нова ефективна хетерогенна каталитична система за синтез на 2-заместени оксазолини, имидазолини, тиазолини и 2-арил-1H-бензимидазоли в отсъствие на разтворител ……..…….15
Ниу Г.И., виж Хуан и др.....323
Носрати А.Х., виж Вазеги и др.....392
Нурахметова М., виж Сасикова и др.....88
Оанча С., виж Ракучу и др.....397
Огнянов М. Хр., Ходжова М. М., Петкова Н. Тр., Денев П. Н., Георгиев Й. Н., Крачанова М. Г., Изолиране и характеристика на растителни клетъчни стени от шипкови плодове.....537
Пализдар И., виж Парвизи и др.....293
Палиулис Д., виж Сенюнайте и др.....81
Панг Х., Фанг Дж., Лиу И., Цаи Х., Лиу Ф., Гао Т., Изотопна идентификация и хидрохимия като инструменти за оценка на източниците на нитрати в плиткия водоносен хоризонт на равнината Хебей, Китай …….....170
Панева С.С., виж Ризов и др.....253
Парвизи Б., Ханлархани А., Пализдар И., Нелинеен предсказващ контрол на основата на изкуствен модел на невронна мрежа за пилотна установка: подход за контрол на съотношенията …….....293
Пашкулева Д., Кирилова-Донева М., Боровинска И., Апостолов А. А., Разлагане на частично абсорбируема хирургична мрежа: химично и механично изследване.....529
Педа Касим Д., Сунета П., Кришна М.С.Р., Динеш Б., Шри Дефти Р., Лакшми Сахитиа У., Идентифициране на летливите съединения от надземните части на царевица, инфектирани с *Chilo partellus*, с помощта на GC-MS анализ..…….....367
Перес-Диас Х.Л., виж Иванов и др.....93
Перес-Диас Х.Л., виж Иванов и др.....99
Петков В., виж Цанова-Савова и др.....73
Петкова Н. Тр., виж Огнянов и др.....537
Петров Л.А., виж Ратер и др.....614
Петрова Св., виж Чаначев и др.....227
Попов Й.П., виж Иванов и др.....93
Попов Й.П., виж Иванов и др.....99
Попова Т.М., Иванова Ст.А., Димитров М.В., Охарактеризиране и лекарствено освобождаване от матрични пелети с удължено освобождаване на монтелукаст натрий …….....410
Попова В.Т., виж Дочева и др.....559
Прасад Р., виж Кумар и др.....444
Прециузо Ф., виж Фиорито и др.....193
Пън У. И., виж Джан и др.....338
Радех Х.М., Абу-Криша М. М., Або-Бакр А. М., Абд-Елсабур М., Граница на откриване и електрохимично отнасяне на малеинова киселина върху платинов електрод ……203
Радойкова Т.Хр., виж Аврамова и др.....416
Радукова Ц., виж Доспатлиев и др.....544
Райчич Вуясинович М., виж Димитриевич и др.....57
Ракучу М., Оанча С., Влияние на 50 Hz магнитно поле върху съдържанието на полифенолни съединения в къпини …….....397
Ралев Я.И., виж Иванов и др.....93
Ралев Я.И., виж Иванов и др.....99
Ратан Г., виж Кумар и др.....444
Ратер С.У., Мухамад А., Ал-Захрани А.А., Юсеф Т.Е., Петров Л.А., Синтез, охарактеризиране и CO_2 адсорбция върху метал-органична мрежа на основата на Cr(III).....614
Рафик С., виж Ур-Рехман и др.....264
Рахбари К., Хасани А.Х., Мерган М.Р., Джавид А.Х., Оценка на ефективността на пречиствателни станции за индустриална отпадна вода с използване на анализ на обхвата на данните с

примерен случай пречиствателната станция на Хузестанския завод за производство на стомана ….....132
Рахметова К.С., виж Сасикова и др.....88
Резаеи З., виж Замани и др.....523
Рефат М.С., виж Наглах и др.....362
Рибарова Ф., виж Цанова-Савова и др.....73
Ризов Т.Н., Панева С.С., Определяне на флуорид в паста за зъби и продукти за орална хигиена с използване на газова хроматография с пламъков йонизационен детектор и автоматично устройство за внасяне на проби (GC/FID/HS) …….....253
Розбахани Б., виж Варшуе и др.....671
Садег Х., Шахриари-гошеканди Р., Джалили М., Чаухан П., Кинетично изследване и моделиране на отстраняването на Zn^{2+} от отпадна вода чрез адсорбция върху многостенни въглеродни нанотръбички.....607
Саедисар С., виж Бакши и др.....382
Сазданова С. В., виж Минков и др.....68
Саил Ц., виж Гокмен и др.....451
Сайнер А.Х.С., Бакир Т., Кандемирли Ф., Волтамперометрично и теоретично изследване на взаимодействието между цефтриаксон и фенилаланин…….....404
Сакан О., Ертик О., Ипчи И., Кабасакал Л., Сенер Г., Янардаг Р., Защитен ефект на екстракт от цвекло върху глюкопроктеиновите съединения и ензимната активност в белите дробове на стрептозодоцин-индуцирани хипергликемични плъхове …….....123
Саклан Накви С. М., виж Ишак и др.....373
Сасикова Л. Р., Башева Ж.Т., Каликбердиев М.К., Нурахметова М., Масенова А.Т., Рахметова К.С., Селективни каталитични реакции за подобряване на характеристиките на газолини…….....88
Селвамеена Р., виж Гомати и др.....36
Сенер Г., виж Сакан и др.....123
Сенюнайте Й., Вайшкунайте Р., Палиулис Д., Утайка от кафе като евтин адсорбент за отстраняване на мед (II) и олово (II) от водни разтвори …….....81
Сет Г. С., виж Мишра и др.....630
Симеонов В., виж Воиславов и др.....422
Симеонов В., виж Гергов и др.....273
Симеонов В., виж Христов и др.....285
Симеонова С., виж Чаначев и др.....227
Стамболова И., виж Блъсков и др.....62
Станкович М.Н., виж Кръстич и др.....242
Стоянова Д., виж Блъсков и др.....62
Сун Г.Л., виж Ян и др.....328
Сун Г.Л., виж Ян и др.....333
Сун Д., виж Шао и др.....144
Сунета П., виж Педа Касим и др.....367
Суо Г.К., виж Джан и др.....338
Сю Л., виж Яо и др.....236
Тадео, В. А. виж Фиорито и др.....193
Такич Л.М., Тодорович Б.Ж., Здравкович А. С., Елезович Н. М., Живкович Н.В., Корелационен анализ на физикохимичните параметри на екологичния статус: пример с река Ибар (Сърбия).....249
Тиан И., виж Шанг и др.....140
Тодоров П., виж Иванов и др.....99
Тодоров П.В., виж Иванов и др.....93
Тодорович Б.Ж., виж Такич и др.....249
Трумич Б., виж Димитриевич и др.....57
У Х.З., Мън Л.Ф., Екстракция при точката на помътняване в съчетание с атомноабсорбционна спектрометрия за анализ на следови количества от сребърни наночастици в отпадни и природни води.....311
Уан И.Д., виж Джан и др.....338
Уанг Ж., виж Кин и др.....160
Уанг З.К., виж Куи и др.....150
Уанг Кс.Б., виж Куи и др.....150
Уанг Ш., виж Шао и др.....144
Уей З.З., виж Хуан и др.....323
Уей Ч., виж Кин и др.....160
Узун Д., виж Арслан и др.....20
Ур-Рехман М., Хурам М.Ш., Рафик С., Мемон Ш.А., Гаури М., Джамил Ф., Джафери М.Х., Догар, М.Г. Моделиране на органичен Rankine цикъл за подходящ работен флуид чрез HYSYS за производство на енергия в Пакистан ……..264
Фаллах Х., виж Мохаммади и др.....118
Фанг Дж., виж Панг и др.....170
Фаскел Д., виж Афкир и др.....432
Фиорито С., Епифано Ф., Прециузо Ф., Тадео, В. А. Дженовезе С., Отпадъчни води от производ-ството на мляко и сирене като ефективен промотор за синтеза на 1,8-диоксо-октахидроксантени.....193
Фу Ч., виж Гуо и др.....175
Фън Г., виж Яо и др.....236
Фън Л., виж Джан и др.....338
Хак А.У., виж Лакат и др.....43
Халид-Рафик М., виж Ишак и др.....373
Халилов А.Н., виж Нагиев и др.....574
Ханлархани А., виж Парвизи и др.....293
Хао Р.Т., виж Ян и др.....328
Хао Р.Т., виж Ян и др.....333
Хасанабади А., виж Калегади и др.....197
Хасани А.Х., виж Рахбари и др. 132
Хашеми С., виж Алирезаеи и др.....646
Хашеми С., виж Вазеги и др.....392
Хейдаринасаб А., виж Варшуе и др.....671
Хлебаров Г. И., виж Лаврова-Попова и др.....280
Ходжова М. М., виж Огнянов и др.....537
Хоу Кс.Дж., виж Джан и др.....338
Хоцеин У.Н., виж Наглах и др.....362
Христева Ц.Х., виж Дочева и др.....559
Христов Хр., Недялкова М., Симеонов В., Поглед към хибридни полимер-боратни филми – структурен подход …….....285
Хуан У.Кс., Уей З.З., Ниу Г.И., Джан И.Дж., Шао Х.Ф., Влияние на натриев полиакрилат и калиев полимер върху растежа и физиологичните параметри на различни опушени тютюни ….....323
Хурам М.Ш., виж Ур-Рехман и др.....264
Хусаин С. М., виж Мишра и др..... 630
Цаи Х., виж Панг и др.....170

Цаковски С., виж Воиславов и др.....422
Цанова-Савова С., Рибарова Ф., Петков В., Съдържание на кверцетин и съотношенията му към общите флавоноли и общите флавоноиди в български плодове и зеленчуци.....73
Цекова Д., виж Велков и др.....458
Чаначев Ал., Симеонова С., Георгиев П., Петрова Св., Иванова Цв., Балашев К., Охарактеризиране на златни наночастици, функционализирани с азоказеин с помощта на атомно-силова микроскопия (AFM) и приложението им за колориметрични ензимни тестове на протеаза.....227
Чаухан П., виж Садег и др.....607
Чеврimли Б.С., виж Арслан и др.....20
Чен З.Г., виж Джан и др.....338
Чън Дж.Г., виж Джан и др.....338
Шанг Л., Ли Дж., Жао Ш., Тиан И., Жанг Ж., Жанг Л., Изследване на сулфидирането на железни оксиди и поведението на сулфидираните продукти при окисление 140
Шао А., Уанг Ш., Сун Д., Модел за предсказване на равновесното адсорбирано количество от солена почва в естуарната област на река Янцзе …….....144
Шао Х.Ф., виж Хуан и др.....323
Шариф А.М., виж Муштак и др.....583
Шарма Р., виж Мишра и др.....630
Шафией Ф., виж Есмаейли и др.....49
Шахриари-гошеканди Р., виж Садег и др.....607
Шахузехи Б., виж Мохаммади и др.....118
Шенарслан Д., виж Арслан и др.....20
Шипочка М., виж Блъсков и др.....62
Шокри А., Маханпоор К., Използване на UV/ZnO процес за разграждане на Кисело червено 283 в синтетична отпадна вода …….....32
Шокри А., Използване на обратна осмоза за отстраняване на *орто*-толуидин от отпадна вода …….....26
Шри Дефти Р., виж Педа Касим и др.....367
Юсеф Т.Е., виж Ратер и др.....614
Ян И.Л., виж Джан и др.....338
Ян Х.Г., Джан Дж.Д., Ли М.Ц., Хао Р.Т., Сун Г.Л., Влияние на наляганeто на отлагане върху филми от Cu_2ZnSnS_4, получени чрез едностадийно разпрашаване с четворна мишена ….....328
Ян Х.Г., Хао Р.Т., Ли М.Ц., Сун Г.Л., Ново електрохимично устройство от изцяло тънък филм за модулиране на оптична пропускливост…..…333
Янардаг Р., виж Сакан и др.....123
Янева З. Л., виж Лаврова-Попова и др.....280
Янков Д., виж Гергов и др.....273
Яо Ш., Сю Л., Фън Г., Тан Л., Оптимизационна схема на типична надлъжна система с Ранкинов цикъл на три нива, използваща студена енергия, за генериране на енергия за рециклиране на течен газ.....….236

SUBJECT INDEX

1,8-diaminonaphthalene……218
^{13}C and ^{31}P-NMR spectroscopy……615
4-amino-N-pyrimidin-2-ylbenzenesulfonamide…….....33
4-hydroxy-6-methyl-2*H*-pyran-2-one……194
acid red 283……27
additives……...82
adsorption isotherms……592
adsorption……74,141,151,602,608
aerosols……89
air pollution……94
alcohol-insoluble solids……530
alkaline solution……171
alumina……..437
Alzheimer's disease……...452
amino acids……351
AMP-activated protein kinase……...111
anodic polarization…….....641
anthocyanins……...393,502
antioxidant activity……553
antioxidant enzymes……..374
antioxidant……...368,502,545
antiurease activities……....37
aqueous medium……274
aqueous/methanol extracts……553
Arisaema flavum……368
aromatic aldehydes…….189,194
arsenic removal……..151
artificial fog……89,94
aspen HYSYS 8.8……..254
atomic force microscopy……...223
azocasein……223
band gap……...……..324
barbiturates…….....44
benzimidazole……100
benzylidenemalononitrile……..568
$Bi_4Ti_3O_{12}$……429
biomimetic catalysis……..615
biosensor…….....16
biosorption…….....7
bisbenzimide……..294
blackberry……..393
boric acid……...281
boron……145
bulky substituent……294
butyric acid……459
carbon dioxide separation…….584
carbon nanocones……..478
carbon paste……16
catalyst-free conditions……..218
catalysts……82,437
cathodic polarization…….....641
ceftriaxone……...……...…...……...……....398
cerium(III).....208
characterization……...429,530
chard……..119
chemical analysis……....204
chemical characterization……..151
chemical profile……538
chemical status……...243
chemometrics……..……..417
cherry laurel puree……467
chickpea beans……...459
chlorophenol wastewater treatment……...638
cholinesterase inhibitor……....452
chromium (VI)……...……417
chronoamperometric measurements……..198
citrinin……383
Clostridium……459
cloud point extraction……306
Co(II) ……433
Co(salen) ……..615
coal dust……171
cobalt……...……..437
coffee grounds……74
cold atmospheric pressure plasma……383
contact angle……..171
contamination……161
copper ions removal……..274
copper……...……74,334
co-precipitation……..423
corn cob……..…...7
cornelian cherry stones……..592
correlation analysis……243
Cr (VI)……..…7
crystal structure……...…....……324
Cu_2ZnSnS_4 (CZTS) thin film……324
cyclic voltammetry …….....198,398
data envelopment analysis……124
desorption……..141
detoxification……383
DFT (density functional theory) method…….....398
dielectric properties……...……484
diisopropyl ether……..82
dimedone……...189
docking studies……....37
dormant site theory……...655
DPPH……351
DRI plant……...286
droplet size distribution……..89,94
drugs……...……...265
Dryopteris ramose……368
DSMC……298
ecological status……243
edge harmonic index……..478
effective moisture diffusivity……...……467
electrochemical characterization……50
electrochromic device……329
electrodeposition……334,560
electrostatic field protection……..641
eliminating pollutants……....638
emeraldine……...……...……...274
empirical correlation……..631
energy consumption……..467
enhanced polymeric blend membrane……..584
enzyme assay……223
estuary region of Yangtze River……141

ethylcellulose……405
evaluating efficiency……124
extended-release……405
Fe_3O_4/TiO_2 composite.....494
fermentation……459
Fe-TiO_2/AC……151
flame atomic absorption spectrometry……306
flavonoid……374
flavonoids……69
flavonols……69
flexible wearable antenna..……484
fluconazole……517
flue-cured tobaccos……315
fluoride……250
free convection……621
freeze drying……467
Freundlich isotherm……7,74
Freundlich model……141
frozen storage……545
fruits……69
galanthamine……452
gas chromatography……250
gas chromatography-mass spectrometry (GC-MS)204,363
gas sensor……298
gasoline……82
glycoprotein……119
gold complex……50
gold nanoparticles……223
gold……437
graph theory generalized formula……478
green chemistry……100,189
green synthesis……218
growth……315
GSR (gunshot residue)……204
hazard index……538
H-beam……145
headspace (HS)……250
heat absorption……621
heated……228
heavy metals……74
HLA/GO……265
HLA/XS……265
HSQC……615
hybrid fillers..……484
hydrazone……218
hydrogen response……655
hydrogenation……82
hydrogeochemistry……161
hydrolyzed lignocellulosic materials……411
hydrothermal……58,429
hyperglycemic……119
Ibar River……243
ilmenite.....494
imidazoline……100
imidazopyridine……568
iminodihydropyridine……568
impinging air jet……631
in situ polymerization……274
indulin lignin……615
industrial wastewater……21
IR……208
iron oxides……133
iron-sulfur compounds……133
isonicotinic acid……452
isotherm……602
Khuzestan steel company……124
kinetic study……655
kinetics……602
Knudsen force……298
Langmuir isotherm……7,74
Langmuir-Hinshelwood, batch photoreactor……27
lead……74
$LiAlO_2$……329
ligand……608
linear sweep voltammetry……198
LiOH activations……592
lipid oxidation……545
liquefied natural gas……228
low-frequency magnetic field……393
low-temperature impact toughness……145
lung……119
LXR agonist……111
M(II) d-metals……237
magnetic properties..……484
magnetron sputtering……324,329
maleic acid……198
Mannich base……37
mathematical modeling……655
matrix pellets……405
mechanical properties……524
membrane permeability……63
MEMS……298
mercaptotriazole……50
metal blocks……82
metal complex……37
metal phthalocyanines……294
metal-organic framework……433,608
methane……437,584
microstructure……171
milli- and micro-interactions……237
minced fish……545
mineralization……27
miR-33……111
model predictive control……286
molar refractivity……44
monoclinic structure……33
monoethanolamine……575
Morchella esculenta……538
morphology……575
mouthwash products……250
multicomponent *p*-toluene sulfonic acid reactions……194
multiple linear regressions (MLR)……44
multiwalled carbon nanotubes……592,602
mycotoxin……383
n –hexadecanoic acid and volatile compounds……363
nanocatalyst……100
nanoclay……423
nanocomposites……423
nanofluid……621
nanometer size……58

nanorods……351
nanoscale diclofenac……208
nano-SSA……517
nano-twin……334
NAP CLS……265
NAS……265
natural rubber based composites……484
neural network……286
nickel……145
nicotinic acid……452
niobium……145
NiO_x……329
nitrate nitrogen……161
non-cyanide gold electrolyte……50
ochratoxin A……383
octanol/water partition coefficient……44
organic Rankine cycle (ORC)……254
organic synthesis……445
organic-inorganic hydrogels……281
ortho-toluidine……21
oscillations……560
osmotic kinetics……63
oxazoline……100
oxidation……133,437
oxide modifying phase……484
paracetamol……208
penicillium……383
perimidine……218
permeance……584
permeate flux……21
phases……423
phenol……16,374,502
phenolics……393
phenylalanine……398
photocatalysis……494
photocatalyst……58
physiological characteristics……315
piperazine derivatives……445
plant cell walls……530
polarizability……44
polarization potential……641
poliglecaprone……524
poly(ethylene glycol)……281
poly(vinyl alcohol)……281
polyaniline (pani)……16
polyaniline activated carbon composite……16
polymer-borate hybrid films……281
polymeric blend membranes……575
polymeric blend……584
polyphasic taxonomy……459
polyphenol oxidase……16
polyphenols……553
polypropylene……524
polysaccharides……530
population balance……655
powder properties……467
power generation……228
pre-concentration……306
propellant powder……204
propylene polymerization……655
QSAR……44
quercetin……69
Quercus leucotricophora……368
Raman……351
ramped temperature……621
rarefied gas……298
rat……119
redox……151
reducible soil fraction……417
reformer……286
rejection percentage……21
reusable catalyst……100
reverse osmosis……21
reverse permeation……171
rose hip……530
round nozzle……631
saline soil……141
salinity……374
selectivity……584
selenium……351
SEM……351
semipermeable membrane……63
Shahid Tondgooyan……638
silver nanoparticles……306
single crystal XRD……33
soils……417
solar-thermal energy……254
sol-gel……429
solvothermal……608
spectral analysis……575
spectral overlap……265
spectroscopy……237
spraying techniques……89,94
sputtering pressure……324
stability……50
stagnation Nusselt number……631
strawberries……502
stress……334
structure……524
succinic acid……198
sulfidation……133
Sunset yellow……592
supercapacitive properties……433
surface area……608
surgical meshes……524
synthesis……517
T0901317……111
Tafel formula……641
target plate material……631
TEM……208
tergitol TMN-6……306
thermal degradation temperature……575
thermogravimetric analysis……608
thiazoline……100
thin layer modeling……467
thiols……194
thorium(IV)……208
three-level Rankine cycle……228
tin-cobalt alloys……560
tobacco……553

toothpaste……...250
total flavonoids……..368
total phenolics…..…….....……..……..368
treatment plant……...124
trichosporon……...638
triethylfluorosilane (TEFS)……...…...…….....250
UV/ZnO process…….....27
validation…….44
vegetables……69
vinylic substitution……445
vinylidene fluoride-hexafluoropropylene copolymer 423
visible absorption……....58
waste heat……..254
waste waters……...189
water treatment……..602
water-retaining agents……...315
wavelength selection…….265
wet extrusion and spheronization……405
wettability……..171
WO_3……...……329
xanthenes……...189
XPS……133
X-ray analysis……....568
X-ray photoelectron spectroscopy…….411
X-ray study……...…….445
XRD……...…351
Zea mays……363
zinc stannate……....58
Zn^{2+}……602
$\delta_{15}N_{NO3}$.....161
$\delta_{18}O_{NO3}$.....161

Instructions about Preparation of Manuscripts

General remarks: Manuscripts are submitted in English by e-mail The text must be typed on A4 format paper using Times New Roman font size 11, normal character spacing. The manuscript should not exceed 15 pages (about 3500 words), including photographs, tables, drawings, formulae, etc. Authors are requested to use margins of 2 cm on all sides

Manuscripts should be subdivided into labelled sections, e.g. **Introduction, Experimental, Results and Discussion**, *etc*. **The title page** comprises headline, author's names and affiliations, abstract and key words. Attention is drawn to the following:

a) **The title** of the manuscript should reflect concisely the purpose and findings of the work. Abbreviations, symbols, chemical formulas, references and footnotes should be avoided. If indispensable, abbreviations and formulas should be givenin parentheses immediately after the respective full form.

b) **The author**'s first and middle name initials and family name in full should be given, followedby the address (or addresses) of the contributing laboratory (laboratories). **The affiliation** of the author(s) should be listed in detail by numers (no abbreviations!). The author to whom correspondence and/or inquiries should be sent should be indicated by asterisk (*) with e-mail address.

The abstract should be self-explanatory and intelligible without any references to the text andcontaining not more than 250 words. It should be followed by key words (not more than six).

References should be numbered sequentially in the order, in which they are cited in the text. The numbers in the text should be enclosed in brackets [2], [5, 6], [9–12], etc., set on the text line. References are to be listed in numerical order on a separate sheet. All references are to be given in Latin letters. The names of the authors are given without inversion. Titles of journals must be abbreviated according to Chemical Abstracts and given in italics, the volume is typed in bold, the initial page is given and the year in parentheses. Attention is drawn to the following conventions:a) The names of all authors of a certainpublications should be given. The use of "*et al*." inthe list of references is not acceptable.b) Only the initials of the first and middle names should be given. In the manuscripts, the reference to author(s) of cited works should be made without giving initials, e.g. "Bush and Smith [7] pioneered...". If the reference carries the names of three or more authors it should be quoted as "Bush *et al*. [7]", if Bush is the first author, or as "Bush and co-workers [7]", if Bush is the senior author.

Footnotes should be reduced to a minimum. Each footnote should be typed double-spaced at thebottom of the page, on which its subject is first mentioned.**Tables** are numbered with Arabic numerals on the left-hand top. Each table should be referred to inthe text. Column headings should be as short as possible but they must define units unambiguously.The units are to be separated from the preceding symbols by a comma or brackets. Note: The following format should be used when figures, equations, *etc*. are referred to the text (followed by the respective numbers): Fig., Eqns., Table, Scheme.

Schemes and figures. Each manuscript should contain or be accompanied by the respective illustrative material as well as by the respective figure captions in a separate file (sheet).As far as presentation of units is concerned, SI units are to be used. However, some non-SI units are also acceptable, such as °C, ml, l, etc.The author(s) name(s), the title of the manuscript, the number of drawings, photographs, diagrams, etc., should be written in black pencil on the back of the illustrative material (hard copies) inaccordance with the list enclosed. Avoid using more than 6 (12 for reviews, respectively) figures in the manuscript. Since most of the illustrative materials are to be presented as 8-cm wide pictures, attention should be paid that all axis titles, numerals, legend(s) and texts are legible.

The authors are required to submit the text with a list of three individuals and their e-mail addresses that can be considered by the Editors as potential reviewers. Please, note that the reviewers should be outside the authors' own institution or organization. The Editorial Board of the journal is not obliged to accept these proposals.

The authors are asked to submit **the final text** (after the manuscript has been accepted for publication) in electronic form by e-mail. The main text, list of references, tables and figure captions should be saved in separate files (as *.rtf or *.doc) with clearly identifiable file names. It is essential that the name and version of the word-processing program and the format of the text files is clearly indicated. It is recommended that the pictures are presented in *.tif, *.jpg, *.cdr or *.bmp format.

The equations are written using “Equation Editor” and chemical reaction schemes are written using ISIS Draw or ChemDraw programme.

EXAMPLES FOR PRESENTATION OF REFERENCES

REFERENCES

1. D. S. Newsome, *Catal. Rev.–Sci. Eng*., **21**, 275 (1980).
2. C.-H. Lin, C.-Y. Hsu, *J. Chem. Soc. Chem. Commun*., 1479 (1992).
3. R. G. Parr, W. Yang, Density Functional Theory of Atoms and Molecules, Oxford Univ. Press, New York, 1989.
4. V. Ponec, G. C. Bond, Catalysis by Metals and Alloys (Stud. Surf. Sci. Catal., vol. 95), Elsevier, Amsterdam, 1995.
5. G. Kadinov, S. Todorova, A. Palazov, in: New Frontiers in Catalysis (Proc. 10th Int. Congr. Catal., Budapest,(1992), L. Guczi, F. Solymosi, P. Tetenyi (eds.), Akademiai Kiado, Budapest, 1993, Part C, p. 2817.
6. G. L. C. Maire, F. Garin, in: Catalysis. Science and Technology, J. R. Anderson, M. Boudart (eds), vol. 6, SpringerVerlag, Berlin, 1984, p. 161.
7. D. Pocknell, *GB Patent* 2 207 355 (1949).
8. G. Angelov, PhD Thesis, UCTM, Sofia, 2001, pp. 121-126.
9 JCPDS International Center for Diffraction Data, Power Diffraction File, Swarthmore, PA, 1991.
10. CA **127**, 184 762q (1998).
11. P. Hou, H. Wise, *J. Catal.*, in press.
12. M. Sinev, private communication.
13. http://www.chemweb.com/alchem/articles/1051611477211.html.

Texts with references which do not match these requirements will not be considered for publication!!!

CONTENTS

L. Zamani, Z. Rezaei, S. Khabnadideh, Improved synthesis of fluconazole by using nano-SSA as a green catalyst…….. 517
D. Pashkouleva, M. Kirilova-Doneva, I. Borovanska, A. A. Apostolov, Degradation of partially absorbable surgical mesh: a chemical and mechanical study……. 524
M. H. Ognyanov, M. M. Hodzhova, N. T. Petkova, P. N. Denev, Y. N. Georgiev, M. G. Kratchanova, Isolation and characterization of plant cell wall material from rose hip fruits…….. 530
L. Dospatliev, M. Ivanova, M. Lacheva, T. Radoukova, *Morchella esculenta* (L.) growing in Bulgaria: chemical profile and hazard index……. 538
P.T.Q. Le, V.M. Nguyen, Effect of polyphenol extract from *Polygonum multiflorum* Thunb. root on the storage of minced red tilapia (*Oreochromis* sp.)…… ……... 545
M. H. Docheva, V. T. Popova, T. A. Ivanova, V. V. Nikolova, T. H. Hristeva, N. N. Nikolov, Polyphenol content and antioxidant activity of aqueous/methanol extracts from different tobacco species (*Nicotiana*) 553
T. T. Valkova, I. N. Krastev, Instabilities during electrochemical deposition of Sn-Co alloys from gluconate/sulphate electrolyte…….. 560
F. N. Naghiyev, A. M. Maharramov, İ. M. Akhmedov, K. A. Asadov, A.N. Khalilov, A. V. Gurbanov, G. Z. Mammadova, A. R. Asgarova, E. Z. Guseynov, I. G. Mamedov, One-pot synthesis of substituted imino- and imidazopyridines under catalyst-free conditions…….. 568
A. Mushtaq, H. Mukhtar, A. M. Shariff, Synthesis and characterization of polymeric blend membranes enhanced by monoethanolamine for CO_2/CH_4 separation……. 575
A. Mushtaq, H. Mukhtar, A. M. Shariff, Effect of MEA on the performance of polysulfone/polyvinyl acetate blend membranes…….. 584
F. O. Erdogan, Comparative study of sunset yellow dye adsorption onto cornelian cherry stones-based activated carbon and carbon nanotubes……... 592
H. Sadegh, R. Shahryari-ghoshekandi, M. Jalili, P. Chauhan, Kinetic study and modeling of Zn^{2+}removal from wastewater by adsorption onto multi-walled carbon nanotubes……. 602
S. U. Rather, A. Muhammad, A. A. Al-Zahrani, T. E. Youssef, L. A. Petrov, Synthesis, characterization and CO_2 adsorption of Cr(III)-based metal-organic framework……. 608
X.-F. Zhou, Structural change of lignin in catalytic oxidation by Co(salen)…… 615
M. R. Mishra, S. M. Hussain, R. Sharma, G. S. Seth, Effect of heat absorption on Cu-water based magneto-nanofluid over an impulsively moving ramped temperature plate…….. 621
K. Jeyajothi, P. Kalaichelvi, Heat transfer performance of stainless steel, mild steel and aluminium target plate for various configurations of impinging air jet…… 631
A Alirezaei, M Bayat, M Alimohmmad, S Hashemi, Study of Chlorophenol Biological Treatment Using Yeast and mold Isolated from Industrial and Petroleum Wastewaters (Isolated from the Petrochemical Wastewater of Imam Khomeini Port (Mahshahr)) 638
X. Wang, Y. Liu, D. Liu, Research on protective method of ship electrostatic field based on metal polarization control 647
Gh. H. Varshouee, A. Heydarinasab, A. Vaziri, B. Roozbahani, Optimizing final product properties and Ziegler-Natta catalyst performance with and without hydrogen in propylene polymerization by kinetic modeling …… 655
AUTHOR INDEX……..……..……..... 672
AUTHORS INDEX (IN BULGARIAN)……...……..……... 678
SUBJECT INDEX ……..……..…….. 683
INSTRUCTIONS TO THE AUTHORS ……..……..……..……. 687

СЪДЪРЖАНИЕ

Л. Замани, З. Резаеи, С. Кабнадидех, Подобрен синтез на флуконазол с използване на наносилика-сярна киселина като „зелен" катализатор …….. 523

Д. Пашкулева, М. Кирилова-Донева, И. Борованска, А. А. Апостолов, Разлагане на частично абсорбируема хирургична мрежа: химично и механично изследване ……..... 529

М. Хр. Огнянов, М. М. Ходжова, Н. Тр. Петкова, П. Н. Денев, Й. Н. Георгиев, М. Г. Крачанова, Изолиране и характеристика на растителни клетъчни стени от шипкови плодове …… 537

Л. Доспатлиев, М. Иванова, М. Лачева, Ц. Радукова, Растеж на обикновената смръчкула в България: химически профил и здравен риск …. 544

П. Т. К. Ле, В. М. Нгуен, Влияние на полифенолов екстракт от корени на *Polygonum Multiflorum* Thunb. върху съхранението на нарязана червена тилапия (*Oreochromis* sp.) …… 552

М. Х. Дочева, В. Т. Попова, Т. А. Иванова, В. В. Николова, Ц. Х. Христева, Н. Н. Николов, Полифеноли и антиоксидантна активност на водно-метанолни екстракти от различни видове тютюни ……... 559

Т. Т. Вълкова, И. Н. Кръстев, Нестабилности при електрохимичното отлагане на Sn-Co сплави из глюконатно-сулфатен електролит …… 567

Ф. Н. Нагиев, А. М. Махарамов, И. М. Ахмедов, К. А. Асадов, А. Н. Халилов, А. В. Гурбанов, Г. З. Мамадова, А. Р. Асгарова, Е.З. Гусейнов, И. Г. Мамедов, Едностадиен синтез на заместени имино- и имидазопиридини в отсъствие на катализатор …… 574

А. Муштак, Х. Мухтар, А. М. Шариф, Синтез и охарактеризиране на подсилени с моноетаноламин смесени полимерни мембрани за разделяне на CO_2/CH_4 …… 583

А. Муштак, Х. Мухтар, А. М. Шариф, Влияние на моноетаноламин върху ефективността на смесени полисулфон/поливинилови мембрани ……. 591

Ф. О. Ердоган, Сравнително изследване на адсорбцията на Сънсет жълто багрило върху активен въглен от костилки на дренки и върху въглеродни нанотръбички …… 601

Х. Садег, Р. Шахриари-гошеканди, М. Джалили, П. Чаухан, Кинетично изследване и моделиране на отстраняването на Zn^{2+} от отпадна вода чрез адсорбция върху многостенни въглеродни нанотръбички …….. 607

С. У. Ратер, А. Мухамад, А. А. Ал-Захрани, Т. Е. Юсеф, Л. А. Петров, Синтез, охарактеризиране и CO_2 адсорбция върху метал-органична мрежа на основата на Cr(III) ……... 614

Кс.-Ф. Жоу Структурни промени в лигнин при каталитично окисление с Co(сален) …….. 620

М. Р. Мишра, С. М. Хусаин, Р. Шарма, Г. С. Сет Влияние на абсорбцията на топлина върху мед-съдържащ магнито-нанофлуид над импулсно движеща се пластина с променяща се температура ……. 630

К. Джеяджоти, П. Калайчелви, Ефективност на топлопреноса на пластини от неръждаема стомана, мека стомана и алуминий за различни конфигурации на ударна въздушна дюза …….. 637

А. Алирезаеи, М. Баят, М. Алимохамади, С. Хашеми, Изследване на биологичната обработка на 4-хлорофенол с мая и плесен от индустриални и петролни отпадни води (пристанище „Имам Хомейни", Махшахр) ……..... 646

С. Ван, И. Лю, Д. Лю, Изследване на защитен метод от електростатичното поле на кораби, основан на поляризационния контрол на металите 654

Г. Х. Варшуе, А. Хейдаринасаб, А. Вазири, Б. Розбахани, Циглер-Ната катализатор в присъствие и отсъствие на водород при полимеризацията на пропилен чрез кинетично моделиране …… 671

Авторски указател на английски..... 672

Авторски указател на български..... 668

Предметен указател..... 683

Инструкция за авторите ……..…… 687